'BIOCHEMICAL AND PHYSIOLOGICAL ANALYSIS OF MICROVESICLE SUBTYPES.'

Presented by

Dan Stratton

Thesis submitted in partial fulfilment of the requirement

for the degree of

DOCTOR OF PHILOSOPHY (Ph.D)

Director of Studies: Prof. Jameel M. Inal

Second Supervisor: Dr. Christopher Bax

Cellular and Molecular Immunology Research Centre (CMIRC)

Faculty of Life Sciences, School of Human Sciences

London Metropolitan University

September 2012

DEDICATIONS

It is with great honour to dedicate this thesis to Tim Jewell, Michael Kagey and Norah Dodson, all people dear to me who I lost over the course of this thesis.

I would also like to include Dr. Bill Revel and Meredith Kercher, two friends who died before their time.

Finally, I would like to dedicate this thesis to my family, friends and colleagues who contributed to my health and well being.

ACKNOWLEDGEMENTS

I would like to thank Memory Pinchbeck for her help, encouragement and support throughout this study, without who this thesis may not have happened. I would also like to thank Diane Kagey for her support and encouragement. Others I am really grateful to are Keiran Furey and Vincent Furey.

I would like to thank my team for their support, Samuel Antwi-Baffour, Samireh Jorfi and Sharad Kholia. All of my colleagues, in particular Sheelagh Heugh and Dr. Chris Bax for their support and interest in this study. Furthermore I would like to thank Dr. Steven Butler, Prof. Chris Palmer, Dr. Ken White, Dr. Gareth Williams, Dr. Nick Chatterton, Dr. N Wardle, Dr. E. Ansa-Addo, Dr. Tim Scott-Taylor, Dr. Una Fairbrother, Dr. B. Awamaria, George Worthington, Masuma Ahmed Ali, Jennifer Jacoby, Ruth Eyob, Louis Stott and Eric Coleman for their kind donations, their help and their advice.

I would *especially* like to thank Prof. Jameel Inal for his support and guidance throughout this study, for both scientific and personal advice. Always having time to listen regardless of the situation. I look forward to productive future collaborations.

ABSTRACT

The research presented in this thesis encompasses a detailed biophysical and biochemical analysis of extracellular vesicles: in particular microvesicles (MVs). The characterisation utilised novel applications of existing protocols, demonstrated for the first time within this thesis, resulting in an up-to-date and greatly improved series of techniques for the analysis of microvesicles.

Application of these techniques revealed two distinct subtypes of MVs that can be collected from the same parent cell types in culture, originating via different pathways of biogenesis. cMVs are constitutively released and sMVs stimulated for release. They express distinct biochemistries leading to the potential to perform different physiological functions. These subtypes exhibit distinct FACs morphologies, distinct protein, non-specific carbohydrate and nucleic acid profiles. The techniques used demonstrated in this thesis also show that the MVs have remarkable differences in size as shown for the first time by TEM, flow cytometry, DLS and Nanosight particle tracking.

FT-IR spectroscopy was used for the first time to profile similarities and differences between cell lines by analysis of the fingerprint region (1800cm^{-1} to 900cm^{-1}). The MV subtypes derived from parent cells were analysed using FT-IR to demonstrate similarity in non-disclosed protein expression. BCA protein analysis, modified schiffs test, spectroscopic and quartz crystal microbalance techniques demonstrated cMVs to be smaller, denser and more slowly released from cells than the sMVs are larger, lighter and released sMVs rapidly in response to a stress stimuli.

Analysis of calcium homeostasis has revealed that MVs contain high calcium levels, that are deliverable to cells via MVs as cargo. Furthermore, the MV subtypes express different arrays of deliverable proteins and receptors that were transiently expressible upon the recipient cell.

Novel research into the role of ultra low-frequency magnetic fields (ULMFs) on cellular viability was explored. Results suggested that 0.3μT 6V A/C 10Hz ULMF exposure to cells increased intracellular Ca^{2+} levels via transiently induced plasma membrane pores. Furthermore, ULMFs stimulated MV release from cells and negated apoptosis by export of pro-apoptotic agents, increasing the health of the cells. ULMFs can be used to significantly enhance the uptake promoting cellular sensitivity to anti-cancer drugs, such that 10% of the therapeutic dose used with ULMFs was able to achieve current levels of therapeutic response. ULMFs significantly reduce HeLa migration during wound healing although they increased cell proliferation, possibly by releasing MVs.

The exciting potential of this research may lead to new possibilities in cancer therapy. Using ULMFs in conjunction with chemotherapy may increase the success rates of existing therapies and reduce unwanted side effects. The data presented in this thesis will allow researchers to better understand subtle differences in MV biogenesis, how this reflects in their composition and morphology. It is the hoped that this research will lead to more laboratories engaging MV research using the techniques pioneered in this thesis to engage within many new areas of biology and biochemistry. This work offers a significant contribution to the field of MV research, but represents the tip of the iceberg.

PUBLICATIONS

Selected Papers

Stratton, D., Williams, G., Antwi-Baffour, S., Jorfi, S., Jurkschat, K., Lange, S. and Inal, J., (2013) Microvesicles released constitutively and upon stimulation retain parental features but exhibit distinct properties, Submitted to J. Biochem

Dan Stratton, Samuel Antwi-Baffour, Gareth Williams, Ryan Grant, Sigrun Lange and Jameel Inal (2012) Characturization of microvesicles released from cells constitutively and upon stimulation, JEV, Vol. 1, 18167

Stratton, D., (2012) The two main microvesicle subtypes are significantly different in construction and have different physiological roles, Journal of Immunology, Vol. 188, Abstract

Inal, J. M., Ansa-Addo, E.*, **Stratton, D.**,* Kholia, S., Antwi-Baffour, S., Jorfi, S., and Lange, S. (2012) Microvesicles in Health and Disease, Archivum Immunologiae Therapiae et Experimentalis, Vol. 60, pp 107-121

Grant, R., **Stratton, D.**, Ansa-Addo, E., Antwi-Baffour, S., Jorfi, S., Kholia, S., Krige, L., Lange, S and Inal. J., (2011) A filtration-based protocol to isolate human Plasma Membrane-derived Vesicles and exosomes from blood plasma, Journal of Immunological Methods, Vol. 371, pp 143-151

Antwi-Baffour, S., Kholia, S., Aryee, Y. K. D., Ansa-Addo, E. A., **Stratton, D.,** Lange, S and Inal, J. M., (2010) Human plasma membrane-derived vesicles inhibit the phagocytosis of apoptotic cells – Possible role in SLE, Biochemical and Biophysical Research Communications, Vol. 396, pp 278-283

Selected Conferences

Dan Stratton and Jameel Inal (2012) Plasma Membrane-derived Vesicle subtypes exhibit distinct physical and physiological properties. Presented at the Biochemical Society meeting, Microvesiculation and Disease.

Dan Stratton (2012) Microvesicle subtypes, invited to talk at ISEV conference, Gotoborg.

Dan Stratton and Jameel Inal. (2012) The two main PMV subtypes are significantly different in construction and have different physiological roles. Submitted to J. Immunol. 99th Annual Meeting of the American Associaton of Immunologists.

Stratton, D., and Inal, J. (2010) Characterisation of cPMVs and sPMVs, constitutive and stimulated plasma membrane-derived vesicles. Immunology, Vol. 131, 135-135. Presented at the Annual Congress of the British Society for Immunology Liverpool.

CONTENTS

List of figures

List of tables

ABBREVIATIONS

ABCA-1	ATP binding cassette transporter 1
ATP	Adenosine triphosphate
Ca^{2+}	Calcium ion
CGM	Complete growth medium
Cm	Centimetres
cMV	Constitutive microvesicle
CO_2	Carbon dioxide
Cyt-C	Cytochrome C
DAF	Decay accelerating factor (CD55)
ddH_2O	Double distilled water
DMEM	Dulbeccos modified eagles medium
DMSO	Dimethyl sulfoxide
DNA	Deoxyribose nucleic acid
ER	Endoplasmic reticulum
FACs	Flow cytometry (Fluorescence-activated cell sorting)
FBS	Foetal bovine serum
fMLP	*N*-formyl -methionyl –leucyl – phenylalanine
FSC-HLog (FSC)	Forward scatter
FTIR	Fourier transform infra red spectroscopy
$GdCl_3$	Gadolinium Chloride (III)
GRN-HLog	Green logarithmic
GTP	Guanosine triphosphate
H_2O	Water
H	Hours
HS	Horse serum

LAMP-1	Lysosome associated membrane protein (CD107a)
MAC	Membrane attack complex
MHC	Major histocompatibility complex
Mins	Mins
MV	Microvesicle
Nm	Nano meters
-OH	Phenol group/ hydroxyl group
OMV	Outer membrane vesicle
$P2X_7$	Purinoreceptor
PBS	Phosphate buffered solution
PC12	Rat neuronal cell line
Pen/Strep	Penicillin and Streptomycin
PIP_2	Phosphotidylinositol 4, 5- bisphosphate
PS	Phosphatidyl serine
RNA	Ribose nucleic acid
ROS	Reactive Oxygen species
RPMI 1640	Roswell park memorial institute (medium 1640)
sMV	Stimulated microvesicle
SSC-HLog (SSC)	Side scatter
THP-1	Monocytic leukaemia cell line
ULMF	Ultra low-frequency magnetic field
YLW-HLog	Yellow logarithmic
PMA	Phorbol 12-myristate 12-acetate

1. Introduction

1.1 General overview of microvesicles

Cells typically produce a variety of microvesicles, some of which remain intracellular (for example lysosomes) and others that are released (Membrane-derived Vesicles [MVs] or exosomes); these two microvesicle subtypes are based upon their biogenesis, size, function and composition (Hugel *et al*, 2004; Gutwein *et al*, 2005; Akoi *et al*, 2007; Pizzirani *et al*, 2007).

Research into the nature of microvesicles has identified various functions including that of intercellular communication (Scanu *et al*, 2008; Muralidharan-Chari *et al*, 2010), control of apoptosis and apoptotic response to stress (Gutwein *et al*, 2005; MacKenzie *et al*, 2005; Boulanger *et al*, 2007; Sarkar *et al*, 2009), cell proliferation (Inal *et al*, 2012), immunological roles (Pizzirani *et al*, 2007; Nolan *et al*, 2008), pro-coagulant roles (Brodsky *et al*, 2002; Kim et al, 2005), cellular repair and housekeeping (Tomas *et al*, 2006), the export of proteins (del Conde *et al*, 2005; Akoi *et al*, 2007; Torrado *et al*, 2009), RNAs (Deregibus *et al*, 2007; Alder, 2010), peptide hormones (Hugel *et al*, 2004) and possibly cellular waste products such as misfolded proteins (Putz *et al*, 2008), cytotoxic agents and cell metabolic waste (Fox *et al*, 1990; Hugel *et al*, 2004; Robertson *et al*, 2006; Torrado *et al*, 2009). Furthermore, parasites have evolved or adapted to exploit the MV release process to evade host immune responses, invade host cells (Gould *et al*, 2003; Temme *et al*, 2010; Meckes Jr *et al*, 2011) or spread infective particles (Gould *et al*, 2003; Silverman *et al*, 2010).

1.2 Membrane-derived vesicles (MVs)

The established characteristics for MVs include their size, 1-2μm in diameter (Deregibus *et al*, 2007), and for all MVs, regardless of cellular origin, the negatively charged phospholipids such as phosphotidylserine (PS) and Phosphotidylcholine (PC) translocated on to the outer leaflet of the plasma membrane (Angelot *et al*, 2009; Scanu *et al*, 2008) as seen during early apoptosis (Bratton *et al*, 1997). However MVs may contain different ratios or be enriched for phospho- and bioactive- lipids, depending on stimulus type or cellular origin (Akoi *et al*, 2007; Pizzirani *et al*, 2007; Nolan *et al*, 2008; Scanu *et al*, 2008). MVs contain RNAs (mRNA, miRNA and ncRNA) (Deregibus *et al*, 2007; Angelot *et al*, 2009; Alder, 2010), cytoplasmic components such as enzymes and cytoskeletal proteins (Fox *et al*, 1990; Solun, 1999). The cytokines and receptors they carry are characteristic of their cellular origins, reflecting cellular health (Leroyer *et al*, 2007; Scanu *et al*, 2008; Angelot *et al*, 2009; Torrado *et al*, 2009), however composition of MVs may undergo substantial remodelling to enable specialised or adaptive functioning (Muralidharan-Chari *et al*, 2010) or enrichment of particular proteins and receptors.

MVs were first discovered and described as 'platelet dust' during the 1970s but it was not until much later that the properties of MVs and their origin would be ascertained. Initially their pro-coagulant properties were investigated with reference to platelet binding, erythrocyte and lymphocyte interactions (Setty *et al*, 2000; Pizzirani *et al*, 2007) although it transpires that there are a multitude of MV types that exhibit different and sometimes seemingly contradictory properties (Nolan *et al*, 2008; Angelot *et al*, 2009). The current thinking is to categorise MVs with reference to their cellular origins and functions (Kim *et al*, 2005; Akoi *et al*, 2007).

MVs are often associated with the cellular responses to activation, membrane depolarisation or apoptosis (Boulanger *et al*, 2007; Scanu *et al*, 2008; Angelot *et al*, 2009). Activation is a broad term that encompasses all manner of stimuli, such as chemical, biochemical and mechanical triggers that possibly would induce apoptotic or pseudoapoptotic events (cells that have been briefly exposed to stress agents will initiate an easily recoverable apoptotic event) and/or increases in $[Ca^{2+}]_i$ (MacKenzie *et al*, 2005). The processes that govern MV formation and release are therefore a cellular response injury that 'sheds' excesses in $Ca^{2+}{}_i$ as well as export of damaging agents (Gutwein *et al*, 2005), allowing the cell to recover (Inal *et al*, 2012). MVs also have the role as vectors to transmit signals between distant cells by transporting cell components or products as a part of the membrane or internally (Scanu *et al*, 2008; Angelot *et al*, 2009; Leroyer *et al*, 2009; Muralidharan-Chari *et al*, 2010). This would allow the passage of easily degraded, immune response provoking or pH sensitive molecules such as RNAs (Alder, 2010; Quesenberry *et al*, 2010b) or particular types of protein (Kim *et al*, 2005; Pizzirani *et al*, 2007) and enzymes (Sarkar *et al*, 2009) through the circulatory system.

It is possible that all eukaryotic cell types release MVs to varying extents while under stress and these exhibit quite different properties (Pizzirani *et al*, 2007; Nolan *et al*, 2008; Angelot *et al*, 2009; Muralidharan-Chari *et al*, 2010). Investigation has shown that MVs are released from most animal cell types from all species investigated. MV-like or double membrane bound lipid-protein bound microvesicles (70-170nm radius), enriched in 'degraded' phospholipid (stimulated in vitro by Ca^{2+}), have been isolated from some plant species in relation to degrading plasma membrane and also cell membrane senescence (Yao *et al*, 1991). Furthermore, lipids comprising MV-like

vesicles are more likely to be oxidised than lipids from the parent cell (Yao *et al*, 1993). It is reasonable to conjecture that plants can microvesiculate owing to many similarities that exist between plant and animal cell metabolism, however in animals, MVs have been described mainly as a communicative vector that exploits a complex circulatory system, and this might not necessarily be the case in plant systems. MV-like vesicles may play a different role or operate unlike mammalian MVs, but any such hypothesis is beyond the scope of this thesis, being concerned with the functions of MVs and to some extent Outer Membrane Vesicles (OMVs).

1.2.1 Outer Membrane Vesicles

Outer membrane vesicles (OMVs) are released from gram negative bacteria in a similar fashion to MV release from eukaryotes (Bauman and Kuehn, 2006; McBroom *et al*, 2006); they are formed from protrusions that are 'pinched off' from the bacterial outer membrane and include periplasmic components (McBroom *et al*, 2006). OMVs contain enriched proteins and lipid derived from the bacterial outer plasma membrane envelope, forming spherical structures (McBroom *et al*, 2006). They have many roles such as increasing invasion (Vidakovics *et al*, 2010), delivering virulence factors (Kouokan *et al*, 2006), evading host immune systems, shedding immune complexes (Vidakovics *et al*, 2010), formation of biofilm and even transfer of toxic agents that destroy competing bacterial species (McBroom *et al*, 2006). OMVs vary depending upon species and whether they are stimulated or released naturally as a communicative vector (Bomberger *et al*, 2009; Vidakovics *et al*, 2010). OMVs can deliver virulence factors and active proteins to host organisms and interact with eukaryotic cells (Kouokam *et al*, 2006; McBroom *et al*, 2006). As with *Helicobacter pylori,* OMVs can transmit carcinogenic agents (Chitcholtan *et al*, 2008) or modify immune responses

without direct immune cell (B cell) contact and cause MV production in host cells that are lipid raft/receptor dense (Vidakovics *et al*, 2010).

Only a small proportion of OMVs are produced in response to membrane instability, the majority being released as a natural process in response to environmental or internal factors such as membrane stress due to misfolded proteins that could cause transcription of OMV genes (McBroom *et al*, 2006). Twenty or more genes have been isolated that directly influence the release of OMVs, increasing OMV populations up to 200 times (McBroom *et al*, 2006). Typically OMVs comprise 0.2-0.5% of the culture medium, and *in vivo* have been shown to be essential for colony success and establishment of host disease states (Chitcholtan *et al*, 2008; Vidakovica *et al*, 2010). OMVs have therapeutic properties and have been shown to be successful in animal models for the slowing or eradication of disease-causing bacteria (Bishop *et al*, 2010) and as a non-replicating vaccine (Lee *et al*, 2009). OMVs could potentially be used as a diagnostic tool to indicate infection of bacterial species by identifying unique bacterial markers on the membrane, such as combinations of proteins.

The release of MVs, OMVs or MV-like vesicles from many diverse species in response to stimulation or stress would indicate that it is a highly conserved process that is vitally integral for cell-cell communication and 'shedding' cellular waste. Other purposes may have arisen depending upon the constraints placed upon the organism.

1.3 Induction of MVs

The plasma membrane is a dynamic structure that is constantly remodelled and responds to many factors (Tomas *et al*, 2006). Its integrity is essential for the normal functioning of 'the cell', there being many processes that ensure membrane asymmetry, protein/lipid recycling and membrane repair (Manno *et al*, 2001). However MV formation is an innate property of most cell types releasing a 'basal' level of MVs and occurs as a natural part of the cellular processes (Mack *et al*, 2000; Pizzirani *et al*, 2007) for a variety of reasons including that cells typically exist in a state of non or early apoptosis due to slight changes in microenvironment causing stress or the direct stimulation of MV release by active stress agents (MacKenzie *et al*, 2005). It has been observed that cells produce increased levels of MVs in response to stress that are larger than constitutively released MVs (Pizzirani *et al*, 2007; Nolan *et al*, 2008) and that they carry different signalling molecules (Angelot *et al*, 2009). There are various methods that have been described to 'induce' MVs by 'activating' cells under differing circumstances. They may be natural or artificial and the resulting MV release therefore exhibit varied and particular properties that have not been investigated sufficiently to be conclusive. However a distinction exists regarding the properties of MVs produced from differing cell types and under diverse stress factors (Agouni *et al*, 2007; Alder, 2010).

Diseased states are often associated with elevated levels of MVs characteristic of the tissues affected (Leroyer *et al*, 2009; Alder, 2010; Antwi-Baffour *et al*, 2010). Possibly due to stressed tissues (such as the presence of a pathogen or toxic substance), the cells release MVs with their readily detectible protein/lipid signature that may be used as a diagnostic tool for the detection of insidious diseases and cancer (Setty *et al*, 2000;

Antwi-Baffour *et al*, 2010; Muralidharan-Chari *et al*, 2010). There are correlations between MV release and evasion of immune responses and tumour malignancy (Akoi *et al*, 2007), pathogens and pro-cancereous cells may use MVs either acting as a decoy for immune cells or to 'programme' immune responses to overlook them (Muralidharan-Chari *et al*, 2010). Furthermore, MVs are implicated in the establishment and progression of certain types of tumour by transferring oncogenetic factors or carcinogens, establishing blood supply by promoting angiogenesis and by changing the tumour micro-environment to facilitate growth and metastasis (Muralidharan-Chari *et al*, 2010).

1.3.1 Biochemical basis of MV formation; control of membrane asymmetry

The formation of MVs is one characteristic marker for cells undergoing the stages of early apoptosis (Hugel *et al*, 2004; Gutwein *et al*, 2005; Angelot *et al*, 2009) and is typified by PS externalisation (Gonzalez *et al*, 2009), and the calpain mediated cleavage of the actin cytoskeleton due to a rise in intracellular or cytoplasmic Ca^{2+}. This rise in $[Ca^{2+}]_i$ originates mostly from external sources (Setty *et al*, 2000; Pizzirani *et al*, 2007; Qu *et al*, 2007; Nolan *et al*, 2008) and enters the cell through ion channels (MacKenzie *et al*, 2005; Qu *et al*, 2007)(Signal transduction [Brookes et al, 2002]), membrane pores or certain types of cell damage. Typically, cells are very good at Ca^{2+} homeostasis, therefore increases in Ca^{2+} must be rapid and beyond the scope of the cell to control effectively.

Calcium controlled proteins and enzymes proceed to degrade cytoskeletal structures so that the plasma membrane loses integrity and membrane blebs that bud from the

plasma membrane form, that will 'pinch' off (in a process that resembles both cytokinesis and viral budding) to generate a MV (Fox *et al*, 1990; Muralidharan-Chari *et al*, 2010). F actin forms a network beneath the plasma membrane that is crucial for maintaining membrane integrity (Li *et al*, 2010) forming a scaffold that phospholipids adhere to and many cell surface receptors are linked to (Fox *et al*, 1990; Wang *et al*, 2006; Li *et al*, 2010). They depolymerise once cytoskeletal degrading enzymes have been activated, to their G actin conformation, that is the globular form (Tomas *et al*, 2006). Actin remodelling and membrane sealing may depend upon shedding $[Ca^{2+}]_i$ that influences cytoskeletal Ca^{2+} dependant degrading enzymes (Tomas *et al*, 2006).

Membrane shedding though microvesiculation involves a host of enzymes, many that require ATP (Solun, 1999). Whether MVs themselves contain ATP however has yet to be established although there is compelling evidence that suggests that membrane and cytoskeletal associated enzymes associated with ATP generation are included within MVs as a part of the cytoskeletal inclusion (Hardin *et al*, 1992).

Although erythrocytes microvesiculate, this could be due to shear stress or membrane insult, though they have low levels of ATP as well as energy generating mechanisms that could allow erythrocyte MV production. Although similar to MVs derived from nucleated cells erythrocyte MVs may have a different classification to MVs released from nucleated cells (Muralidharan-Chari *et al*, 2010). They can influence nucleated cells but more often are described in terms of clotting (Chung *et al*, 2007). Little research into their biogenesis and physiological roles have been performed, however Ca^{2+} is essential to their formation (Chung et al, 2007; Harry *et al*, 2012).

1.3.2 Enzymes involved in maintenance and loss of membrane asymmetry and subsequent MV release

Membrane asymmetry is crucial for normal membrane function (Gurr *et al*, 2002). It is maintained by enzymes such as aminophospholipid translocase, flippase and floppase that 'patrol' the plasma membrane and continually readjust the orientation of phospholipids and proteins to their optimal alignment (Bratton *et al*, 1997; Brooks *et al*, 2002). Aminophospholipid translocase acts in a contradictory manner to scramblase whose activity is slower so that PS and PC appears internalized against the charge gradient; an increase of $[Ca^{2+}]_i$ inactivates aminophospholipid translocase and enhances scramblase activity leading to PS and PC externalization. Gelsolin and Calpain are crucial for the maintenance and remodelling of the actin cytoskeleton and integral membrane proteins. It is the breakdown of these processes and the cleavage of the actin cytoskeleton (Yermen *et al*, 2007) that leads to the formation of membrane blebs and the subsequent release of MVs.

1.3.3 Aminophospholipid translocase

PS expression on the outer membrane is attributed in part to the loss of aminophospholipid translocase activity, whose role is to prevent non specific 'flip/flop' of most classes of phospholipids and so help regulate membrane asymmetry against an electrochemical gradient (Solun, 1999; Manno *et al*, 2001; Brooks *et al*, 2002). The increased expression of PS that is detected during apoptotic events is due to increases in $[Ca^{2+}]_i$ (Bratton *et al*, 1997; Hugel *et al*, 2004). This increased $[Ca^{+2}]_i$ inhibits the action of aminophospholipid translocase, leading to increased scramblase activity

(Brooks *et al*, 2002) that is localised to the lipid raft or in some cases cell wide expression of PS on the outer membrane (Solun, 1999; Manno *et al*, 2001).

The expression of aminophospholipids on the outer membrane leaflet is a prerequisite for the production of MVs (Solun, 1999). However actin remodelling must occur before membrane blebs appear that lead to MV release (Gutwein *et al*, 2005; Muralidharan-Chari *et al*, 2010). Bleb growth rates may contribute towards determining MV properties. Failure of the cell to release a MV may lead to cell death or be due to effective homeostatic mechanisms overriding MV formation.

1.3.4 Calpain

Calpains are a Ca^{2+} dependant family of cysteine protease enzymes that are ubiquitously expressed in mammals. They are one of the key enzymes responsible for the degradation and remodelling of cytoskeletal and membrane proteins (Fox *et al*, 1990) by cleaving protein kinase C, breaking down receptors and other proteins (Emori and Saigo, 1994; Nolan *et al*, 2008). The role of calpains during wound healing, cell migration, by regulating the expression of signalling molecules (Dourdin *et al*, 2001), and during the cell cycle (Potter et *al*, 1998) provide examples of this. There are two subtypes of calpain that exhibit different $[Ca^{2+}]$ requirements; m calpain and μ calpain (Emori and Saigo, 1994), each having a homologous small subunit that is 28-kDa but each have a distinct 80-kDa isoform subunit with varying properties (Dourdin *et al*, 2001). However for the purposes of this study these differences were unimportant as both forms are implicated in actin cleavage and so the calpain inhibitors used had no specificity for either of these subtypes. Activation of calpain therefore leads to actin

cleavage when bound to free Ca^{2+} (Solun, 1999; Brooks *et al*, 2002), this actin cleavage is essential for cytoskeletal degredation and membrane instabilities that lead to the production of MVs (Fox *et al*, 1990; Brooks *et al*, 2002; Gonzalez *et al*, 2009).

1.3.5 ATP binding cassette transporter 1 (ABCA-1)

The ATP binding cassette transporter 1 (ABCA-1) is a 220-kDa protein that is associated with the plasma membrane (Smith *et al*, 2002). It is a major regulator of phospholipid and cholesterol homeostasis within the cell, functioning to translocate PS from the inner leaflet to the outer leaflet of the plasma membrane (Smith *et al*, 2002; Inal *et al*, 2012) hence 'floppase' activity. Floppase is an ATP dependant enzyme that transports lipids across the plasma membrane to maintain asymmetry. Its action is slower than aminophospholipid translocase (Solun, 1999). Indeed ABCA (-1-) mice have reduced MV levels due to decreased PS expression (Morel *et al*, 2011).

1.3.6 Scramblase

Scramblase is a part of the family of proteins called flippases, enzymes whose role it is to maintain membrane asymmetry by transporting lipids across monolayers of the lipid bilayer in opposition to aminophospholipid translocase (Brooks *et al*, 2002). Scramblase activity depends of intracellular $[Ca^{2+}]$. During normal cellular activity these concentrations are low, however while under stress intracellular $[Ca^{2+}]$ rise leading to the activation of scramblase (Brooks *et al*, 2002) and the rapid externalization of PS and PC that is essential for MV shedding (Gonzalez *et al*, 2009). Scramblase is a constituent of the MV membrane (Solun, 1999).

1.3.7 Gelsolin

Gelsolin is an 82-kDa protein that is a member of the actin filament serving and capping family (Sun *et al*, 1997; Yermen *et al*, 2007), found within the cytoplasm and in mitochondria. It is activated by the binding of Ca^{2+} (Fox *et al*, 1990) and inhibited by polyphosohoinositides (notably phosphotidylinositol 4, 5- bisphosphate [PIP_2]) (Sun *et al*, 1997). Gelsolins varied roles within different cell types include the assembly and disassembly of the actin cytoskeleton, transduction of signals across the plasma membrane to the cytoskeleton by interactions with PIP_2 and regulation of cell motility, secretion and apoptosis by controlling cytoskeletal architecture (Tomas *et al*, 2006; Yermen *et al*, 2007).

Gelsolin can slow or prevent apoptosis by repairing damage to mitochondrial structures and so prevent the leakage of cyt^{450} that leads to the formation of the apoptosome. Caspase -3 cleavage residues are activated by gelsolin causing it to increase actin depolymerisation (Yermen *et al*, 2007) that first leads to membrane blebbing and then microvesiculation or to apoptosis.

1.3.8 A paradigm for MV biogenesis

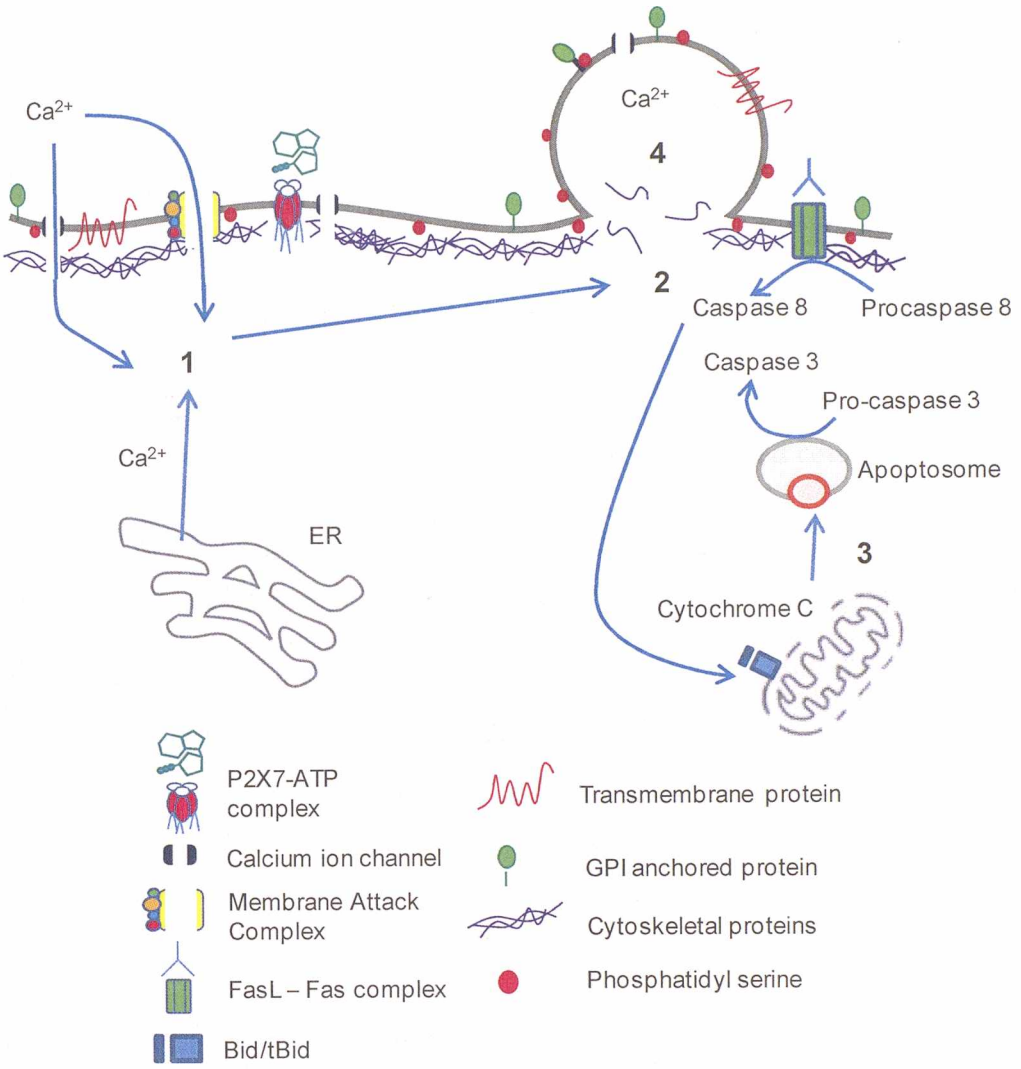

Fig 1. Cellular pathways to MV release. Ca^{2+} influx via calcium channels, Membrane Attack Complexes (MACs) or P2X7-gated calcium channels leads to a microenvironment with increased $[Ca^{2+}]_i$, resulting in the deactivation of cytoskeletal-associated enzymes, membrane instabilities and cytoskeletal protein degradation. Intracellular Ca^{2+} may also originate from organelles, in particular the endoplasmic reticulum (ER). **1**, Flippase, Floppase and Aminophospholipid translocase are unable to maintain membrane asymmetry leading to increased external expression of phosphatidyl serine. **2**, The simultaneous activation of calpain by free $Ca^{2+}{}_i$ causes the degradation of the actin cytoskeleton, leading to the formation of the membrane bleb. **3**, Mitochondrial stress can lead to MV formation via a different pathway to Ca^{2+} activation. Pro-apoptotic Bd-2, Bax, Bak insert into the mitochondrial outer membrane causing an increase in membrane permeability leading to reactive oxygen species (ROS), cytochrome C and AIF (apoptosis inducing factor) to leak into the cytoplasm, stimulating the caspase cascade causing cytoskeletal degradation, and the formation of the apoptosome that leads to apoptosis. If the 'spill' is relatively small and the damage minimal, the cell can use the apoptosome to form a MV and export the hazardous agents (pseudoapoptosis). Stimulation of FasL leads to the stimulation of caspase 8 and the subsequent stimulation of caspase 3, and the translocation of tBid to the mitochondrial membrane, leaking cytochrome C, leading to formation of the apoptosome. The membrane bleb expresses receptors and proteins typical of the parent cell, enriched externally for phosphotidyl serine. **4**, Internally, the bleb is enriched for actin and contains a sample of the 'local' cytoplasm components such as RNA, protein, peptide hormones and esterases. The bleb also contains undesirable components such as apoptotic agents, notably $Ca^{2+}{}_i$ which is enriched in MVs as apart of the cell's calcium homeostatic mechanisms. The bleb finally pinches off, forming the MV.

Fig 1.1 by Stratton (Inal *et al*, 2012)

1.3.9 Other factors leading to MV formation

Response to stress factors such as NHS deposited sublytic MAC on plasma membrane causes localised rises in intracellular Ca^{2+}, that via differing pathways, leads to cleavage of the actin cytoskeleton and membrane blebbing (Inal *et al*, 2012). Other stress factors include fMLP, a bacterial peptide that has been shown to stimulate MVs (Nolan *et al*, 2008) and Calcium ionophore (Thomas and Salter, 2010). As previously stated MV exhibit very similar characteristics but will have different properties depending upon their mode of formation (Agouni *et al*, 2007). MVs are released constitutively, possibly as a response to changes in mitochondrial viability resulting in leakage of ROS/cyt^{450} or some otherwise undiscovered process (Sato *et al*, 2004; Kim *et al*, 2005; Mackenzie *et al*, 2005) such as calcium homeostasis or as a part of a complex communication network, eluding to complex biochemical components.

1.3.10 Lipid rafts

Lipid rafts are cholesterol and sphingolipid enriched 'islands' in the plasma membrane that have highly ordered associated protein microdomains and receptor complexes (Mandal *et al*, 2005; Martinez-Seara *et al*, 2010; Levitan *et al*, 2010; Wang *et al*, 2010). They have a distinct composition from the majority of the plasma membrane (a non-lipid raft membrane has a cholesterol : protein ratio of 50 : 1 whereas in raft containing membranes it is 20 : 1 [Martinez-seara *et al*, 2010]) and they are typically of diameter 10-200nm (Levitan *et al*, 2010). Lipid rafts diffuse laterally across the plasma membrane allowing interactions between activated receptors and transduction molecules such as GTP (Wang *et al*, 2010). The receptor micro-domains have been implicated in many cellular interactions such as cell migration, communication and

apoptosis (therefore MV generation). Lipid rafts are also thought to be the site of MV production and consequently MVs exhibit lipid raft properties or may themselves be included on the released MV (Vidakovics *et al*, 2010; Inal *et al*, 2012).

The high cholesterol content of the lipid rafts leads to increased membrane rigidity that may regulate ion channel function or may directly interact with residues on the receptors to regulate their action (Levitan *et al*, 2010). Although lipid rafts are essential for the formation of MVs (del Conde *et al*, 2005) they are instrumental in a range of other cellular mechanisms and these may also be properties carried by MVs. Lipid rafts may act as the site of microvesiculation (Inal *et al*, 2012), possibly due to receptor interactions with extra/intra cellular signals. Indeed, lipid rafts may be implicated in cell surface protein and receptor sorting, leading to enrichment of classes of proteins and receptors (de Gassart et al, 2003; Schuck and Simons, 2004).

Membrane fluidity is essential for normal microvesiculation (Gonzalez *et al*, 2009; Muralidharan-Chari *et al*, 2010), the variable lipid content of cellular membranes from different tissues may account for the change in number of MVs that are typically shed from cells types and explain (in part) their range of properties (Levitan *et al*, 2010). In particular, cancer cells express a different lipid profile to normal cells (Shah *et al*, 2008) and may be linked to specific properties of cancer derived MVs.

1.3.11 Mechanosensitive ion channels (Ca^{2+})

Mechanosensitive calcium channels are found on a large variety of cell types, including epithelial cells and neurons (Ohata *et al*, 2001). They respond to mechanical, shear or osmotic stress that causes the ion channel to 'open' due to a conformational change in shape allowing the influx of Ca^{2+}, thereby initiating Ca^{2+}-mediated protein synthesis by stretch-induced gene expression (Chang *et al*, 2001; Ohata *et al*, 2001).

There are at least 5 types of mechanosensitive receptors. Calcium activated potassium channels (K_{Ca}) have been extensively researched, being responsible for membrane repolarisation and are modulated by external 'stretch' stress and intracellular ATP (Kawakubo *et al*, 1999). However other classes will allow the passage of ions for different physiological roles. The mechanosensitive receptors open in response to pressure on the lipid membrane local to that receptor. Although these receptors are uniformly distributed throughout the plasma membrane a holistic cellular response will only occur if the majority or whole of the membrane is stressed (Ohata *et al*, 2001). The influx of Ca^{2+} in response to mechanosensitive receptor stimulation will initiate cellular remodelling (Ohata *et al*, 2001) and MV production through activation of actin cleavage and associated enzyme responses.

1.3.12 $P2X_7$

The P2X family of receptors (purinoreceptor) are extensively expressed on most terminally differentiated animal cells (Zhang *et al*, 2009) and can respond to extracellular ATP stimulation (Qu *et al*, 2007; Zhang *et al*, 2009). They are 5'-triphosphate ATP-gated ion channels that are implicated in ion influx. Upon stimulation

they facilitate the rapid bidirectional movement of cations triggering the collapse of the Na^+ and K^+ gradient and a next influx of Ca^{2+} (Zhang *et al*, 2009) thus influencing cell morphology such as PS translocation and membrane blebbing (Mackenzie *et al*, 2005; Qu *et al*, 2007). $P2X_7$ have also been linked with MV shedding (Bianco *et al*, 2005; Qu *et al*, 2007; Thomas and Salter, 2010), because blocking this receptor in the presence of the appropriate activator has been shown to diminish MV release by 65% (Pizzirani *et al*, 2007; Thomas and Salter, 2010). MVs in turn also express P2X receptors as well as many types of associated ion channels (Levitan *et al*, 2010).

1.3.13 Integrins

Integrins comprise a group of approximately 24 cell surface receptors (90 – 160 kDa) composed of 18 α- and 8 β- subunits (Legate *et al*, 2009), that are connected to the F actin cytoskeleton regulating cell attachment, the cell cycle and apoptosis via signal transduction both externally and internally (Li *et al*, 2010). They are transmembrane receptors that recognise and bind to the extracellular matrix and counter receptors that have 'overlapping' substrate affinity and cell specific expression patterns (Legate *et al*, 2009). Unique combinations of integrins will determine cell type binding and will be tissue specific (Legate *et al*, 2009).

1.3.14 Membrane Attack Complex (MAC)

Complement with its resulting membrane attack complex (MAC) are a part of the innate immune response and are composed of self assembling protein subunits found within NHS (blood serum), When complement C5 is cleaved into C5a and C5b the MAC deposition is initiated. Essentially C5b is inserted into the plasma membrane, allowing

the binding of C6-9 consecutively, polymeric C9 comprising the protein pore. Sublytic pores that allow the cytoplasmic contents of the cell to spill into the extracellular space and would help encourage macrophages to migrate to this site. The sublytic pores formed also allows the passage of extracellular Ca^{2+} to the cytoplasm along a concentration gradient, so increasing $[Ca^{2+}]_i$ (Halperin *et al*, 1993). This rise in $[Ca^{2+}]_i$ would activate the host of enzymes that lead to the release of MVs.

The release of MVs and OMVs may be a process employed by eukaryotic cells and bacteria respectively to evade destruction by complement mediated lysis through shedding MVs with MAC embedded within the plasma membrane (Moskovich and Fishelson, 2007; Inal *et al*, 2012).

1.3.15 Mitochondrial stress

Mitochondria are an important cause of apoptotic stress (Aleo *et al*, 2006) that can lead to the formation of MVs (Laytin *et al*, 2009) via a different pathway to membrane activation and $[Ca^{2+}]$ influx. Pro-apoptotic Bcl-2, Bax and Bak insert into the mitochondrial outer membrane causing an increase in membrane permeability. Permeablisation of mitochondrial membranes leads to ROS, and cytochrome C (Cyt-C) that affects ATP and ROS production, and AIF (apoptosis inducing factor) to leak into the cytoplasm (Sato *et al*, 2004). Cytochrome C release from mitochondria is considered to be the first irreversible stage of apoptosis. If this stimulus is left to accumulate it can cause activation of the caspase cascade and the formation of the apoptosome (DuBmann *et al*, 2003; Aleo *et al*, 2006) leading to DNA/RNA damage and protein malformations that could cause apoptotic or under certain circumstances, necrotic cell death. However, cellular machinery cleans up this 'spill' and causes the

formation of the apoptosome through a series of reactions, leading to apoptosis (Aleo *et al*, 2006). If the 'spill' is relatively small and the damage minimal, the cell can use the apoptosome to form a MV and export the hazardous chemicals to be ingested by macrophages that have mechanisms to control ROS or to be filtered out of the body (pseudoapoptosis) (Akoi *et al*, 2007; Inal *et al*, 2012). MVs containing activated caspases and leaked mitochondrial contents are deliverable to cells as cargo and will cause pseudoapoptosis/apoptosis in the recipient cell (Inal *et al*, 2012), in particular if the cell is undergoing stress before MV fusion.

Furthermore mitochondria respond to prions and misfolded proteins, leading to the initiation of apoptotic reactions. These prions and apoptotic reactants may be exported within MVs (Robertson *et al*, 2006; Mecke Jr *et al*, 2011).

1.4 Eukaryotic cells produce a host of other extracellular vesicles (EV)

Extracellular vesicles (EV) have certain common features in common such as being membrane bound, either single or double layered, and containing or expressing proteins and lipids reminiscent of the 'parent' cell. However they can be divided into classes depending upon their mode of action, size and specific construction; due to content, membrane constituents or method of synthesis.

There are strict guidelines to differentiate between the different EVs to ensure purity. This is important to ensure that biological effects really are due to MVs and not to an assortment of EV types (Thomas and Salter, 2010). The techniques used to ensure

sample purity include ultracentrifugation which would be preceded by sonication and/or filtration to disaggregate exosomes that otherwise would sediment with MVs (resulting in confounding factors if unpurified). Finally diagnostic FACs analysis can act as a quality control for MV purity (Antwi-Baffour *et al*, 2010) with or without binding annexin V to phosphatidyl serine.

Furthermore, distinct types of MV, stimulated MVs (sMVs) and constitutive MVs (cMVs) have been described (Stratton *et al*, 2012), each 'sub-type' exhibiting different physical and physiological properties, although classifiable as MVs by generalised morphology, PS expression and structure. sMVs are produced while a cell is undergoing stress, inducing early apoptosis: pseudoapoptosis that is potentially recoverable or late apoptosis: possibly recoverable with extensive damaged protein export, including misfolded proteins and mitochrondria derived ROS, cytochromes, $[Ca^{2+}]_i$ and so forth (Stratton *et al*, 2012). sMVs are stimulated using agents otherwise foreign to a typical cell culture, such as NHS, calcium ionophore, *N*-formyl-methionyl –leucyl – phenylalanine (fMLP), a chemotactic bacterial peptide to attract phagocytic leukocytes. cMVs are constitutively released as a part of usual cellular processes that are not due to atypical stimulation.

1.4.1 Apoptotic bodies

Apoptotic bodies are EVs that typically express PS and $\alpha_V\beta_5$ receptor (Xie *et al*, 2009) but that are typically of greater diameter than MVs and can contain complete or fragmented cellular organelles and components from cells undergoing apoptosis (Narula and Strauss, 2003; Muralidharan-Chari *et al*, 2010). Caspases constitute a

family of aspartate-directed cysteine proteases -1 to -14, that are typically activated during mitochondrial directed apoptosis. Their activation (notably -3 and -8) leads to loss of aminophospholipid translocase activity causing an increase in PS externalisation (Narula and Strauss, 2003; Mandal *et al*, 2005). This coupled with the protein degrading activity, with regard to cytoskeletal proteins leads to apoptotic body formation (DuMann *et al*, 2003; Yermen *et al*, 2007).

Apoptotic bodies are often phagocytosed by a multitude of cell types, in particular macrophages that respond to the enriched levels of PS externally expressed (Narula and Strauss, 2003), the $\alpha_V\beta_5$ and CD36 receptors aiding macrophage apoptotic body engulfment (Xie *et al*, 2009). They have diverse functions, their stimulatory effects having been extensively documented (Hristov *et al*, 2004), However there is increasing evidence to show that apoptotic bodies also deliver signals to surrounding cells and can act as a vector for gene transfer (Muralidharan-Chari *et al*, 2010) and that apoptotic bodies released from tumour cells modulate T cell immune responses by antigen presentation derived from the apoptotic cell (Bastos-Amador *et al*, 2012) and stimulate macrophage maturation (Xie *et al*, 2009).

1.4.2 Exosomes

Exosomes are vesicles composed of a membrane bilayer (30-100nm in diameter) with a characteristic 'cup-shaped' morphology (Chaput *et al*, 2006; Quesenberry *et al*, 2010b) that are stimulated for release or constitutively released from a multitude of cells by exocytosis (Robertson *et al*, 2006; Hogan *et al*, 2009). Lysosomes fuse with the endosome to form a pro multivesicular body composed of membrane components

derived from the cell membrane and defunct organelles. The inward budding of endosomes form membrane microdomains composing signalling molecules such as protein and miRNA, that 'pinch' off to form exosomes contained within multivesicular bodies (Gould *et al*, 2003; Koga, *et al*, 2005; Muralidharan-Chari *et al*, 2010). Exosome shedding is an active process requiring ATP and RNA synthesis with no observable apoptotic or necrotic markers (Akoi *et al*, 2007; Qu *et al*, 2007). Established biomarkers for exosomes are CD63, CD81 and CD82. They also have a unique profile (forward and side scatter) using flow cytometry (Subra *et al*, 2010).

Like MVs, exosomes contain proteins that are characteristic of their cell of origin (Mack *et al*, 2000; Gutwein *et al*, 2005; Muralidharan-Chari *et al*, 2010). However they are enriched for certain groups of proteins, such as histones (Kesimer *et al*, 2009), major histocompatibility complex proteins I and II, a variety of heat shock proteins (for example HSP70 and HSP1), enzymes such as phospholipid scramblase and GTPases (Subra *et al*, 2010) as well as a number of other proteins, whose list is constantly being updated (Aoki *et al*, 2007) depending on their 'intended' roles and degree of remodelling (Muralidharan-Chari *et al*, 2010). Indeed exosomes produced by antigen presenting cells will have particular functional relevance to CD4+ T cells and subsequent immune responses (Chaput *et al*, 2006; Bastos-Amador *et al*, 2012). Exosomes are implicated in a broad range of activities ranging from immunological responses (Nolan *et al*, 2008) such as antigen presentation stimulating T cell proliforation (Bastos-Amador *et al*, 2012), control of cellular activities (Kesimer *et al*, 2009) and protein homeostasis (Putz *et al*, 2008). mRNA and miRNA, also present in exosomes are deliverable to other cells and therefore implicated in communication (Parolini *et al*, 2009; Quesenberry *et al*, 2010b).

Exosomes are internalised by recipient cells through direct plasma membrane fusion (Parolini *et al*, 2009). Furthermore Parolini *et al*, 2009 suggest that low pH is crucial for increased exosome release as well as internalisation and proton pump inhibitors lead to reduced exosome uptake by recipient cells.

As well as taking part in cellular communication by transferring proteins and RNAs between cells (Robertson *et al*, 2006; D'Souza-Schorley and Clancy, 2012) exosomes have been shown to carry misshapen proteins such as prions, namely CJD from cell to cell (Schultz *et al*, 2005; Robertson *et al*, 2006; Putz *et al*, 2008; Quesenberry *et al*, 2010b) and amyloid precursor protein implicated in Alzheimer's disease (Subra *et al*, 2010). Viral particles such as Human Immunodeficiency Virus (HIV) also use exosomes to evade immune detection and invade cells by being enveloped in proteins and lipids reminiscent of their host (Gould *et al*, 2003; Chaput *et al*, 2006; Izquierdo-Useros *et al*, 2009) by hijacking their biogenesis pathways (Subra *et al*, 2010). Exosomes released from tumour cells release RNA typical of its mutated genome and are able to subvert the function of immune cells so allowing tumour progression for example, by suppression of cytotoxic T cells (Szajnik *et al*, 2010). Furthermore, exosomes may carry transmissible oncogenic factors capable of transforming healthy cells into cancer and are implicated in cancer metastasis (Parolini *et al*, 2009; D'Souza-Schorley and Clancy, 2012).

Often exosomes and microvesicles are confused, indeed, there is a degree of overlap in size between both microvesicle types, although they may differ biochemically (Thomas and Salter, 2010).

1.4.3 The endosomal pathway

The organelles of the late endocytic pathway are highly coordinated (Duclos *et al*, 2003) and are in a state of dynamic equilibrium, so that contents and membrane mixing occurs (Pryor *et al*, 2000); the contents of late endosomes are delivered to lysosomes through a direct fusion or a transient interaction (kiss-and-run fusion events) (Pryor *et al*, 2000; Duclos *et al*, 2003). The fusion depends on ATP, temperature, *N*- ethyl maleimide-sensitive factor (NSF) and soluble NSF proteins (SNAPs) and is inhibited by GDP dissociation inhibitor (Pryor *et al*, 2000).

1.4.4 Exocytosis

Exocytosis is the process of cellular export that involves transport vesicles containing proteins, wastes and other macromolecules, fusing to the plasma membrane and releasing their contents into the extracellular matrix. There are two distinct types of exocytosis, [Ca^{2+}]-triggered (Lourido *et al*, 2010) and non [Ca^{2+}]-triggered also known as constitutive (Qu *et al*, 2007). These vesicles 'pinch off' the golgi body and are trafficked through the cytoplasm by a series of cytoskeletal proteins until they 'dock' with the membrane associated cytoskeleton. These vesicles contain the proteins that the golgi body 'repackaged'. SNARE proteins allow the vesicle to fuse with the plasma membrane and the vesicle contents are exocytosed into the cell matrix (Gurr *et al*, 2002). This process has many functions, including export of cellular components such as wastes, signalling molecules and plays roles in membrane repair (Lourido *et al*, 2010).

1.4.5 Lysosomes

Are single membrane bound organelles that express LAMP-1 (Lysosomal Associated Membrane Protein 1) a biomarker for lysosomes, and contain more than 50 acid-dependant hydrolases such as lipases and proteolytic enzymes (Dell'Angelica *et al*, 2000). Their role is to degrade defunct or surplus organelles for recycling, internalisation of nutrients, regulation of cell surface receptors (Duclos *et al*, 2003) and to digest intracellular parasites or internalised pathogens; the breakdown of parasites and formation of peptides that bind MHC class II is an important feature of the T cell mediated B cell immune response (Rosenfeld *et al*, 2001). Cell surface receptors can be endocytosed and degraded by lysosomes as a method to control signal transduction (Dell'Angelica *et al*, 2000) and lysosome fusion is regulated by [Ca^{2+}] (Pryor *et al*, 2000; Qu *et al*, 2007)

Lysosomal single membrane contains highly gycosylated, Lysosomal Associated Membrane Proteins (LAMP-1, -2 and -3) (Dell'Angelica *et al*, 2000) that regulate pH (4-5), amino acid content and various solutes. Lysosomes are a family of vesicles that strongly resemble one another; melanosomes, lytic granules, major histocompatibility complex class II (MHC class II) compartments, Platelet dense granules, basophil granules and neutrophil azourophil granules (Dell'Angelica *et al*, 2000). However for the purposes of this thesis, all subclasses will be referred to as lysosomes. Lysosomes have been shown to 'plug' plasma membrane breaches to ensure the viability of the cell. Typically these patched breaches will exhibit lysosome associated proteins such as LAMP-1 (Thomas *et al*, 2009).

1.4.6 Schematic of microvesicle types and their formation

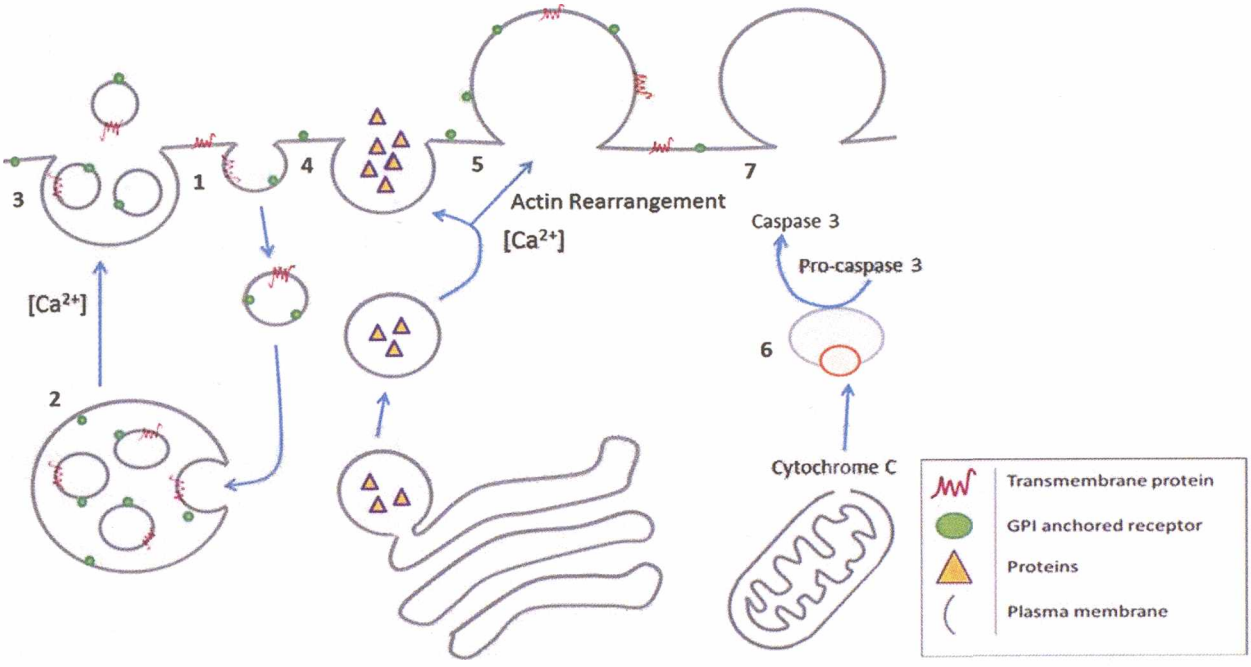

Fig 1.2 An overview of extracellular vesicle types and their formation; 1. Endosmomes form by an invagination of the plasma membrane. The vesicle thus contains redundant or defunct membrane associated proteins and lipid expressed internally, is either degraded by lysosomes (not shown) or fuses with a multivesicular body; **2.** Multivesicular bodies are formed by the fusion of endosomes and other vesicles. They undergo a process of invagination to form a number of **3.** exosomes; that express an assortment of membrane proteins (expressed externally), cytoplasmic inclusions, such as RNA, peptide hormones and mitochondrial proteins. The multivesicular body migrates to the plasma membrane and fuses, so externally releasing the exosomes into the extracellular spaces. **4.** Vesicles 'pinch off' from the golgi body and traffic cargo (proteins, receptors, carbohydrates or lipid) to the plasma membrane or to organelles; **5.** MVs arise from membrane blebs, containing a sample of the cytoplasm and membrane of the parent cell. Due to membrane instabilities, PS is expressed externally, actin rearrangement causes the inclusion of cytoskeletal components; **6.** Apoptosome forms when mitochondrial damage leaks cytochrome C and ROS into the cytoplasm, the initiation of apoptosis leads to the formation of capsase 3 from procaspase 3 (cysteine protease); 7. Apoptotic Bodies are shed expressing external PS, cytoskeletal and cellular components, containing toxic substances and occasionally organelles. (Sato *et al*, 2004; Xie *et al*, 2009) By Stratton, 2012.

1.5 The physical and physiological functions of MVs

MVs have a multitude of functions within an organism ranging from postponing/preventing apoptotic events, initiating apoptosis (Sarkar *et al*, 2009), cellular communication (Agouni *et al*, 2007), delivery of cytoplasmic cargo to recipient cells (Thomas and Salter, 2010), immunity (Antwi-Baffour *et al*, 2010), proliferation, exporting senescent proteins (Putz *et al*, 2008), chemotaxis, and both as pro-inflammatory (Bianco *et al*, 2005; Pizzirani *et al*, 2007; Nolan *et al*, 2008), and anti-inflammatory agents (Gasser and Schifferli, 2004).

There is a threshold in the number of MVs that fuse or interact that has to be reached before cells will elicit a response; they typically have to be in a significantly greater number that would be constitutively released (Nolan *et al*, 2008). This number will vary depending upon the cell type and the signal molecule.

MVs have been shown to 'programme' stem cell progenitors to influence the eventual cell type differentiated. Although this mechanism is not entirely clear it has been speculated that the receptor, protein/enzyme and microRNA constituents would be important in the process of commitment and that the parent cell type that the MV is derived from can initiate stem cell differentiation (Agouni *et al*, 2007; Leroyer *et al*, 2009; Quesenberry *et al*, 2010b) and indeed, preliminary trials using MVs containing microRNAs to control cancer stem cells is underway (Viaud *et al*, 2010). Ischaemic tissues will release MVs to postpone apoptotic damage (Gutwein *et al*, 2005), these MVs containing differential instructions giving rise to tissue growth (Sarkar *et al*, 2009) as

well as containing cell death signals (Andreola *et al*, 2002) (these are important for tissue modelling).

Although different MV subtypes will elicit different responses as they will have been created through different processes and will therefore contain a distinct assortment of proteins, lipids, RNAs and so forth, they do contain similar features such as actin, HSP 70 and PS, allowing them to be identifiable as MVs and act through similar mechanisms such as receptor mediated endocytosis or plasma membrane fusion with recipient cells. Furthermore, any sample of MVs may include a mixture of vesicles that contain different signal molecules, or varying abundances of one signal molecule, even though they derive from the same tissue culture (Inal *et al*, 2012).

Tumour cells release MVs that aid in their survival (Muralidharan-Chari *et al*, 2010), either by transferring growth factors or RNAs to transform surrounding cells (Quesenberry *et al*, 2010b), regulating metastasis and/or by using them to avoid immunological detection (Aoki *et al*, 2007; Szajnik *et al*, 2010). However tumour cells behave in much the same way as non-tumour cells do, given that they release growth factors, regulate tissue homeostasis, cell-cell communicative factors and immune subversion.

In vitro experiments show a multitude of potential roles for MVs in classical biology and as stated before microvesicles can operate as communicative vectors. Once shed, circulating vesicles can act as markers for tissue damage and inflammation, in particular as chemo-attractants for immune cells or metastatic cancer cells

(chemotaxis) (Muralidharan-Chari *et al*, 2010). Moreover, tumour cells not only transmit oncogenic vectors, they use MVs to synchronise cellular activity (Quesenberry *et al*, 2010b). Experimental limitations *in vitro* do not allow for holistic organism responses to be observed although cellular mechanisms and modes of interaction can be studied in detail. MV therapeutic effects are still being unravelled and animal models for disease states are the next step in the progression of MV immunology.

1.5.1 Why cells release MVs

Almost all eukaryotic cell types release MVs, and although there are many reasons why cells release MVs, they can be defined in four broad categories.

1) Apoptotic events (Sarkar *et al*, 2009) are initiated via cell death signals that originate externally (extrinsic) by ligands such as FasL or internally (intrinsic) by the activation of caspases (Mandal *et al*, 2005). The complex processes that control the apoptotic pathways lead to the cleavage of caspase -3 and the activation of the subsequent caspase cascade causing the degradation of cellular protein, including actin and membrane associated enzymes that contain cysteine residues.

2) Mediating novel cellular communication (Agouni *et al*, 2007; Scanu *et al*, 2008; Muralidharan-Chari *et al*, 2010) and the control of homeostatic mechanisms such as inflammation, tissue modelling, cell migration and cellular differentiation (Akoi *et al*, 2007; Deregibus *et al*, 2007; Stowell *et al*, 2009).

3) Response to cell stresses such as parasites (Inal *et al*, 2012); causing damage or irritation to cells, some virus hijack the formation of microvesicles to form membrane enveloped virus (Gould *et al*, 2003; Jorfi and Inal, 2012).

4) Export of defunct proteins by MVs to maintain normal cell physiology has been observed (Putz *et al*, 2008). Prions for example are exported in this manner. As a cell ages, its ability to synthesize correctly configured proteins diminishes. However a study by Grant *et al*, 2011 demonstrated a decline in plasma MVs in patients over 55 years old, the cohort was too small to be conclusive. Should the cells ability to release MVs decrease with age, it may shed light on possible causes of misfolded protein accumulative diseases such as Alzheimer's and their ability to remodel tissues. Furthermore, patients who smoke show a significantly decreased ability to release MVs, as nicotine inhibits actin cleavage (Grant *et al*, 2011) MV release may also play a role in infectibility of cells by parasitic agents (Cestari *et al*, 2012).

$[Ca^{2+}]_i$ microdomains greater than 100 μM can form within the cytoplasm of many cell types, typically adjacent to ion gated Ca^{2+} channels (Oheim *et al*, 2006); this $[Ca^{2+}]_i$ is either compartmentalised with in cellular organelles, dissipated (although this will have biological consequences such as signal transduction [Oheim *et al*, 2006] or initiate actin cleavage) or removed from the cell; conceivably this $[Ca^{2+}]$ domain could cause MV release and be included within their cytoplasmic contents. However microdomains (tens of nM) or high molarity can be tolerated for nanoseconds, possibly to quicken signal transduction. Interestingly $[Ca^{2+}]_i$ is typically associated with many types of membrane depolarisations, such as synaptic (Oheim *et al*, 2006), apoptotic events

(Alder, 2010) or membrane breach sealing; MACs for example are shed via microvesicles (Halperin *et al*, 1993; Inal *et al*, 2012).

1.5.2 MVs mediate cellular communication

MVs exhibit properties of a small world network (Deregibus *et al*, 2007) that is a communicative network having a small number of intermediates to govern a system. It is flexible allowing adaption as appropriate (Gross and Blasius, 2008), such as tissue homeostasis (Akoi *et al*, 2007), where differing stimuli will alter the behaviour of the tissue either for proliferation (Agouni *et al*, 2007), apoptosis (Kim *et al*, 2005), transdifferentiation (reprogramming) or differentiation (Leroyer *et al*, 2009). MVs arise either constitutively or as a response to stress, the dose dependant mode of MVs allowing a fine control of the signals (all or nothing type response to influence cells) they convey such that a stress agent will produce a larger quantity of MVs and so have a larger impact upon the surrounding/distant tissues (the more MVs released, the greater the number of possible cellular responses) (Quesenberry *et al*, 2010b).

Signalling molecules and proteins can be transported on the surface or within the MV (Kim *et al*, 2005; Scanu *et al*, 2008; Sarkar *et al*, 2009). MVs are often enriched for proteins, enzymes and signalling molecules, some of which can only be sufficiently exported via microvesicles (Bianco *et al*, 2005). The signal being transduced depends upon the interaction of the MV with the target cell, so that surface ligand interaction can induce a response within the cell that could later be countered by the inclusion of the MVs cytosolic components. Alternatively, MV binding stimulates a response that will either alter the metabolism of the cell or cause the cell to release messengers to

distal stimulatory cells to alter their metabolism (an example of a homeostatic mechanism).

A complex system of MVs and MV interactions exist within mammalians, conceivably all cell types releasing a 'specie' of MV that acts as a communicative organelle both locally and distally. Control mechanisms within this network ensure that appropriate responses to signals are elicited and signals therefore cannot go astray; this can only be guessed at as the models and interactions are complex and still being investigated. The recipient cell-MV membrane fusion events are important for the transduction/delivery of internally transported molecules. PS and PS receptor is essential for this type of membrane fusion; membrane fusion events are mediated by Ca^{2+} (Gurr *et al*, 2002)

1.5.3 Apoptotic signals

Fibroblast associated receptor (FasR or CD 95) is a type 1 transmembrane protein (Kim *et al*, 2005) from a family of receptors with 7 distinct isoforms. FasR acts as a cell death signal receptor that may be essential for MVs formation (Mandal *et al*, 2005) when FasR is translocated into lipid rafts, cell death signalling platforms being initiated.

FasL is a 42 kDa type 2 transmembrane protein that interacts with FasR (Kim *et al*, 2005). FasL and Fas are tumour necrosis factors (TNFs) that interact forming Fadd (Fas associated death domain) causing the formation and activation of caspases that in turn rearrange actin and lead to protein degradation. The FasR/FasL pathway mediates pro-inflammatory responses and acts as an apoptotic signal (Andreola *et al*, 2002; Kim *et al*, 2005).

Reactive Oxygen Species (ROS) are formed as a bi-product of oxidative phosphorylation (Agouni *et al*, 2007), causing nucleic acid and protein damage. Notably, cells cultured in growth media supplemented with antioxidants such as N-acetly cysteine, release fewer MVs (Aoki *et al*, 2007).

Microvesicles carry caspase -1 (Andreola *et al*, 2002; Sarkar *et al*, 2009), as well as Caspase -3 (Andreola *et al*, 2002) and may also contain Bcl2 and Bax. The delivery of these cell death signals are dependent upon the catalytic activity of the enzyme delivered and on the viability of the microvesicle (Sarkar *et al*, 2009). Apoptotic cell derived microvesicles propagate the cell death signal by transmitting it to adjacent cells (Andreola *et al*, 2002; Quesenberry *et al*, 2010b).

1.5.4 Proliferation signals

MVs have been shown to stimulate cell proliferation and differentiation through the interaction of the lipids and proteins that they carry (Agouni *et al*, 2007; Angelot *et al*, 2009; Leroyer *et al*, 2009). In particular, THP-1 will differentiate into monocytes when co-cultured with MVs (Ansa-Addo *et al*, 2010).

Proliferative effects of MVs vary significantly depending upon the cell line studied and the origin of the MVs, often, contradictory results being observed and published. MVs carry proteins and 'signal molecules' that are deliverable to recipient cells, but the nature of the MV binding and the cellular response to the cargo may vary considerably, leading to distinct responses (Inal *et al*, 2012; Stratton *et al*, 2012). Often MVs are shed

as a reaction to stress agents, which may be due to cellular damage where proliferation of monocytes or B cells may be required to mediate immune responses.

1.5.5 Other signals

MVs express adhesion proteins allowing them to influence cell-cell interactions (Nolan *et al*, 2008; Scanu *et al*, 2008) such as CD11a, CD14 and CD18 (Pizzirani *et al*, 2007) and in turn allowing internal MV signalling molecules to be delivered to the recipient cell (Pizzirani *et al*, 2007).

Cytokines are signalling molecules operating between and within cells that function at low concentrations, behaving like hormones in an autocrine, paracrine and endocrine manor (Benjaminin *et al*, 2000). They are often produced in response of stress stimuli and create concentration gradients that can act as a chemotactic attractor (Benjaminin *et al*, 2000). Interleukins are a subfamily of cytokines that exert their biological functions by cell surface receptor interactions (Walsh, 2002).

MVs bearing unique arrays of signalling molecules and miRNAs have the potential to be used for disease state diagnostics (Chen *et al*, 2011), showing both the type of disease and the relative involvement of the particular cell type. This type of research has yielded positive results (ISEV meeting, 2012) and technology is being developed to maximise the potential of MV diagnostics. Micro array assays and RTPCR are techniques currently employed and have yielded detailed MV profiles from many cell types (Chen *et al*, 2011).

1.5.6 Export of unwanted cellular components

Many bio-accumulative agents and toxic cellular substances are exported via MVs, such as misfolded proteins (Putz *et al*, 2008), ROS, apoptotic components (Sarkar *et al*, 2009), prions (Quesenberry *et al*, 2010b). Intracellular calcium and bioactive ions/molecules are also exported (Stratton *et al*, 2012). Recently, viral particles have been observed exploiting MV release processes, it is possible that infective particles are exported by MVs (Jorfi *et al*, 2010).

1.5.7 MVs transfer proteins and receptors

MVs carry protein and receptors that can be transmitted to a recipient cell (Deregibus *et al*, 2007; Sarkar *et al*, 2009), which can influence the biological activity of recipient cells (Agouni *et al*, 2007; Scanu *et al*, 2008; Quesenberry *et al*, 2010b). Evidence shows that microvesicles can alter the activity of the recipient cell transiently towards a phenotype of the originating cell, being able to perform significant biological roles (Agouni *et al*, 2007; Quesenberry and Aliotta, 2010a; Quesenberry *et al*, 2010b).

Glycolytic enzymes can associate with cytoskeletal structures as well as mitochondrial membranes, during cytoskeletal remodelling and MV formation these enzymes may be included, indicating that MVs carry the necessary enzymes and associated ion channels for oxidative phosphorylation (Hardin *et al*, 1992).

1.5.8 Surface receptor

Surface receptors can be transmitted to recipient cells by MVs. Should the recipient cell have the necessary 'machinery', it will transiently acquire the receptor properties until endocytosed (Quesenberry and Aliotta, 2010). GPI anchored proteins associate with lipid rafts and are also present on the surface of MVs. Fusion events allow for the transport of GPI proteins from cell to cell (Ansa-Addo *et al*, 2010; Inal *et al*, 2012). The implications for receptor transfer are far reaching, hinting towards a temporary borrowing of properties by similar tissues during conditions leading to cellular stresses that could help alleviate damage to the tissues and organs by helping with cellular roles (Quesenberry *et al*, 2010b). Ion channels are included in the membrane of MVs, these are often implicated in MV formation (appendix fig 10.3 indicates that calcium stretch receptors are not present on MVs). Adhesion molecules that account for their adhesive properties of MVs and may also be an important factor in cell interaction/fusion (Nolan *et al*, 2008). During MV formation, surface protein/receptor sorting occurs allowing their enrichment or absence on the released MV (Muralidharan-Chari *et al*, 2010).

1.5.9 Internal proteins

MVs contain a large array of cell derived proteins, for instance, structural proteins such as actin, protein machinery, enzymes and regulatory proteins (Inal *et al*, 2012). Macrophage migratory inhibiting factor (MIF) is a 12.5 kDa cytokine that is produced in response to pro-inflammatory, hormonal or mitogenic stimuli (Merk *et al*, 2009). MIF is associated with microvesicles from many cell types (Merk *et al*, 2009) and can be used as a standard marker for MVs. Esterases are a family of ubiquitous enzymes found in the cytoplasm of mammalian cells, that are inevitably included in MVs as a random

sample of cytoplasmic inclusions and will remain active within the MV (Stratton *et al*, 2012).

1.5.10 Associated proteins

Transforming growth factor beta (TGF-β, -1, -2 and -3) is associated with apoptosis, cancer progression and blocking lymphocyte and monocyte macrophage differentiation. It is a highly complex molecule associated with many metabolic pathways, however it has been found to associate with the outer leaflet of MVs and performs its varied roles either external to the microvesicle of internal to the cell (Ansa-Addo *et al*, 2010). Diseased cells, such as cancer cells exhibit increased expression of protein/ receptor types (Biasi *et al*, 2002; Broom *et al*, 2009) that are transmissible via MVs.

1.5.11 Transfer of RNA

Naked RNA has a short half life and cannot be transferred between cells through the extracellular fluids with any significant success, MVs therefore offer the RNA a protective vector for cellular transmission (Deregibus *et al*, 2007; Aliotta *et al*, 2011). MVs are among a host of microvesicles that act as vectors for RNAs, transferring them from one cell type to another, thereby influencing the phenotype and function of the recipient cell (Quesenberry *et al*, 2010b). Recently, research groups have focused on MVs as a RNA vector, and its increasing importance in altering cellular metabolism and even the progression of disease states such as cancer (Aliotta *et al*, 2011; Inal *et al*, 2012) This is an example of horizontal RNA delivery (Deregibus *et al*, 2007; Alder, 2010; Inal *et al*, 2012).

1.5.12 MV lipid export

Membrane lipids derived from parent cells constitute MVs (Chattopadhyay *et al*, 1979; Yao *et al*, 1991; del Conde *et al*, 2005; Muralidharan-Chari *et al*, 2010). Typically cells such as immune cells and nerve cells have distinct but similar lipid profiles (Garver *et al*, 2010). However diseased cells, such as cancer cells have unique lipid profiles that are transmissible between cell types (del Conde *et al*, 2005; Thomas and Salter, 2010) and may be implicated in their biogenesis and frequency of release.

1.5.13 MV diagnostics and applications

In view of the uniqueness of MV types and classification in relation to their cellular origins it has been speculated that MVs derived from patients could be used as a diagnostic tool of disease. Indeed, pharmaceutical companies such as Caris life sciences' patented 'carisome' have already developed simple assays targeting certain cancer types. The full potential of MVs in diagnostics and as a drug delivery system is far from realised, but has become a main focus in microvesicle research.

1.6 Ultra low-frequency magnetic fields (ULMFs)

Magnetic fields are a conceptual description of the magnetic attractive and repulsive effects on materials and charged particles. They are produced by the movement of charged particles, molecules or the 'spin' of fundamental particles such as electrons (charged leptons and heavy quarks) (Lederman, 1982). ULMFs are low frequency oscillations of pulsed magnetism within the range of 3-300Hz. They are generated easily using electrical equipment or specialised apparatus, and overlay with the Earth's

natural magnetic field (Lacy-Hulbert *et al*, 1998). Magnetic fields are quantified in terms of field density (teslas) and strength (voltage). The purpose of this study is not a detailed examination of the mathematical and physical laws that govern magnetism and its interactions, but rather an observation of bio-magnetic interactions and their effects.

Low frequency electromagnetic fields are generated by electronic devices abundant within the normal human environment, epidemiological studies indicating their possible links to cancer (Lacy-Hulbert *et al*, 1998 ;Ansari and Hei, 2000; Dini *et al*, 2010) leading to concerns about their ever growing effect on human development, health and disease (Hung *et al*, 2010). Concerns about magnetic field dosage caused by power lines, mobile phones and other electrical equipment are being addressed by health organisations and government agencies.

1.6.1 ULMF effects on health

Studies into the role of magnetic fields and cancer progression show conflicting results (Ansari and Hei, 2000; Ventura *et al*, 2000; Villeneuve *et al*, 2000; Nakahara *et al*, 2002; Nikolva *et al*, 2005; Hung *et al*, 2010) as tissue types respond differently to magnetic stimulus (Ventura *et al*, 2000; Dini *et al*, 2010). Studies on cell lines derived from different tissues and organisms show many potential effects or no effects at all (Lacy-Hulbert *et al*, 1998; Nikolva *et al*, 2005). Electromagnetic exposure of neuronal progenitor cells results in transient DNA damage and up-regulation of genes relating to apoptosis. It is conjectured that cellular repair mechanisms compensate for these magnetic effects (Nikolova *et al*, 2005). For tumour development, at least three

mutations in the genome must occur (in most cases) (Lacy-Hubert *et al*, 1998), and magnetic fields may contribute to a tumour state but not necessarily be the only causative agent. Nevertheless weak or low frequency magnetic fields could acts as a mutagen or interfere with signalling pathways (Lacy-Hubert et al, 1998; Hung *et al*, 2010) leading to disease states or tissue damage.

1.6.2 ULMFs interaction with membrane phospholipids and proteins

Phospholipids are usually associated with membranes. They are molecules in a fluid state that have a net negative charge (complex polar molecules) (Eyre *et al*, 2004), being essential for the selective permeability properties of membranes. These phospholipids flow around the cell, within either the outer or inner membrane leaflet upon a dynamically changing but for these purposes, rigid cytoskeleton composed of α-helical proteins (Eyre et al, 2004). When magnetic fields of sufficient strength are applied to plasma membrane, magnetic torque causes alignment of the polar component of the phospholipid with the magnetic field (Roberts and Redfield, 2004; Dini *et al*, 2010). The extent of magnetic alignment is proportional to density and strength of the magnetic field (Roberts and Redbridge, 2004), creating membrane pores sufficiently large enough to allow the passage of ions and molecules to pass into and out of the cell. The transient nature of these membrane pores is due to the fluid behaviour of the membrane that will cause micro fluctuations in magnetic field strength allowing membrane ruffling (Dini *et al*, 2010) and pores to open and close as the lipids align and loose alignment with the magnetic field (Roberts and Redbridge, 2004). This alignment is short-lived and ceases when the magnetic field is removed (Dini *et al*, 2010; Stratton *et al*, 2012). Indeed, pores induced by electroporation contract within milliseconds and seal completely mins to hours later (Lado *et al*, 2004).

Although brief changes in hydrocarbon tail configuration may lead to ultra short lived polarity, this is not relevant to this study; the hydrocarbon tail is considered non polar in this instance as molecular charges are well balanced (Petrache *et al*, 2006). Magnetic field alignment can be deflected or its strength diminished in the presence of an electrical current, metallic ions or artefacts within or adjacent to the sample, temperature variations associated with the sample or the presence of a stronger magnetic field.

Proteins which are often hydrogen bonded at the secondary level of organisation to help maintain stability may behave in a similar manner. Magnetic fields however may affect 'moving' or flexible components of proteins such as opening ion pore channels (Lopez *et al*, 1991) or altering the configuration of enzyme binding sites leading to a temporary loss of function. Protein functionality may be lost permanently if a strong magnetic field causes denaturation or temporarily altered by changes in conformation with a weak magnetic field (Lopez *et al*, 1991). Furthermore, magnetic fields interacting with polar groups of proteins may create novel biological properties (Gartzek and Lange, 2002). Although cells stimulated by various magnetic fields do not upregulate HSP60 or other studied chaperones (Henderson *et al*, 2003; Shi *et al*, 2003). Chaperones assist in protein folding and protein repair (Lado *et al*, 2004), suggesting that structural protein stress causes the increased production of chaperone class proteins.

1.6.3 ULMFs effects on DNA

Although CHO-K1 subjected to strong magnetic fields exhibited no significant DNA damage (Nakahara *et al*, 2002), in mouse embryonic stem cells and rat neuronal cells there was a dose dependant increase in dsDNA damage with time, quantified with rtPCR (Nikolva *et al*, 2005; Hung *et al*, 2010). This damage itself was temporary and was 'mostly' repaired by cellular mechanisms (Nikolva *et al*, 2005).

1.6.4 Magnetic Field effects on proliferation or growth suppression

Studies have shown the growth effects of magnetic fields on particular cell lines (Lacy-Hulbert *et al*, 1998; Ventura *et al*, 2000; Gartzek and Lange, 2002) Typically, *in vitro* magnetic studies demonstrate proliferative stimuli to particular cell lines, initiating G_1 from cells in G_0 (Lacy-Hulbert *et al*, 1998). Furthermore, Hung *et al*, 2010 demonstrated that low frequency magnetic fields caused *C. elegans* to develop and age faster than the control group due to atypical gene transcription of *age-1, unc-3, lim-7 and chk-1* (having human homologues). THP-1 differentiate into monocytes after treatment with PMA *in vitro*, usually takes 72 h. However when PMA treated THP-1 are stimulated with 6mT magnetic field, their differentiation is halted (Dini *et al*, 2010). Low frequency magnetic fields alter cell morphology via cytoskeletal interactions or remodelling (Dini *et al*, 2010; Hung *et al*, 2010)

1.6.5 ULMFs and calcium

Calcium influx across plasma membrane in conjunction with magnetic fields of 50-300nT is well documented (Glogauer et al 1995; Nakahara *et al*, 2002; Hung *et al*,

2010), the subsequent biological effects often being attributed to the excess internal calcium levels. How low frequency magnetic fields interact with calcium and transfer free energy is a matter for debate, with differing 'schools' of thought offering feasible theories (Gartzek and Lange, 2002). Indeed, this thesis proposes a simple model of diffusion along concentration gradients (Stratton *et al*, 2012) allowing enough free calcium to effect physiological responses. Other work proposes that F-actin components of microfilaments interact with magnetic fields, their polyelectrolyte properties allowing calcium ion conductance into the cytosol, analogous to a disjointed conductive cable (Gartzek and Lange, 2002). The movement of Ca^{2+} along a concentration gradient down a magnetically induced 'conductive axis' leads to typical Ca^{2+} induced cellular responses. Once the induced Ca^{2+} conductance begins the signal is amplified until V_{max} is achieved or the magnetic field is removed (Gartzek and Lange, 2002). The F-actin affinity for cations causes a barrier to anion entry. Furthermore, Ca^{2+} 'flow' and microvilli warping causes membrane stress and dissociation with cytoskeletal elements (Gartzek and Lange, 2002; Dini *et al*, 2010). These observations allow theoretical models for powering nanomachines to be designed.

Calcium also enters via stretch activated ion channels (Glogauer et al, 1995) during membrane deformation, leading to cytoskeletal remodelling (Dini *et al*, 2010; Hung *et al*, 2010). Magnetically induced calcium influx increases apoptotic occurrence (Hung *et al*, 2010).

1.6.6 Magnetic therapies

Ultra Low Magnetic Fields have been used in medicine mainly for imaging tissues *in situ* (Dini *et al*, 2010; Hung *et al*, 2010), although, recently ULMFs have been shown to provide the optimal conditions for interaction with biological systems, so providing various therapeutic roles such as increased proliferation of cells, in particular, for the repair of bones (Lacy-Hulbert *et al*, 1998; Gartzek and Lange, 2002), for the induction of apoptotic/necrotic cell death (Dini *et al*, 2010; Hung *et al*, 2010) or the altered expression of genetic systems (Dini *et al*, 2010). Often, magnetic therapies are used in conjunction with other magnetic or non magnetic agents to achieve a therapeutic response (Ansari and Kei, 2000; Polanaik *et al*, 2010; Tomasini *et al*, 2010).

Magnetic nanoparticles (50μm) in high frequency magnetic fields have been shown to rupture lipid membranes by pore formation, however the nanoparticles lead to increased temperature of the tumour cells examined *in vitro* and contributed significantly to the observed cell death. However the temperature increase was not observed *in vivo* (Tomasini *et al*, 2010) attributing membrane damage to the nanopartical vibration within the magnetic field.

Treatment of tocopherol (vitamin E) and low frequency electromagnetism with murine epithelial cell carcinoma found a dose dependant increase in protective activity of membrane lipid to peroxidation (Polanaik *et al*, 2010). However, the exact mechanism was not described, and it was hypothesised that the molecular shape of topopherol was modified into a more effective form or that the magnetic field allowed for an increased

cellular uptake. Calcium signalling is often the target for magnetic based therapies (Gartzek and Lange, 2002, Hung *et al*, 2010).

It is difficult to separate the effect of magnetism and side effects generated as a single causative agent (Nakahara *et al*, 2002; Tomasini *et al*, 2010) and it could be conjectured that they have an accumulative effect leading to tumour death. However, studies to date are inadequate to evaluate the effects of magnetic fields on human health (Gartzek and Lange, 2002; Nakahara *et al*, 2002), both in short and long term exposure. Many attempts to replicate results lead to only partial success based upon differing methodologies or cell types (Lacy-Hulbert *et al*, 1998; Dini *et al*, 2010). However reproducible results using lymphocytes are common and minimising previous exposure and handling is essential to obtain valid data (Lacy-Hubert *et al*, 1998), it is possible that humans are used to interacting with magnetic fields and that any therapies would depend on the extent and strength of previous exposure.

2. Research Objectives

2.0 Aims

The purpose of this thesis is to undertake a detailed biochemical and biophysical analysis of microvesicles and their biogenesis, relating to their physiological roles and to pioneer new techniques using up-to-date technology. Furthermore, this thesis will propose a formal reproducible technique for the isolation of pure MVs.

Although it is generally accepted that microvesicles are reminiscent of their parent cell types, the degree of similarity has yet to be elucidated. Investigation of whether microvesicle release from a parent cell or their fusion with a recipient cell alters their metabolism.

Finally, investigation of the effect of electromotive force on microvesicle biogenesis and its novel roles in cellular behaviour should be investigated due to the increased incidence of magnetic fields in the human environment.

The aims of this thesis are to investigate the hypothesis that MV release alters cellular metabolism, confering distinct cellular properties from the parent cell to the recipient cell. The MVs can also export 'unwanted' cellular components via MVs to enhance the cell's viability. Furthermore, microvesicles are stimulated for release by many environmental factors such as A/C magnetic fields, potentially harming cells. This thesis will investigate the roles, if any, of Ultra Low-frequency magnetic fields effects on cell viability and microvesicles biogenesis.

3. MATERIALS AND METHODS

3.1 Materials

12 well plate (Sigma-Aldrich), 15ml centrifuge tubes 24 well plate (Sigma-Aldrich), 50ml centrifuge tubes, 96 well plate (Sigma-Aldrich), Aluminium backed silicon TLC plates, Megamix beads, Pipette tips 10µl, 200µl and 1000µl, Tissue Culture Flasks, 1.5ml and 2ml eppendorf tubes.

3.1.1 Chemicals

Acetone (99.5%) (Sigma-Aldrich)

Agar resin (Sigma-Aldrich)

Annexin V Alexa Fluor 488 (Invitrogen)

Annexin V, Fluorescein-conjujated Annexin V (NX50) (R and D systems)

ATRA (all-trans-retinoic acid) (Sigma-Aldrich)

Bacitracin (Sigma-Aldrich)

Barbituric acid (Sigma-Aldrich)

BCA protein assay kit (Pierce Biosciences)

Bioguard® disinfectant (BoundTree Medical)

Bromophenol blue (Fisher Scientific)

BSA (Bovine serum albumin) (Sigma-Aldrich)

$CaCl_2$, Calcium Chloride (Sigma-Aldrich)

Calcium green-AM dye (Invitrogen)

Complement diluent buffer (CDB) (Oxoid)

Coomassie brilliant blue (BDH Limited, Poole, England)

DAPI-VECTASHIELD (Vector Laboratories Inc, Ca, USA)

DMSO (Dimethyl sulfoxide) (Sigma-Aldrich)

Docytaxol (Sigma-Aldrich)

EDTA, Ethylene-diamine-tetraacetic Acid (Sigma-Aldrich)

EGTA, Ethylene-glycol-tetraacetic Acid (Sigma-Aldrich)

Ethanol (Fisher Scientific)

Etoposide (Sigma-Aldrich)

FBS (Foetal Bovine Serum) (Fisher Scientific)

$GdCl_3$ (Gadolinium chloride) (Reaction Product, Cheshire)

Glacial acetic acid (Fisher Scientific)

Glucose (Acros Organics)

Guava Nexin Reagent (Guava Technologies, UK)

Guava ViaCount reagent (Guava Technologies, UK)

Halt Protease Cocktail (Pierce, Thermo-Scientific)

HCl (Hydrochloric acid) (Fisher Scientific)

HEPES (Sigma-Aldrich)

Horse serum (HS) (Sigma-Aldrich)

Hybrid nitrocellulose membrane (Amersham Biosciences)

IMS, Industrial Mentholated Spirit

Kanamycin (Sigma-Aldrich)

Methanol (Fisher Scientific)

Methotrexate (Sigma-Aldrich)

Methyl nadic anhydride (MNA) (Agar Scientific)

$MgCl_2$, Magnesium Chloride (Sigma-Aldrich)

Milk powder (Marvel Original, Dublin)

Na_2HPO_4 (BDH Lab supplies, England)

NHS (Normal Human Serum) (Sigma-Aldrich)

Nutrient Agar powder (Sigma-Aldrich)

Osmium tetroxide (Sigma-Aldrich)

Paraformaldehyde (Sigma-Aldrich)

PBS, Phosphate Buffer Solution (Fisher Scientific)

Penicillin and Streptomycin (Sigma-Aldrich)

Phosphotungstic acid (PTA) (Agar Scientific)

PMA (Phorbol-12-myristate-13-acetate) (Sigma-Aldrich)

Ponceau S (Sigma-Aldrich)

Potassium chloride (KCl) (Sigma-Aldrich)

Propidium Iodide (Sigma-Aldrich)

Protein molecular weight marker (BioRad)

Reynolds Lead Citrate stain (Agar Scientific)

RPMI 1640 (Fisher Scientific)

SDS (sodium dodecyl sulphate) (Sigma-Aldrich)

Sodium azide (Avocado Research Chemicals)

Sodium barbital (Sigma-Aldrich)

Sodium chloride (NaCl) (Sigma-Aldrich)

Sodium hydroxide (NaOH) (Sigma-Aldrich)

Sucrose (Sigma-Aldrich)

TEMED (Sigma-Aldrich)

Tris base (Sigma-Aldrich)

Triton X-100 (Sigma-Aldrich)

Trypsin, 0.25% EDTA (Sigma-Aldrich)

Trypsin/EDTA solution (Sigma-Aldrich)

Tween 20 (Sigma-Aldrich)

Uranyl acetate (Agar Scientific)

3.1.2 Biological Substances

FBS (centrifuged 4000 *g* for 1 h pre use)

NHS (sterile filtered 2µm nitrocellulose membrane pre use)

HS (sterile filtered 2µm nitrocellulose membrane pre use)

3.1.3 Apparatus

Bacterial incubator (Heraeus Incubator), Centrifuge 5804R (Eppendorf), Centrifuge 5810R (Eppendorf), Centrifuge, Microcentrifuge 5417R (Eppendorf), F-20 micron rotor (Sorvall), FLUOstar Omega plate reader (BMG Labtech, UK), Gel loading tips (Corning) GraphPad Prism 4 from GraphPad Software Inc., Guava EasyCyte flow cytometer (Guava MilliPore Technologies, UK), IR-Fourier Spectrometer (Bruker, Germany), Leica Ultracut R ultra microtome (Leica, Wein, Austria), Nikon Inverted Microscope TS100 (Nikin Eclipse, Japan), Fluorescent microscope (1X81 Olympus Corporation, Germany), Orbital shaker, pH meter 766 Calimatic (Jenway), Pioloform film copper grids (Agar Scientific), Pipette 2-20µl, 20-200µl and 100 to 1000µl (Sigma-Aldrich), Quartz crystal microbalance (Q-sense), Roto-Shake Genie (Denley), SE012 Rotor (Sorvall), Semi-dry transfer system (BioRad), Sorvall T-865 rotor (Sorvall), Sorvall ultracentrifuge RC6 (Thermo Electron Corp.), Spectrofluorimeter (Lambda Advanced Technology Ltd.), EMF tester gauss electromagnetic field meter TES-1390 (China), Ultra Low-frequency Magnetic Field Generator, Waterbath (Townson & Mercer Ltd, Croydon) and NanoDrop 1000 spectrophotometer (Thermo Scientific).

3.1.4 Antibodies

Anti-Annexin V Alexa Fluor 488 (eBiosciences)

Anti-LAMP-1 Alexa Fluor 488 (eBiosciences)

Anti-CD11b PE (AbD Serotec)

Anti-CD14 FITC (AbD Serotec)

Anti human H1R mouse antibody (R and D systems)

Anti human CD55 goat antibody (DAF) (Complement Technology)

Anti human CD11b mouse antibody (AbD Serotec)

Anti human CD107a mouse antibody (R and D systems)

Anti human C9 mouse antibody (Complement Technology)

Anti mouse rabbit FITC labelled antibody (AbD Serotec)

Anti human Phosphatidyl Serine (R and D systems)

3.1.5 Cell Lines

THP-1 (ECACC ref 88081201)

HeLa (Received as a kind gift from Dr Steven Butler, Middlesex University)

MCF-7 (ECACC ref 89012803)

PC3 (Received as a kind gift from Prof Chris Palmer, London Metropolitan University)

PNT2 (ECACC ref 95012613)

PC-12 (ECACC ref 88022401)

MBA-MB-231 (Received as a kind gift from Dr David MacDonald, London Metropolitan University)

CHO-K1 (Received as a kind gift from Dr Ken White, London Metropolitan University)

Salmonella typhimurium (Received as a kind gift from Dr Brigit Awamaria, London Metropolitan University)

3.2 Solutions

Eukaryotic Cell Freezing Solution

10% DMSO (v/v), 20% FBS (v/v), 69% RPMI 1640 (v/v) and 1% Penicillin and Streptomycin (v/v). Stored at 4^0C for 3 months.

Complete Growth Media (CGM)

25 ml FBS, 5 ml Penicillin and Streptomycin was added to 500 ml RPMI 1640 to make 5% CGM. 50ml FBS, 5 ml Penicillin and Streptomycin was added to 500 ml RPMI 1640 to make 10% CGM. The media was always handled in sterile conditions. After 250 ml was used, 5 ml was cultured without cells as a diagnostic for potential contamination.

Complete Growth Media with Kampomycin (CGM+K)

25 ml FBS, 5 ml Penicillin and Streptomycin was added to 500 ml RPMI 1640 to make 5% CGM. 50 ml FBS, 5 ml Penicillin and Streptomycin was added to 500 ml RPMI 1640 to make 10% CGM. 5 ml Kanamycin was added every 4 - 6 weeks.

Preparation of ethylenediaminetetraacetic acid (EDTA)

0.5 M stock solution was prepared; 2.92 g EDTA was dissolved in 1 ml distilled H_2O. 10 M NaOH was added a drop at a time until the EDTA was dissolved and pH 8 balanced with HCl using calibrated pH meter. The solution was made up to 100 ml with ddH_2O. EDTA solution was then sterilized by passing through a 0.2 µm pore size nitrocellulose membrane. The prepared EDTA was stored at -20°C.

Preparation of Sodium Hydroxide (NaOH) 10M

39.99 g NaOH was dissolved in 100 ml distilled H_2O. Stored at room temperature.

Annexin V Binding Buffer

10 mM Hepes, 140 mM NaCl and 25 mM $CaCl_2$ were dissolved in 200 ml ddH_2O and pH adjusted to 7.4 with 10 M NaOH and 1 M HCl. The binding buffer was autoclaved and stored at 4 ^{0}C.

Preparation of Phosphate buffered solution (PBS)

1 PBS tablet/100 ml ddH_2O was mixed using a magnetic stirrer in a durans bottle until dissolved. The PBS was sterilised using an autoclave preset 130 ^{0}C and then allowed to cool. The PBS was stored at 4 ^{0}C for 1 month.

Preparation of calcium green-AM dye

Calcium green-AM (50 µg) was dissolved in 50 µl of DMSO, in sterile conditions, as instructed by the manufacturer. Calcium green-AM was stored in the dark at -20 ^{0}C.

Periodic and acetic acid reagent for use with modified schiff's reagent

0.06% Periodic acid and 7% Acetic acid was added to 92.94% ddH_2O; for immediate use.

Preparation of Etoposide

1000 µg of Etoposide was dissolved in 1 ml of 99% Ethanol and stored -20 ^{0}C until use.

Preparation of Methotrexate

1 mM stock solution was prepared by dissolving 10 mg/ml methotrexate in 1 M NaOH pH 9.0.

Preparation of Docetaxel

1 mM stock solution was prepared by dissolving 10 mg/ml docetaxel in absolute alcohol.

Preparation of Phorbol- 12- Myristate- 13-Acetate (PMA)

5 mg/ml of PMA was dissolved in 1 ml DMSO and vortexed until fully dissolved. The PMA was then dispensed into 50 µl aliquots and stored in the dark at -20 °C.

Lysis buffer pH 7.4

100 mM HEPES-KON, 2 mM $CaCl_2$, 0.2% Triton X-100 (v/v) and Protease inhibitor (AEBSF), made up to 50 ml with Millipore water and stored in 1 ml aliquots at -20 °C.

SDS-PAGE solutions

(4x) SDS sample buffer pH 6.8

200 mM Tris-HCl, 25% glycine (w/v), 2% SDS (w/v), 0,2% bromophenol blue (w/v) and 20 mM DDT (added upon use).

(1.5 M) Resolving buffer pH 8.8

18.17 g Tris base dissolved in 100 ml ddH_2O and adjusted to pH 8.8.

(0.5 M) Stacking buffer pH 6.8

6.06 g Tris base dissolved in 100 ml ddH_2O and adjusted to pH 6.8.

Resolving gel solution (12%)

2 ml ddH_2O, 1.25 ml 1.5 M Tris-HCl pH 8.8, 0.05 ml 10% SDS (w/v), 1.66 ml acrylamide/Bis 30% (w/v), 0.025 ml 10% APS (w/v) and 0.0025 ml TEMED.

Stacking gel solution

1.53 ml ddH_2O, 0.625 ml 0.5 M Tris-HCl pH 6.8, 0.025 ml 10% SDS (w/v), 0.335 ml acrylamide/bis 30% (w/v) and 0.0025% TEMED.

Electrophoresis running buffer (1 L)

30 g Tris-HCl pH 8.3, 144 g glycine, 50 ml 20% SDS (w/v) and 950 ml ddH_2O.

Coomassie brilliant blue G-250

0.025% coomassie blue (w/v), 10% acetic acid (v/v) and 90% ddH_2O (v/v), mixed and filtered (Whatman number 1 paper).

Destain solution (500 ml)

35 ml acetic acid, 25 ml methanol and 440 ml ddH_2O.

Transfer buffer (10X)

250 mM Tris base, 1925 glycine, 500 ml ddH_2O.

Sartoblot buffer (500 ml)

40 ml Transfer buffer (1X), 100 ml methanol, 360 ml ddH_2O.

Ponceau solution

0.25% Ponceau S (w/v), 3% trichloroacetic acid (v/v) and ddH_2O.

Phosphate buffer saline (PBS) solution (1 L)

140 mM NaCl, 2.7 mM KCl, 10 mM Na_2HPO_4, 1.8 mM KH_2PO_4 and ddH_2O.

Phosphate buffer saline tween 20 (PBS-T)

1 L PBS and 1 ml tween 20.

Blocking buffer

6% Milk powder (w/v) and 100 ml PBS-T.

Antibody dilution buffer (WB)

3% Milk powder (w/v) and 100 ml PBS-T.

Permeabilisation buffer (PB)

0.5% tween 20 (v/v) and PBS.

Immunofluorescence antibody dilution buffers

Cell dilution medium

10% FBS, 1% NaN_3 and PBS solution.

Primary and secondary antibody dilution buffer

3% BSA (w/v) and PBS.

Flow cytometry analysis buffer

3% BSA (w/v), 1% NaN_3 (w/v) and PBS.

Veronal buffer pH 7.4

0.15 mM $CaCl_2$, 141 mM NaCl, 0.5 mM $MgCl_2$, 1.8 mM Na barbital and 3.1 mM Barbituric acid, dissolved in 500 ml ddH_2O.

Dulbeccos Phosphate Buffer Saline (D-PBS)

40 gm NaCL, 1 gm KCl, 5.75 gm Na_2HPO_4, 1 gm KH_2PO_4, pH adjust to 7.3 and make up to 5 L with ddH_2O.

Complement diluent buffer

Dissolve 1 tablet (Oxoid) in 100 ml ddH_2O. Stored at 4° C until use.

Nutrient Agar broth and culture plates

31 g Nutrient gar powder dissolved in 1 L of distilled H_2O was autoclaved for 15 min at 130 °C and allowed to cool to ~50 °C before pouring into ~50 agar plates.

8 g of Nutrient agar powder was dissolved in 1 L of distilled H_2O and autoclaved for 15 min at 130 °C and allowed to cool. 5 ml aliquots were stored in sterile universal bottles and stored at 4 °C until use.

3.3 Methods

3.3.1 Methods of MV analysis to date

The general consensus dictates that MVs have a particular morphology based upon size, physical and chemical properties as well as their biochemical interactions (Nolan *et al*, 2008). MVs however can be subdivided into sMVs and cMVs (Stratton *et al*, 2012a), as is shown in this thesis, so that a greater understanding of their origins and roles can be explained.

When analysing MV subtypes and OMVs, quantification based upon microvesicle number was employed as opposed to weight of protein content, to allow for meaningful comparisons between samples. Data obtained is comparable within sample type and with other subtypes. The reason for microvesicle counting is that absolute numbers of different subtypes will express different weight of protein naturally, however the protein content may not account for the physiological roles of the MV subtypes. Conversely, equal weight of protein in different subtypes will result in different microvesicle counts, leading to unequal quantities of other agents such as RNA, cytochrome c or specific levels of individual types of proteins.

3.3.2 Flow cytometry

The flow cytometer used throughout this thesis was the Guava Millipore Easycyte flow cytometer, with CytoSoft data acquisition and analysis software version 3.6.1 and FCS data manipulation and presentation software. Data collected was statistically analysed using GraphPad Prism 5 or SPSS 18.

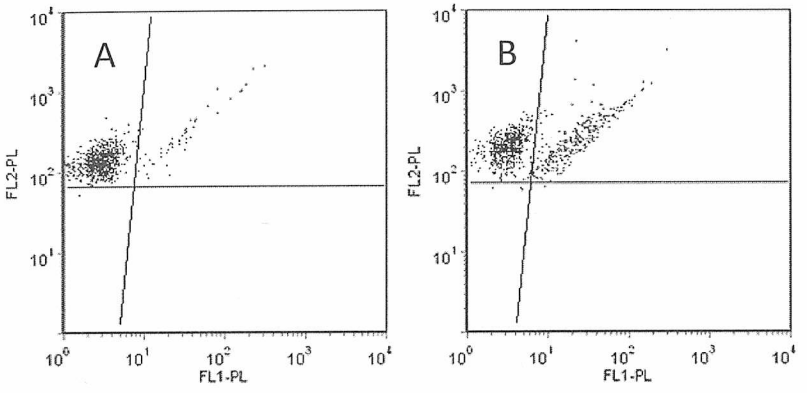

Fig 3.1 Guava Millipore ViaCount assay. Typical 'gating' to quantify viability and cell number. The upper left quadrant denotes healthy cells, the upper right denotes apoptotic and dead cells. FL1-PL measures the expression of PS by annexin V FITC chromophore, FL2-PL measures 7-AAD bound to DNA. (A) is a typical dot plot for a 95% viable cell population (7.5 x 10^5 /ml), (B) indicates a cell population undergoing apoptosis and death, 75% viability (7.5 x 10^5 /ml) (Image produced for this thesis by Dan Stratton).

The flow cytometry was used to determine cell number and viability of cell populations by viacount assay (Antwi-Baffour *et al*, 2010), the assay determining % viability by sampling 1 x 10^3 cells, measuring the % annexin V chromophore and % 7-AAD fluorescence and comparing the results to the calibrated control. The results would also indicate the viable cell number/ml and total cell number/ml (% viability).

Flow cytometry is a powerful tool used to count and quantify particles, cells and MVs. It's resolving power ranges accurately from ~0.05 μm to 3 μm, using a photocell to determine size of 'particles, (FSc-HLog)'. Side scatter (SSc-HLog) determines the angle of laser light that is scattered due to 'roughness' of the surface of the MV (Grant *et al*, 2011). Flow cytometry uses one or more lasers tuned to specific wavelengths to identify and quantify the presence of fluorescent dyes and antibodies conjugated to

fluorescent dyes. Binding of Annexin V to PS, size and morphology can be quantified, expressed PS being a typical feature of MVs.

Use of unlabelled standard cMVs to compare all experimental conditions was employed for standard calibration and if required, to demonstrate the presence of increased fluorescence due to the experiments performed.

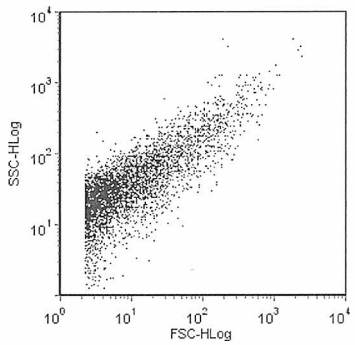

Fig 3.2 Typical FACS dot plot showing MV morphology, obtained using Guava Millipore ExpressPlus Programme (Grant *et al*, 2011). FSC-HLog (forward scatter) is a measure of particle/cell size, SSC-HLog (side scatter) is an evaluation of the surface granularity by measuring refracted laser light angle.

Figure 3.2 shows a typical FACS MV morphology for cMVs, the x axis showing forward scatter (FSC) and the y axis side scatter (SSC). There is a positive relationship between FSC and SSC such that as the MV size increases so does its surface granularity thereby depicting a characteristic dot plot graph shape for the presence of MVs.

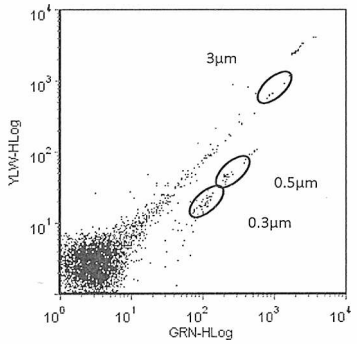

Fig 3.3 FACS dot plot for MVs showing GRN-HLog vs YLW HLog, with Megamix sizing beads using Guava Millipore, ExpressPlus programme (Grant *et al*, 2011). MVs fluoresce 'slightly' green, therefore it is essential to 'gate' or calibrate the control sample so that bound FITC (green fluorescent dye) will cause a stronger quantifiable fluorescence. The Megamix sizing beads shown also fluoresce for ease of identification and are used as a measure of known sizes (0.3, 0.5 and 3 µM).

Figure 3.3 shows the ratio of Green (GRN-HLog) to Yellow fluorescence (YLW-HLog), Megamix being included with this sample to demonstrate cMV size, Megamix sizes shown are 0.3 µm, 0.5 µm and 3 µm. There is a strong positive correlation between GRN-HLog and YLW-HLog for MVs as their size increases indicating that they have a natural fluorescence in this range. The background fluorescence is observed as the plots between 10^0 – 10^1 for both GRN-HLog and YLW-HLog. RED-HLog is used to analyse TRITC labelled features using the same protocol as GRN-HLog and YLW-HLog.

3.3.3 Nanosight tracking analysis

Nanosight tracking analysis (NTA) LM10 uses a laser (640 nm) that tracks particles 10 nm – 1000 nm. NTA works in a similar way to dynamic light scattering (DLS) using the brownian motion of the media to infer particle size, however DLS does not image the particles and is unreliable to estimate absolute size. NTA has a greater resolving power than flow cytometry and is more reliable than DLS. (Gyorgy *et al*, 2011).

NTA can size and track particles in real time, allowing video capture (Vallhov *et al*, 2011), however is limited by the viscosity of the media, the concentration of the particles and cannot size larger particles, i.e., over 1000 nm. The data is extrapolated from interference patterns caused by changes in the fluids refractive index due to brownian motion of the particles (Gyorgy *et al*, 2011).

3.3.4 qNano particle analysis

qNano is a non-optical technique for assessing particle size, instead using resistive pulse sensing on 40 µl of 'diluted' sample (typically $1 \times 10^5 - 1 \times 10^6$ particles /ml).

qNano counts and measures charged particles as they pass through a pore of known size. Therein lies its limitations and to build up accurate data multiple analyses at various pore sizes must be performed to generate an overall data set. This type of analysis is suitable for MVs as they carry an outer leaflet negative charge due to increased expression of PS. (Inal *et al*, 2012)

The unique feature of qNano is that it measures blockade baseline duration, so that it is able to quantify of the 'flight time' of the particles within an electric field, thereby measuring particles' relative charge per unit surface area.

3.3.5 Microplate affinity assays

Affinity assays are designed to measure the presence of many types of molecule, such as specific antibodies, proteins and lipids. They are used to quantify the presence of the molecule of interest by comparing the sample to a standard curve of varying concentration (often referencing the optical densities). Using this method, the concentration of PS and various proteins can be accurately assessed. Microplate assays are often used as an alternative or confirmatory test for flow cytometry.

3.3.6 Western blot

Western blot is a powerful tool for identifying proteins based on their size and charge. Lysed MVs were applied to Western blot analysis and common proteins were identified, indicating a specific protein component for all subtypes of MVs (Inal *et al*, 2012, Stratton *et al*, 2012a) however, these subtypes varied with the combination and concentration of proteins that they included based upon the originating cell and mode of stimuli, if any (Gutwein *et al*, 2005; Muralidharan-Chari *et al*, 2010). Actin and associated cytoskeletal proteins are ubiquitously included in mammalian MVs, as are esterases, membrane associated receptors.

3.3.7 ELISA

Enzyme-linked immunosorbant assay (ELISA) was used for the detection and quantification of MV components such as enzymes, receptors and structural proteins. Often used in conjunction with Western blot although requiring a smaller initial MV sample, they are very sensitive, using a calibration curve of known quantities of the

analyte and compared, usually by optical density, to the MV sample. This method can highlight differences between samples, allowing for experimental manipulation and observation to a great degree of accuracy.

3.3.8 Fluorescent microscopy

Fluorescent microscopy was used in conjunction with fluorescent antibody staining and/or fluorescent staining of enzymes or lipids to identify either MVs or proteins such as receptors that are expressed on MVs. It was used as a comparative tool to measure the presence or relative abundance of a protein/lipid and to visualise them in relation to cell physiology.

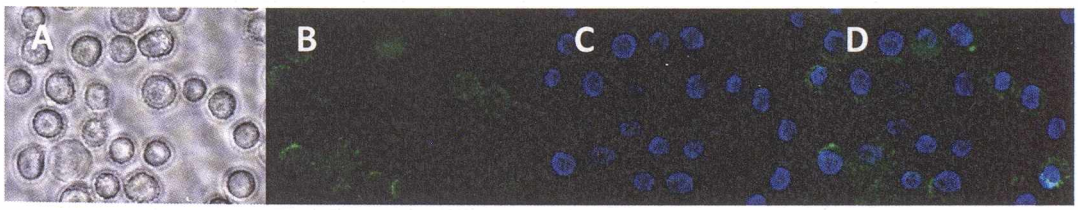

Fig 3.4 THP-1 undergoing anti phosphatidyl serine receptor antibody conjugated to FITC labelling. (**A**) The fixed THP-1 were located and captured in a bright field image. (**B**) Then the FITC chromophore was stimulated using a specialised lamp, the FITC specific filter allowed the PSR-antibody-FITC to be captured. (**C**) The DAPI nuclear stain was then captured and finally (**D**) the FITC and DAPI images were superimposed allowing for a composite image to be produced (Images produced by Dan Stratton for this thesis).

Proteins were often used as a target for the photosensitive dyes –FITC, green; -PE, yellow; -TRITC, red and DAPI, blue, however any fluorescent dye can be imaged with reference to its wavelength. MVs themselves are too small to be captured in detail, however a fluorescent 'pin point' would indicate the labelled MV.

3.3.9 NanoDrop analysis

NanoDrop is a specialised spectrophotometer that analyses 0.5 – 2 µl samples accurately and is ideal for biological material where yield or sample size is min (NanoDrop, 2008). This procedure was used to identify and confirm the presence of DNA, protein and carbohydrate (CH_2 -OH) (Hansen *et al*, 2007; NanoDrop, 2008) relative abundances in different MV and OMV samples, where MV subtypes and OMVs were diluted to 1 x 10^6 /ml and prior to analysis were thoroughly mixed to give 2000 microvesicles in 2 µl (Stratton *et al*, 2012).

The NanoDrop is an excellent tool for quantification of molecular abundances using frequency at the appropriate spectral ranges, 260 nm showing the presence of DNA, 280 nm the presence of protein and 230 nm carbohydrate (Hansen *et al*, 2007). The ratio of 260 nm:280 nm was also used to show that DNA was present and associated with nuclear proteins or with cellular proteins.

The results were recorded and displayed on the NanoDrop software and data collected was analysed using GraphPad version 5 to quantify and compare MV subtypes and OMVs (Appendix).

3.3.10 Fourier Transform Infrared Spectroscopy

Fourier Transform Infrared Spectroscopy (FT-IR) is a highly accurate technique used to identify chemical bonds and molecular motifs present in a compound or biological sample using Infrared absorption or transmission (Buttner *et al*, 2009; Du *et al*, 2009).

More recently FT-IR has been used to observe spectral information from biological samples with mid-infrared frequencies (Martin, 2011). Using published data, it is possible to identify protein features such as α-helices, β-pleated sheets and random coils (Buttner *et al*, 2009; Du *et al*, 2009) [see Table 5.1]. It is also possible to derive a unique spectral signature for cell types and to derive specific chemical data for any relevant sample (Martin, 2011; Nasse *et al*, 2011).

DNA is identifiable within 900 - 1200 cm^{-1} (Du *et al*, 2009), carbohydrates with associated C=O bonding (Buttner *et al*, 2009). Lipids and lipid functional groups also are identifiable within the definable spectral range 2800 - 3000 cm^{-1} (Gousset *et al*, 2002; Buttner *et al*, 2009). Often, samples are prepared in a dry form, but with cells it is possible to work with sample suspended in media. Using medium as a blank removes many erroneous features.

The fingerprint region, a spectral range from 900 - 1800 cm^{-1} shows a high degree of variability in biological models, encompassing the DNA region (900 - 1300 cm^{-1}) and proteins (1475 - 1680 cm^{-1}). Notably ratios of intensity for amide I and amide II, and ratios for DNA intensity can be used to identify differences between samples.

Table 3.1 Summary of particular spectral features of FT-IR (adapted from Dagneaux *et al*, 1996; Gousset *et al*, 2002; Popova and Hincha, 2005; Nara *et al*, 2006; Buttner *et al*, 2009; Du *et al*, 2009).

Wavelength cm^{-1}	*Molecule*	*Feature*
750 – 900	Sugar	842 - 865 cm^{-1} sugars associated with nucleotides
900 – 1300	DNA	965 cm^{-1} C-C bonds
		1080 -1086 cm^{-1} PO_2^- bonds
		1240 cm^{-1} asymmetric DNA 1253 -1262 cm^{-1} P=O peaks (lipid)
1400 – 1700	Protein	1538 cm^{-1} amide II, C-N-H bending/ stretching
		1640 cm^{-1} amide I, C=O stretching
		1613 - 1637 cm^{-1} β-pleated sheets (1615 - 1620 cm^{-1} aggregated proteins)
		1637 - 1645 cm^{-1} random coils
		1645 - 1662 cm^{-1} α-helix
		1662 - 1682 cm^{-1} β-turns
1700 – 1750	Lipid	1720 cm^{-1} C=O stretching of COOH (COO^-) 1737 - 1743 cm^{-1} C=O bond
2800 – 3000	Lipid	CH_2 and CH_3 are apparent in this range
3000 – 3500	Water and Other features	3090 cm^{-1} ROS of Water

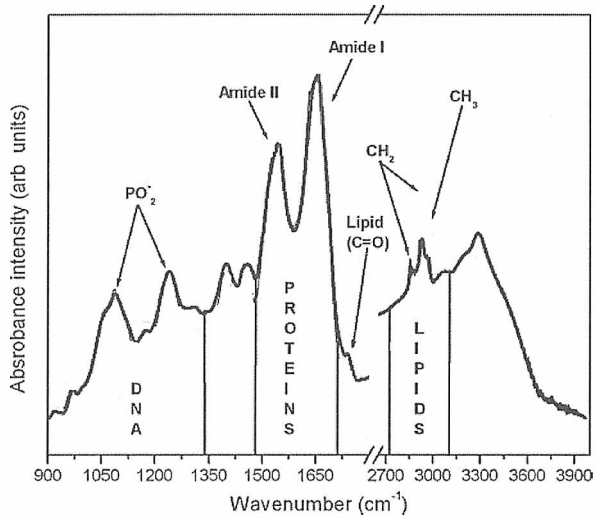

Fig 3.5 FT-IR profile of cancer cells. 900 - 4000 cm^{-1} typical topography of cancer cells using FT-IR, showing the fingerprint region and extending to the lipid region; adapted from Buttner *et al*, 2009.

FT-IR produced unique profiles depending upon the quality and quantity of sample analysed (Gazi *et al,* 2007; Ghosal *et al*, 2010) and pioneering work (presented in this thesis) proposes novel uses as a diagnostic tool, indeed, there is growing evidence that FT-IR spectroscopy can be used to diagnose disease based upon the standard (normal) FT-IR profile and how this deviates from the test FT-IR profile (Ghosal *et al*, 2010).

FTIR has many advantages over other diagnostic and research techniques as no special preparation of samples is required, the results are compelling, non destructive, no biomarkers being necessary and measurements can be taken quickly and compared directly to other samples (Martin, 2011; Nasse *et al*, 2011).

3.3.11 Quartz Crystal Microbalance

The quartz crystal microbalance (from Q sense) is a versatile device used for measuring changes in mass and fluidity within samples of interest, whether it be a chemical or biological assay (Luo *et al*, 2006). Wafer thin quartz crystals coated with gold electrodes resonate when applied to an electric field, the piezoelectric effect (Chou *et al*, 2002). The resonation is controllable and very precise, generating a standing shear wave that is measured in Hz. As mass is deposited upon the surface of the quartz crystal sensor the resonant frequency decreases and a corresponding change in mass is measurable. Similarly mass is removed from the quartz crystal sensor, the resonance increases (Benes, 1984). Application of the sauerbrey equation allows a calculation of mass change by measuring frequency change; $\Delta Hz \times 17.7 = \Delta mass\ \mu g$ (Chou *et al*, 2002; Luo *et al*, 2006). Furthermore, the viscosity changes of a fluid can be determined using Q sense QCM by detecting energy dissipation changes of the shear waves within the fluid. Application of the Quartz crystal microbalance to the field of microvesicles has been demonstrated for the first time in this thesis (Stratton, 2012; Stratton *et al*, 2010), however QCM techniques are more commonly used as diagnostics for immunoassays owing to the apparatus' sensitivity (Chou *et al*, 2002; Luo *et al*, 2006).

3.3.12 Thin layer chromatography

Thin layer chromatography (TLC) is a powerful technique used to identify molecules based upon their polarity (Pasciak *et al*, 2003) with reference to a known control sample and the relative 'front' of the solvent on the TLC plate. Most biological molecules are detectible using TLC (Fried and Sherma, 1999). Mobile phases contain

either an apolar or polar solvents and spots are detectible using UV light (Fried and Sherma, 1999)

3.3.13 MV functional assays

Comparing the interactions of cells and MV subtypes. Functional assays are designed to observe the response of cells to MVs subtypes from various cells. They can measure:

1) Complement protective roles: assessment of cell viability and number.

2) Proliferation of cells/ apoptosis of cells: assessment of cell viability, apoptotic stages and number.

3) Communicative vectors: assessment of change in cellular metabolism or expression of molecule types.

4) Pro-coagulant roles: assessment of coagulation efficiency.

5) Stress agent receptacles: assessment of changes in viability or apoptotic stages.

6) Delivery of cargo: assessment of changes in concentration of particular molecules or ions, such as calcium, enzymes or RNA (Thomas and Salter, 2010).

Functional assays measure the change in viability, cell number or molecule in particular protein (however RNA is also frequently monitored) expression in association with cells.

3.4.0 Tissue culture and microbiology

3.4.1 Maintaining cell lines

Exponentially growing cells with a viability of >95% were used in all experiments, their viability was quantified using a Guava Millipore flow cytometer, ViaCount assay. Foetal Bovine Serum (FBS), Normal Human Serum (NHS) and Horses Serum (HS) were centrifuged for 1 h at 4°C in sterile 50ml centrifuge tubes and then filtered through a 0.22 μm nitrocellulose filter to ensure removal of cellular debris and bacteria. Flow cytometry analysis of filtered serum revealed negligible presence of microvesicles (MVs), when diluted in RPMI 1640, MVs would typically ~1 – 4 x 10^3 /ml. Serum was frozen at -20 °C prior to use.

Sterility was ensured, all tissue culture apparatus and consumables were autoclaved or cross linked with a UV illuminator and wiped with IMS prior to use. Cells were treated respectfully, once used were destroyed using industrial methylated spirit (IMS) and autoclaved at 130 °C for 15 min.

3.4.2 Non-adherent cell lines

THP-1 were cultured using RPMI 1640 supplemented with 10% filtered (0.22 μm) foetal bovine serum (FBS) and 1% penicillin-streptomycin. Cells were occasionally cultured with 1% kanamycin to treat potential micoplasma infection, this was performed every 4 - 6 weeks to avoid antibiotic resistance. All cell cultures were grown in 5% CO_2 humidifiers at 37 °C. Cells were washed 3 - 4x a week, the THP-1 (or other non-adherent cell lines) were transferred to 50ml centrifuge tube and spun 160 *g* for 5

min. The pelleted cells were re-suspended in serum free RPMI 1640, discarding the resulting supernatant. The previous centrifugation regimen were repeated 2x, the THP-1 finally suspended in the desired volume of complete growth media and seeded into new 75cm^2 tissue culture flasks. Usually, THP-1 were initially cultured at a concentration ~1 x 10^5 /ml until the cell numbers had reached ~1 x 10^6 /ml.

3.4.3 Adherent cell lines

HeLa were cultured using DMEM supplemented with 10% filtered (0.22 μm) foetal bovine serum and 1% penicillin-streptomycin. PC3, PNT2, MCF-7, MBA MB 231 and CHO-K1 were cultured using RPMI 1640 supplemented with 10% filtered (0.22 μm) foetal bovine serum and 1% penicillin-streptomycin. PC12 were cultured using RPMI 1640 supplemented with 10% filtered (0.22 μm) foetal bovine serum, 5% filtered (0.22 μm) horse serum and 1% penicillin-streptomycin. Cells were occasionally cultured with 1% kanamycin as before. All cell cultures were grown in 5% CO_2 humidifiers at 37 ^{0}C. They were washed 3 - 4x a week using serum free media.

At >85% confluence the adherent cell cultures were split, cells were washed 2x using serum free medium followed by 0.25% (v/v) trypsin/EDTA in serum free media. After 3 - 10 min incubation at 37 ^{0}C in 5% CO_2, the culture flask was gently 'tapped' to encourage cells to detach, upon which complete growth media (CGM) was added to de-activate trypsin. The cells were centrifuged 160 *g* for 5 min followed by a wash in RPMI 1640 serum free medium. The cells were finally re-suspended to the desired concentration in CGM and seeded using 75cm^2 tissue culture flasks.

3.4.4 Freezing Eukaryotic cells

To prepare cells for long term cryogenic storage, cells usually within the range of 5 x 10^6 – 1 x 10^7 /ml were counted using Guava Millipore ViaCount assay. Adherent cells were removed by incubating with 0.25% (v/v) trypsin/EDTA for 3 - 10 min at 37 °C. Non-adherent and adherent cell supernatant was centrifuged at 160 *g* for 5 min. The cell pellet (~1 x 10^7 cells) was re-suspended in 1 ml cell freezing solution and transferred to cryo-vials (Grenier) and cooled -1 °C/min in cryo-boxes until -80 °C. The frozen cells were transferred to liquid nitrogen cell storage tanks.

3.4.5 Defrosting Eukaryotic cells

Cryo-vials containing the desired cell line(s) were removed from liquid nitrogen storage and immediately thawed in a 37 ^{0}C water bath. After sterilising the exterior of the cryo-vial using IMS, the cells were transferred to a 15 ml centrifuge tube containing 9 ml of pre-warmed (37 ^{0}C) CGM upon which the cells were centrifuged 160 *g* for 5 min. To ensure complete removal of DMSO the cells were washed 2x using pre-warmed CGM as before and finally seeded in a 75 cm^2 tissue culture flask and maintained at 37 ^{0}C in 5% CO_2 humidifier.

3.4.6 Salmonella typhimurium *culture*

All microbiology work and was performed within tissue culture cabinets that were dedicated to microbiology work. All sterilisation was performed using autoclaving, IMS and Bunsen burner techniques. Personal protective equipment was clean and sterile. Disposable equipment and salmonella cultures were destroyed by following in-house

protocols. Asceptic techniques were observed following protocols for microbiology work.

Salmonella typhimurium were cultured on nutrient agar spread plates at 37 ^{0}C. One colony was collected and diluted as appropriate in sterile PBS and pippetted on to prepared sterile nutrient agar plates.

In brief, a sterilised (flames and cooled) sterilised loop was used to collect on pure colony of *Salmonella Typhimurium* to inoculate 5ml of nutrient broth (CM001B, Oxoid, UK) in a sterilised universal bottle that was aerobically incubated at 37 ^{0}C for 24 h. After incubation, using a disposable loop (sterile), 10 µl of the culture was collected and streaked on the surface of pre-prepared nutrient agar plates (CM003B, Oxoid, UK) and the plates were incubated (as before). From the fresh colonies a dilution series was made, diluting by a factor of 10 (final volume of 100 µl) and spreading the bacteria on the agar spread plates. Colonies were counted and the dilution selected contained 30 – 300 colony forming units (CFU), usually 10^{-5}.

3.4.7 Freezing salmonella typhimurium

Nutrient agar cultured *salmonella typhimurium* were grown on spread plates for 24 – 48 h, one or two colonies were collected using a sterilised hoop and dispensed into a vial of cryo-beads and mixed by pipetting. The cryo-beads were then frozen at -20 ^{0}C. All salmonella were collected from this stock to ensure little or no genetic or phenotypic variation and ensure reproducibility for microbiology work.

3.4.8 Defrosting salmonella typhimurium

Nutrient agar broth (5 ml) was prepared as directed by the manufacturer, typically diluting 25 g of nutrient broth powder in 1 L of sterile H_2O and autoclaving at 121 ^{0}C for 15 min. Once autoclaved the nutrient agar broth was allowed to cool. The *salmonella typhimurium* vial was removed from -20 ^{0}C storage and 2 cryo-beads were removed and cultured in nutrient agar broth at 37 ^{0}C for 24 h. The salmonella were collected and then grown on a nutrient agar spread plates.

3.5 Biochemical methods

3.5.1 Flow cytometry

All flow cytometry was performed using a Guava Millipore EasyCyte Flow Cytometer. The Guava Millipore has assays and specific programmes to assay cell culture viability and cell number (ViaCount), particle morphology (ExpressPlus), size and number (ExpressPlus), fluorescent label detection (ExpressPlus), apoptotic stages (Nexin), cell cycle by DNA content (Cell Cycle reagent) and a variety of other programmes not used for this thesis.

3.5.2 Cell counting and viability assessment

The cell count and viability was quantified using a Guava Millipore flow cytometer and the manufacturer's ViaCount assay. The ViaCount assay uses a membrane dye exclusion principle to discriminate between viable (membrane intact) cells and non-viable (membrane compromised) cells, therefore non-viable cells allow the uptake of the ViaCount dye, so staining the cell. The ViaCount dye contains nuclear dye (7-

aminoactinomycin D: 7-AAD) and annexin V. Annexin V binds to PS indicating early apoptosis and 7-AAD binds to DNA by entering the cells nucleus through the plasma membrane and nuclear membrane by apoptotic pores, indicating late apoptosis or cell death.

Typically cells were optimally suspended in media, 150 µl of cells in culture were dispensed into a corstar 96 well sterile plate to which 50 µl of ViaCount reagent was added. The assay was kept in the dark and analysed by flow cytometry, typically quantifying 1,000 cells in at least x3 per control and more for analysis of experiments.

3.5.3 Microvesicle counting using flow cytometry

Sterile PBS (180 – 190 µl, depending upon the expected concentration of the isolated MVs) were dispensed into a sterile 96 well mictotitre plate (Corstar). Purified MVs (10-20 µl) suspended in sterile PBS were sonicated in a sonicating waterbath (Townson and Mercer Ltd) for 5 min at 4 ^{0}C and then added to the dispensed PBS and mixed by gentle pipetting. The Guava Millipore ExpressPlus programme was used as per the manufacturer's instructions and MVs were counted and the population morphology recorded. Typically 5,000 events were analysed by ExpressPlus, quantified 3x for controls and more for analysis of experiments.

MVs have a natural green fluorescence, the GRN-HLog was gated upon the control (1st marker) so that FITC labelled antibodies could be compared to the control. Increased GRN-HLog was expressed by % change on the 2nd marker.

3.5.4 Identification of proteins and receptors by immunofluorescence staining with antibodies

To establish cellular and microvesicle expression of proteins and receptors, cells were immunofluorescence stained with antibodies and analysed using flow cytometry. Cells >95% viability (determined using ViaCount assay, as before) were washed 2x by centrifugation at 160 *g* for 5 min and typically transferred to 1.5 ml eppendorf tubes at the required concentration (depending upon the assay type or manufacturer's requirements) for the remainder of the staining protocol, after which the cells or cell sample was transferred into a 96 well microtitre plate for flow cytometry analysis (ExpressPlus).

Cell surface and microvesicle surface expression of CD55, H1R, CD107a, CD14b, C5b-9, CD209 and CD11 was analysed by flow cytometry, ExpressPlus programme. Typically, THP-1 (but also HeLa and CHO K1: were removed from their culture flasks using 0.25% trypsin EDTA, as before) were washed 2x by centrifugation at 160 *g* for 5 min with sterile PBS and finally suspended in cold PBS supplemented with 10% FBS and 1% NaN_3. Cells were incubated in the dark with the appropriate primary antibody (2 µg/million cells, R & D systems, UK) against the receptor or protein of interest at 4 ^{0}C for 1 h while shaking. After 3x washes at 400 *g* for 5 min, the cells were stained with the isotype matched control antibodies: anti-mouse or anti-rabbit IgG-FITC, R & D systems, UK) diluted 1:320 in sterile PBS supplemented with 3% BSA and incubated while shaking in the dark at 4 ^{0}C for 1 h. The cells were washed 3x in cold, sterile PBS and finally suspended in 200 µl PBS supplemented with 3% BSA and 1% NaN_3 before being immediately analysed by flow cytometry using the ExpressPlus programme, gating on the negative control.

Gating based upon negative and/or positive controls allow the flow cytometer to quantify % fluorescent tagged antibody binding (normally GRN-HLog or YLW-HLog) and therefore measure changes in protein/receptor expression caused by experimental constraints.

3.5.5 Immunofluorescence staining following microvesiculation

To investigate whether MVs carry cell receptors and proteins once released, immunostaining was performed. Typically 5 x 10^6 cells/ml were prepared as before and stimulated for microvesicle release using pre-warmed (37 ^{0}C) RPMI 1640 supplemented with 10% filtered (0.22 μm) NHS and 2 mM $CaCl_2$ and purified using the MV isolation/purification technique. However, occasionally MVs were immunostained after release, particularly in the case of C5b-9 (labelling the C5b-9 complex prevented microvesiculation) and cMVs (being released over a longer period of time, the antibodies would have been assimilated by the cells) the microvesicles were concentrated to 5 x 10^6 MVs/ml in cold PBS supplemented with 10% FBS and 1% NaN_3 2 ng/ml primary antibody was added in the dark at 4 ^{0}C for 1 h. The MVs were washed 2x by initially adding 200 μl sterile PBS to the eppendorf tubes to dilute the antibody and then centrifuged 25,000 *g* for 15 min. The MVs were then suspended in PBS supplemented with 3% BSA and the appropriate isotype matched secondary antibody (as before) and were shaken in the dark at 4 ^{0}C. The MVs were washed 2x by centrifugation at 25,000 *g* for 15 min and immediately analysed using flow cytometry, ExpressPlus Programme. Variations of the centrifugation speed were assessed, although to confirm MVs the protocol for MV purification was adhered to.

3.5.6 Isolation of MVs from culture medium

Cells were separated from RPMI 1640 supplemented with 10% foetal bovine serum and 1% penicillin-streptomycin (CGM) by centrifugation at 160 *g* for 5 min. The supernatant was collected and submitted for a further centrifugation of 4000 *g* for 60 min at 4 ^{0}C to remove cell debris. The pellet was discarded, the supernatant was transferred to 1.5 ml sterile eppendorf tubes and sonicated for 5 min at 4 ^{0}C in a sonicating water bath then immediately centrifuged at 25,000 *g* for 90 min at 4 ^{0}C. The supernatant was discarded and the pellet composed of MVs was suspended in 250 µl PBS before a final centrifugation at 25,000 *g* for 15 min at 4 ^{0}C (Antwi-Baffour *et al*, 2010) to remove loosely attached proteins such as albumin that may lead to confounding data. The pellet was finally suspended in 100 µl PBS. The MVs were stored at -80 ^{0}C until required. MVs were quantified using a Guava Millipore flow cytometer, ExpressPlus programme, or stained with annexin V conjugated to FITC, to ascertain surface PS expression on the MV membrane.

For experiments that evaluated the effective sedimentation of MVs through different ultra-centrifugation speeds, the procedure for MV isolation was followed as before until the final ultracentrifugation step whereby centrifugation speeds were tested at 10,000 *g* for 30 min, 10,000 *g* for 60 min, 15,000 *g* for 60 min and 25,000 *g* for 60 min as well as 25,000 *g* for 90 min at 4 ^{0}C to ascertain optimal MV centrifugation speeds.

3.5.7 Isolation of stimulated MVs

Cells >95% viability were washed 2x using RPMI 1640 at 160 *g* for 5 min and finally re-suspended at the desired concentration, usually 1 x 10^5 – 1 x 10^6 cells/ml in RMPI 1640 supplemented with 10% normal human serum (filter sterilised) and 2 mM $CaCl_2$ to induce MV release. The cells were usually incubated using 15 ml centrifuge tubes at 37 ^{0}C in a rotating water bath for 30 min after which they were immediately placed on ice to stop microvesiculation and transferred to 1.5 ml eppendorf tubes. The cells were pelleted using centrifugation at 160 *g* for 5 min and cellular debris removed by centrifugation at 4000 *g* for 60 min at 10 ^{0}C. The pellet was discarded and the supernatant was sonicated for 5 min at 4 ^{0}C and then centrifuged at 25,000 *g* for 90 min at 4 ^{0}C. The pellet containing mainly MVs (possible low contaminating exosomes) was re-suspended in 250 µl sterile PBS and centrifuged for a further 15 min at 25,000 *g* at 4 ^{0}C before the pelleted MVs being finally suspended in 100 µl of sterile PBS. Isolated MVs were immediately quantified using a Guava Millipore flow cytometer, ExpressPlus programme, or labelled using annexin V conjugated to FITC as before. Finally stimulated MVs were frozen -80 ^{0}C until required, typically within 1 week.

Other stress agents were sometimes used (where stated) and if so the NHS would be substituted for fMLP, LPS, calcium ionopore or ULMF; the procedure was not otherwise altered.

3.5.8 Annexin V labelling of MVs

Isolated MVs were suspended in annexin binding buffer and annexin V conjugated to FITC (5 µl annexin V (Sigma-Aldrich)/100 µl buffer) in a 200 µl final volume and wrapped in foil to prevent photo-bleaching of the FITC. The sample was incubated at room temperature for 45 min on shaking, before being centrifuged at 25,000 *g* for 30 min to pellet MVs. Samples were immediately re-suspended in sterile PBS and analysed using Guava Millipore flow cytometer, ExpressPlus programme, gating against an unlabelled control.

3.5.9 Quantification of lipid rafts on MV subtypes

Lipid rafts have been described on MVs, however owing to their differences in biogenesis it was essential to quantify differences that may indicate different physiological roles and how important lipid rafts are between MV subtype biogenesis.

MV subtypes were quantified (as before) and suspended to 1 x 10^6 /ml. Manufacturers protocol. In brief, MV subtypes (1 x 10^6 /ml) were suspended in 200 µl of fluorescent CT-B conjugate working solution and incubated for 10 min at 4 °C. The MVs were washed at 25,000 *g* for 15 min and re-suspended in 100 µl chilled PBS. Then they were added to 200 µl of chilled anti CT-B antibody working solution and incubated for 15 min at 4 °C. The MVs were washed at 25,000 *g* for 15 min, the MVs re-suspended in 200 µl PBS. The MVs were the quantified by flow cytometry ExpressPlus YLW-HLog, gating against an unlabelled control.

3.5.10 Sizing MVs by flow cytometry

Isolated MV subtypes were quantified and sized with Megamix beads, particles of known sizes (0.3, 0.5 and 3 μm). The Megamix beads were warmed to room temperature and agitated using a vortex mixer for 30 seconds to ensure thorough separation of the particles. 20 μl of MV subtypes were pipetted into the wells of a 96 well microtitre plate (Corstar) and 20 μl of Megamix beads were added to the MV subtypes. Sterile PBS was used to make the solution up to 200 μl. The MVs were sized by using Guava Millipore ExpressPlus programme. The MV subtype populations were gated using the Megamix beads as a scale for comparison.

3.5.11 The effect of cell concentration on sMV release

THP-1 >95% viability cultured in 10% CGM were washed 2x by centrifugation at 160 *g* for 5 min using RPMI 1640 and finally suspended in RPMI 1640 supplemented with 10% NHS and 2 mM $CaCl_2$ at ascending cellular concentrations: 1 x 10^5 /ml, 5 x 10^5 /ml and 1 x 10^6 /ml before being incubated at 37 ^{0}C in a rotating water bath for 30 mins The cells were immediately cooled to 4 ^{0}C using ice and submitted for sMV isolation. The purified sMVs were quantified using flow cytometry, ExpressPlus assay.

3.5.12 Extracellular calcium effects on sMV release

THP-1 (>95%) viability were washed x2 and finally suspended in RPMI 1640 supplemented with 10% NHS and either 0, 0.5, 1, 2, 4 or 6 mM $CaCl_2$ to a concentration of 5 x 10^5 THP-1/ml being cultured in eppendorf tubes. The cells were incubated at 37

^{0}C in a rotating water bath for 30 min, after which they were immediately cooled to 4^{0}C and submitted to sMV isolation and quantification (as before).

3.5.13 Measurement of intracellular calcium

Cells, typically THP-1, were washed and suspended in sterile D-PBS at a concentration of 1 x 10^6 /ml. 9 µl of 50 mM calcium green-AM (FITC) dye (pre-diluted to correct concentration in DMSO, as directed by the manufacturer) was added to the cells and incubated at room temperature while wrapped in aluminium foil to minimise photo-bleaching of the fluorophore's, slowly shaking for 45 min. The cells were washed x3 in cold, sterile D-PBS at 160 *g* and finally suspended in CGM. Calcium green fluorescence was ascertained using FLUOstar Ω multiplate reader using the fluorescence programme, stimulating the calcium green at A_{485} and reading calcium green bound fluorescence at A_{520}.

THP-1 loaded with calcium green-AM (FITC) dye were stimulated for sMV release using RPMI 1640 supplemented with 10% NHS and 2 mM $CaCl_2$ at 37 ^{0}C for 30 min, ensuring minimum exposure to light to prevent photo-bleaching of the FITC dye. THP-1 were quantified for changes in internal free calcium levels, the results being ascertained as above. Simultaneously, collected cMVs were loaded with calcium green dye (as before), equal numbers of both cMVs and sMVs, (~1 x 10^5 /ml) stimulated from the calcium green dye loaded THP-1 cells previously used were quantified for calcium green dye fluorescence.

3.5.14 Assessment of free Ca^{2+} in MV subtypes using calcium green-AM

THP-1 loaded with calcium green-AM (as before) were stimulated for sMV release. The sMVs were collected, purified and quantified (as before). They were finally suspended 2 x 10^6 /ml in sterile D-PBS. Co-currently cMVs were loaded with calcium green-AM and quantified (as before) and finally suspended 2 x 10^5 /ml in sterile D-PBS. THP-1 loaded with calcium green dye were stimulated for sMV release using ULMFs (0.3 μT 6V A/C) for a total of 30 min. THP-1 were analysed for changes in internal free calcium using FLUOstar Ω (as above) at 0, 5, 15 and 30 min.

3.5.15 Re-stimulation of MVs from THP-1

THP-1 (1 x 10^6 /ml) >95% viability were rested in RPMI 1640 at 37 ^{0}C in 5% CO_2 for 60 min whereupon they were washed 2x with RPMI 1640 and stimulated for microvesicle release using RPMI 1640 supplemented with 10% NHS and 2 mM $CaCl_2$ for 30 min at 37 ^{0}C with mixing. The supernatant was collected and sMVs were isolated and quantified (as before). THP-1 cells were washed 2x with RPMI 1640 and finally suspended in RPMI 1640 at 37 ^{0}C until required. Time points for re-stimulation of microvesicle release using RPMI 1640 supplemented with 10% NHS and 2 mM $CaCl_2$ at 37 ^{0}C with mixing were applied: 0, 10, 20, 30, 60, 90 and 120 min. After re-stimulation for a 30 min period the cells were pelleted at 160 *g* for 5 min. The supernatant was then collected and submitted for MV isolation and analysis using the ExpressPlus programme (Guava Millipore). 1 x 10^6 THP-1/ml >95% viability were rested in RPMI 1640 for 60 min at 37 ^{0}C and the procedure as above was applied. The MV inducing agent was RMPI 1640 supplemented with 10% FBS and 2 mM $CaCl_2$ (complete growth media and calcium: calcium and non-calcium conditions yielded no difference in cMV release).

3.5.16 Increasing concentration of α-tocopherol effects on cMV release

Prior to the experiment, different concentrations of α-tocopherol: 0 pM, 12 pM and 50 pM was added to RPMI 1640 supplemented with 10% FBS and 1% penicillin and streptomycin. THP-1 (>95%) viability were washed x2 and suspended at 5 x 10^5 /ml in one of the 3 α-tocopherol regimes and incubated at 37 ^{0}C in 5% CO_2 for 24 h. The cells were removed by centrifugation at 160 *g* for 5 min and the supernatant was submitted for cMV isolation (as before). The cells were assessed for their viability using Guava Millipore ViaCount assay. The cMVs were sized (as before) and counted using Guava Millipore, ExpressPlus assay.

3.5.17 Collected cMVs were assessed for ROS using an oxygen electrode

In brief, the oxygen electrode was calibrated for oxygen pressure in the presence of saturated KCl dissolved in ddH_2O eliminating oxygen from the system. MV subtypes were then added to the system one at a time: sMVs 1 x 10^5 /ml, cMVs 1 x 10^5 /ml collected from cells cultures in no α-tocopherol, then cMVs 1 x 10^5 /ml collected from THP-1 cultured in 12 ng/L α-tocopherol and finally the cMVs 1 x 10^5 /ml collected from THP-1 cultured in 50 ng/L of α-tocopherol, the electrode being cleaned and reset after each measurement. The MV subtypes were counted by FACs and suspended in PBS.

3.5.18 Isolation of exosomes by ultracentrifugation

Constitutively released exosomes were collected from cell culture media. The exosomes were subject to centrifugation to remove cells: 160 *g* for 5 min, to remove debris: 4000

g for 60 min and to remove MVs: 25,000 *g* for 90 min. Exosomes were finally pelleted by ultracentrifugation at 160,000 *g* ultracentrifugation for 16 h and re-suspended in 100 µl of PBS. The exosomes were frozen at -80 ^{0}C until required.

3.5.19 Exosomes were compared to cMVs by flow cytometry

Exosomes and cMVs were isolated from the same culture medium in 1 ml aliquots, the cMVs isolated first using MV purification protocol and exosomes were isolated from the resultant MV deficient medium using exosomes purification protocol, to compare known extracellular vesicle released from the same parent cells over the same duration: 24 h. cMVs were analysed using Guava Millipore flow cytometer, ExpressPlus programme and used as a control to compare exosomes with. The cMVs and exosomes were compared for population numbers, population morphology and auto fluorescence (GRN-HLog).

3.5.20 Quartz crystal microbalance (QCM) analysis of microvesiculation

QCM analysis of microvesiculation was performed on the q-sense quartz crystal microbalance. The apparatus was set up as per manufacture's specifications and manufacturer specified sub-harmonic frequencies: 1st and 3rd were established. THP-1 (1 x 10^{6} /ml) with a viability >95% were washed 3x and suspended in CGM were loaded on to the QCM sensor and incubated at 37 ^{0}C for 1 h and their mass and viscosity (fluid rigidity) activity recorded at all established sub-harmonics to establish baseline data and observe normal cellular behaviour.

THP-1 (>95%) viability were washed 3x before being suspended in RPMI 1640 supplemented with 10% NHS and 2 mM $CaCl_2$ at a 1 x 10^6 THP-1/ml concentration. They were immediately loaded onto the QCM sensor and incubated at 37 ^{0}C for 1 h and their activity was measured as before to observe changes in mass and viscosity that were associated with MV release.

During analysis the 1st and 3rd sub-harmonics were selected as these surveyed the middle and edges of the sensor and typified the resonance of the whole sensor. The average density of the MV sample is proportional to the frequency and the loss of amplitude.

3.5.21 Dynamic Light Scattering

Dynamic light scattering (DLS) was primarily used as a confirmatory test for MV subtype size difference. The test assumes near perfect spherical structures in a homogenous or well mixed solution. In brief, the diluted MV subtypes in equal concentrations (1 x 10^6 /ml) were transferred to a quartz micro-cuvette and placed into the apparatus. The molecules of PBS were undergoing Brownian motion, scattering and refracting the incidental laser light into a sensor at 90^0 to the laser. As the analyte was in flux the refracted laser intensity varied. Typically, smaller MVs diffuse faster than larger MVs. The translational diffusion coefficient (D_T) was derived using the DLS computer software, the hydrodynamic radius (R_H) was calculated from the D_T. Although it was possible to derive MW of the MVs, the test was not considered robust enough as it relied on to many assumptions.

3.5.22 Nanosight analysis of MVs

Nanoparticle Tracking Analysis (NTA) performs real time sizing and counting of suspended particles (10 nm – 1000 μm), assuming a near perfect sphere it tracks individual particles moving by Brownian motion (Wright, 2012). However particles it cannot track non-metal particles below ~40 nm.

MV subtype samples (1 x 10^6 /ml) were prepared by diluting 1/1000 with sterile RPMI 1640 prior to use and kept at 4 ^{0}C until required. The Nanosight was cleaned using IMS and calibrated following the manufacturer's instructions. 100 μl of MV subtypes were loaded into the reservoir and the software activated to track and record the particle movement and ascertain size. MV film was made by the Nanosight software and VideoPad Video Editor.

3.5.23 qNano particle analyser

The qNano particle analyser was used to detect the presence of MVs and relate their size based upon the impedance of electric current caused by their presence within an electrically conducting stream of buffer or electrolyte that was passed through a pore of known size. MV subtype surface charge was also determined by their baseline blockade duration, that is their flight time in response to an electric field.

The qNano particle analyser was set up and operated as directed by the manufacturer. In brief, the correct size polyurethane pore was selected (1000 nm) and wet using the selected sample buffer, PBS. 75 μl of buffer was pipetted onto the sensor and dried using blue roll to ensure even spread of buffer, before the polyurethane pore was

attached to the sensor by way of specialised grips or 'teeth'. Callipers were used to measure the distance of the teeth and was interpolated to calibrate the pore size by inputting the calliper measurement's on to the qNano computer software. The reservoir beneath the polyurethane pore was filled again using 75 µl of PBS. 40 µl of PBS was then pippetted into the sensor chamber before the vacuum pump was applied and set to 7 or 8 (arbitrary units, recommended by the manufacturer). The voltage was selected, typically 0.3V, however 0.04V was occasionally used should the qNano be unresponsive to the sample, whereupon the controls would be re-calibrated. A check was performed to ensure the current range was 100 – 120nA and that there was little to no noise (below 10pA) during the qNano warm up for 5 min. The pressure pump was then removed and the 40 µl of PBS removed and replaced with 1:100 diluted calibration beads: SKP200 (200 µm) in PBS. The pressure was applied as before until a minimum of 500 particle counts was reached. The scan was recorded for all subsequent sample calibration to a known standard. By removing the SKP200 beads and washing 2x with PBS the MV subtypes were scanned as before and the data processed using the qNano software and calibrated against the SKP200 beads.

Blockade baseline duration is a measure of 'flight time' in an electromagnetic field as a quantification of particle charge. MVs were analysed as before, without pressure being applied so that the particles would not be forced through the pore but would pass through based upon their response to the electromagnetic field.

3.5.24 BCA Protein assay of MV subtypes

The concentration of protein in MV subtypes was determined using BCA Protein Assay kit from Pierce Bioscience, Thermo. Using a biuret reaction, the reduction of Cu^{2+} to Cu^{+} by protein in an alkaline medium and the colorimetric detection of Cu^{+} by bicinchoninic acid colour reagent.

BSA was dissolved in sterile diluent to make a concentration of 2 mg/ml. The BSA solution was then pipetted into a 96 well microtitre plate as per the manufacturer's instructions (BCA Protein assay kit, Pierce Bioscience) to create a standard curve using: 0, 5, 25, 50, 125 and 250 µg/ml in sterile H_2O. 25,000 (1 x 10^6 /ml) MV subtypes were lysed using 1% Triton x-100 at room temperature on a rotating platform for 10 min and then 25 µl were added to empty wells on the micro titre plate. Working reagent was made following the manufacturer's guidelines by adding a ratio of 50:1 Reagent A: Reagent B and was mixed before adding to each well. The microtitre plate was wrapped in foil to minimise photo-bleaching and shaken on a rotating platform for 30 seconds to ensure thorough mixing, after which the plate was incubated at 37 ^{0}C for 30 min. The plate was then cooled to 20 ^{0}C before being analysed using the FLUOstar Ω plate reader measuring absorbance at A_{540}. Unknown protein concentrations of the MV subtypes were determined by interpolation on the generated standard curve.

3.5.25 NanoDrop spectroscopy

MV subtypes were suspended in PBS concentrated to 1 x 10^6 /ml prior to use. The NanoDrop was cleaned with IMS and dried with lint free blue roll before the apparatus was initiated by loading the NanoDrop computer programme. The correct assay

programme was selected, for example a protein assay or an assay for nucleic acids, and the blank controls were measured by pippetting 2 µl of PBS into the sensor. The armature appendage was closed over the sample and the blank control was performed. The apparatus was cleaned after each use with IMS and dried with lint free blue roll before the 2 µl samples were loaded, containing ~2,000 microvesicle subtypes. The armature was closed and the samples were analysed for either DNA or protein, the data being recorded after being analysed. Multiple repeats for each sample type were performed. Re-blanking was also performed as tests may be performed at different times.

MV subtypes were assayed for protein as a confirmatory test using the absorbance of UV light at A_{280} and a general test for DNA or nucleic acid was performed by measuring absorbance at A_{260}. Other data was collected such as absorbance at A_{230} as a measure or CH_2OH and used in conjunction with other biochemical techniques.

3.5.26 Preparation of cell and microvesicle lysates

THP-1 cultured in CGM were washed x2 in RPMI 1640 and finally re-suspended in RPMI 1640 (2 x 10^8 /ml in 10 µl aliquots) before be being lysed using detergent as directed by the manufacturer of the BCA kit. In short, THP-1 were lysed using 2% Triton X-100 (w/v) containing protease inhibitor. To dissolve the proteins, the sample was thoroughly mixed by pipetting the sample and the insoluble debris was pelleted by centrifugation at 5000 rpm for 5 min at 4 ^{0}C, A-4-62 swing out rotor, using 5810R eppendorf centrifuge). The total protein was then subjected to SDS-PAGE analysis.

3.5.27 SDS-PAGE Sample preparation

SDS sample buffer was added to the samples in a 1:4 ratio followed by incubation at 95 ^{0}C for 4 min. The samples were then centrifuged at 2,000 *g* for 2 mins in order to collect all of the liquid, at the bottom of the reaction microtube. The samples were then loaded into the gel wells.

3.5.28 SDS-PAGE Protein molecular weight standards

Prestained Protein-Marker 1 (BioRad) was used as a molecular weight standard. Markers from 10 to 194 kD or 10 to 250 kD were used when interpolating protein gels. The protein markers were loaded into the appropriate positive control wells in 5 µl aliquots.

3.5.29 SDS-Polyacrylamide gel electrophoresis(SDS-PAGE)

The separation of proteins by their molecular mass using SDS-PAGE was carried out by following the protocol published by Laemmi, 1970. The proteins were denatured using sodium dodecyl sulphate (SDS) and separated on an polyacrylamide gel by electrophoresis, using Mini PROTEAN III electrophoresis System (Bio-Rad). Polyacrylamide gels were moulded (102 x 73 mm with a thickness of 0.75 mm) by pouring freshly prepared 12% separating gel solution containing acrylamide/bisacrylamide between two glass plates into the gel cassette firmly placed in a casting frame. Unset separating gel was overlain with H_2O saturated butanol ensuring an even top edge. Once the gel was set the H_2O saturated butanol was poured off and the gel was washed 2x with ddH_2O, the excess water was removed by blotting

with filter paper (Whatman 3 MM, Whatman AG), before stacking gel was poured into the cassette and a comb was inserted into the top of the gel to form the loading wells in the stacking gel.

Once set the polyacrylamide was inserted into the electrode assembly apparatus, inside a clamping flame within the tank of the Mini PROTEAN III electrophoresis system. Electrophoresis running buffer was added to both the inner and outer chambers of the tank and the comb was removed. The wells were washed with running buffer to remove unset gel artefacts. Samples were loaded into the wells using extra long pipette tips. Protein separation by electrophoresis was carried out using 150 V until the bromophenol blue sample front had reached the end of the resolving gel. Gels were stained with Coomassie Brilliant Blue dye and photographed. Unknown proteins were determined by interpolation of the protein ladder standard curve.

3.5.30 Modified Schiff's carbohydrate assay

The modified Schiff's assay was adapted from Kilcoyne et al, 2011. The periodic acid/ schiff's stain was used to detect nonspecific polysaccharides, glycolipids and glycoproteins. Periodic acid oxidises the vicinal diols (adjacent hydroxyl groups on a carbon chain molecule) present in carbohydrates and sugars preventing interaction between carbon molecules not involved in glycosidic links and ring closure, leading to the formation of aldehyde groups. The aldehydes form a ligand complex with the schiff's reagent to give a quantifiable purple colour using colourmetric spectroscopy. 120 µl of periodic and acetic acid reagent were pipetted into each well of a 96 well microtitre plate. 25 µl MV subtypes (2 x 10^6 /ml) lysed using 1% Triton X-100, were

added to the microtitre plate and mixed by pipetting. The plate was then incubated at 37 ^{0}C for 90 min and wrapped in aluminium foil to minimise photo-bleaching of the reagents. The microtitre plate was cooled to 20 ^{0}C and 100 µl Schiff's reagent was added and mixed by pipetting. The modified schiff's assay was allowed 40 min to develop and the absorbance measured at A_{590} using the FLUOstar Ω multiplate reader.

3.5.31 Fourier Transform Infra Red Spectroscopy (FT-IR)

Prior to use, the Bruker FT-IR spectrometer was cleaned using industrial methylated spirit (IMS), set to display absorption and calibrated by performing a background scan, blanking on air. The apparatus was covered to minimise extraneous light, followed by scanning the control calibration media, usually RPMI 1640 or sterile PBS forming a seal with a glass coverslip. The glass coverslips were scanned as a part of the control so that any absorbance from the silicon could be removed from the test samples, control samples using different glass coverslips were taken every 5th scan to reduce the occurrence of impurities within the coverslips that may distort the sample results (however, no such impurities were observed), and scanned 32 times at 1cm^{-1} frequency intervals from 750cm^{-1} to 4000cm^{-1}; however 900cm^{-1} to 2800cm^{-1} was analysed as 3000cm^{-1} plus had interference from H_20. However there were no phosphate bond peaks from the sterile PBS in the fingerprint region (controls and samples were shielded from all external light sources by aluminium foil). Cells were grown on glass coverslips and their viability ascertained using Guava ViaCount assay before being submitted to FT-IR analysis. All samples were washed 3x in sterile PBS to remove media proteins and cellular waste before being mounted on the diamond plate. The coverslips along with sterile PBS were held against the diamond reader and the sample scanned 100 times at 1cm^{-1} intervals from 750cm^{-1} to 4000cm^{-1} and the results baseline

corrected and recorded. Each sample was scanned 3x and an average was taken. Each condition being analysed was repeated 10 – 15 times to ensure reproducibility of the results.

MVs were quantified using Guava ExpressPlus and diluted to $1x10^6$ MVs/ml in sterile PBS. 10-20µl of media or PBS was used as a control calibration and scanned 32 times at $1cm^{-1}$ intervals from $750cm^{-1}$ to $4000cm^{-1}$ (as before with the control cells). 10-20µl of sample was mounted onto the diamond reader and a glass coverslip formed a vacuum seal before being scanned 100 times and the results recorded (as before). Manipulation of the data was carried out using Bruker software to correct baselines, smooth peaks, minus the control sample and pick peaks before statistical and comparative analysis was performed.

For cells and MVs the recorded FTIR data was interpreted using Bruker OPUS software. The scans for the wash or suspension media (typically PBS) were loaded and then scans for a particular cell or MV type were baseline corrected and smoothed (using the smooth by 13 option) and an average of every scan for that cell or MV type (usually 15 or more) would be created, the background wash/suspension media profile values being deducted from the cell or MV type to generate a true profile. The scan profile was cropped and y axis adjusted to show the maximum size plotted graph. Amide 1 at $1640cm^{-1}$ was used as an internal standard (as it was impossible to incorporate an appropriate standard as they were toxic to cells) and all relevant peaks were normalised as a ratio to amide 1 and presented in a bar graph format. Peaks of

particular interest were found at 2350cm^{-1}, 1538cm^{-1} (amide 2), 1460 cm^{-1}, 1253 cm^{-1}, 1240 cm^{-1} and 1080cm^{-1} (Table 1.1).

FT-IR had indicated that MV subtypes carry nucleic acids. To quantify nucleic acid, MV subtypes (1 x 10^6/ml) were lysed by incubating with 1% triton x-100 at 4^{0}C shaking for 5 min. The resulting lysate was immediately quantified for nucleic acids using NanoDrop.

3.5.32 Fluorescence microscopy

For non-adherent cells, coverslips were deposited in the cells of a 6 or 12 well plate (Corstar) and sterilised using UV light for 30 min. 100 – 200 µl of polylycein was deposited on each cloverslip and incubated for 1 h at 37 ^{0}C in 5% CO_2 conditions. Cells, typically THP-1, were split from culture in CGM (>95% viability) and washed 3x by centrifugation at 160 *g* for 5 min before being finally suspended to the required concentration for the experiment. The polylycein was removed from the coverslips and the non-adherent cells were added at a high concentration and incubated at 37 ^{0}C in 5% CO_2 for 1 h. Cells were fixed using 4% paraformaldehyde at 37 ^{0}C for 10 min and then gently washed 2x using sterile PBS before being mounted on microscope slides with DAPI-VECTASHIELD medium (Vector Laboratories Inc, Burlingame CA).

For adherent cells, coverslips were deposited in the wells of a 6 or 12 well plate (Corstar) and sterilised using UV light for 30 min. Cells were spilt from >85% confluent culture by washing 2x with sterile RPMI 1640 and removal using 0.25% trypsin EDTA

for 3 - 10 min at 37 ^{0}C. The trypsin was deactivated by adding CGM once the cells had detached and the cells were washed 2x by centrifugation at 160 *g* for 5 min before finally suspending in CMG at a concentration of 1 x 10^{5} cells/ml and incubated at 37 ^{0}C in 5% CO_2. The cells were allowed to grow to confluence before being experimented upon. The cells were then labelled using fluorescently tagged antibodies, such as anti-human CD55 or anti-human H1R by following immune-labelling protocols as directed by the supplier. Fixing protocol was followed (as before). Fluorescence microscope (1X81 motorised inverted fluorescence microscope, Olympus Corporation) was used to collect images.

3.5.33 Transmission Electron Microscopy of MV subtypes

The use of hazardous chemicals required that the protocol was performed in a fume cupboard. THP-1 (5 x 10^{6} /ml) were washed 2x with RPMI 1640 and suspended in prewarmed RPMI 1640 supplemented with 0.5 mM $CaCl_2$ (37 ^{0}C) in 15 ml centrifuge tubes. They were either stimulated or not (control) with 5% NHS and incubated in a waterbath at 37 ^{0}C for 30 min, after which the cells were fixed by adding 1ml of 0.1 M fixative solution (3% glutaraldehyde in 0.1 M sodium cacidylate buffer pH 7.2) and incubated for 1 h at 37 ^{0}C. Fixed cells were collected by centrifugation at 300 *g* for 5 min using an A-4-62 swing out rotor for 5810R centrifuge (Eppendorf). Before fixing, pelleted cells were transferred to 1,5ml microtubes and washed 2x with 0.1 M sodium cacodylate buffer pH 7.2 using a microfuge at 300 *g* for 5 min. Samples were post fixed by incubation at 0 ^{0}C for 1 h with 1% osmium tetroxide solution (Sigma-Aldrich) 1:1 0.2 M sodium cacodylate buffer, followed by 3x washes with ddH_2O and block stained by suspending cells in 1% uranyl acetate (aq) for 12 h shaking. The cells were washed 2x using ddH_2O and suspended in 1% hot aragose and pelleted by centrifugation at 5,000

g for 5 min, before agargose solidified. Once solidified the cell pellects embedded in aragose were removed from the 1.5 ml microtubes and cut into small slices. They were placed into a 10 ml glass vial for processing.

The cells were dehydrated in an ascending ethanol series (from 70% to 100% absolute ethanol (v/v) for 30 min each regimen) and washed 2x for 30 min with propylene oxide. Once the propylene oxide was removed the cells were saturated with 1x propylene oxide: 1x agar (mix of 4,.8 g agar resin, 3.6 g MNA, 1.9 g DDSA and 0.2 g BDMA from Agar Scientific, Essex, UK) and were incubated at 20 °C for 12 h shaking.

Infiltrated samples were changed 2x with 100% agar resin for 1 h at 20 °C and embedded in capsules using applicators. Then the samples were polymerised at 60 °C for 24 h.

Furthermore, MV subtypes and exosomes were separately fixed and infiltrated with agar resin. The polymerised blocks were sent for cutting, staining and image capture at the London School of Hygiene and Tropical Medicine, Electron Microscopy Unit. Ultra thin sections were cut on a Leica Ultracut R ultra microtome and picked up onto Pioloform film copper grids. The secrions were stained for 10 min in Reynolds Lead Citrate stain before washing in ddH_2O and examined using a Jeol JEM – 1200 Ex II Electron Microscope. Digital images were taken with a 1K, slide mounted AMT digital camera (Advanced Microscopy Techniques Corp. 3 Electronics Ave., Danvers, MA 01923 USA, supplied by Deben UK Ltd., IP30 3QS).

Negative staining for MV subtypes and exosomes were also performed at the EM Unit at the London School of Hygiene and Tropical Medicine. They were stained with 2% uranyl acetate (aq) or 2% phospotungstic acid pH 6.8 and Bacitracin (aq) (300 µg/ml diluted 1:10 in the negative stain, as a spreading agent). Using fine tipped forceps to manipulate the 400 mesh copper grids with a pioloform support film (grids and Pioloform powder from Agar Scientific Ltd., Essex, CM24 8DA). The grids were pre-treated with 1% Alciam Blue 8GX (aq) for 10 min before washing with ddH_2O. 5 µl of sample was placed in the grids for 1 min. This was then removed by touching the grid edge with a strip of filter paper and replaced with 5 µl of the stain for 1 min. The stain was then removed in the same way and the grid was air dried before examining using the Transmission Electron Microscope. Digital imahes were recorded using the AMT digital camera (as before).

3.5.34 Delivery of calcium via MVs

THP-1 (>95% viability) were loaded with calcium green-AM (as before) washed 2x with D-PBS before being suspended in sterile veranol buffer at a concentration of 1 x 10^6 /ml. The THP-1 were co-incubated with cMVs 2 x 10^5 /ml (10 µl ~2,000 cMVs) and sMVs 2 x 10^6 /ml (5 µl ~10,000 sMVs) respectively for 1 h at 37 ^{0}C in 5% CO_2. THP-1 were then cooled rapidly to 4 ^{0}C before being washed 2x with cold RPMI 1640 and finally suspended in RPMI 1640 (at 4 ^{0}C). They were analysed for changes in internal free calcium levels using the FLUOstar Ω multiplate reader (as before) as a measure of deliverable free calcium by MV subtypes.

3.5.35 C5b-9 expression after MV release

NHS containing membrane attack complex C5b-9 and 'random' antibodies derived from the donor are able to initiate the formation of Membrane Attack Complex (MAC), leading to the formation of sMVs. Adherent HeLa cells were used to cut down on wash and centrifugation steps. In short, sublytic MACs were deposited on the cells stimulating MV release, the HeLa were labelled before and after MV release and the relative abundance inferred as the release of MACs on MVs.

HeLa cultured in CGM (>95% viability at 5 x 10^5 /ml) were washed 2x by centrifugation at 160 *g* for 5 min with sterile PBS and finally suspended in 200 µl of 10% FBS 1% NaN_3 in PBS, containing 2 µl/ml of mouse anti human C5b-9 and incubated at 4 ^{0}C for 45 min shaking in dark conditions. The HeLa were then washed 2x by centrifugation at 160 *g* for 5 min in cold sterile PBS and finally suspended in 200 µl cold PBS containing 3% BSA and rabbit anti mouse FITC conjugated antibody 1:320. The cells were shaken at 4 ^{0}C in dark conditions for 1 h after which the cells were washed 3x in sterile PBS and finally suspended in 200 µl PBS containing 3% BSA and 1% NaN_3. HeLa were immediately analysed using flow cytometry and the ExpressPlus programme, gating against an unlabelled control.

HeLa were analysed both before (incubated with sublytic MAC however analysed 15 - 5 mins. The cells were also kept at 4 °C and suspended in NaN_3 to prevent protein synthesis) and after sMVs had been released. sMV release was stimulated using RPMI 1640 supplemented with 10% NHS and 2 mM $CaCl_2$. Co-currently a negative control of HeLa were also incubated with RMPI 1640 supplemented with 10% Heat Inactivated

NHS (previously, NHS was incubated at 56 ^{0}C to deactivate the heat labile complement proteins, primarily complement C2) and 2 mM $CaCl_2$.

3.5.36 Receptor transfer from HeLa (DAF$^+$) to CHO (DAF$^-$) via HeLa sMVs (DAF$^+$)

HeLa (5 x 10^5 /ml) were cultured in RPMI 1640 supplemented with 10% FBS, 1% Penicillin and streptomycin with 50 nM PMA, incubated at 37 °C in 5% CO_2 humidifier for 24 - 48 h, to increased expression of DAF. This was measured using rabbit anti human DAF and mouse anti rabbit FITC labelled antibody (as before), quantified by Guava Millipore FACS, ExpressPlus programme.

HeLa expressing increased levels of DAF were cultured with RPMI 1640 supplemented with 10% NHS and 2 mM $CaCl_2$ to stimulate MV production. The sMVs were collected as previously described (1x CHO K1: 1x sMV, unless otherwise stated).

CHO K1 (DAF$^-$; 1 x 10^6 /ml) were cultured in Costar 6-well plates (some were grown on glass coverslips to enable fluorescent microscopy). HeLa MVs DAF$^+$ were incubated with CHO K1 at the desired ratios (0:1, 1:1, 2:1 and 5:1) in RPMI 1640 for 1 h at 37 ^{0}C. CHO K1 were washed with sterile PBS 3x and finally cultured in 200 µl of 10% FBS 1% NaN_3 in PBS. 2 µl/ml rabbit anti human DAF antibody (Complement Technology) was incubated with CHO K1 at 4 ^{0}C for 45 min on a rotating table. The cells were washed x3 in sterile PBS at 4 ^{0}C and suspended in PBS supplemented with 10% FBS. Mouse anti rabbit FITC conjugated antibody (1/3000) was incubated for 45 min with the primary

antibody labelled cells (as before). The cells were finally washed 3x with 4 ^{0}C PBS supplemented with 3% FBS and 1% NaN_3 (200 µl) to supplement the cells and prevent protein synthesis and receptor uptake (CHO K1 DAF$^+$ that were assessed for their receptor functionality were not suspended in 3% FBS and 1% NaN_3). CHO K1 and HeLa were labelled with rabbit anti human CD55 and mouse anti rabbit FITC were gently removed from culture flask using PBS (without calcium) with 5% EDTA for 15 min at 37 °C. The resultant supernatant was washed (160 *g* for 5 min) and the cell pellet was suspended in 4 ^{0}C sterile PBS. The cells were analysed for DAF using Guava ExpressPlus programme.

CHO K1 DAF$^+$ (5 x 10^5 /ml) >95% viability were cultured in RMPI 1640 supplemented with 0 - 25% NHS to assess the function of the transplanted DAF. The cells were incubated for 60 min at 37 ^{0}C in 5% CO_2 humidifier and were immediately quantified for changes in viability using Guava ViaCount assay.

3.5.37 Growth assay

Typically, healthy cells (>95% viability) cultured in CGM were washed 2x in RPMI 1640 before being suspended to the required concentration in the appropriate growth medium. Cells were monitored at 24 h intervals and their viability and cell number was assayed using Guava Millipore's ViaCount assay. Experiments would be allowed to run 24 - 96 h depending upon the phenomenon being observed. Different growth assays were used, either to observe the effects of MV subtypes on cell behaviour, to observe the effects of ULMFs with a treatment of anticancer drugs on cell health or the effects of ULMFs on cell growth and migration.

THP-1 >95% viability were washed 2x and finally suspended at a concentration of 1 x 10^5 /ml in RPMI 1640 supplemented with 10% NHS and 1% penicillin and streptomycin (except for the negative control, that was cultured in complete growth media) and transferred to sterile 12 well plates (Corstar). Microvesicle subtypes were added to the cells to observe the effects of either cMVs or sMVs on cells (except the negative control and the positive control that was cultured in sublytic NHS without the addition of MVs) in different ratios: 1:1, 2:1 and 5:1 before being incubated at 37 ^{0}C in 5% CO_2. At 24 h intervals for a total of 96 h 50 µl of the THP-1 from each well were assayed using flow cytometry, ViaCount assay. At 72 and 96 h the individual wells of the plates were photographed using the bright field image using the Fluorescent microscope (1X81 Olympus Corporation, Germany).

MV subtypes derived from THP-1 were co-cultured in a 0:1, 1:1, 2:1 or 5:1 ratio with THP-1 at 37 ^{0}C in 5% CO_2 for 96 h. At 72 and 96 h the THP-1 were evaluated for their viability and cell number, comparing to the controls, using the Guava Millipore ViaCount assay and digital microscopy using an Fluorescent microscope (1X81 Olympus Corporation, Germany)to record images.

3.5.38 THP-1 lysis and avidity assay MV avidity for MAC

MV subtypes have a quantifiable difference in avidity for MACs or protein S. whether this could be used to identify difference in physiological roles. THP-1 (5 x 10^5 /ml) were cultured with 2x THP-1:1x MV subtype in halving dilutions to 64x THP-1:1x MV subtype.

MV subtypes were counted by flow cytometry, ExpressPlus and 2.5 x 10^5 MV subtypes/ml suspended in halving serial dilutions from 1/2 to 1/64 and suspended in RPMI 1640 supplemented with 45% NHS diluted in complement diluent buffer (CDB) for 10 min at 37 ^{0}C. THP-1 (5 x 10^5 /ml) were washed 2x with sterile RPMI 1640 and suspended in complement diluent buffer and incubated with one of the preselected concentrations of MV subtypes. THP-1 were incubated at 37 ^{0}C for 90 min before being washed 2x with sterile RPMI 1640 and finally suspended in RPMI 1640 and assessed for viability using ViaCount.

3.5.39 Salmonella *lysis assay*

Salmonella typhimurium were cultured on nutrient agar spread plates at 37 ^{0}C for 24 - 48 h (as before). *Salmonella* colonies were collected and suspended in sterile PBS and mixed thoroughly by pipetting. *Salmonella* were then diluted with PBS containing 45% NHS and 1 x 10^5 MV subtypes/ml and incubated for 1 h before being cultured on a dilution series of nutrient agar plates (10^{-4}, 10^{-5}, 10^{-6} and 10^{-7}) and incubated at 37 ^{0}C for 24 - 48 h (as before). The colonies were counted and the data collected.

3.5.40 ULMFs generate plasma membrane pores

ULMFs interact with the polar groups on phospholipids and proteins, causing them to align to lines of magnetic force. Stimulation with ULMFs would vary across a 12 or 24 well plate (not significantly), however, repeat experiments were designed to used wells in the same co-ordinate position to minimise field fluctuations. All ULMF densities used were 0.3 μT 6V A/C current unless otherwise stated.

The ULMF plates were housed with the Heraeus incubator set to 37 ^{o}C 5% CO_2, the magnetic field was quantified using TES-1390 EMF Tester using the Tesla option. The A/C magnetic field was found to vary from 0.1 – 1 μT depending upon the plate settings, the background field was 0.08 μT while the magnetic field generator was switched on, but fell to negligible when the generator was switched off. It was decided to set the plates to generate 0.3 μT 6V A/C electromagnetic field.

3.5.41 Nexin assay in ULMF

Nexin assay was used to assess the apoptotic stages of a population of cells using flow cytometry. The Nexin assay contained two dyes, annexin V and 7-AAD. Annexin V binds to outer membrane expressed PS as a measure of early apoptosis and 7-AAD passes through outer membrane pores and the nuclear membrane breaches binding to dsDNA as a measure of late apoptosis. Cells were incubated with the Nexin assay before being analysed by flow cytometry using the Guava Nexin programme.

THP-1 cultured in CGM (>95% viability) were washed 2x by centrifugation at 160 *g* for 5 min using RPMI 1640 before being suspended at 5 x 10^5 /ml in CGM and dispensed into sterile 12-well plates (Corstar) and the cells exposed to 0.3 μT 6V A/C ULMFs within a 37 ^{o}C incubator for 2 h. After this the cells were immediately incubated with Nexin assay following the manufacturer's protocol. Cells were typically incubated at 37 ^{o}C for 20 min in the dark to reduce photo-bleaching before being analysed using Guava Millipore Nexin programme to assess apoptotic stages. The labelled, untreated control was initially used to set up the relevant gating on the Guava Millipore Nexin programme before the experimental cells were analysed. Gating was used to

discriminate healthy cells from cells in early or late apoptosis and the gating also included identification of dead cells.

3.5.42 Incubation of THP-1 with PI with ULMF

Using PI it was possible to determine the extent of the membrane damage and indeed whether membrane pores had formed of whether ViaCount and calcium was entering the cells via ion channels or some other undetermined route.

THP-1 (5 x 10^5 /ml) were washed 2x with RPMI 1640 and suspended in RPMI 1640 supplemented with 10% FBS and 1% penicillin and streptomycin and dispensed into 24 well plates (Corstar). 5 μM PI was added to the cells in culture before one plate was incubated at 37 ^{0}C, the other plate was stimulated with 0.3 μT 6V A/C ULMFs in 37 ^{0}C for 30 min. THP-1 were cooled at 4 ^{0}C and washed 2x with RPMI 1640 and finally suspended in cold PBS before being assessed for PI inclusion by flow cytometry, ExpressPlus and FLUOstar Ω multiplate reader A_{626}.

3.5.43 Lamp-1 expression

Calcium influx causes rapid membrane repair mechanisms whereby lysosomes or other organelles 'plug' the transmembrane breach to limit damage caused by calcium. Membrane damage caused by ULMFs was measured by quantifying membrane increase in CD107a (LAMP-1) after ULMF stimulation.

THP-1 (5 x 10^5 /ml) were washed 2x with RPMI 1640 and finally suspended in RPMI 1640 supplemented with 10% FBS and 1% penicillin and streptomycin before being dispensed into sterile 24 well plates (Costar). One plate was incubated at 37 ^{0}C while the other plate was stimulated with 0.3 μT 6V A/C ULMF at 37 ^{0}C for 30 min, after which both THP-1 plates were rapidly cooled to 4 ^{0}C, washed 2x with RPMI 1640 and suspended in sterile PBS. Anti-LAMP-1 (50 μM) was added to the THP-1 and incubated at 4 ^{0}C for 45 min, shaking in the dark to prevent photo bleaching of the fluorescent dye. THP-1 were washed 2x with sterile PBS and quantified for anti-LAMP-1 using flow cytometry, ExpressPlus programme.

3.5.44 Stimulation of microvesicles using Ultra Low-frequency Magnetic Fields

The usage of ULMFs to generate MVs was assessed. Cells (typically THP-1) were washed 2x with RPMI 1640 and finally suspended in RPMI 1640 supplemented with 10% FBS and 1% penicillin and streptomycin. The cells were assayed for their viability and number using ViaCount reagent and Guava Millipore flow cytometer before being suspended at the required concentration (typically 5 x 10^5 /ml) and dispensed into 12 or 24 well plates (Costar). The cells were then stimulated with 0.3 μT 6V A/C ULMFs for 30 min at 37 ^{0}C. Then the cells were centrifuged at as before to isolate sMVs. They were quantified by flow cytometry using the ExpressPlus.

3.5.45 Assessment of membrane re-sealing and calcium influx after ULMF-mediated damage

Lysosomes migrate rapidly to the membrane in response to uncontrolled increases in intracellular calcium and fuse with the plasma membrane to 'patch' the breach. The

fusion event was detectible by lysosomal proteins that were transiently expressed externally after such a fusion event. LAMP-1 was the most suitable candidate to assay as it typically is not associated with healthy cell plasma membranes.

THP-1 (>95% viability) cultured in CGM were washed 2x in RPMI 1640 and suspended at 5 x 10^5 /ml in CGM and dispensed into 12 well microtitre plates. The cells were stimulated with ULMFs for 30 min after which they were rapidly cooled to 4 ^{0}C. As directed by the manufacture, anti-LAMP-1 Alexa Fluor 488 (1 μg/10^6 cells) was incubated with THP-1 at 4 ^{0}C for 1 h while shaking. Labelled cells were washed by centrifugation at 160 *g* for 5 min 3x with RPMI 1640 and finally suspended in cold RMPI 1640 before being analysed by both flow cytometry Guava Millipore ExpressPlus programme and FLUOstar Ω multiplate reader absorbance programme at $_A$488. In both cases and labelled but un-stimulated control was used for gating.

To investigate calcium influx in response to ULMF induced membrane breaches, THP-1 (>95% viability) were washed and plated as above before being stimulated with ULMFs. Cells were stimulated for 5, 10, 15 20 and 30 min with ULMF, after which they were rapidly cooled to 4 ^{0}C and loaded with calcium green-AM as previously described. The cells were washed 2x with sterile PBS and finally suspended in PBS. The cells were assessed for Ca^{2+} influx by comparison to an untreated control using the FLUOstar Ω multiplate reader absorbance at A_{520} programme as previously described.

3.5.46 Blocking stretch Calcium ion channels or quenching Calcium with EGTA

ULMFs cause MV release and lower the viability of cells both transiently for short exposure or forcing the cells into late apoptosis for longer exposure. This was due to the formation of membrane pores or interactions with ion channels. To investigate the role that ion channels and membrane pores play in ULMF MV release and changes in cell viability, THP-1 (5 x 10^5 /ml) were washed 2x with RPMI 1640 and finally suspended one of the following culture regimens: RPMI 1640, RPMI 1640 supplemented with 10% NHS and 2 mM $CaCl_2$, RPMI 1640 supplemented with 5 mM EGTA or RPMI 1640 supplemented with 200 µM $GdCl_3$. The cells were dispensed into 24 well plates (Costar). The control cells were incubated at 37 °C, the experimental cells were stimulated with 0.3 µT 6V A/C ULMFs for 30 min at 37 °C before being removed from the magnetic field.

Immediately, the cells were cooled to 4 °C and the cells pelleted and re-suspended in RPMI and their viability assessed by flow cytometry ViaCount assay. The supernatant was submitted for MV isolation (cMV isolation as the cells had been stimulated) and the MV morphology and population count was assessed by flow cytometry ExpressPlus (as before).

3.5.47 Assessment of H_2O_2 uptake under the influence of ULMFs

ULMF induced membrane breaches may enhance the uptake of membrane permeable H_2O_2. THP-1 (>95% viability) cultured in CGM were washed 2x by centrifugation at 160 *g* for 5 min with RPMI 1640 and suspended at 5 x 10^5 cells/ml before being suspended in RPMI 1640 supplemented with 10% FBS and 1% penicillin and

streptomycin and 1 mM H_2O_2. THP-1 were then stimulated with ULMFs for 30 min and the cells were immediately assayed for their viability using ViaCount reagent and Guava Millipore flow cytometer. The ULMF stimulated cells were compared to H_2O_2 stimulated and non stimulated controls.

3.5.48 Treatment of cancer cells with chemotherapeutic agents in the presence of ULMFs

Cultured cells were washed and treated with various concentrations of Methotrexate and stimulated with ULMFs for 30 min. The cells were cultured for 48 h with Methotrexate, cells being assayed for viability and cell number at 24 h intervals. Repeats were performed with experimental conditions being reproduced at the same co-ordinate positions to reproduce exact ULMF stimulation.

THP-1 were cultured in CGM (>95% viability) and washed 2x by centrifugation at 160 *g* for 5 min and finally suspended in CGM to a concentration of 1 x 10^6 /ml and dispensed into sterile 12 well plates (Costar). THP-1 were subjected to 10, 1 and 0.1 µM concentrations both with and without stimulation with ULMFs. THP-1 within ULMFs were stimulated for 30 min at 37 ^{0}C and then incubated for 48 h at 37 ^{0}C in 5% CO_2.

PC12 were grown in 12 well plates (Costar) to 1 x 10^6 /ml in CGM with >95% viability and were washed 2x with RPMI 1640 and re-cultured in CGM supplemented with 1 and 0.1 µM concentrations of methotrexate for 48 h at 37 ^{0}C in 5% CO_2. PC12 were then washed 2x with RPMI 1640 and removed by 0.25% Trypsin EDTA and washed in CGM

to deactivate the trypsin before being analysed by flow cytometry ViaCount assay to assess both cellular proliferation and viability.

3.5.49 Scratch injury

HeLa (>95% viability) cultured in RPMI 1640 supplemented with 10% FBS and 1% penicillin and streptomycin were grown to confluency in 6 well plates at 37 ^{0}C in 5% CO_2. The HeLa adherent culture were injured by scratching a 200 µl pipette tip along the equator of the well causing a 1500 µm 'clean scratch', devoid of cells. The HeLa were washed x2 in RPMI 1640 and finally suspended in 1 ml RPMI 1640 – phenol red, supplemented with 10% FBS and 1% penicillin and streptomycin. The injured HeLa cultures were all bright field photographed using a fluorescent microscope (1X81 Olympus Corporation, Germany) along the entire length of the scratch injury using x40 lens. The test wells were subjected to ULMFs in a 37 ^{0}C incubator for 30 min. The control cells were not exposed to the ULMF but were incubated at 37 ^{0}C. After this the culture was removed from the ULMF or the 37 ^{0}C incubator and cultured at 37 ^{0}C in 5% CO_2 for 48 h.

After 24 h the cells were washed 2x and re-suspended in 1 ml RMPI 1640 supplemented with 10% FBS and 1% penicillin and streptomycin. The cells were then photographed under bright field (as before) using the fluorescent microscope (1X81 Olympus Corporation, Germany). The control and test samples were then assessed for their viability and cell number using Guava Millipore ViaCount reagent (as before). The HeLa were washed using RPMI 1640 2x before 100 µl of 0.25% trypsin EDTA was added to the wells and incubated for 3 - 10 min at 37 ^{0}C, in order to detach the cells.

Once detached the 0.25% trypsin EDTA was deactivated by adding 900 µl of CGM and the cells were pelleted by centrifugation at 160 *g* for 5 min. The HeLa were re-suspended in 1 ml RPMI 1640 and analysed using ViaCount reagent. After 48 h the procedure was repeated. The scratch injury in each well was measured randomly at 20 points at right angles along the entire scratch and the collected data was interpreted by GraphPad prism 4 statistical analysis.

3.6 Statistical analysis

Statistical analysis were performed using students' *t*-tests or ANOVA, a P-value of <0.05 was considered significant. Data was presented as means ± SEM. Statistical analysis was performed using GraphPad Prism 4.0 software package, SPSS 12.0 or radial graph using Microsoft Office Excel 97. Fourier transform was performed as a part of the OPUS software package.

4. Isolation and physical characterisation of microvesicles

4.0 Introduction

Many biological functions have been assigned to MVs, ranging from immunological roles to delivery of miRNAs or virulence factors to cells. No consensus currently exists for the isolation and characterisation of MVs, although there is a degree of similarity between actively publishing groups. One major consideration is mistaking exosomes for smaller MVs and even confusion of MVs for apoptotic bodies. Moreover MVs can be divided into two distinct subtypes depending upon their mode of isolation and stimulatory conditions, as was referred to in the literature review detailing that MVs were either stimulated or collected from culture media (Jayachandran *et al*, 2012; Palmisano *et al*, 2012; Zhang *et al*, 2012a). To this end MVs were stimulated (sMVs) or collected (cMVs [constitutively produced]) and quantified in terms of cell number. A rigorous assessment of centrifugation speeds was also performed as MVs may not be robust enough to withstand strong shear stresses.

MV subtypes were subjected to rigorous biophysical tests to quantify differences in the physical characteristics of subtypes. Key differences examined were size and mass (further biochemical differences are discussed in Chapter 5). Biophysical tests included flow cytometry, q sense microbalance, Nanosight particle tracking, qNano, spectroscopy, NanoDrop, dynamic light scattering and TEM/ microscopy.

Microvesicles (MVs) are released from the plasma membrane of cells for a variety of reasons and therefore have a diverse range of physiological functions. The constitutively MVs, cMVs (released without stimulus) or the stimulated ones, sMVs,

were stimulated, usually with RMPI supplemented with 10% NHS and 2mM Ca^{2+} (ions formed by dissolving $CaCl_2$ in RPMI or PBS).

Beyond a detailed physical characterisation of cMVs and sMVs the data presented in this chapter will attempt to identify any differing biological roles between these two MV subtypes.

4.1 CGM, NHS or RPMI culture medium has no significant effect upon cell viability

Differing culture media containing RPMI 1640 supplemented with 1% penicillin and streptomycin, and either 10% FBS, 10% NHS or no serum were investigated for their effects on cell viability as an initial step to determine whether extended periods of THP-1 cultured in different media would adversely affect their typical physiological behaviour. THP-1 maintained high levels of cell viability, however RPMI 1640 cultured cells dropped 2% to 93%, indicating that the serum-free condition has a small effect on cell health over 24 h.

Although statistically insignificant, 10% NHS cultured cells had a lower viability than 10% FBS (Fig 4.1) owing to the possible deposition of sublytic Membrane Attack Complex (MAC) on THP-1 that may have 'tipped the balance' in the fate of pseudoapoptotic cells leading to late apoptosis and cell death. Experimental procedures were designed around potential limitations of THP-1 and HeLa in culture medium, HeLa for example optimally growing in DMEM supplemented with 10% FBS and 1% penicillin and streptomycin.

4.2 Phosphatidyl Serine (PS) levels are expressed differently on healthy and stressed THP-1

Stimulation of THP-1 with 5 and 10% NHS caused membrane poration by the deposition of MACs. The insertion of MAC into the plasma membrane or use of activating/damaging agents allows the influx of Ca^{2+} into the cell down a concentration gradient increasing cellular Ca^{2+} levels. Free Ca^{2+} binds to membrane associated enzymes scramblase and flippase inhibiting their action of maintaining membrane

asymmetry and allowing PS to reach an approximately equal equilibrium laterally across the membrane and be externally expressed. Increased PS expression is typical of a cell undergoing early apoptosis as healthy cells maintain membrane asymmetry. The increased PS expression is typically identified using Annexin V binding, either conjugated to a fluorescent marker such as FITC or detected using a fluorescent antibody to Annexin V typically conjugated to FITC. The PS Annexin V complex was detected using Guava Millipore ExpressPlus programme. This proved to be an invaluable diagnostic tool in conjunction with the EasyCyte programme for the Guava flow cytometer and the Viacount assay, for the detection of apoptotic behaviour in cell populations.

The relevance of increased PS expression in NHS stimulated cells indicated (Fig 4.2) that a pseudoapoptotic process had been initiated and that the membrane associated enzymes had been inactivated and membrane asymmetry resulted. This process did not lead to late apoptosis as THP-1 populations cultured in 10% NHS for 24 h did not show any significant decrease in viability or increase in cell death. The pseudoapoptotic effect of increased PS expression was transient and membrane integrity was naturally recovered and the viability of the cells increased to >95%.

4.3 THP-1 number affects MV production in 10% NHS

The initial cell number influences sMV production when using a fixed volume of RPMI 1640 supplemented with 10% NHS and 2 mM CaCl to stimulate microvesiculation. To ascertain optimal conditions for 10% NHS stimulated MV release, THP-1 populations were counted 1 x 10^5 /ml, 5 x 10^5 /ml and 1 x 10^6 /ml respectively. The cells were

stimulated to microvesiculate and the resultant MVs collected were quantified using Guava Flow Cytometer, ExpressPlus, where MV numbers were compared.

As seen in Fig 4.3 there were significant differences between 1 x 10^5 /ml and both 5 x 10^5 /ml and 1 x 10^6 /ml, indicating that the deposition of MACs is essential to MV formation in this instance. Furthermore a fixed amount of NHS was used as a stimulus, such that only an absolute amount of MAC could be deposited upon the cells. If only one MAC per cell were required for the formation of a MV, then the levels of MVs released should have remained constant across all THP-1 concentrations. However there were significantly more MVs within the 1 x 10^5 /ml THP-1 populations, indicating that more than one MAC per cell was required to release one MV. The cell: MAC ratio was lower, therefore more MAC per cells was deposited onto the membrane. When the cell: MAC ratio decreased, MACs would have been deposited approximately evenly cross the cell population. However the MV number decreased showing that more than one MAC were required to produce one MV.

Optimal sMV conditions were pinpointed at 1 x 10^5 THP-1 /ml. *In vivo* implications of this observation are that serum-acclimatised cells would produce less MVs /ml as the cell density /ml is higher in a complete organism. Furthermore, repairable membrane damage would have to be reasonably extensive to cause sMV release.

4.4 The effect of [Ca^{2+}] on the release of sMVs from THP-1 monocytes

Free intracellular calcium leads to MV release (Fig 4.4) by binding to cytoskeletal associated enzymes such as calpain, leading to cytoskeletal cleavage and the depolymerisation of F-actin to the poorly organised G-actin and the formation of a membrane bleb that eventually pinches off.

Intracellular calcium is stored within organelles until required, an excess of calcium causing a multitude of undesirable effects. Consequently the cell needs to regulate excess calcium effectively. Cells are efficient at sequestering excess calcium into the rough endoplasmic reticulum and other suitable organelles. However should the bio-available calcium exceed the cell's calcium storage potential or remain localised to an insult site then microvesiculation is an important calcium homeostatic mechanism. Microvesiculation of MVs resets internal calcium levels to safe levels (Fig 4.5a).

Typically 1 – 2 mM of extracellular Ca^{2+} leads to microvesiculation (Fig 4.4) and the release of sMVs by influx into the cytoplasm. However sMVs were released at each calcium concentration observed. At 0 - 0.5 and 4 mM [Ca^{2+}], microvesiculation was at basal levels. At 6 mM+ release (not shown) many vesicles counted were not accountable as MVs as the cells were undergoing irreversible apoptosis (Giorgi *et al*, 2012; Roos *et al*, 2012) releasing many potential apoptotic bodies.

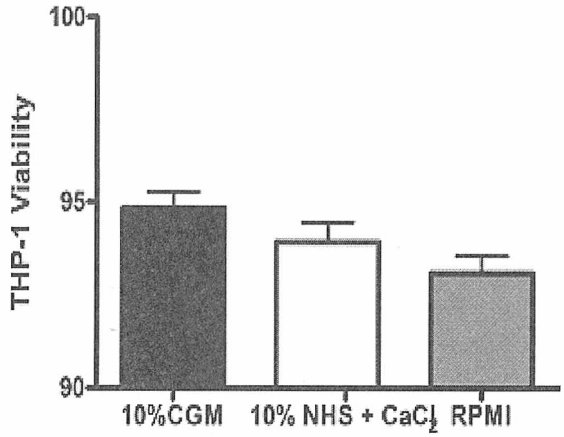

Fig 4.1 CGM, NHS or RPMI culture medium has no significant effect upon cell viability. THP-1 (1 x 10^6 /ml) were cultured in RPMI 1640 or RPMI 1640 supplemented either FBS, NHS to observe changes in viability. The cells maintained high viability for 24 h, although RPMI 1640 viability dropped to approximately 93 ± 0.5%.

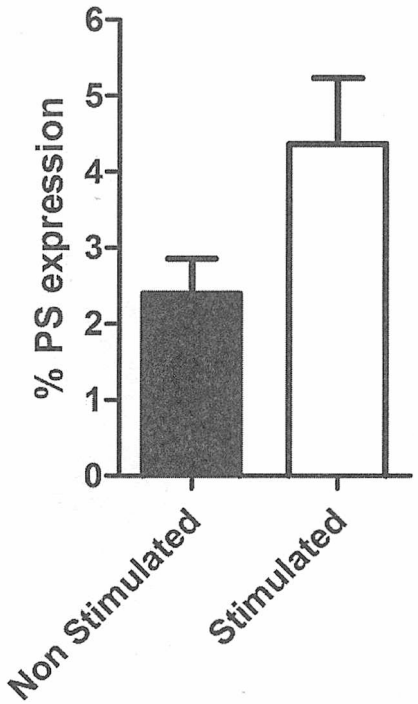

Fig 4.2 Phosphatidyl Serine (PS) levels are expressed differently on healthy and stressed THP-1. Non stimulated THP-1 express lower levels of externalised PS ~2.5% than stimulated (stressed) THP-1 ~4.5% using RPMI supplemented with 5% NHS and 2 mM Ca^{2+}. This is a typical result for any stressed, activated or stimulated cell that may be membrane attacked, damaged or entering apoptosis.

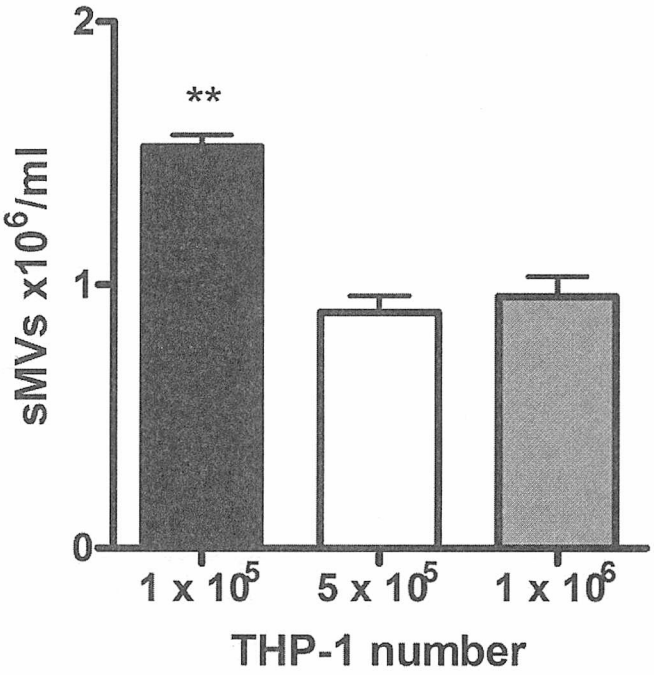

Fig 4.3 The number of THP-1 cells effects MV production when stimulated with a fixed volume of 10% NHS. THP-1 were serially diluted; 1 x 10^5, 5 x 10^5 and 1 x 10^6/ml and cultured in RPMI 1640 supplemented with 10% NHS and 2 mM Ca^{2+}. 1 x 10^5 THP-1 /ml was the optimum concentration of cells for sMV production, generating ~1.5 x 10^6 sMVs /ml. THP-1 concentrated to 5 x 10^5 and 1 x 10^6/ml produce significantly fewer sMV numbers ~ 1 x 10^6 sMVs /ml.

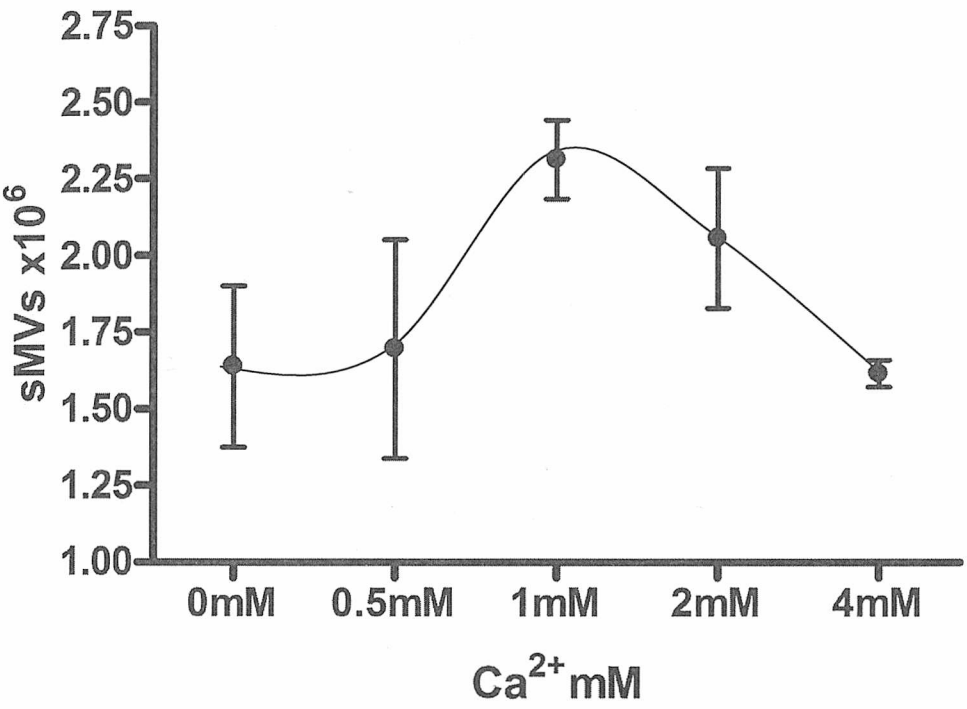

Fig 4.4 The effect of [Ca^{2+}] on the release of sMVs from THP-1 monocytes. THP-1 cells were cultured to a concentration of 5 x 10^5 cells /ml in RPMI 1640 supplemented with 10% NHS with differing Ca^{2+} ($CaCl_2$) concentrations. The effect of varying Ca^{2+} concentration on MV release was determined by enumerating MVs released using the Guava EasyCyte flow cytometer. This showed the optimum concentration of Ca^{2+} for microvesiculation ranged between 1 - 2 mM. MV release was significantly higher compared to 0 - 0.5 and 4 mM.

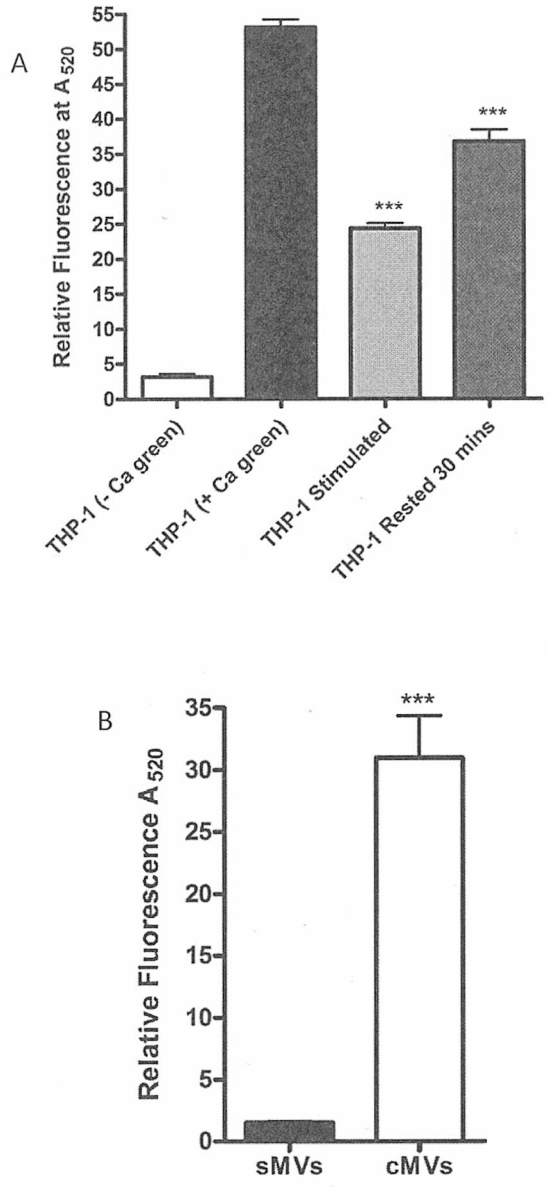

Fig 4.5 Intracellular calcium concentration mediates MV production as a homeostatic mechanism. (**A**) Calcium green-AM was incubated with THP-1 to bind with free intracellular calcium. When the THP-1 were stimulated with 10% NHS, resultant membrane pores lead to sMV release accompanying a significant decrease in free intracellular calcium. After a 30 min refractory period the cells showed a significant increase in the cells internal calcium levels. Calcium green fluorescence was measured with the FLUOstar Ω multiplate reader, stimulating at A_{485} and reading at A_{520}. (**B**) sMVs collected from A, show low levels of calcium green fluorescence, however, cMVs collected independently were incubated with Calcium green-AM. cMVs contain significantly more calcium than sMVs. Also the Calcium green-AM required cytoplasmic esterases to cleave the steroid (AM) molecule and accumulate within a continuous plasma membrane, such as cMVs. The accumulation of calcium green confirmed the presence of an active esterase within MVs.

4.5 Intercellular calcium concentration mediates MV production as a homeostatic mechanism

Calcium green-AM dye passes freely across plasma membrane as a steroid based molecule. The dye component is cleaved from the steroid by cytoplasmic esterases causing the dye to accumulate within the cytoplasm and the steroid component to be lost by passing out of the cell and being removed from the culture during the cell washing steps in the protocol.

The relative fluorescence of the positive control (THP-1 loaded with calcium green-AM) was a standard to compare the experimental values obtained. Fluorescence was measured using the FLUOstar omega multiplate reader. THP-1 preloaded with calcium green-AM were stimulated for MV release, the cells showing a significant decrease in free Ca^{2+} after microvesiculation (Fig 4.5A), indicating that the 'excess' Ca^{2+} was removed, contained within the MVs themselves. Indeed microvesicles did contain the calcium green dye in small amounts. Notably when cMVs were incubated with calcium green-AM for comparison to sMVs released in this experiment, a significant amount of Ca^{2+} was found within the cMVs. The presence of Ca^{2+} within the cMVs demonstrated that Ca^{2+} is essential for all types of MV release. However the comparatively high levels of Ca^{2+} in cMVs may be attributed to their slower release, and that they are released in smaller numbers or that some unknown mechanism for their biogenesis is in operation. Of interest, this result also shows the presence of the active esterase in the cMVs to allow for dye accumulation. Active enzymes and receptors show that MVs have functional properties (Fig 4.5B).

When the cells were left to recover for 30 min, there was a significant increase in intracellular calcium. (Fig 4.5A) this increase corresponding with the necessary refractory period to allow for subsequent MV release. The result also confirms that MVs are essential for calcium homeostasis, removing excess that may initiate undesirable metabolic events. Furthermore the low level of calcium in sMVs reflects their main role as biologically functional vesicle to circumvent cellular apoptosis (see chapter 5) and to attract macrophages to the site of injury. Conversely cMVs contain large levels of calcium that is essential for driving and directing many cellular processes. Their roles are those of communicative vectors (see chapter 5) containing sufficient [Ca^{2+}] to initiate or drive many intracellular reactions.

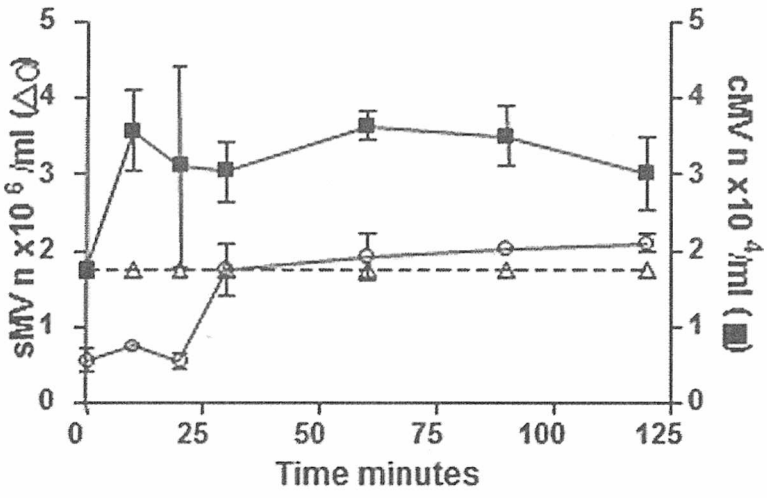

Fig 4.6 Analysis of MV production after an initial MV release event. (sMVs), THP-1 were stimulated with 10% NHS and the resulting MVs collected and quantified by FACs analysis. The cells were then stimulated with 10% NHS at progressive time intervals (0, 10, 20, 30, 60, 90 and 120 min) and the MVs collected and quantified. The cells were unresponsive to stimulation for up to 30 min after an initial stimulatory event. After 30 min, sMV numbers released reached approximately the initial amount collected and progressively increased over time to equal initial stimulatory numbers. (cMVs), THP-1 were washed and incubated in RPMI, MVs were collected and quantified as before. cMVs were collected at progressive time points (as with sMVs) and quantified. The first time point produced the lowest levels, thereafter there was no significant difference in the numbers of cMVs collected.

4.6 Analysis of MV production after an initial MV release event

Stress constraints cause cells to release sMVs in large numbers, as previously shown (Fig 4.3 and 4.4). Investigation into whether cells can release MVs in quick succession or whether a refractory period is required, were performed.

Cells were initially stimulated for sMV release, rested at 37^{0}C in RPMI 1640 and re-stimulated at progressive time points (0, 10, 20, 30, 60. 90 and 120 min) to ascertain the maximal frequency at which sMVs are released from cells. There was an initial stimulation that lead to sMV release followed by a 30 min refractory period where no or very low levels of sMVs were produced (Fig 4.6). The figure shows a small increase in sMV number at 10 min. This was the latent release of sMVs from the initial stimulation that was not evident at 20 min. At 30 min sMVs were released at levels closely approximating the initial MV stimulatory event. This level continued to rise until 120 min, where upon sMV numbers equal the initial event. THP-1 were washed and rested in RPMI 1640 for 1 h at 37^{0}C, cMVs were harvested and the THP-1 rested in RPMI 1640 at 37^{0}C for progressive periods of time, whereby the cMVs were collected and isolated. Initially at 0 min, low cMV numbers were reported. However at every successive time point there was no significant difference in cMV numbers collected. This shows that cMVs are released at a constant, slow rate.

The data collected typically demonstrates the potential mechanisms of stimulated cells to shed excess Ca^{2+}, given that a 'natural/unaided' Ca^{2+} refractory period is 30 min and that Ca^{2+} levels recover within that time frame to levels below that of the initial

concentration but sufficient to allow subsequent MV release. As Ca^{2+} reaches normal intracellular levels, the cell is able to release more MVs.

4.7 Real time observation of microvesiculation from THP-1

The Quartz crystal microbalance (QCM) was employed to record real time sMV release from THP-1 by measuring mass changes in the THP-1 and by observing changes in media fluidity. The behaviour of THP-1 suspended in RPMI 1640 supplemented with 10% NHS and 2 mM Ca^{2+} behaviour was recorded; mass and fluidity was observed. The cells were incubated at 37^0C on the Q-sense sensor for 1 h. Fig 4.7A shows the increase in mass as the THP-1 cells are deposited on the censor up to ~1000s (corresponding to the frequency decrease). Upon addition of the stimulus (10% NHS) at 1000s, there is then a significant loss of mass from THP-1 between ~1300 – 2000s. Fig 4.7B reproduces the results for A, using a different sub-harmonic. Fig 4.7C shows no change in mass from un-stimulated THP-1 cells cultured in NHS-deficient medium. Fig 4.7D demonstrates the changes in fluidity/rigidity associated with microvesiculation. As MAC deposits into the membrane, the cell surface blebs, increasing the cells surface area therefore changing their behaviour within the media. The fluid becomes rigid as the cells displace one another. This bleb eventually forms a microvesicle and pinches off, increasing the rigidity (clarity) of the media and so decreasing its fluidity as submicron vesicles were present.

4.8 C5b-9 complex is expelled during sMV release

THP-1 were stimulated for sMV release using sublytic MAC (C5b-9) present in NHS. MACs were used as a model for membrane damage that leads to sMV release. Other

membrane damaging stimuli produce sMVs reminiscent of MAC-induced damage (See Chapter 6). MAC inserts into cell membranes within 5 - 10 min of incubation and is detectible until 30 min after initial stimulation with NHS using αC5b-9 (Fig 4.8). After 30 min MAC was no longer detectable on THP-1. It was reasonable to conjecture that MACs allowing cytoplasmic Ca^{2+} influx could then be located at the site of MV release and so being included on the released MV itself. Once removed from the cell, the damage caused by the MACs ceased and the cell recovered. As complement proteins are heat labile, heat inactivated NHS does not deposit MACs and no microvesiculation is observed.

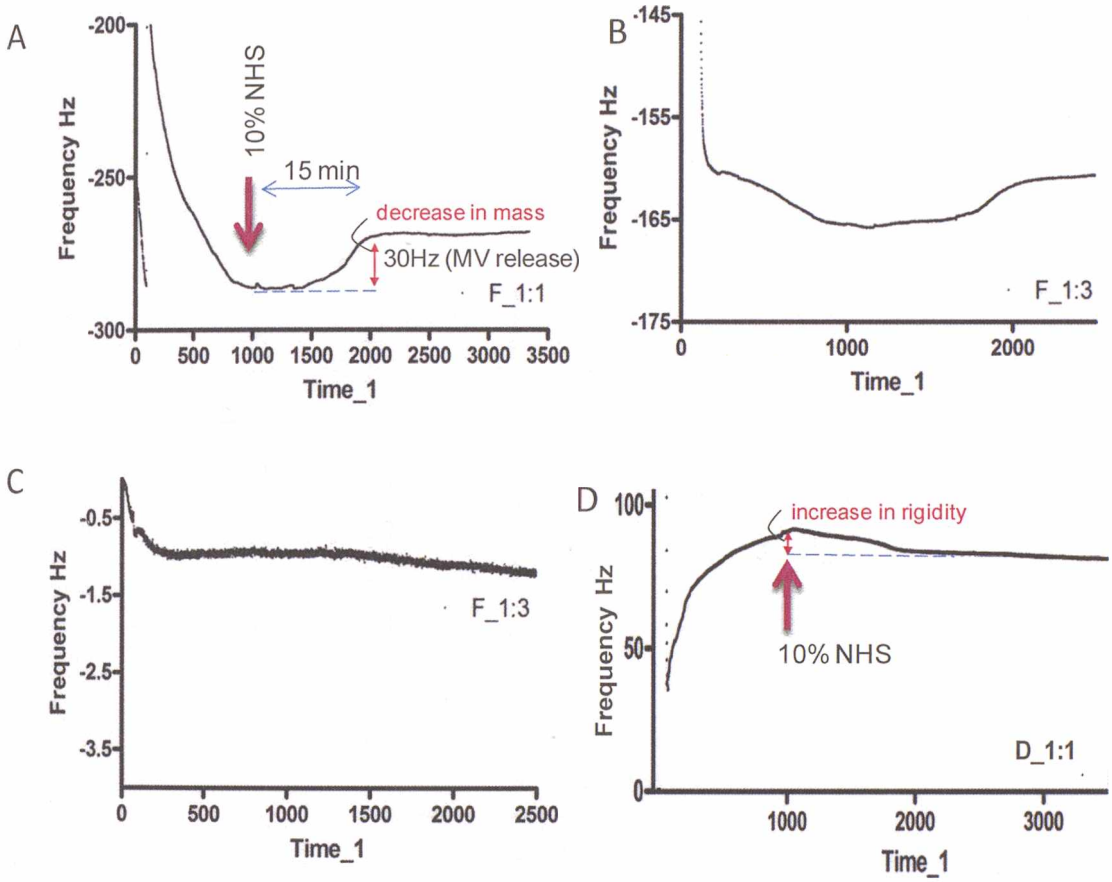

Fig 4.7 Q-sense data for microvesiculation from THP-1. (**A**). Using sub-harmonic F_1:1, the mass of the THP-1 increased as they settled onto the sensor; 0 – 800s shows a sharp increase. The mass remains constant 1000 - 1800s after which there was a sudden loss in mass (decrease in frequency). This loss in mass remains constant thereafter. (**B**). The THP-1 settle from 0 - 800s, then mass remains constant until MV release at 1800 - 2000s, where there is a loss of mass from THP-1. (**C**). No mass change occurred over the 2500s duration, the THP-1 were suspended in 10% NHS and EDTA. Notice that the cells settle quickly, this is because the base line had already been established for THP-1 on previous experiments. (**D**). Using sub-harmonic D_1:1, the 'rigidity' of the media containing the cells was assessed. As the cells settled on to the piezoelectric sensor the media clarifies, becoming less rigid, however as NHS deposits MACs ~1000s, the membrane begins to bleb, correspondingly there is an increase in media rigidity until the blebs 'pinch off' ~1800 - 2000s, to form sMVs, leading to a permanent increase in media rigidity.

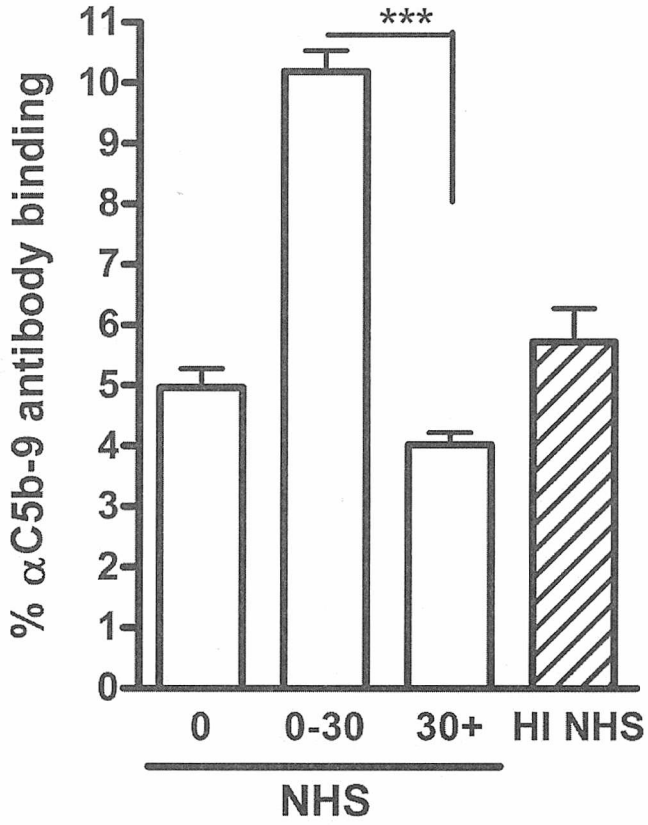

Fig 4.8 C5b-9 binds to THP-1 membrane stimulating sMV release. THP-1 were incubated with 10% NHS allowing sublytic levels of MAC (C5b-9) deposition leading to sMV release. FITC conjugated αC5b-9 was used to detect the presence of lytic pores on THP-1. Between 0 - 30 min, C5b-9 complex had assembled spanning THP-1 membrane. After 30 min C5b-9 complex was no longer detectible on THP-1 membrane. No C5b-9 was detected when THP-1 were incubated in heat inactivated NHS.

4.9 The effect of MVs on the proliforative status of the promonocyte cell line THP-1

MVs deliver factors to cells (THP-1) that stimulate proliferation. Although physiological conditions contain fewer MVs/ml, the results mimic micro-environments whereby MVs will be concentrated, such as the site of injury and stressing environments localised to tissues. MVs have reportedly contradictory physiological functions in the literature. The sMVs used in this experiment were generated by stressing THP-1 with 10% NHS. cMVs were collected from CGM, containing a plethora of growth factors and communicative signals. The cells throughout this experiment maintained viabilities above 95% and in some cases above 99%.

Although it has been suggested by this study that cMVs are communicative vectors and sMVs are produced to shed cell stress agents, it cannot be ignored that excessive growth signals may also be a stress agent to cells. It should also be noted that sMVs produced by NHS contain MACs, that at sublytic levels (as are expressed on sMVs) cause cellular proliferation (Ansa-Addo *et al*, 2010). Significant differences in THP-1 incubated with or without MV subtypes was observed by 72 h (Fig 4.8A), whereupon MV stimulated cells had shown significant proliferation. However differences between cMVs and sMVs were clearly evident but not statistically significant (Fig 4.8B). 96 h demonstrated that 10% NHS incubated THP-1 displayed significant increases in proliferation and that the difference in proliferation between subtypes had become more apparent.

4.10 MV subtypes protect Salmonella typhimurium *from complement mediated lysis*

Salmonella typhimurium are destroyed by complement mediated lysis (C5b-9 MAC) when incubated with 45% NHS. However when incubated with MVs (1:1) and 45% NHS, the salmonella had an increased chance for survival (Fig 4.10). The MV subtypes offer different levels of protection; while cMVs offer significant protection from MACs (22.2%), sMVs offer significantly higher levels of protection (62.9%). It is conjectured that this significantly enhanced protective role of sMVs is due in part to their increased size, offering a greater surface area for MACs to adhere to. MACs seemingly bind to non-self identified membrane in a 'random' manner, so that MVs with a larger surface area will have an increased probability of encountering complement protein C5b, hence using the complement proteins and increasing the Salmonella's chances for survival. The results obtained were highly reproducible. Furthermore, PS on the outer leaflet of MVs, covalently binds to C4 binding protein activating the classical complement cascade (Gigli *et al*, 1979) to adhere to MV membranes. Complement mediated lysis of salmonella is inhibited or significantly reduced in the presence of MVs.

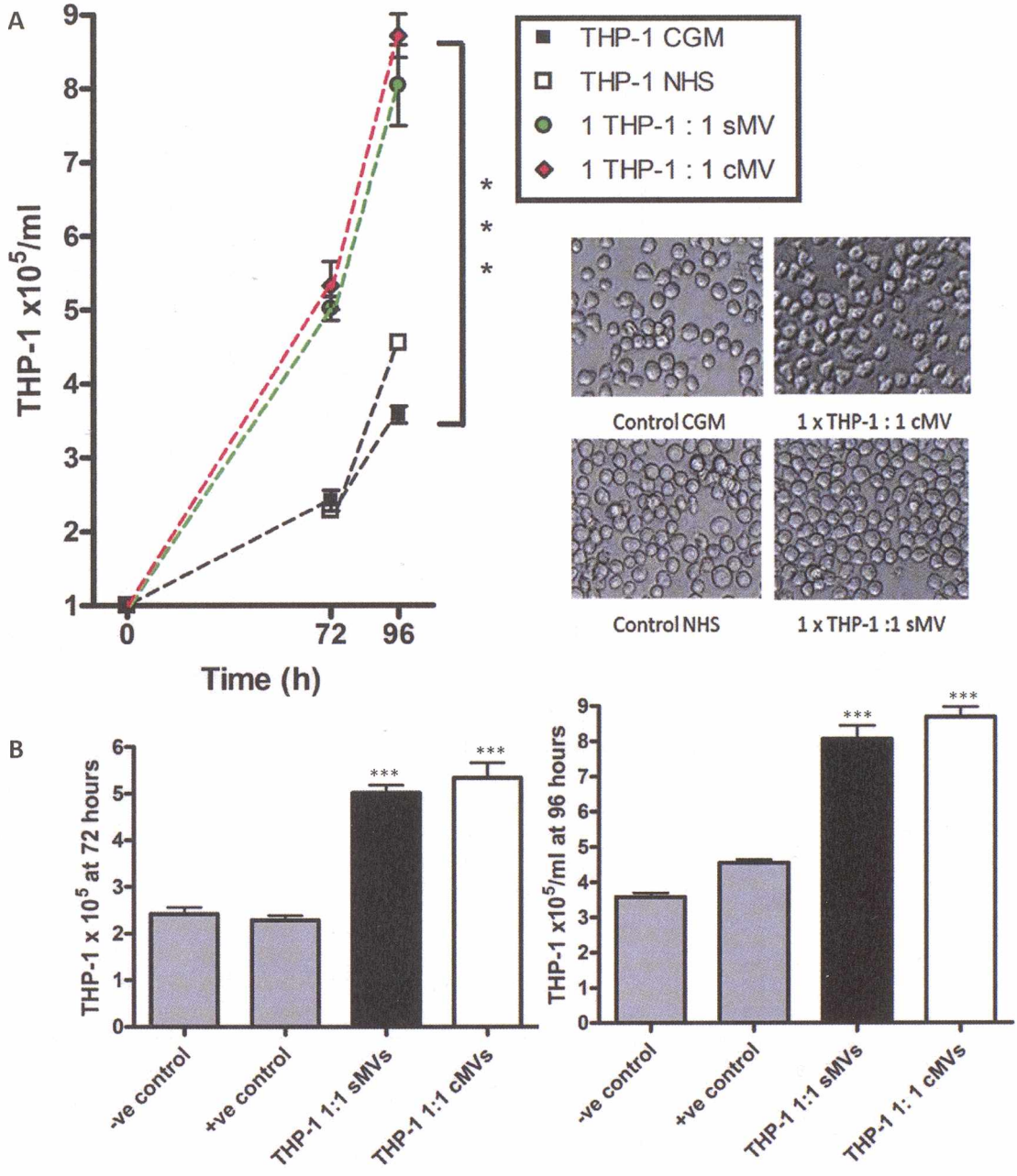

Fig 4.9 Physiological roles for MVs. (**A**) THP-1 (1 x 10^5 /ml) were incubated with MVs (1 x 10^5 /ml) in 10% NHS. THP-1 MV subtypes significantly increase growth over 96 h. There is no significant difference between the MV subtypes for stimulating growth however sMVs have a greater capacity to stimulate growth. There is a significant difference between the means for cMVs (8.04 x 10^5 /ml) and sMVs (8.72 x 10^5 /ml) at 96 h. Photo inset shows 96 h for all conditions listed shows increased proliferation in all THP-1 stimulated with MV subtypes. (**B**) Cell count at 72 h and 96 h for the incubation of MV subtypes with THP-1 cultured in RPMI 1640 supplemented with 10% NHS and 1% penstrep.

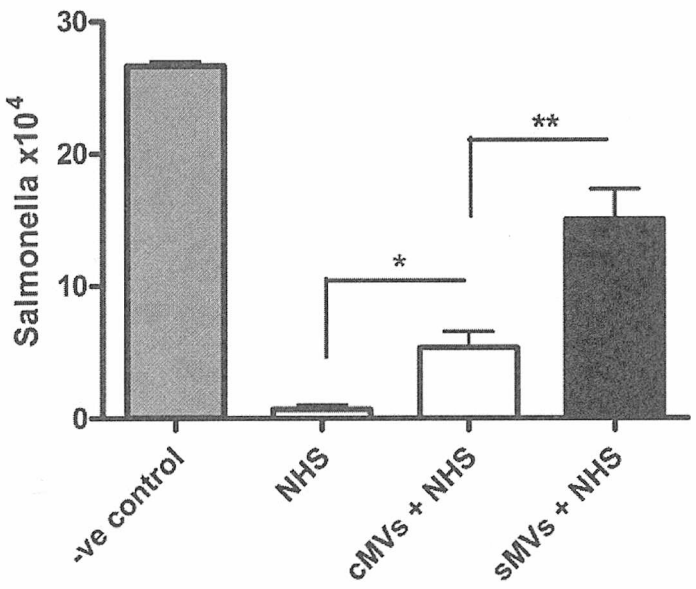

Fig 4.10 MV subtypes offer different levels of protection to *S. typhimurium* against complement mediated lysis. Salmonella incubated with cMVs receive a significant level of protection from complement mediated lysis; ~6 ± 1 x 10^4 (~22.2%) however sMVs offer a highly significant level of protection to salmonella from complement mediated lysis; ~17 ± 2.5 x 10^4 (~62.9%).

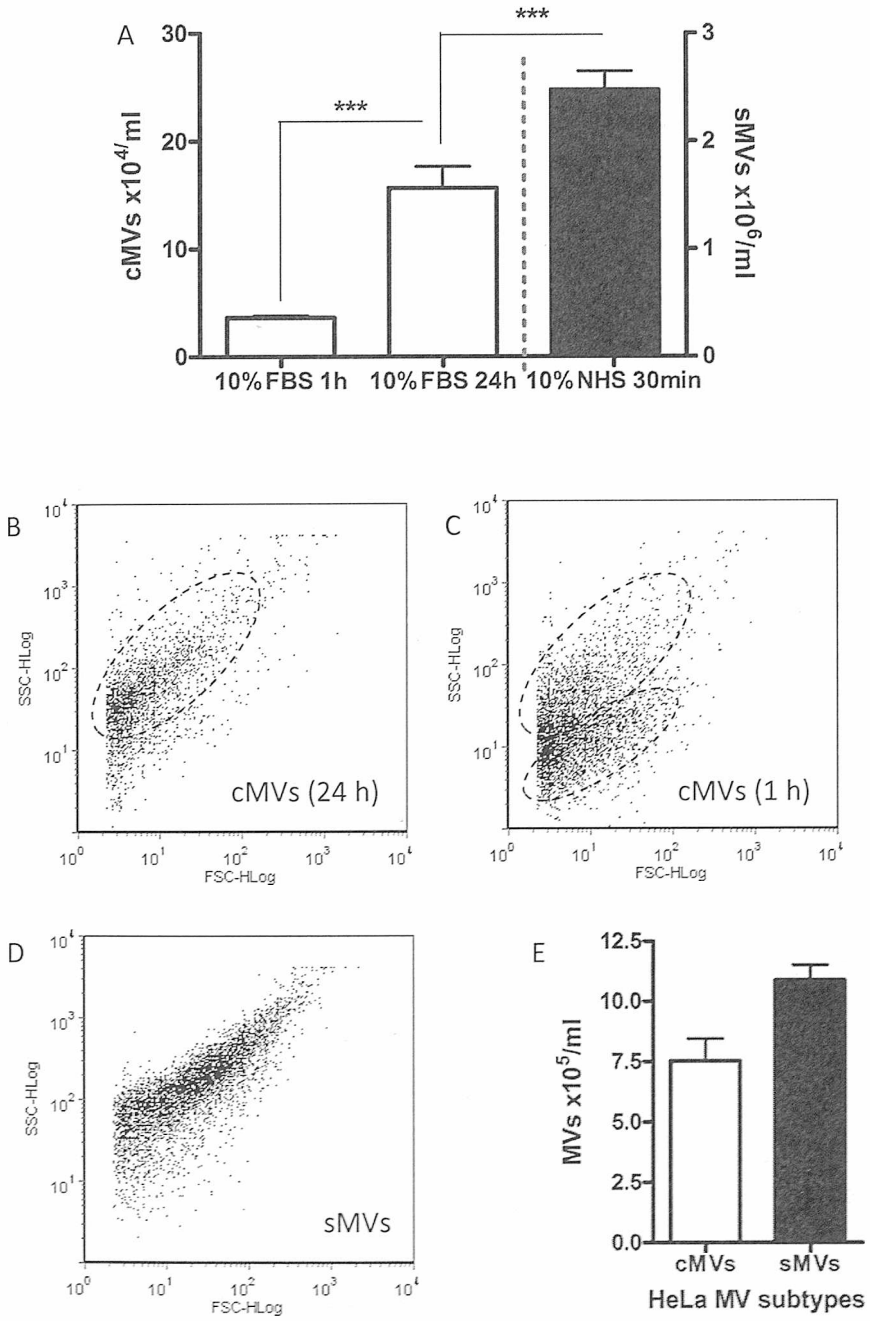

Fig. 4.11 Comparison of THP-1 MVs isolated from different media. Fresh cMVs were isolated from CGM after 1 h incubation with cells. 'cMVs media' were isolated from CGM after 24 h and 'fresh sMVs' were isolated from 10% NHS in RPMI 1640 + 2 μM $CaCl_2$. The data was collected by FACS analysis and shows significant differences in the number of MVs subtypes isolated. (A) MVs were isolated from various media and quantified, there were significantly more sMVs than cMVs isolated from 24 h media. (B) – (D) (C) show the dot plot profiles obtained, sMVs showing a distinctive profile (D) compared to cMVs (B, C)(E) HeLa MV subtypes were quantified. HeLa shed significantly more cMVs /ml over 24 h than THP-1 but significantly less sMVs than THP-1 when stimulated by RPMI 1640 supplemented with 10% NHS and 2 mM Ca^{2+}.

4.11 Comparison of THP-1 MVs isolated from different media.

MVs were isolated from various culture media, replicating conditions used for THP-1 (1 x 10^6 /ml) as cultured before. THP-1 were incubated in RPMI 1640 for 1 h, in CGM for 24 h and THP-1 were stimulated with 10% NHS for 30 min. All culture supernatant's were submitted for MV isolation and analysed and quantified using FACs. cMVs population count was 1.5 x 10^4 /ml for 1 h, one tenth that of cMVs allowed to accumulate over 24 h (Fig 4.1A). Furthermore the 'fresh' MVs contained two distinct populations leading to the conclusion that actual cMV numbers were lower still. cMVs accumulated in culture media for 24 h were counted at ~1.5 x 10^5 /ml. sMVs were showed a significant increase in population numbers, a more than 10 fold increase, 2.5 x 10^6 /ml over 24 h for cMVs. This demonstrates that cMVs accumulate in the culture medium slowly, demonstrating a slow release from un-stimulated cells. sMVs were released in large numbers over 30 min in response to stressing agents.

THP-1 incubation in CGM for 24 h showed the accumulation of cMVs, exhibiting 'classical' cMV morphology performed by FACs (Fig 4.11B). Different incubations times for MV isolation were necessary to ensure a maximal yield for analysis. Optimal conditions were applied in each case, THP-1 in RPMI 1640 for 1 h would yield newly released cMVs. Unexpectedly, FACs analysis revealed two distinct populations of microvesicle. The larger of the two approximating to 'classical' or expected cMV FACs morphology. The smaller population occupies the position expected for exosomes, however this was unconfirmed by further analysis (Fig 4.11C). 30 min incubation cultured in RPMI 1640 supplemented with 10% NHS and 2 mM $CaCl_2$ stimulated the release of sMVs, showing 'classical' sMV morphology by FACs analysis (Fig 4.11D). HeLa (1 x 10^6 /ml) release MV subtypes reminiscent of THP-1 MV subtypes, however HeLa

release MVs in different concentrations when collected using the same methodologies. Most remarkably THP-1 release ~1.75 x 10^5 /ml cMVs per 1 x 10^6 cells compared to HeLa that release ~7.5 x 10^5 /ml cMVs per 1 x 10^6 cells. Furthermore THP-1 release ~2.5 x 10^6 /ml sMVs compared with HeLa ~1.2 x 10^6 /ml sMVs (Fig 4.11E). This indicates that different cell types release MV subtypes in a similar fashion to THP-1, therefore biogenesis is conserved between cell types although MVs of the same subtype are released in different concentrations (See Chapter 5).

4.12 Exosomes are distinct to cMVs

Media collected from THP-1 cultured with RPMI 1640 supplemented with 10% FBS and 1% penicillin and streptomycin was separated from cells by low speed centrifugation (160 *g* for 5 min) and then was centrifuged to remove debris (4000 *g* for 1 h). The resulting debris free culture medium was dispensed into 1ml aliquots and submitted for MV isolation, the pellet suspended in PBS and then the resulting supernatant was submitted for exosome isolation, both the cMVs and exosomes were analysed using Guava Millipore flow cytometry for comparative numbers released into culture media and relative fluorescence to distinguish the eMVs. Indeed, the FACs demonstrated different FACs population morphologies, sizes, relative numbers and auto fluorescence, revealing the exosomes to be distinct from cMVs. This was confirmed by TEM (Fig 4.14).

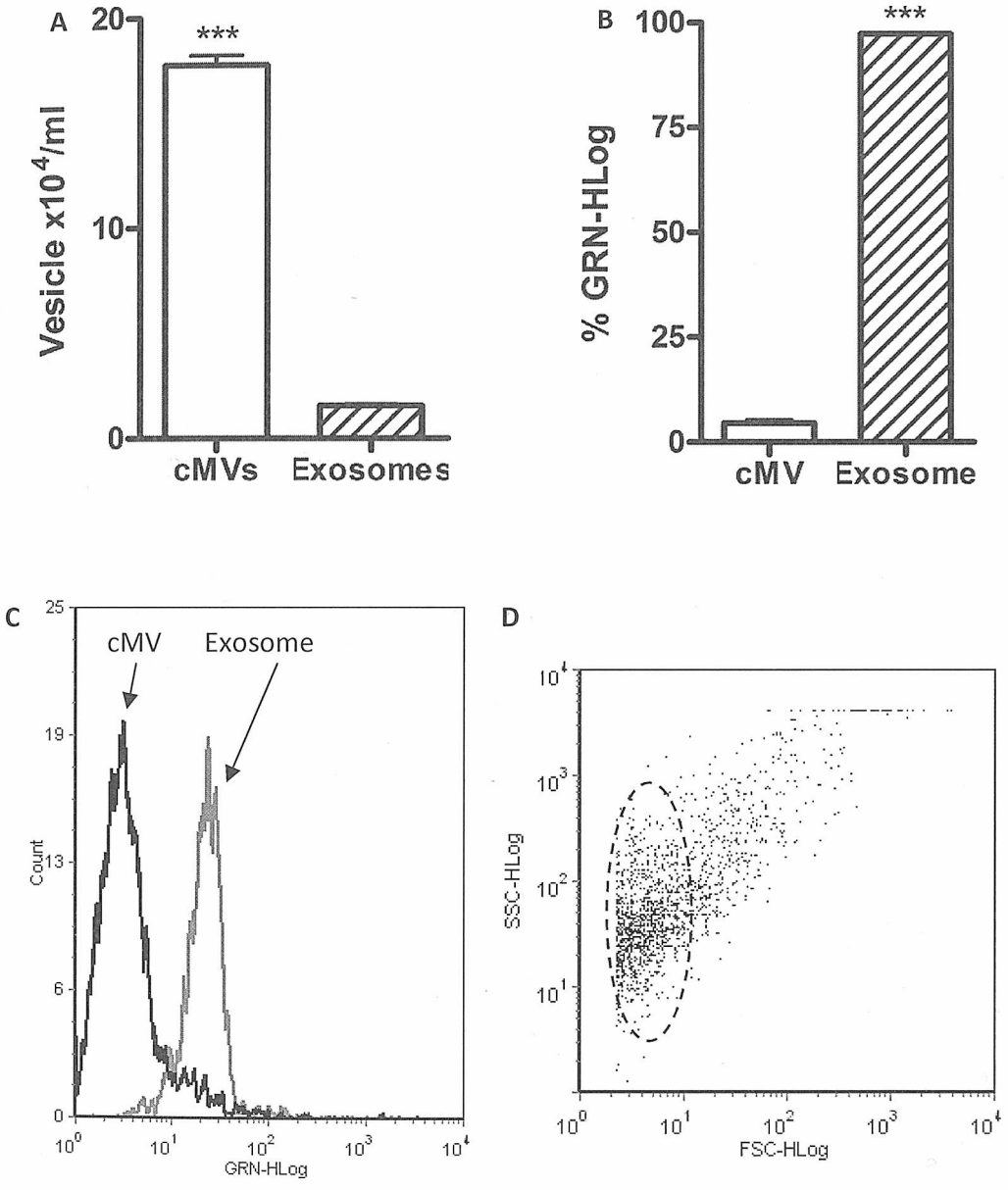

Fig 4.12 cMVs are distinct from exosomes. (**A**) Vesicles isolated from THP-1 24 h culture medium contains ~1.8 x10^5 /ml cMVs and ~1.5 x10^4 /ml exosomes. This indicated that cMVs are released >10 fold that of exosomes. (**B**) Relative auto fluorescence of exosomes is ~90% greater than cMVs when measured using Guava Millipore ExpressPlus GRN-HLog. (**C**) GRN-HLog of cMVs natural fluorescence (black) and exosome natural fluorescence (grey). (**D**) FACs dot plot of exosomes (within the elliptical region) FSC-HLog and SSC-HLog.

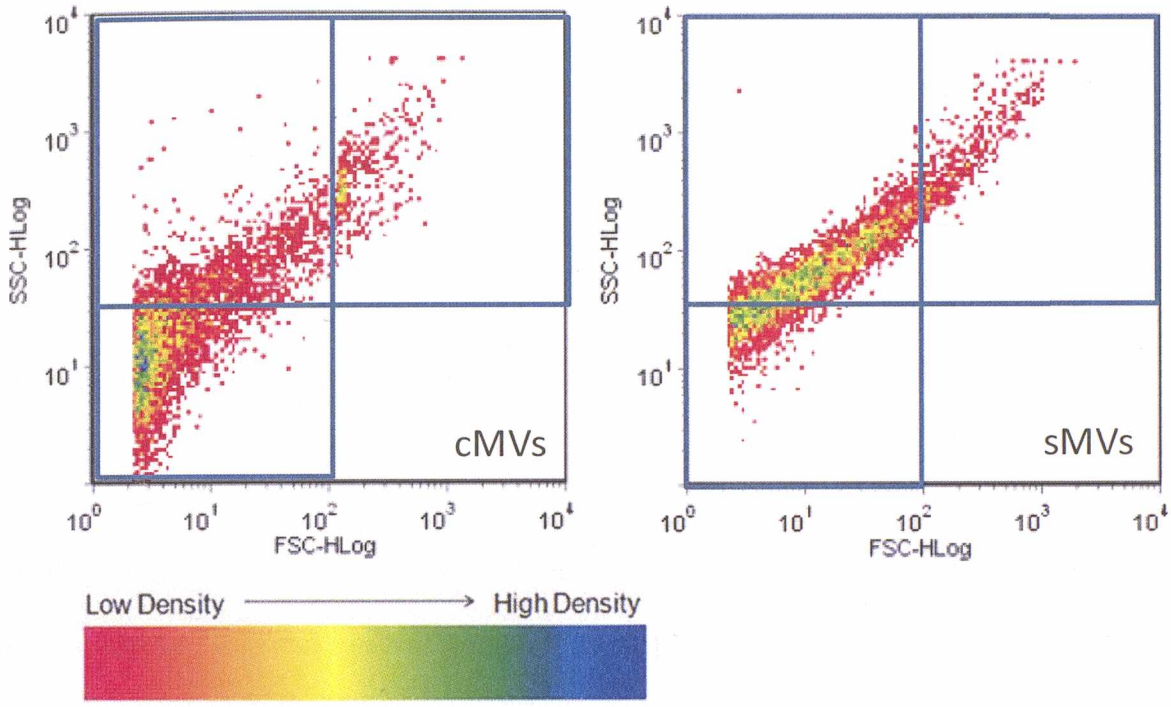

Fig. 4.13 MV subtype FACS population density distribution. cMVs and sMVs have differing population density when analysed by flow cytometry, according to forward scatter (FSC-Hlog) and side scatter (SSC-Hlog). cMVs have a higher population density within the 0 - 0.3 μm gate whereas sMVs have a greater population density Within the 0.3 - 0.5 μm gate. Although both MV subtypes have MVs in the 0.5 – 3 μm range, the sMVs have significantly more with a more uniform morphology of the scatter plot than cMVs. Overall, sMVs have a more uniform density and scatter plot morphology. The FACS gating shown is based upon multimix sizing beads. Any debris or possible exosomes have been excluded from the 0 - 0.3 μm gate. 0 - 0.3 μm, lower left quadrant; 0.3 - 0.5 μm, upper left quadrant; 0.5 – 3 μm, upper right quadrant.

4.13 MV subtypes have different FACS population density distributions

A typical MV distribution dot plot showing size and granularity as obtained on the Guava EasyCyte flow cytometer is highlighted in Fig 4.13 and shows that sMVs are significantly larger than cMVs. The identification of distinct MV subtypes lead to the necessity for characterisation. Both sMVs and cMVs are released for contrasting functions via potentially different metabolic pathways.

Detailed analysis of MV subtypes by FACs showed that they differed considerably with regards to average size and general population morphology. MVs were 'sized' using megamix sizing beads (0.3 μm, 0.5 μm and 3.0 μm), the distribution of MV sizes being analysed using Guava complementary software. The data shows that cMVs population distribution has highest density 0 - 0.3 μm, whereas sMVs have a more uniform size distribution across all sizes measured. However the sMV population density is highest (0.3 - 0.5 μm) indicating a significantly larger average size than cMVs.

The population morphology of the subtypes also differs, each having a unique signature, sMVs having a narrower SCC-Hlog than cMVs which appear 'messier' and less coherent. SCC-Hlog is a measure of surface granularity, the larger sMV varies less than the cMVs.

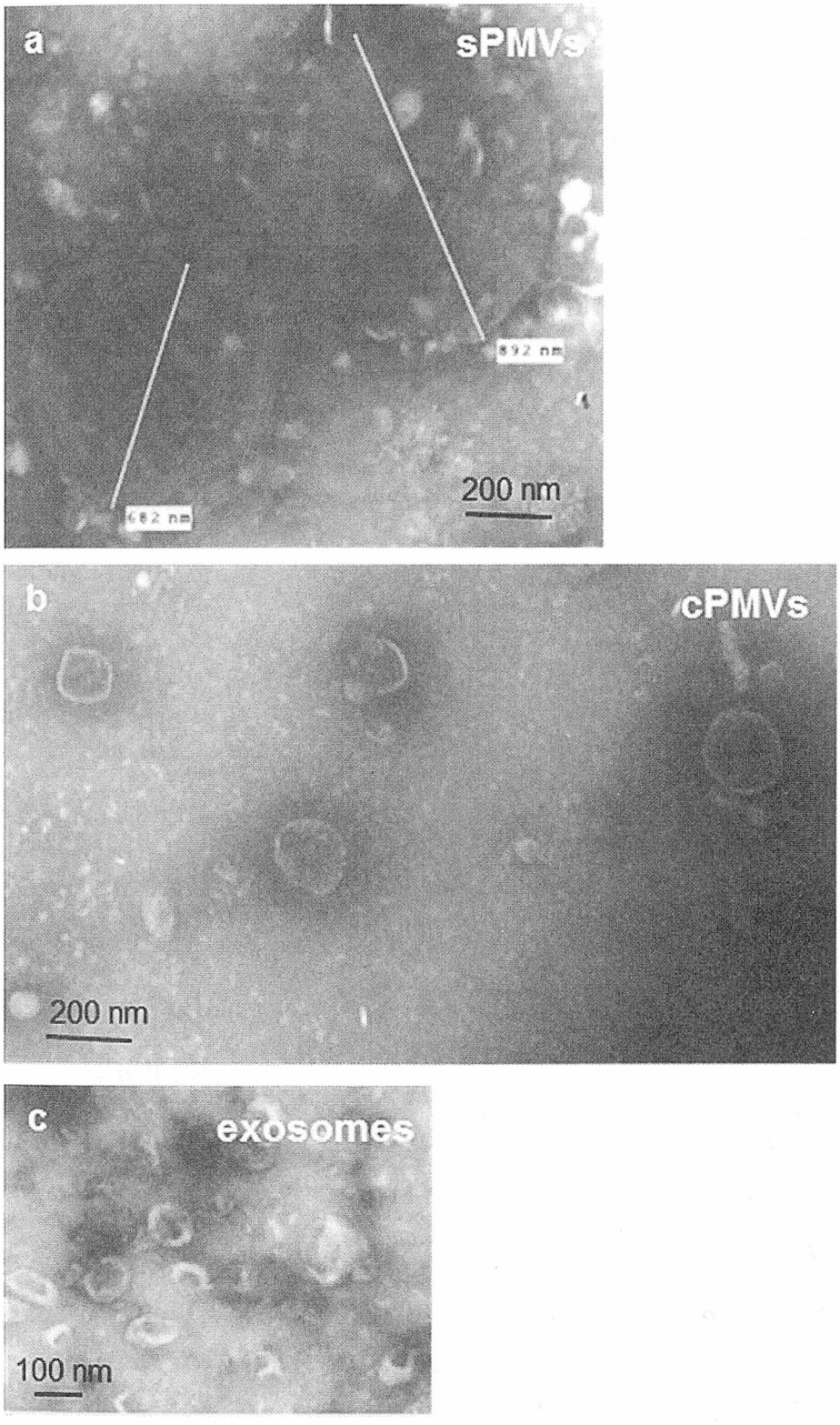

Fig 4.14 Transmission electron microscopy of sMVs, cMVs and exosomes. All microvesicles were released from THP-1 monocytes. MVs were isolated by centrifugation from cell-free supernatants at 25,000 *g* for 60 min. Images prepared by negative staining and samples examined on a JEOL JEM-1200 EXII electron microscope. Exosomes were isolated by centrifugation at 160,000 *g* for 16 h. (3x magnification) Scalebars: 200 nm (a, b), 100 nm (c).

4.14 Transmission electron microscopy of sMVs, cMVs and exosomes

Transmission electron microscopy visually highlights the differences in MV subtype morphology and size. Fig 4.14a, sMVs are large (892 nm and 682 nm), roughly spherical vesicles that appear to vary considerably in size. Fig 4.14b reveals that cMVs are small (<200 nm), near spherical vesicles that are consistent in size. Exosomes were examined to highlight the physical differences to cMVs. Exosomes are flattened, concave disk structures that are approximately 100 nm diameter. sMVs were stimulated for release with 5% NHS from THP-1. Conversely cMVs were collected from CGM containing THP-1.

The importance in the size and morphology distinction between MV subtypes are related to their roles. It can be conjectured that cMVs will act as communicative vectors as they are small and less likely to be impeded by structures within the extracellular medium, sMVs are larger and more likely to interact with cells close to the sight of release. It was suggested that cMVs being smaller, heavier, denser and containing many cellular elements will be much more robust than sMVs that are lighter, larger and containing few cellular elements.

As cMVs act as communicative vectors, it is essential that they can withstand degeneration so to transmit cellular instructions and components. As sMVs are formed as a response to stress, they will have a shorter half-life, as typically they will be engulphed by macrophages. They may also split open, spilling little cellular components that would cause inflammation.

4.15 Comparison of MV subtypes size distribution

Comparison of MV subtype size distribution (Fig 4.15) confirmed that sMVs were larger than cMVs. Typically 80% of cMV populations were 0 - 0.3 μm, 15% were 0.3 - 0.5 μm and 5% were over 0.5 μm. Whereas 17% of sMVs were 0 - 0.3 μm, 65% were 0.3 - 0.5 μm and 18% were over 0.5 μm. At each size there were significant differences between MV subtype sizes, confirming that cMVs, (typically ≤ 0.3 μm) were much smaller than sMVs, (typically 0.3 - 0.5 μm).

Assuming a perfect sphere, the surface area of a cMV is πd^2 (d is the diameter of the MV as measured by FACs). If cMVs are 0.3 μm (maximum) then the maximum average surface area of cMVs (over 80% of the FACs population) are $\pi 0.3$ μm^2 ~0.2328 μm^2. If sMVs are 0.5 μm (maximum) then the maximum average surface area of sMVs (over 65% of the FACs population) are $\pi 0.5$ μm^2 ~0.7855 μm^2. The difference in surface area is significant when considering expression of membrane lipids, proteins, carbohydrates and receptors. The results make some generalised assumptions, but may be used to indicate potential differences.

Likewise the volume of a perfectly spherical MV $=\frac{3}{4}.\pi r^3$. Using the assumptions above we obtain $3/4\pi 0.15$ μm^3 ~0.0079531 μm^3 for cMVs and $3/4\pi 0.25$ μm^3 ~0.036823 μm^3 for sMVs. Although MV subtypes are unlikely to form perfect spheres, this is a model demonstrative of the potential difference in volume (sMVs have a ~4.3x larger volume than cMVs and ~3.4x greater surface area).

4.16 Light scattering determination of MV subtype size

Light scatter analysis of MV subtypes was used as confirmatory test for the FACs analysis with sizing beads (Fig 4.16). The results confirmed a consistent pattern of MV subtype distribution; cMVs are smaller (7.34 ± 0.82) than sMVs (29.63 ± 7.3). However the sizes derived were different to FACs. Light scatter analysis assumes a perfectly spherical body and extrapolates size by a model of scattered light patterns. Unfortunately, although the concentration for MV subtypes was ~1 x 10^6 /ml the suspension medium (PBS and RPMI 1640) appeared to alter the data. Furthermore, a change in subtype concentration would change the DLS size interpretation, so that DLS can only be used as a relative MV subtype size comparison.

cMVs are nearly spherical (Fig 4.14B). However they have a grainier morphology than sMVs (Fig 4.13) and would therefore alter perception of light scatter and lead to small inaccuracies in the parameters for analysis. sMVs are roughly spherical so again the light scatter would not give a true account of size. However the patterns observed fit the expected differences in size. Although light scattering gives a rough estimation of size, it is an excellent tool for showing marked differences in size and population distributions of size.

4.17 Comparison of the effects of centrifugation speed and time on MV population size and morphology

Many different studies indicate different methods for MV isolation. Fig 4.17 shows that although centrifugation regime varies with respect to time and speed, MVs *are* isolated.

Confirmatory tests for MVs include annexin V analysis, analysis of size and typical morphology of MVs.

As indicated by the figure, increasing speed and duration of centrifugation leads to an increase in the smaller sized MV population. A distinction between small MVs and exosomes must be made to prevent confounding data. It is generally accepted that exosomes (40 – 100 μm) are the same size as the smallest MVs (~100 μm or more) and that exosomes need considerably longer centrifuge times to pellet. To minimise exosomal contamination therefore, MVs must be pelleted using shorter times, and sonicated for 5 min at 4 ^{o}C.

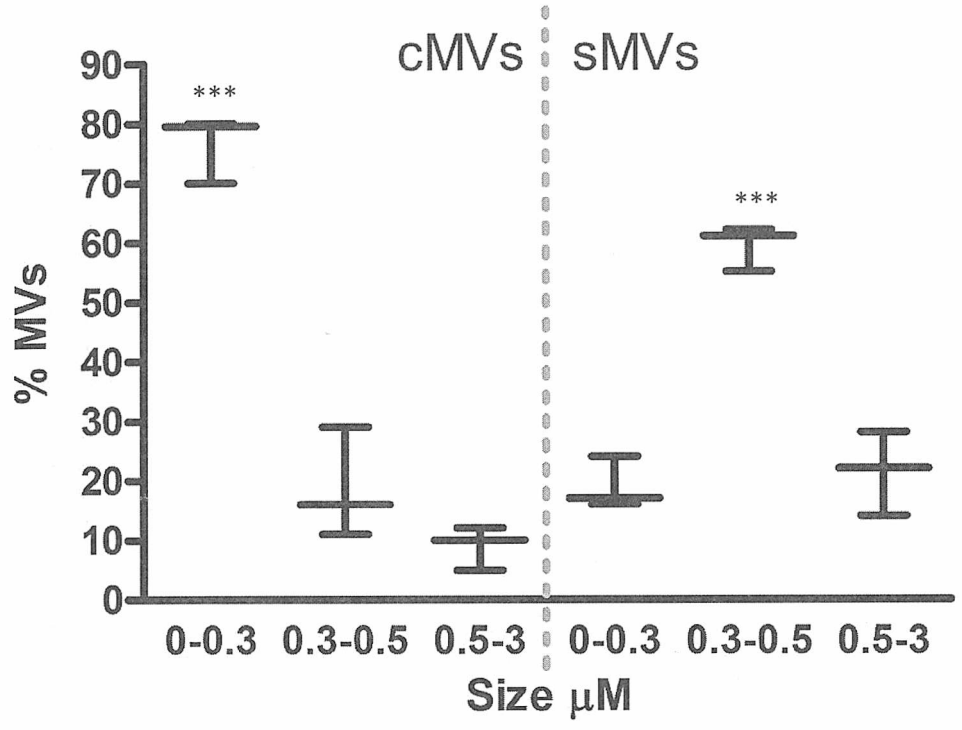

Fig. 4.15 Comparison of MV subtypes size distribution. cMV purity was assessed to have very low to no levels of exosomes, 80% of the cMV lie in the range 0 - 0.3 μm in diameter, 15% between 0.3 - 0.5 μm and 18% over 0.5 μm. 17% of the sMV population lie in the range 0 - 0.3 μm in diameter, 65% in the range 0.3 - 0.5 μm in diameter and 18% over 0.5 μm. There are significant differences between the sizes at each measured size interval. The data shows that cMVs are generally smaller vesicles (usually $\leq$ 0.3 μm in diameter) with sMVs having a mean population diameter of 0.3 - 0.5 μm.

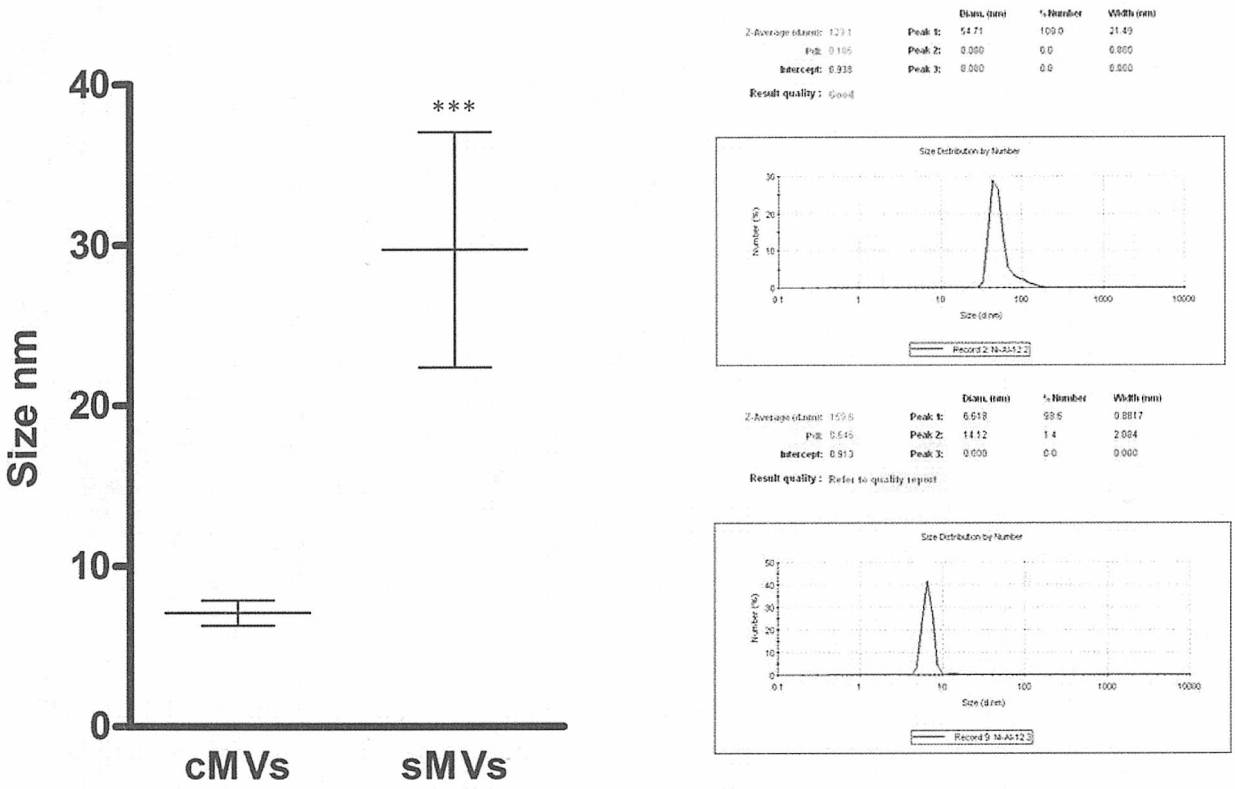

Fig 4.16 Light scattering determination of MV subtype size. (**A**) Light scatter analysis of MV subtypes indicates a significant difference in size. sMVs are 4x larger on average than cMVs, sMVs having a greater variation in size than cMVs, that have a more or less consistent size definition. (**B**) Raw data taken from analysis software shows typical result.

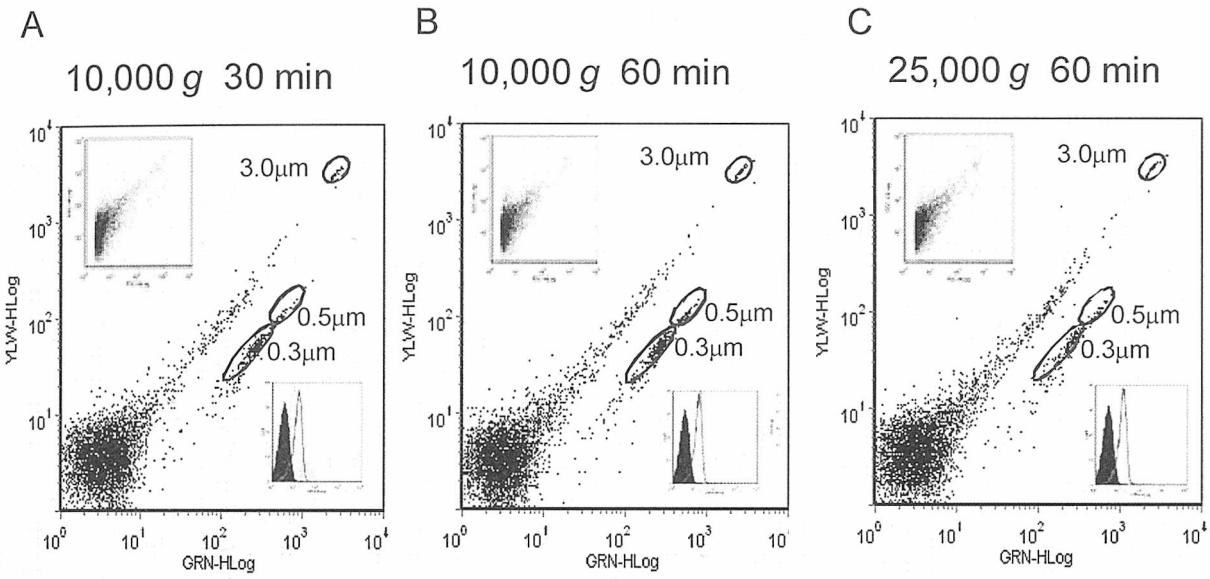

Fig 4.17 Comparison of the effects of centrifugation speed and time on MV population size and morphology. Increasing centrifuge regimes with speed and duration leads to an increase in MV deposition and a more even distribution of MVs in the smaller size range. Top inset shows little difference in MV population morphology across the regimes. Bottom inset confirmatory MV analysis for the presence of PS expression by annexin V.

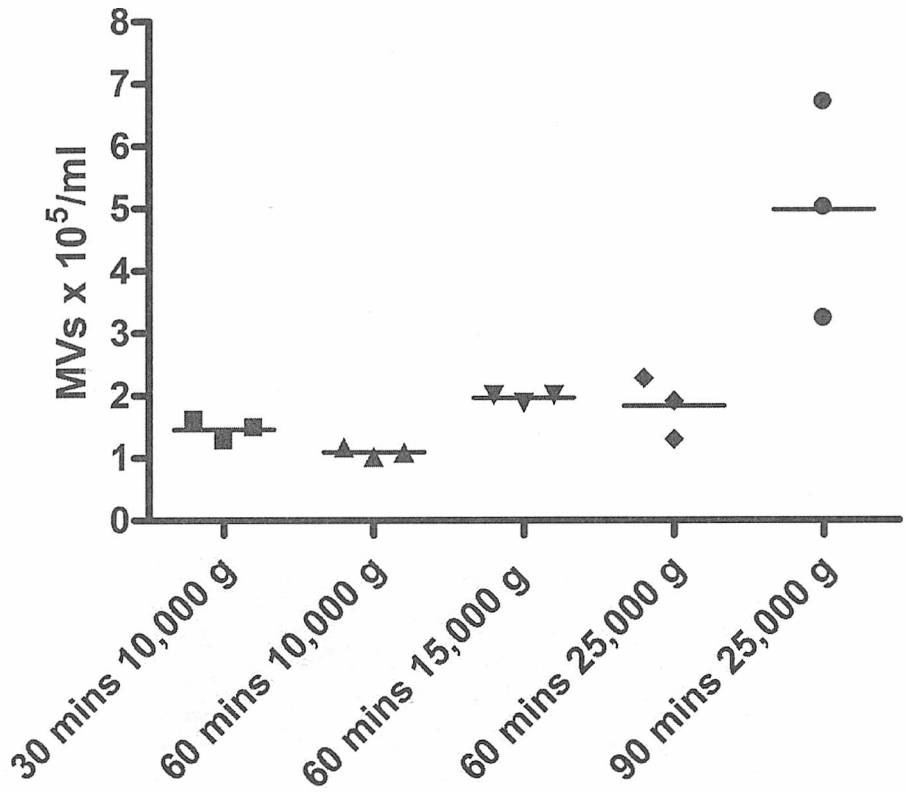

Fig 4.18 The effects of different centrifugation speeds and duration on MV isolation. 1 x 10^6 THP-1 were stimulated for MV release and submitted for isolation by different centrifugation speeds for different durations. Isolated MVs were quantified by Guava FACs Analysis. As centrifuge regimes significantly increase in speed and duration, larger quantity of MVs are pelleted. 30 min 10,000 *g* to 60 min 25,000 *g* isolated similar quantities of MVs, however 90 min at 25,000 *g* isolated significantly more (cMVs).

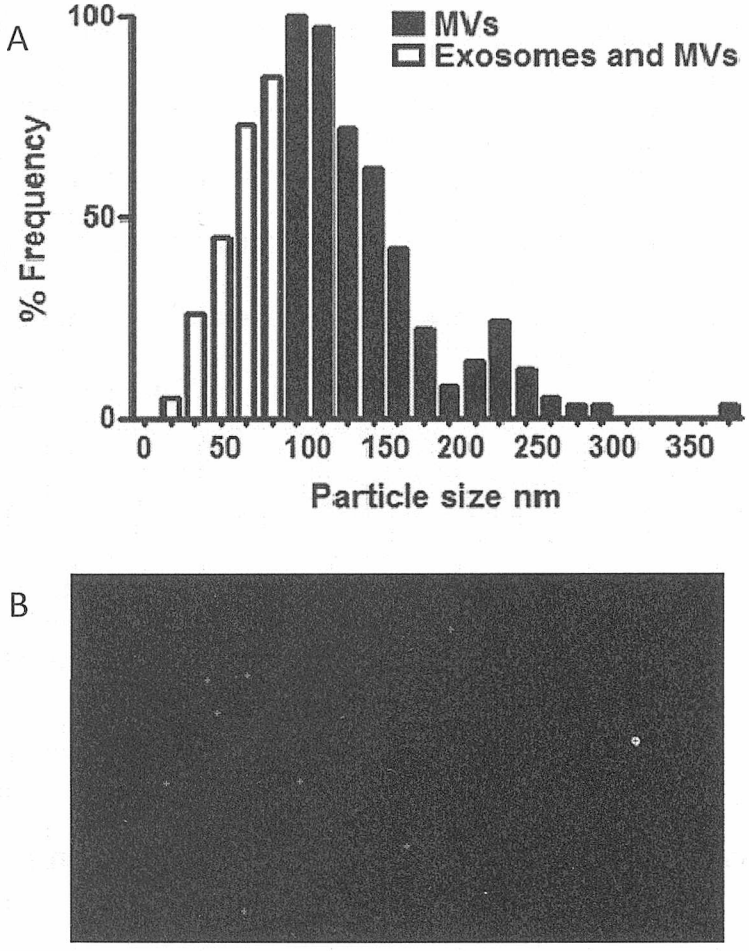

Fig 4.19 NanoSight analysis of all THP-1 MVs released over 1 h resting in RPMI 1640. (A) THP-1 (5 x 10^5/ml) were washed x3 at 160 *g* and finally rested in RPMI 1640 for 1 h at 37 ^{0}C. The cells were pelleted at 160 *g* and the supernatant diluted 1:100. The diluted supernatant was analysed using NanoSight. The results processed and presented using GraphPad Prism 4. Exosomes, typically in the range of 20 nm – 90 nm are released constitutively, cMVs typically 90+ nm overlap exosomes sizes. The figure shows two distinct sized populations, the smaller being a mix of exosomes and cMV 20 – 175 nm, the larger are cMVs 175 – 320 nm. (B) A sample image depicting cMVs in RPMI 1640 captured from NanoSight, nanoparticle tracking analysis, Version 2.2. No scale is available, however the software projects the average particle size ~135 nm (inclusive of exosomes (20 – 90 nm) and cMVs (90+ nm).

4.18 The effects of centrifugation speeds and time on levels of recoverable MVs

Techniques to isolate MVs are varied and there is no consensus with research methods, so the following experiments were carried out. THP-1 (1 x 10^6 /ml) were stimulated for MV release and the MVs isolated using the usual protocol except for the final centrifugation step where 5 different treatments were applied; 30 min at 10,000 *g*, 60 min at 10,000 *g*, 60 min at 15,000 *g*, 60 min at 25,000 *g* and 90 min at 25,000 *g*. The MVs were counted by FACs analysis and their morphology ascertained. Confirmatory tests of MVs were Annexin V binding to PS.

The assessment of various centrifuge speeds and times indicated that 25,000 *g* for 90 min isolates larger MV numbers and a wider variety of MV sizes.

4.19 Nanosight particle tracking analysis (PTA) of MV and exosomes from THP-1 cells

THP-1 (5 x 10^5 /ml) were rested in RPMI 1640 for 1 h. The supernatant was collected and analysed using Nanosight (PTA) to reveal two distinct populations of microvesicles that were constitutively released (Fig 4.15). PTA offered new insights into the nature of vesicles released, showing them to be released rapidly over the course of 1 h. Interestingly, exosomes and cMVs overlap leading to a large population of mixed particles 80 – 90 nm (Fig 4.19A). Although exosomes and cMVs have distinct protein markers and different shaped morphologies, it was beyond the scope of the Nanosight as this time to differentiate between the two. Other data (Fig 10.4) indicates that exosomes account for a smaller proportion of 90 nm vesicles, their population size peaking at 80 nm; therefore cMVs could be smaller than first anticipated. Without

further analysis including microscopy and ratios of CD63 : PS being analysed all that is certain that there is an overlap in this region (Ansa-Addo *et al*, 2009). The nanosight image depicts exosomes and cMVs 1/100 dilution, indicating that vast numbers of vesicles are rapidly released into the fresh media (RPMI 1640 was analysed and found to be totally abscent of microvesicles), mainly as communicative vectors.

Fig 4.20 Quantification of sizes of MV subtype using qNano

Samples of sonicated MV subtypes were analysed for size differences using qNano (Fig 4.20). The profile produced is reminiscent of the profiles produced by both flow cytometry ExpressPlus and nanosight particle tracking. This data consolidates a general rule for MV subtype identification using biophysical techniques.

MVs were diluted 1 x 10^5 /ml in PBS to optimise this technique. Limited by the pore size, particles below 700 nm were not observed (typically exosomes in this region). Both MV subtypes show a distinctive morphology identifying them as MVs. However 95% of cMVs were 700 – 2250 nm and sMVs extend into a significantly larger size range, 95% lying in the range 700 – 3550 nm.

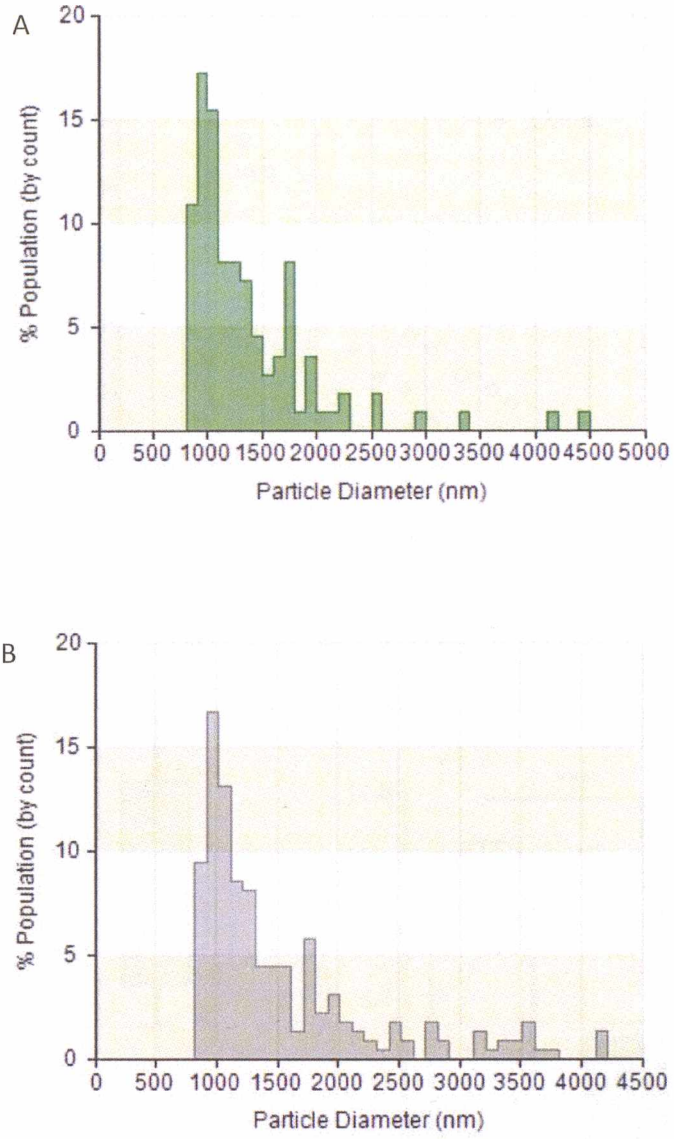

Fig 4.20 qNano size quantification of microvesicle subtypes. Microvesicle subtypes were isolated from THP-1, sonicated for 5 min and diluted to 1 x 10^5 /ml with PBS before being submitted for qNano size analysis. (A) cMVs (green) vary 700 – 2200 nm >95% with a mean particle sample size ~1.3 µm and a mean particle span 2.1 e^{-3} (B) sMVs (grey) vary 700 – 3800 nm >95% with a mean particle sample size ~1.5 µm and a mean particle span 2.6 e^{-3}. All microvesicle subtypes have a small distinct population at ~1700 nm.

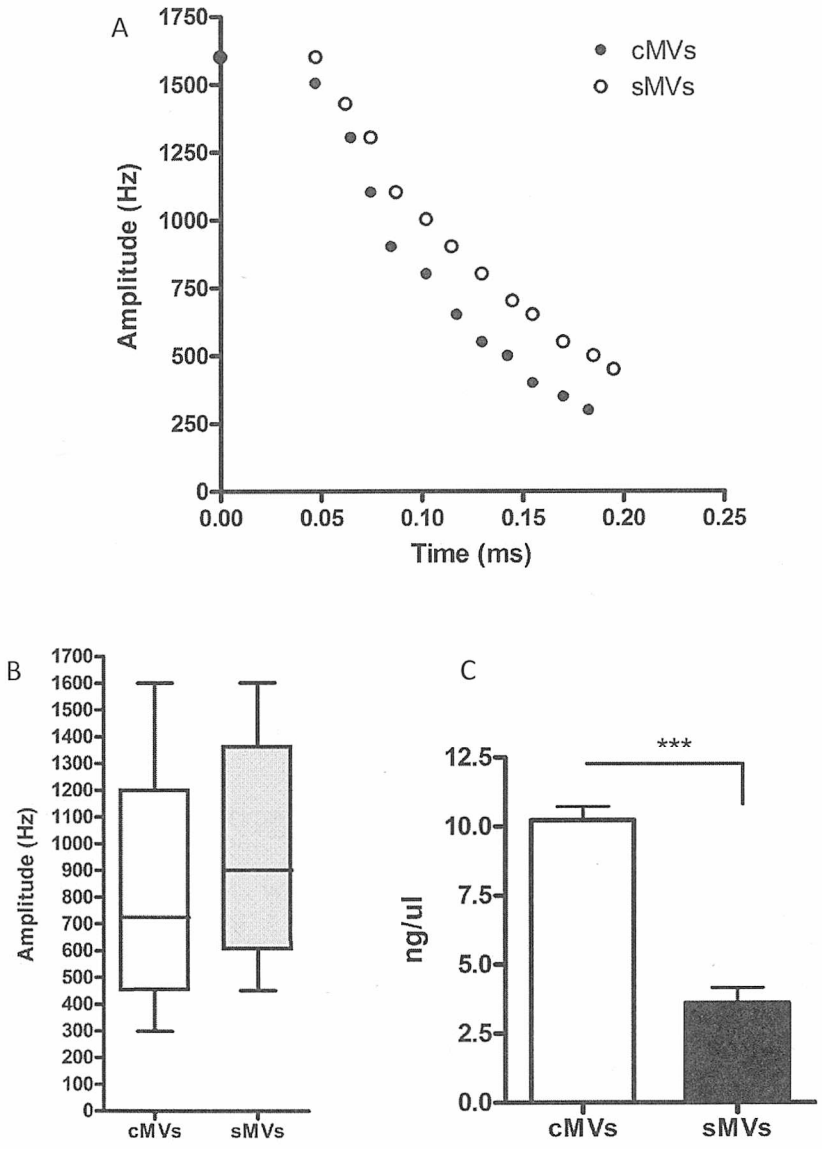

Fig 4.21 Q-sense (QCM) analysis of MV subtype population rigidity/mass suspended in PBS. (**A**) MV subtypes were analysed for their ability to quench oscillating momentum using QCM F3_1. cMVs amplitude dissipates significantly faster than sMVs indicating that cMVs were deposited on the sensor faster than sMVs. This suggests that cMVs have a larger mass that sMVs. (**B**) MV subtypes were pulsed on the QCM at 1485679 Hz (1.48 MHz), their amplitude was measured for a duration of 0.16 ms. cMVs had 11 oscillations compared to sMVs that had 12 oscillations. cMVs dissipate their energy for motion quicker than sMVs, as they display a shorter half life, indicating that cMVs are denser than sMVs. (**C**) 1 x 10^6 MVs/ml were quantified using NanoDrop microbalance, 2 µl of MV subtypes typically contained 2000 MVs, were assessed for their weight. cMVs (~10.0 ± 1.0 ng/ul) were consistently significantly heavier than sMVs. (~3.5 ± 1.0 ng/ul).

4.21 Q-sense quartz crystal microbalance analysis of MV subtype population rigidity/mass suspended in PBS

MV subtypes were analysed on the Quartz Crystal Microbalance (QCM) by Q-sense to ascertain their mass. This was determined by their behaviour when applied to a pulsing resonant frequency of 5,000,000Hz. The sub-harmonic frequency '3' (1,485,679Hz) was selected as this frequency tended to resonate the centre of the sensor and yield clearer results. cMVs were found to quench the amplitude of the wave significantly faster than sMVs (Fig 4.21A). This quenching of the wave shows that the cMVs have greater mass than sMVs as their energy of momentum dissipates faster than sMVs and they more rapidly accumulated on the QCM sensor.

The weight of the MV subtypes differs considerably as measured using a NanoDrop microbalance. The results were repeatedly consistent showing that cMVs are significantly heavier that sMVs. (Reasons for this anomaly are thoroughly explored in Chapter 5.)

cMVs vary little across populations and the weight is highly conserved; 11 ng/ul. sMVs vary more although their weight is more or less consistent; 4 ng/ul. cMVs being smaller must contain more and/or heavier components than sMVs; this result is consistent with the calcium data previously presented and the quenching of momentum as measured with the QCM (q-sense).

Fig 4.22 Blockade baseline duration of MV subtypes

Blockade baseline duration (BBD) is the 'flight time' of MVs in a electromagnetic field and indicated the relative surface charge of particles. Approximately 5 x 10^4 MV subtypes/ml were sonicated and applied to qNano for measurement of their BBD. Owing to the larger surface area, there is a larger amount of negatively charged lipids such as PS and PC on sMVs than cMVs. Indeed, sMVs had a BBD of ~2.6 ms and cMVs of ~1.4. Furthermore the BBD of ≥90% cMVs was below 2 ms where as the BBD of ≥90% sMVs was below 6 ms.

Fig 4.23 Freeze thaw action on sMV viability

Storage conditions play an important role in MV viability and recovery. DMSO was used as a cryoprotectant and compared to conditions without cryoprotectant at different storage temperatures. sMVs exhibit greater susceptibility to freeze induced damage/lysis than cMVs (Fig 4.23). Furthermore it was found that cMVs are robust enough to survive at both 4 °C and -20 °C with negligible reduction in numbers. sMVs were most damaged by freezing without cryoprotectants.

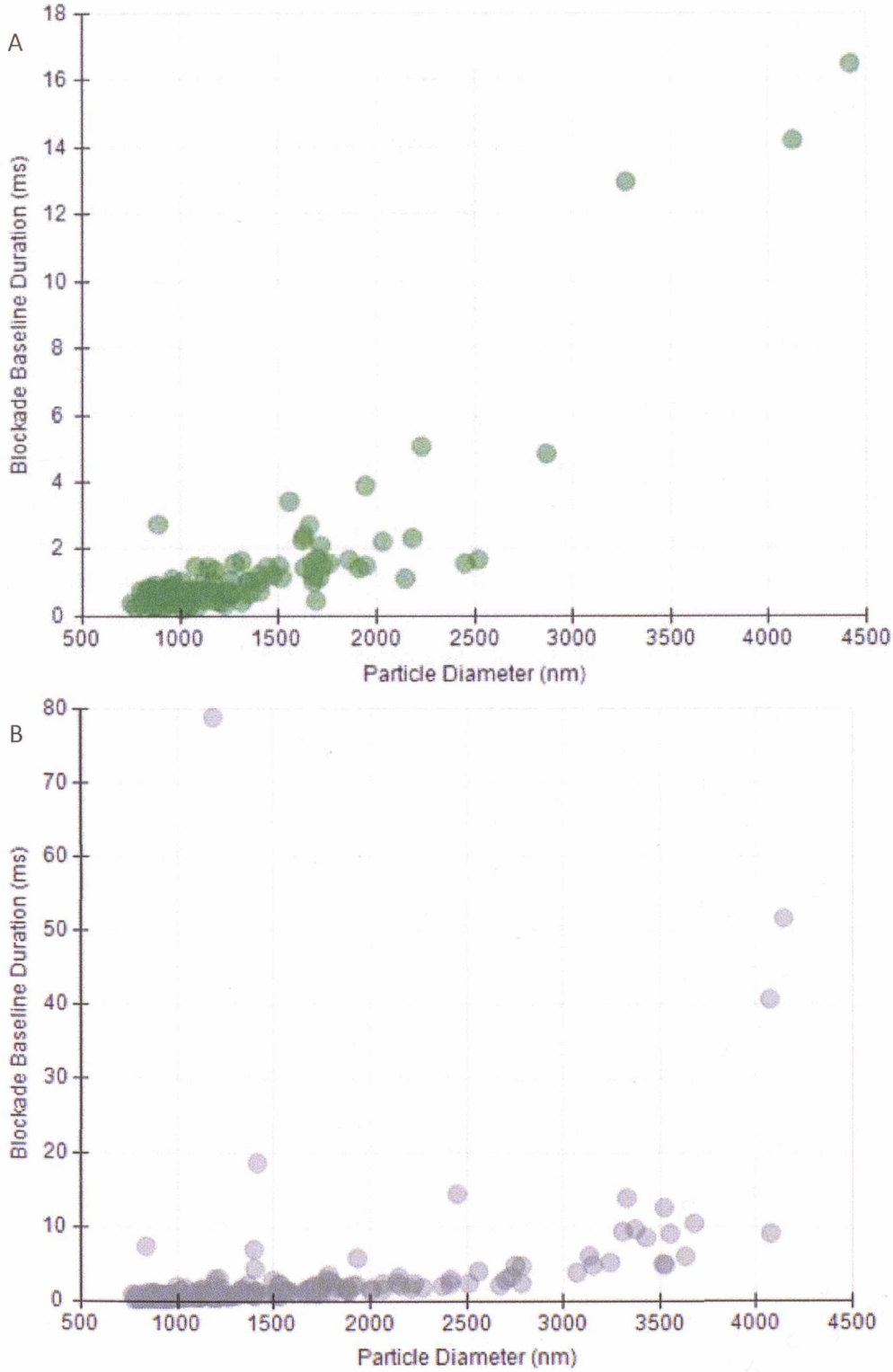

Fig 4.22 The blockade baseline duration (ms) of microvesicle subtypes. Microvesicle subtypes isolated from THP-1 were diluted 1/20 with PBS and submitted for qNano analysis, (A) cMVs (green) blockade baseline duration >90% population was an average of 1.42 ± 1 ms for particle size in the range 700 – 2500 nm. (B) sMVs (grey) blockade baseline duration >90% 2.6 ± 1 ms for particle size in the range 700 – 2700 nm and a subpopulation of particles (3000 – 3700 nm) has a blockade baseline 5 – 15 ms.

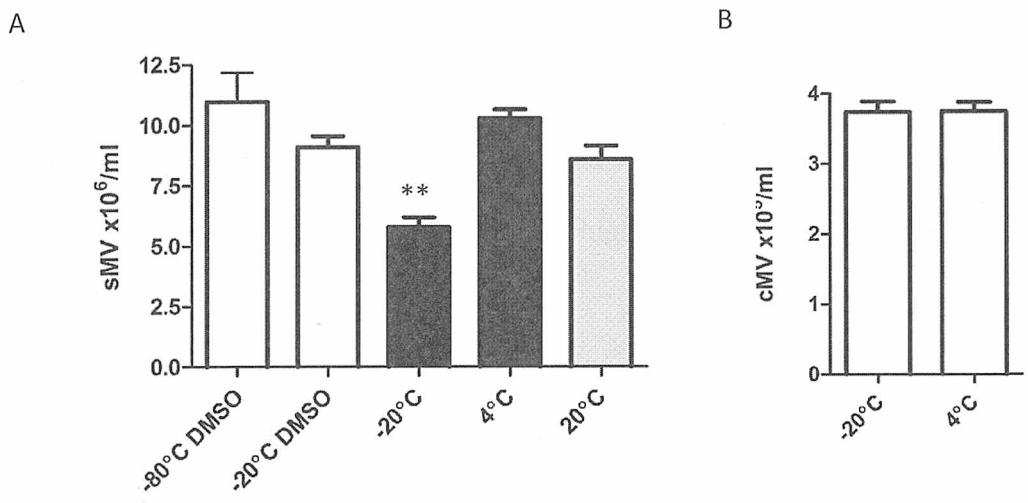

Fig 4.23 sMVs were stored using different conditions. (**A**) sMVs (~1.2 x 10^6 /ml) were subjected to different storage conditions. It was found the optimal storage conditions were -80 ^oC with DMSO and 4 ^oC. While DMSO offered protection against freeze thaw lysis, -20 ^oC were the worst storage conditions for sMVs. These results indicate that sMVs are relatively fragile. (**B**) cMVs (~4 x 10^5 /ml) were subject to either -20 ^oC or 4 ^oC for 24 h. The data collected indicates that for 24 h there were no significant loss in MVs stored.

4.24 Discussion

The data presented supports the hypothesis that cells release two distinct types of MV, that vary considerably in size and morphology as well as their biogenesis. Cells release low levels of cMVs into the culture medium and high levels of sMVs when stimulated.

THP-1 were cultured in media containing RMPI 1640, 1% penicillin and streptomycin and 10% FBS (filtered) for 1 h and 24 h, MVs were collected and analysed by FACS, and compared to 10% NHS stimulated MVs for 30 min. The MVs displayed different population morphologies and were released in different numbers (Fig 4.11) It can be concluded that the MV subtypes observed had different biogenesis.

MVs derived from differing media produce two distinct MV subtypes (exosomes are not included as they are not the focus of this thesis), constitutively released MVs (cMVs) from tissue culture media and stimulated MVs (sMVs) from RPMI 1640 with 5 - 10% NHS and 2 mM $CaCl_2$. cMVs are released from cells that are not undergoing stress (Fig 4.6, 4.11), rather a product of normal cellular functioning (Inal *et al*, 2012). cMVs are distinct from exosomes (Muralidharan-Chari *et al*, 2010); expressing a variety of different receptors such as CD9 and CD63 on exosomes (Kushlich *et al*, 2010) and PS as a biomarker for MVs (Angelot *et al*, 2009) (Fig 4.16 and 5.5B). sMVs, cMVs and exosomes have characteristically different sizes with distinct physical morphologies (Fig 4.11 – 4.16, 4.21 and 4.23), biochemistries (Fig 4.22 and See Chapter 5) (Heijnen *et al*, 1999; Akoi *et al*, 2007) and pathways for biogenesis (Muralidharan-Chari *et al*, 2010; Inal *et al*, 2012).

MVs are released from most mammalian cell types (D'Souza-Schorley and Clancy, 2012), indeed as described in this thesis they have been observed them from THP-1, HeLa (Fig 4.11), PC3, PNT2, MCF7, MBA MB 231 and CHO K1 (Chapter 5). HeLa released cMVs in greater numbers than THP-1 but HeLa released sMVs in smaller numbers than THP-1 (Fig 4.11). Indeed, HeLa proliferate faster than THP-1 so it may be expected that the biogenesis of cMVs would be elevated. However HeLa are adherent and grow in clusters until at confluency, they typically expose their 'upper' surface to stress agents compared to the non-adherent THP-1, that exposes their entire surface. Essentially stress agents have a larger surface area to bind to on THP-1 than HeLa. Furthermore HeLa will have different tolerances to various types of membrane damage. It was found that the numbers of MV subtype shed varied considerably across cell types, owing to their unique morphologies and biochemistries (Chapter 5).

Cells produce MVs at a constant low basal level, that are small, 80%≤ ~0.1 - 0.3 μM (Fig 4.15, 4.16, 4.19 and 4.20) robust (Fig 4.23B) and appear to have different ability in their biological roles (Fig 4.9 and 4.10). Their biogenesis is not fully understood, but their biochemistry is considered in detail in Chapter 5. However they contain relatively high concentrations of bio-available calcium (Fig 4.5B). cMVs are released into tissue culture medium and require no special conditions to stimulate their release.

sMVs biogenesis is better understood. They are released in response to cellular stresses, such as sublytic MACs formed from treatment with NHS. They are larger than cMVs, 65% ≥ ~0.3 - 0.5 μM and 20% ≤ ~0.5 μM+ (Fig 4.15, 4.16, 4.19 and 4.20). They are more susceptible to damage such as freezing than cMVs (Fig 4.23 and Fig 10.4).

The TEM of sMVs reveal them to be larger, approximately 600+ nm, less dense vesicles than cMVs, that are smaller, with sizes approximating 200 nm and electron dense. Exosomes have a biconcave morphology with sizes up to 100 nm (Fig 4.14)(Koga *et al*, 2005; Akoi *et al*, 2007). The MV subtypes are released in different quantities, cMVs accumulated in media 24 h old number 1.5 x 10^4 /ml however sMVs number 2.5 x 10^6 /ml (Fig 4.11 A).

sMVs are released from the cell surface responding to stressing agents as a mechanism to circumvent apoptosis. Typically most mammalian cells exist in a state of pseudoapoptosis as their environments (MacKenzie *et al*, 2005), although well maintained are fragile and fluctuations within micro-environments constrain cells (Fig 4.1), such as local changes in osmolarity, protein availability, ion concentration and so forth (Mackenzie *et al*, 2005; Bevilacqua *et al*, 2010). Furthermore, cells are also subject to a host of potential stress triggers including rapid environmental change, pathogen related stresses or mechanical stresses (Brereton and Blander, 2011). These stresses, if left to accrue will ultimately result in apoptosis or in extreme cases necrosis (Janssen *et al*, 2009; Bevilacqua *et al*, 2010). Membrane pores, such as MACs, typically cause an uncontrolled rise in intracellular calcium that could lead to many types of metabolic damage (Fig 4.5A) in particular, the deactivation of scramblases and flippases that maintain membrane asymmetry leading to increased PS expression on the outer leaflet of the cell (Fig 4.2). Calcium drives many biochemical reactions and may act as second messengers for many intracellular signalling pathways (Rizzuto and Pozzan, 2006). However this calcium influx may be localised to a micro-environment adjacent to the membrane breach rather than being completely cytosolic and therefore recoverable (Rizzuto and Pozzan, 2006).

Homeostatic mechanisms operate within the cell that initially sequesters intracellular calcium to specialised organelles. However excess cytosolic calcium causes the formation of a membrane bleb containing damaged cell components, the excess intracellular calcium (Gutwein *et al*, 2005; Mackenzie *et al*, 2005) (Fig 4.5B), externally expressed PS and the MAC that will 'pinch off' to form sMVs (Moskovich and Fishelson, 2007), expelling the breach that would allow continuing damage (Fig 4.8) (Moskovich and Fishelson, 2007). Indeed optimal concentrations of calcium in the media for sMV production are 1 – 2 mM (Fig 4.4) in conjunction with membrane breaches, 4+ mM causeing significant irreversible cell damage that leads to apoptosis (Vindis *et al*, 2005; Roos *et al*, 2012). The degree of plasma membrane damage directly influences the number of sMVs released, Fig 4.3 shows that increasing THP-1 cell number in a fixed volume of 10% NHS decreases the sMV number released. If one MAC caused the formation of one sMV, changing the cell number would not affect the number of sMV released, thus demonstrating that multiple MACs and therefore more than one membrane breach is required to produce a microvesicle. The Q-sense QCM measured a significant change in cellular mass at 27 min typical of sMV release (Fig 4.7A and 4.7B), measured at 2 subharmonics. The Q-sense QCM detected a decrease in media fluidity, attributed to increases of membrane blebbing on THP-1 (Mackenzie *et al*, 2005) at 27 min due to MV release (Fig 4.7D). MAC inserted into the membrane of THP-1 are present until microvesiculation has occurred up to ~30 min (Fig 4.8) whereby the MACs have been shed with the MV.

Once released, sMVs export significant amounts of calcium (Fig 4.5B), so that immediate re-stimulation is not possible and a 30 min refractory begins (Fig 4.5A and 4.6), whereby the cell recovers sufficient intracellular calcium concentration to enable

subsequent microvesiculation (Fig 4.5A and 4.6). Calcium induced refractory periods are a typical feature of many cellular vesicle pathways (Rizzuto and Pozzan, 2006). The sMVs contain low levels of calcium (Fig 4.6B), that is deliverable to cells thus temporarily increasing intracellular calcium of the recipient cell (Fig 5.1), whose typical resting Ca^{2+} potential is 100 nM (Rizzuto and Pozzan, 2006). Although sMVs have low calcium levels, they are released in large numbers, all capable of delivering a small calcium cargo (Muralidharan-Chari *et al*, 2010) or releasing it into interstitial fluid or culture medium.

cMVs are released as communicative vectors and are produced in a different manner to sMVs. They are not produced as a response to stress agents, so do not respond to extracellular calcium concentration *per se* and cMVs are released at a low constant rate (Fig 4.6) accumulating in the culture media, no significant differences in numbers released having been observed over the course of these experiments. cMVs contain significantly more calcium than sMVs (Fig 4.5B).

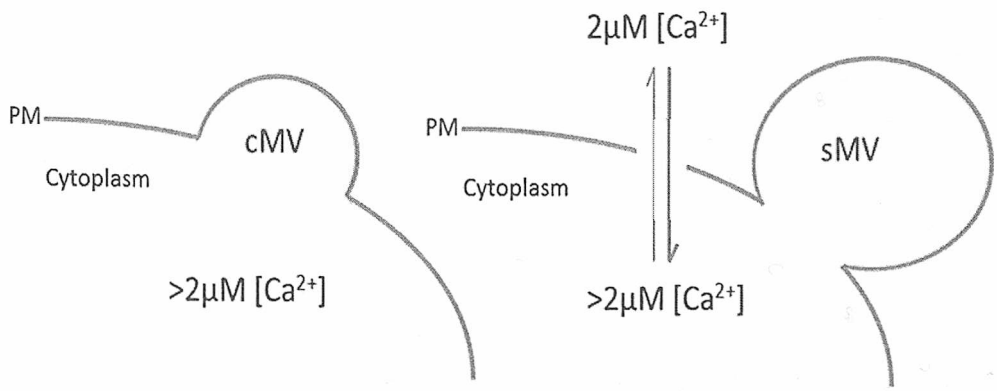

Fig 4.24 Free calcium leads to MV development. cMV formation arises by including internal cellular sources of Ca^{2+} , sMV formation arises from a net Ca^{2+} influx through a membrane pore as well as internal cellular Ca^{2+}, inducing stresses leading to membrane and cytoskeletal damage. This damage causes membrane blebs, where Ca^{2+} can be exported, minimising Ca^{2+} induced cellular damage. This bleb pinches off to form sMVs.

Typical MV subtypes were weighed using NanoDrop microbalance (Fig 4.8), 2000 MVs were weighed, the highly consistent results demonstrate that cMVs, although much smaller, weigh (10 ng for 2000 cMVs) significantly more than sMVs (3.8 ng/μl for 2000 sMVs). When MV subtype density was measured by Q-sense QCM, it was found the cMVs have a higher density than sMVs (Fig 4.21). cMVs' BBD is lower than for sMVs indicating that cMVs have a lower surface charge and contain less PS and/or charged proteins (Fig 4.22) owing to surface area size constraints.

MV isolation techniques were assessed for their effectiveness. A range of centrifugation speeds were selected and MVs stimulated from THP-1 and isolated identically until the final centrifugation step (Fig 4.18). MVs were isolated at different published (Heijnen *et al*, 1999; Akoi *et al*, 2007; Grant *et al*, 2011) centrifugation speeds. The quantities increased significantly at 25,000 *g* for 90 min (Fig 4.18). The centrifugation speeds were increased, smaller sized MVs were isolated (Fig 4.18), thereby eliminating the possibility of shearing forces as a possible MV degrading step.

THP-1 respond to MV subtypes derived from THP-1 by undergoing significant proliferation, cMV stimulated THP-1 underwent more rapid proliferation than sMVs, although the difference was barely statistically significant (Fig 4.9), see Chapter 5. This indicates that an undetermined mechanism other than proliferation due to sublytic MACs had caused this phenomenon. It could be conjectured that MV subtypes carry both signalling molecules and Ca^{2+} that contribute to cellular proliferation. MV subtypes were also found to aid in *salmonella typhimurium* survival when cultured in lytic levels of NHS. sMVs offer salmonella ~63% survival rate compared to ~22% with cMVs. It can

be speculated that MV subtypes can 'soak up' MACs in a competitive way to salmonella or that MACs themselves contain complement regulatory proteins that aid in protecting *Salmonella* from complement mediated lysis.

To summarise, there are two distinct MV subtypes that can arise from the same parent cell type, exhibiting characteristic morphologies and modes of origin. Although identifiable as MVs, their distinct physical profiles specialise them for different biological roles, cMVs are communicative vectors, whereas sMVs act primarily as a response to apoptotic triggers as transmitters of apoptotic signals or may play a role in inflammation and attraction of macrophages to sites of stress or injury. Their construction is different owning to their biogenesis. cMVs are well constructed and potentially having a longer half life. Conversely sMVs are produced as a rapid response to stress, are poorly constructed with a shorter half life (Fig 4.22) acting to offer cellular protection from lysis and as a chemotactic attractant for monocytes i,e., large surface area with enriched PS expression (Chapter 5 and Fig 4.23).

The release of cMVs from a cell is due to a number of variables, both observable and undetermined, leading to highly similar but not identical cMVs. The molecular data that they carry may vary, giving rise to all or nothing responses. The 'instruction' being delivered by an MV may be lost or insufficient on its own to alter the metabolism or effect change within the recipient cells. Therefore no measurable change within a recipient cell can be observed (the observation is often sought, such as change in particular protein expression, or change in morphology; this in itself is dependent on an operating mechanism, that would be initiated by the release or receipt of a signal).

The entropy (s=0) because $H_{n+1}(MV_1,..MV_n, 0)$ $\{H_{n+1}\}$ total energy and or molecular input from the tissue or cell, $\{MV_{1...n}\}$ are the possible population of MVs released. However MVs contain molecular information or Ca^{2+} able to effect change thereby increasing the entropy of the system because $H_{n+1}(MV_1,..MV_n, 1)$. MVs are released in quantifiable amounts into a tissue culture, however one cell may only release one MV per day therefore on a cellular level, the likely outcome of a MV increasing entropy is (s) ≥ 0, but as a tissue the likely outcome of MVs increasing entropy (s) ≤ 1. Indeed the observed change in mass using the QCM indicates that MV release from a cell increases its own entropy (Fig 4.7), changing its biochemical profile and possibly preventing apoptosis. sMVs are released as a direct response to stress, their ability to affect change is (s) ≤ 1, as they are produced in larger numbers, are bigger and most likely carry the initial or derived stress agent. This has been observed experimentally where sMVs carry apoptotic signals to recipient cells (Jorfi *et al*, 2010), their ability to prevent complement mediated lysis is enhanced and so on.

The distinction between MV subtypes originating from the same parent cell type is important when studying their biological functions to avoid conflicting and confounding results. Not only are MVs subject to different release pathways, but sMV biochemistry may also vary according to the stress agent used to stimulate them.

5. MV SUBTYPE BIOCHEMISTRY AND BIOCHEMICAL ANALYTICAL TECHNIQUES

5.0 Introduction

There are significant biochemical and biophysical differences between MV subtypes, such as size, mass and protein profile, such that a detailed characterisation needs to be performed. MVs have been described as extracellular membrane vesicles (eMVs) that only express PS, PC, proteins and receptors that are present on the originating cell and that and where in some circumstances protein enrichment can occur. However, due to their seemingly different properties, for example, protection against lysis, it is feasible that MV subtypes are released for distinctive biological roles. The contradictory roles for MVs being released from the same parent cell are due to a lack of consideration of MV subtypes.

eMVs (exosomes, MVs and apoptotic bodies) are implicated in many biological roles, eluicidation of the biogenesis pathways are crucial for the effective exploitation of eMVs. This can indicate their physiological roles and offer the potential to engineer MVs for specific functions and even to be used as vectors to administer therapies (Zeelenberg *et al*, 2008).

The research presented in this chapter used different biochemical techniques to highlight significant differences between MV subtypes and their parent cells. Although research has investigated biochemical components of MVs, this is the first research (as of ISEV 2012) to investigate MVs of distinct population subtypes with different origins.

FT-IR analysis has been used recently to describe holistic differences between cell types, changes in cellular chemistry and even organelle function. Investigation into the similarity between MVs and their parent cells may lead to a method to identify disease using MVs subtypes derived from particular cells contained within blood plasma or lymph. In reality FT-IR is a powerful classical chemistry tool and the application to biological systems is somewhat progressive, however FT-IR is still in its initial stages for analysing whole cells and rigorously defined criteria needed to be adhered to for meaningful comparisons. Identification of regions with strongly associated biochemical features was essential i.e., DNA region and where available identification of particular proteins, such as amide I (one). Amide I became an internal standard for all the samples, so that ratios of selected peaks relative to amide I would allow generation of meaningful and comparable data.

As previous work concluded that apoptosis could be determined using FT-IR, it became essential to ensure that all cells being investigated were maintained in optimal conditions and at high viability.

A thorough investigation of general biochemistry was undertaken, with regard to protein, carbohydrate, calcium, reactive oxygen species and both GPI anchored and transmembrane receptors for MV subtypes. Furthermore, physiological roles for MVs were investigated such as receptor transfer or cargo delivery between cell types and protection against complement.

5.1 MV subtypes deliver different concentrations of calcium cargo to THP-1 cells

THP-1 (5 x 10^5 /ml) were loaded with 9 µl of calcium green-AM (50 µM) dye and incubated at room temperature for 30 min on an orbital shaker. The THP-1 were washed 2x by centrifugation using sterile PBS and finally suspended in CGM. cMVs (2 x 10^5 /ml) were incubated with calcium green loaded THP-1 and sMVs (2 x 10^6 /ml) were incubated with calcium green loaded THP-1 for 1 h. The cells were analysed with FLUOstar Ω multiplate reader, stimulating at A_{485} and reading at A_{520}.

cMVs have been shown to carry a significant concentration of calcium (Fig 4.5B) relative fluorescence ~31 ± 3 A_{520} compared to an unlabelled control. Unlabelled cMVs were incubated with calcium green labelled THP-1 to assess the increase in calcium concentration upon binding or fusion of cMVs to THP-1. cMVs deliver a significant concentration of free calcium to THP-1, increasing calcium green fluorescence ~3.0 ± 0.8 A_{520}. Small numbers of cMVs were used to simulate physiological conditions (1x cMV: 50x THP-1).

sMVs also carry free calcium (Fig 4.5B) relative fluorescence ~15 ± 1.1 A_{520} compared to an unlabelled control, although in much lower concentrations than cMVs. A larger quantity of sMVs was used to observe any differences in free calcium concentration. There was a smaller but significant concentration of free calcium delivered to THP-1 via sMV cargo, increasing calcium green fluorescence ~3.0 ± 1.2 A_{520}, even though (1x sMV: 5x THP-1). It should be nated that variability in delivered calcium may also be due to the non-uniform nature of sMV construction. The implications of this result demonstrates that low concentrations of cMVs can deliver sufficient free calcium to

cells such that they may affect cellular metabolism; however sMVs would have to bind to cells in greater numbers (≥50 fold) to deliver the same concentration of free calcium that cMVs deliver (Thomas and Salter, 2010).

5.2 MVs transfer DAF receptor to deficient cell lines CHO-K1 (DAF^-)

Incubation of HeLa derived MVs $CD55^+$ (DAF^+) with CHO-K1 (DAF^-) leads to CHO-K1/HeLa MV fusion events and transient transfer of DAF receptor to CHO-K1 (DAF^+); other proteins and receptors (not measured) would also be transferred from HeLa to CHO-K1 via MV fusion events. Optimal conditions for fusion were achieved by incubating 1x HeLa MVs (DAF^+): 1x CHO-K1 (DAF^-). HeLa (5x MVs: 1x CHO-K1) when incubated with CHO-K1 lead to lower incidents of fusion ~3.6%. Fluorescent microscopy and flow cytometry was used to examine the presence of anti-DAF antibody conjugated to FITC label. This confirmed the transfer of DAF from HeLa to CHO-K1, albeit at a low but statistically significant ~5.3% level (Fig 5.2B), however HeLa DAF expression was ~10% (Fig 10.5).

Receptor transfer was confirmed by fluorescent microscopy, CHO-K1 (DAF^+) can be observed, with a weak signal, CHO-K1 (DAF^-) showing no fluoresce. Furthermore the FITC labelled DAF appears to have mixed with the CHO-K1 and is not observable as distinct packets, indicating membrane fusion and lipid mixing (Fig 5.2A)

A lysis assay using 25% NHS was performed on CHO-K1 (DAF^+). The presence of DAF transferred to CHO-K1 conferred protective properties enabling CHO-K1 (DAF^+) to

withstand the formation of MACs leading to a higher viability >5.3% than the control (Fig 5.2C). This reaction demonstrates that receptor transfer is possible, even between different species and that the receptor can retain its original function on the recipient cell.

5.3 MV subtypes have different avidity for complement proteins, conferring different capacity for protection against MACs

MV subtypes were assessed for their avidity for MAC (Fig 5.4A and 5.4B). Although both MV subtypes exhibit different capacity for complement protective roles (Fig 4.10), serial dilutions of MV subtype ratios to THP-1 was performed to identify differences in ability for preventing C3b formation and subsequent changes in cell population viability. The results were significant for cMVs a ratio of 1:64 (THP-1: cMVs) but were not significant for sMVs 1xTHP-1:64x sMVs, however a trend of decreasing viability was apparent (Fig 5.4A and 5.4B). Furthermore the error bars for sMVs were larger than for cMVs as sMVs have less homogeneity in size than cMVs (Fig 4.15) and because biogenesis of sMVs releases vesicles of variable construction.

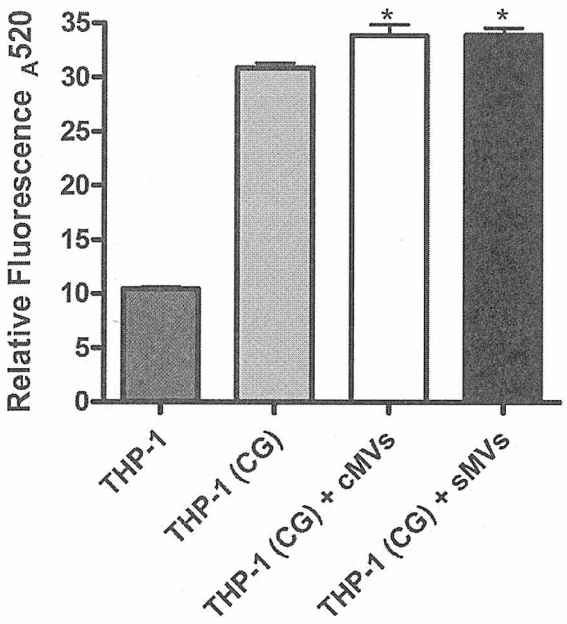

Fig 5.1 MV subtypes deliver different concentrations of calcium cargo to THP-1 cells. THP-1 (5 x 10^5 /ml) were incubated with calcium green-AM dye (CG), the total internal calcium measured $_A$520 THP-1 (CG). Approximately 1 x 10^4 cMVs were incubated with THP-1 for 1 h at 37 ^oC, the total internal calcium measured of cMVs fused to THP-1, approximately 1 x 10^5 sMVs/ml were incubated for 1 h with THP-1 at 37 ^oC and the total internal calcium of THP-1 + sMVs was quantified using FLUOstar Ω multiplate reader, measuring fluorescence stimulated at $_A$485 and measured $_A$520. cMVs deliver significant concentrations of calcium cargo to THP-1 (33.85 ± 2.89 $_A$520), sMVs deliver slightly more (33.94 ± 2.91 $_A$520).

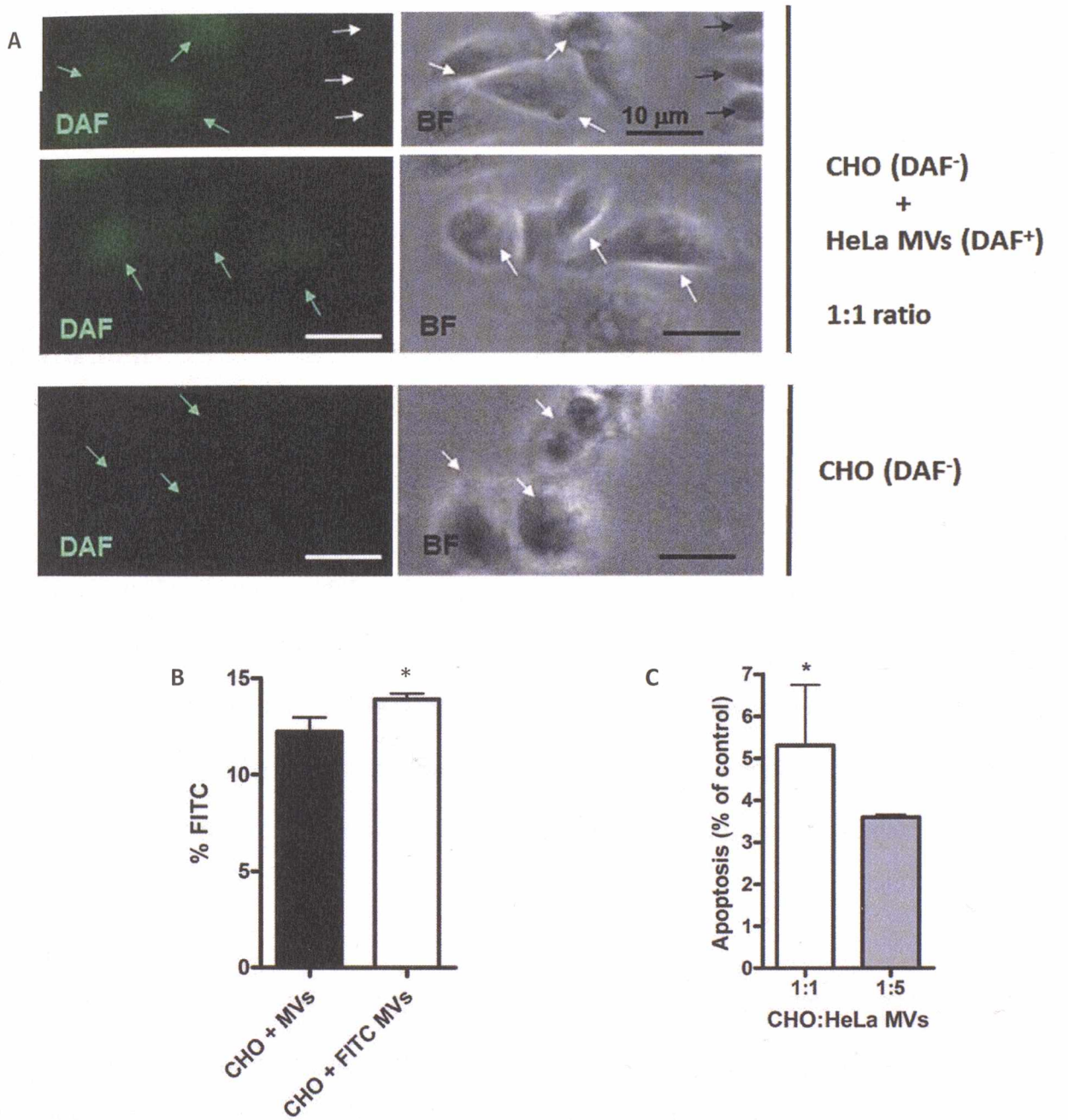

Fig 5.2 MVs derived from HeLa (DAF$^+$) transfer ~5% DAF to CHO-K1 (DAF$^-$) and confer the physiological properties of DAF to CHO-K1 (**A**) Fluorescent microscopy revealed the transfer of HeLa derived DAF$^+$ MVs to DAF$^-$ CHO-K1. (**B**) CHO-K1 incubated with DAF$^+$ MVs and labelled with Human anti DAF FITC labelled significantly increased fluorescence in the FITC spectrum >3 – 5% using flow cytometry, ExpressPlus. (**C**) The Transfer of DAF to CHO-K1 via HeLa MVs (1:1) significantly protects the cells from complement mediated lysis; ~5.3%, however (1:5) is not statistically significant; ~3.6%. Viability was assayed using ViaCount.

5.4 MV subtypes carry different concentrations of proteins

The amount of the protein content of MV subtypes was carried out in two ways. Firstly a protein assay was performed. This method compared lysed MVs expressing total protein to a standard of known BSA protein concentrations. This method revealed that cMVs contained significantly more protein ~44.0 ± 1.5 ng/ml than sMVs ~28 ± 3 ng/ml. However this method did not indicate the nature of proteins that were being measured (Fig 5.4A).

The second method was direct measurement of proteins A_{280} using a NanoDrop spectrometer. A similar pattern to the assayed proteins was observed, whereby cMVs contained more protein ~0.40 A_{280} than sMVs ~0.17 A_{280} (Fig 5.4B). The Lowry method of protein determination indicates total protein content by the presence of Cu^{+} reduced by alternate peptide bonds. However the NanoDrop spectroscopic method of protein method, measures the UV absorption of amino acid associated aromatic rings.

Interestingly, this simple spectroscopic assay highlighted that there was a higher proportion of proteins in cMVs than sMVs and that these proteins contained phenylalanine, tryptophan, histidine and tyrosine with an associated aromatic ring structure responding to A_{280} that also ~3x more abundant in cMVs (Fig 8.5B).

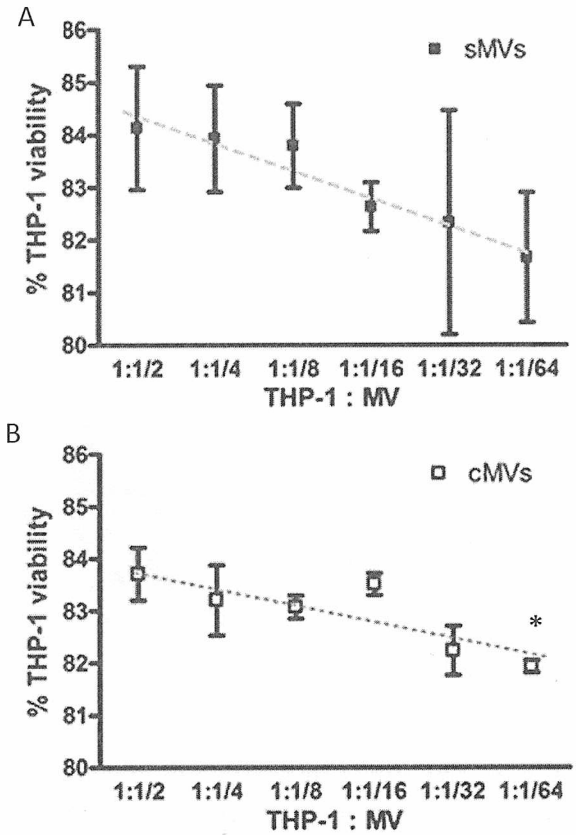

Fig 5.3 MV subtypes have significantly different avidity for complement proteins offering protective properties to THP-1. (**A**) sMVs offer less protection to THP-1 against complement mediated lysis while suspended in 45% NHS as their concentration decreases from 1:1/2 affording ~84% viability to 1:1/64 affording ~81.5% viability. (**B**) cMVs offer significantly less protection to THP-1 against complement mediated lysis while suspended in 45% NHS as their concentration decreases from 1:1/2 affording ~83.8% viability to 1:1/64 affording ~81.9% viability.

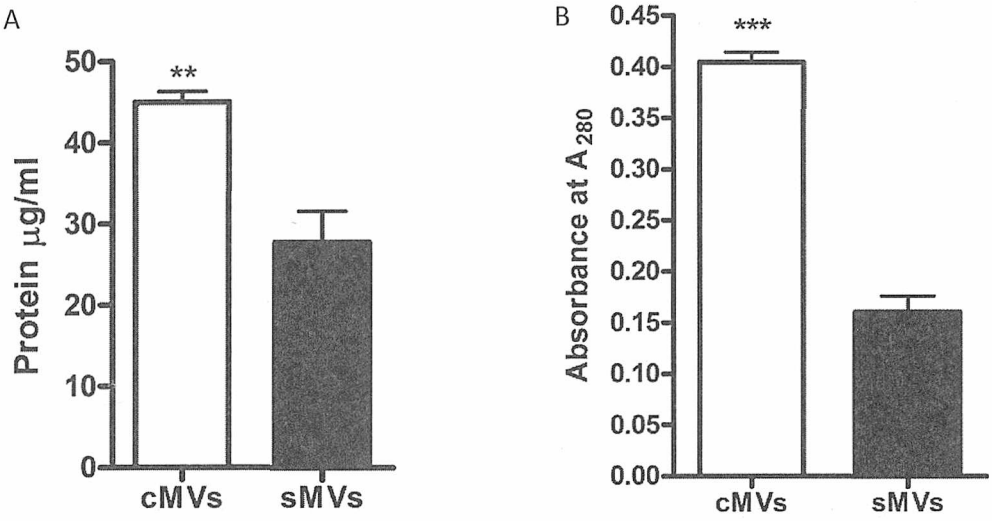

Fig. 5.4 Protein content analysis of MV subtypes. (**A**) 25,000 MVs were lysed in 1% (v/v) Triton X-100 and assayed for their protein content using a BSA protein assay kit. Measurements were taken with a spectrophotometer at A_{500} and optical density converted into µg/ml referencing a protein standard curve. cMVs were found to carry ~45 ± 2 µg/ml significantly more protein than sMVs ~28 ± 3.75 µg/ml. (**B**) Protein content, measured in terms of A_{280} using a NanoDrop showed cMVs to carry at least two-fold more protein (optical density 0.40 ± 1) than sMVs (optical density 17 ± 2). Results are the mean of multiple measurements of 2000 MVs for each subtype.

5.5 MV subtypes contain different protein types

The SDS-PAGE reveals all proteins present in THP-1 MV subtypes. All MVs show an enrichment of a 70 kDa protein. There are few protein bands congruent across MV subtypes, notably ~250 kDa, ~23.5 kDa and a ~33.4 kDa protein (Fig 5.9).

cMVs consist of a protein complement analogous to the parent cell, in particular ~48, ~55, ~60, ~62, ~70 and ~150 kDa. sMVs are enriched for a few proteins and others are totally absent, such as ~125 kDa. However both MV subtypes are enriched for particular proteins, most notably ~70 – 80 kDa (Fig 5.9). 62.5 and 150 kDa proteins may be monocytic differentiation markers that are present in cMVs but absent in sMVs, indicating different biogenesis pathways. Furthermore cMVs contain a 42 kDa protein that is possibly actin, sMVs do not contain significant concentrations of actin.

This confirms the initial protein data (Fig 5.8), indicating that sMVs may have less potential to carry out and perform communicative roles owing to a less diverse protein assemblage. It further emphasizes the potential for conflicting data should MV subtype be overlooked. Although the SDS-PAGE shows radical differences between subtypes, it was not possible to accurately describe the proteins present. This would require an in-depth proteomic study.

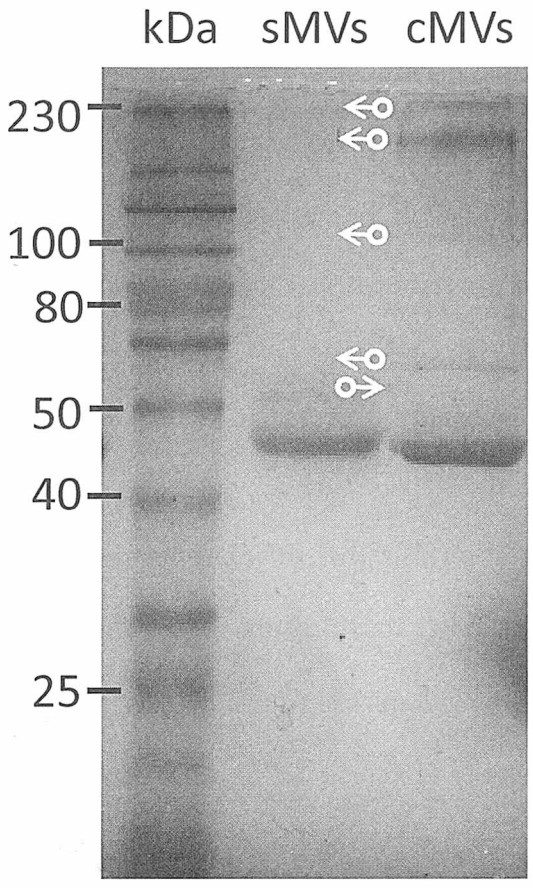

Fig 5.5 SDS-PAGE stained with silver stain showing protein profile of MVs and Cells. Profiles presented are of stimulated versus non-stimulated THP-1 monocytes as well as constitutively released (cMVs) and stimulated MVs (sMVs). 10μg protein was run per lane. Proteins bands lacking or severely diminished upon stimulation of cells are indicated by an asterisk. The band of ~130 kDa lacking upon stimulation that is common to THP-1 monocytes is shown by a red asterisk. Proteins in cMVs apparently lacking in sMVs are shown with clear circles. The protein that seems enriched in MVs compared to untreated or stimulated THP-1 cells is shown with a filled circle.

5.6 CD55 expression is regulated by microvesiculation

Whilst both HeLa and THP-1 express CD55 (Fig 5.2 and 5.6), HeLa were chosen for analysis for ease of use. HeLa were gated against a negative control using FACs analysis. CD55 is a Glycophosphadidylinositol (GPI) anchored complement inhibitory receptor that is expressed on the outer membrane leaflet and 'flows' with lipid across the cell surface. The HeLa were cultured with 50 nM PMA to increase CD55 (Hindmarsh and Marks, 1998) expression from ~3% to ~7% (Fig 10.5).

HeLa stimulated with DMEM supplemented with 10% NHS and 2 mM Ca^{2+} for 30 min at 37 ^{o}C released sMVs that coincided with a significant decrease in CD55 expression ~15% of the CD55 expressed (Fig 5.6A). It can be reasonably conjectured that the CD55 was released on sMVs (Fig 4.7 and 4.8A), in particular as the decrease in expression coinsides with the typical time taken for sMV release.

THP-1 stimulated for sMV release, showed significantly reduced CD55 expression ~19% (Fig 5.6B). THP-1 releasing cMVs reduce CD55 ~14% (Fig 5.6B) However, 1 x 10^5 cMVs/ml express ~10% more CD55 that 1 x 10^5 sMVs/ml (Fig 5.6C). As sMVs are released in larger numbers the DAF released from the THP-1 is distributed between more sMVs than in the case of cMVs. The DAF labelled THP-1 were gated against an unlabelled control, and although DAF is not highly expressed on THP-1 the calibration was against 100% of labelled DAF.

Many cell types express CD55; a GPI anchored receptor that is expressed on the outer leaflet of the plasma membrane and moves in a similar manner to lipid across the

surface of the cell. As MVs form, the cytoskeleton loses rigidity by actin depolymerisation and this causes the plasma membrane to bleb; the plasma membrane being in constant flux causes any associated GPI anchored protein and receptors to flow over the surface of the bleb and integrate with lipid rafts (Fig 5.5A). As the bleb grows, more lipid and associated membrane features will accumulate and become a part of the microvesicle once it 'pinches off'.

5.7 MV subtypes express different concentrations of histamine receptor (H1R)

Histamine receptor (H1R) is transmembrane and ubiquitously expressed receptor in mammals. Indeed THP-1 express ~33.8% H1R gated against an unlabelled control. When stimulated for sMV release, THP-1 decrease H1R expression to ~17% and THP-1 releasing cMVs express ~26% H1R (Fig 5.7A and 5.7B).

MV subtypes derived from THP-1 express H1R. sMVs (5 x 10^5 /ml) express ~4.4% H1R and cMVs (1 x 10^5 /ml) (less cMVs available) express ~3.5% H1R. This indicates that H1R is more readily included in sMVs than cMVs (Fig 5.7C).

H1R is anchored with the cytoskeleton. Its inclusion on MVs indicates that protein sorting occurs in MV formation and their biogenesis may involve homeostatic mechanisms for working receptor transport as well as removal of stress agents.

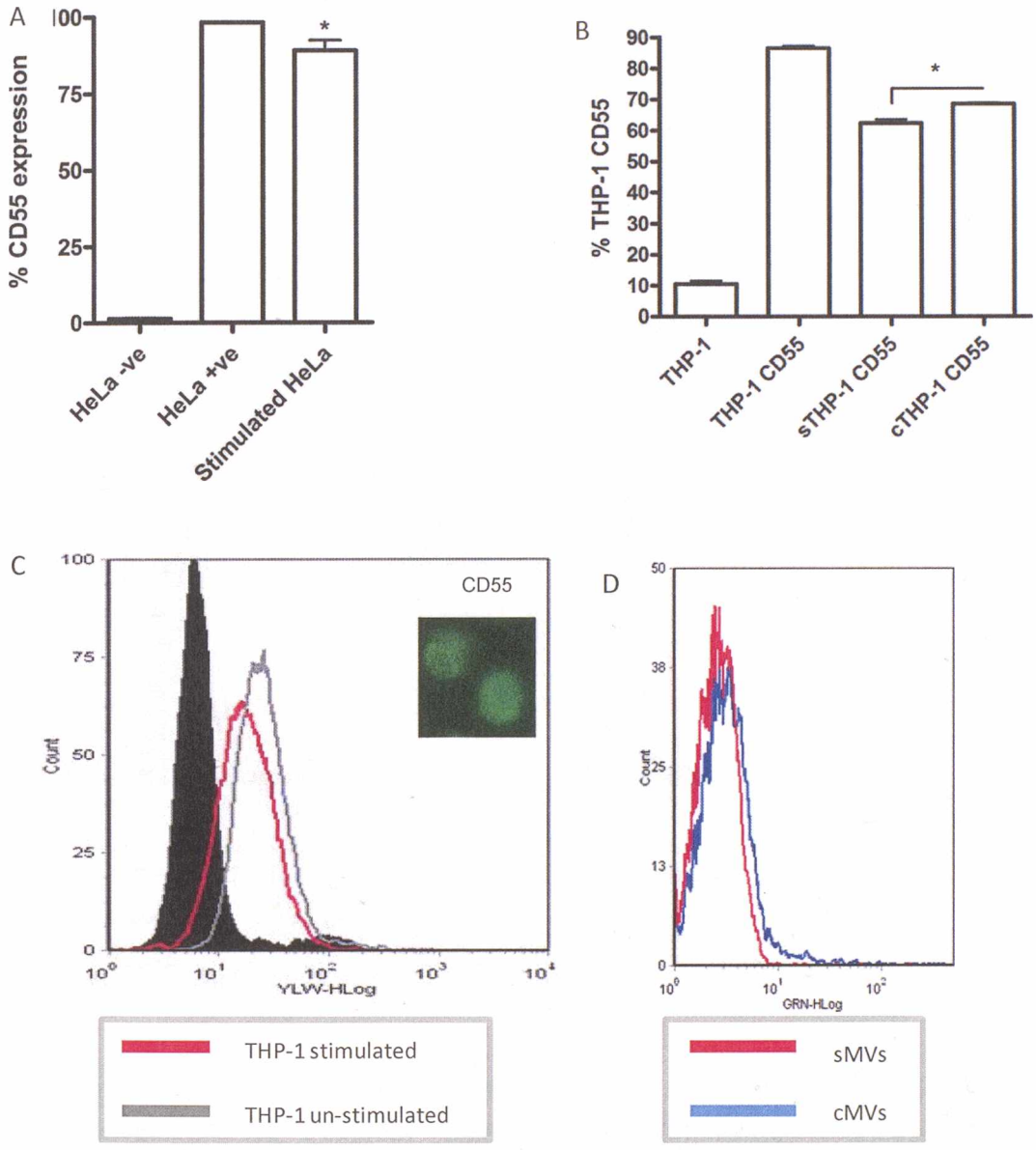

Fig 5.6 CD55 (DAF) expression is regulated by microvesiculation. (**A**) 5 x 10^5 HeLa/ml were cultured in 50 nM PMA to increase CD55 expression (Fig 10.5) before being stimulated with DMEM supplemented with 10% NHS and 2 mM Ca^{2+} to microvesiculate. HeLa releasing sMVs express significantly less CD55 ~86 ± 3% than un-stimulated cells ~98%. CD55 was labelled using anti human CD55 conjugated to FITC and quantified by flow cytometry, ExpressPlus. (**B**) THP-1 express ~85% CD55 gating against unlabelled THP-1. Stimulation with RPMI 1640 supplemented with 10% NHS and 2 mM Ca^{2+} leads to sMV release, significantly decreasing THP-1 DAF ~19%. Allowing THP-1 to release cMVs decreases THP-1 DAF expression ~14% (**C**) GPI anchored CD55 expression significantly decreases after 10% NHS stimulation of THP-1 to release sMVs. Inset, FIT-C fluorescently labelled Human αCD55 antibody bound to THP-1, confirms the presence and relative abundance of CD55. (**D**) FITC labelled CD55 on MV subtypes were quantified for the presence of CD55. cMVs express ~10% more CD55 than sMVs. .

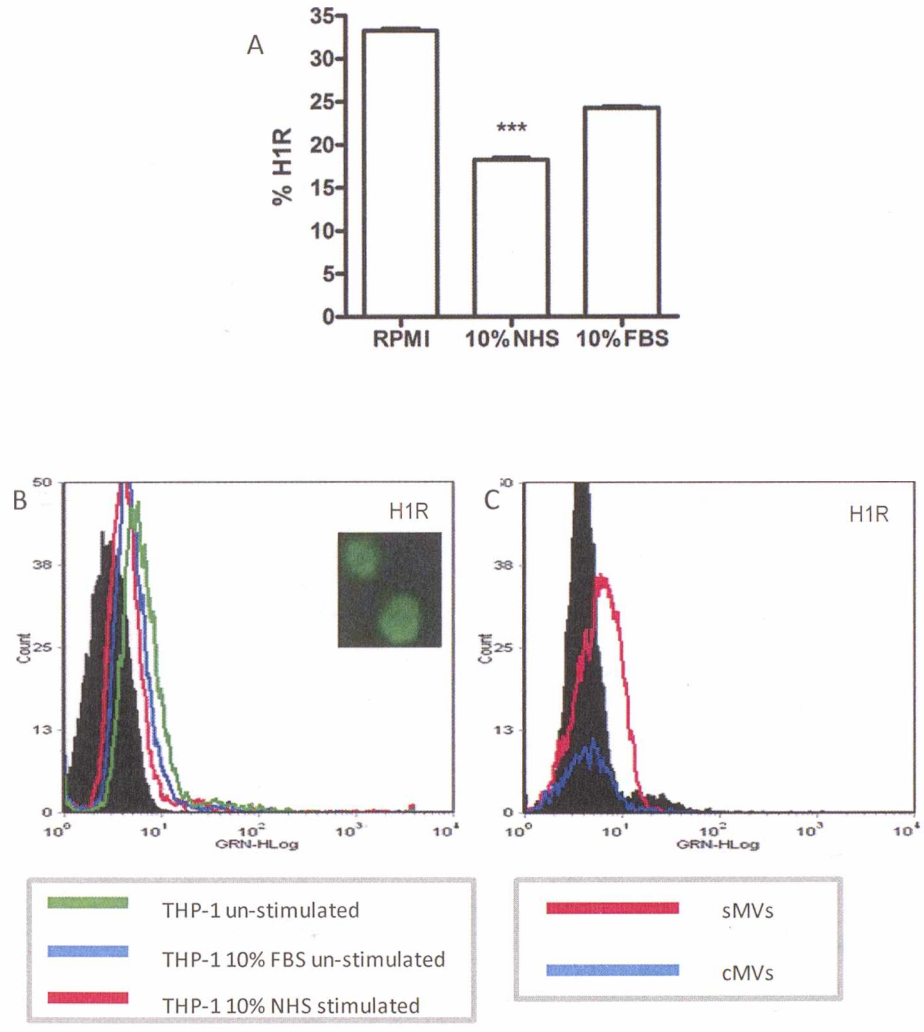

Fig 5.7 THP-1 expression of H1R is reduced after microvesiculation of MV subtypes. (**A**) THP-1 express ~33.8% H1R, when stimulated to release sMVs the THP-1 express significantly less ~ 17% H1R. cMV release lead to a decrease in H1R ~7.0%. (**B**) H1R was quantified on THP-1 using flow cytometry, insert H1R fluorescent microscopy (FITC). (**C**) THP-1 were stimulated for sMV release and H1R quantified by FACS, there was a significant decrease in expression. The sMVs were themselves assessed for H1R using FACs ~4.4%, showing that sMVs carry H1R derived from THP-1. cMVs were quantified, albeit in smaller numbers ~3.5%, there was a corresponding decrease in expression in THP-1. Black solid is control cells, FITC- cells (B) and FITC- MVs (C).

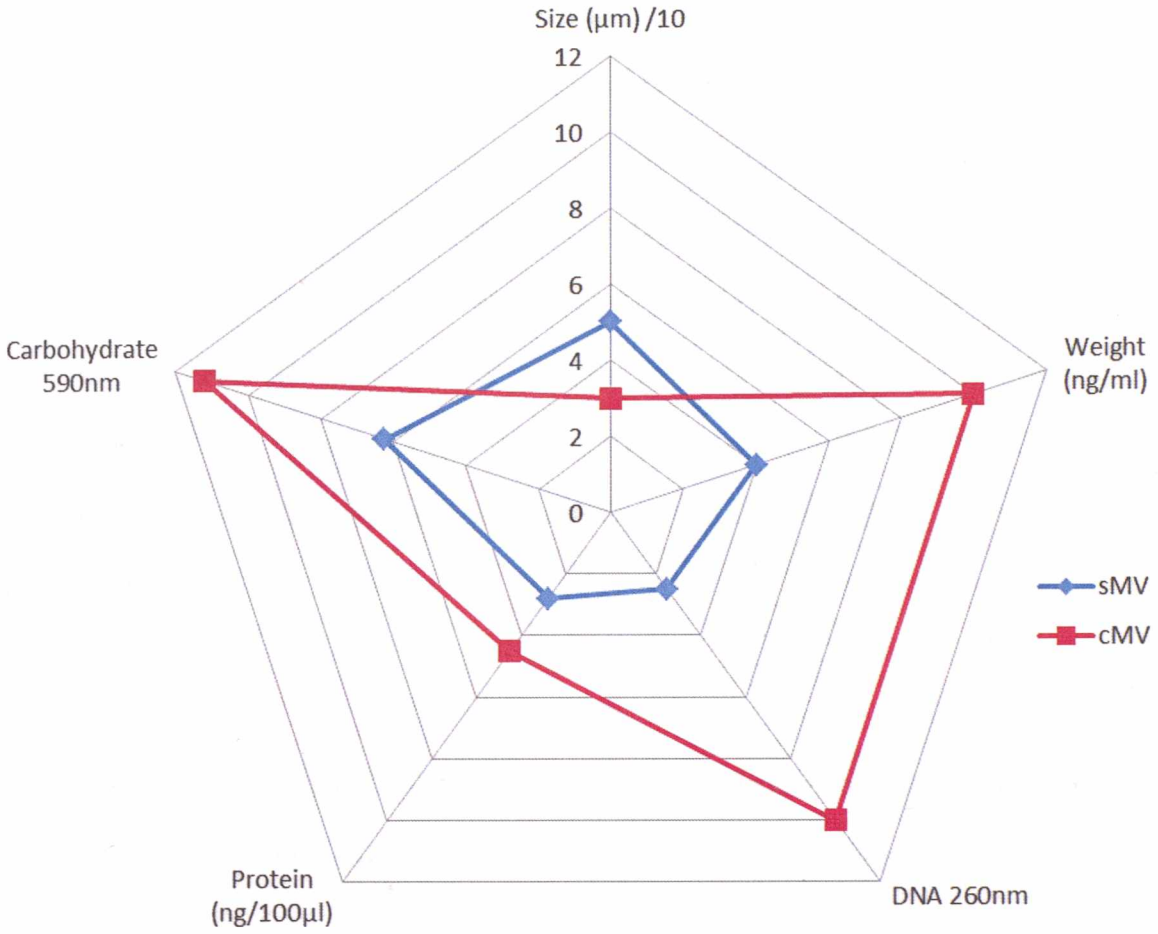

Fig 5.8 Radar graph comparing MV subtypes: cMVs and sMVs for measurable characteristics. Comparison of cMVs and sMVs features reveals significant differences in cMV size ~3 µm compared to sMVs ~5 µm, weight: cMVs ~10 ng/ml and sMVs ~4 ng/ml, DNA absorbance at 260 nm: cMVs ~10 and sMVs ~2.5, protein: cMVs ~4.5 ng/100 µl and sMVs ~2.8 ng/100 µl and carbohydrate abundances: cMVs ~11.2 and sMVs ~6.25. Both subtypes vary considerably in typical morphology and biochemical characteristics.

5.8 Summary of MV subtype biochemical profiles

The radar chart shows 5 physical characteristics of MV subtypes; size, weight, DNA content, protein content and carbohydrate content (Fig 5.8). These criteria are plotted with an appropriate scale to allow them to be compared easily. It should be noted that protein and size scale had to be adjusted for meaningful comparison. Unfortunately, error bars could not be plotted, however the average value was displayed. For every feature, except size, cMVs exhibit significantly greater amounts of each feature represented than sMVs (having a significantly larger size than cMVs). This figure aims to graphically highlight the significance of the data collected and show the need for considering MV subtypes.

5.9 Alexa fluor-488 labelled Cholera toxin B binding indicates relative expression levels of lipid rafts and retention of phosphatidyl serine in MV subtypes

Cholera toxin B was selected as an assay for the quantification of lipid rafts as it binds to ganglioside G_{m1} in the plasma membrane, that is selectively sequestered in to lipid rafts (Gitz *et al*, 2012). Lipid rafts are implicated in microvesicle release however thus far have not been shown to be released with microvesicle membranes. Fig 5.5A demonstrates that sMVs carry more lipid rafts ~5±0.5% than cMVs ~3±0.5% based on $1x10^6$ MV subtypes/ml.

Equal concentrations of MV subtypes were quantified for PS using annexin V conjugated to FITC by flow cytometry ExpressPlus programme. cMVs express >85% PS sMVs, conversely expressing significantly more PS >90% (Fig 5.4B). PS is localised in lipid rafts during early apoptosis. sMVs are larger that cMVs, this difference in size

possibly being responsible for the difference in % PS expression. However sMVs biogenesis is a response to cell stress agents that initiate pseudoapoptosis, during which PS expression is elevated in the outer membrane leaflet and may be included on the released sMV.

MV subtypes have different modes of biogenesis, cMVs therefore having different physiological roles to sMVs. The increased PS expression in sMVs (carrying stress agents) may facilitate their more rapid phagocytosis by macrophages (Antwi-Baffour *et al*, 2010). Conversely cMVs may be less likely to be engulfed and pass relatively unhindered through the tissues to perform their communicative role.

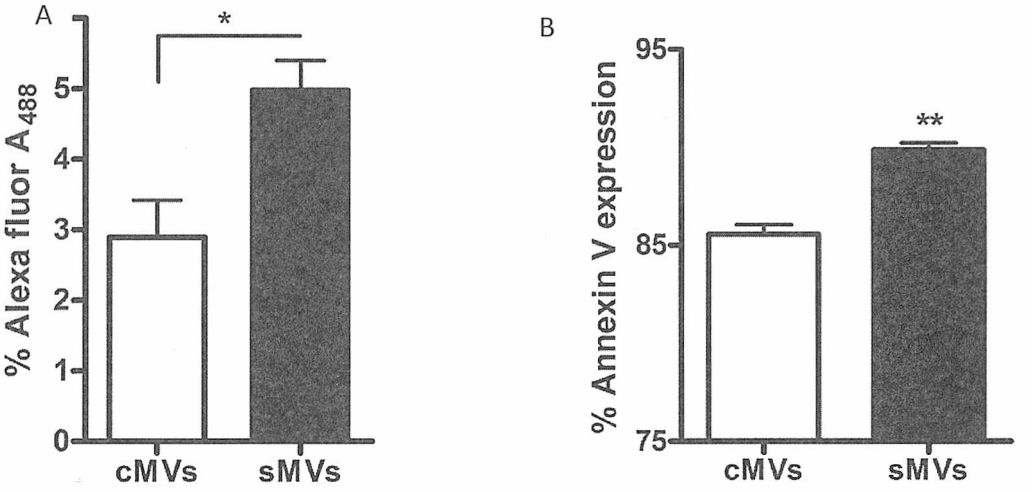

Fig 5.9 Relative abundance of alexa fluor binding to MV subtypes and MV subtype PS expression. (**A**) sMVs carry significantly more lipid raft ~5 ± 0.5% than cMVs ~3 ± 0.5%. The data was obtained by FACs analysis of alexa fluor A_{488} cholera toxin binding to GPI anchored ganglioside $_{M1}$ that is highly concentrated in lipid rafts. (**B**) Isolated THP-1 MV subtypes were analysed for %PS presented on the outer membrane leaflet using annexin V conjugated to FITC. cMVs expressed ~85 ± 0.5%, sMVs expressed significantly more ~90 ± 0.5%.

5.10 MV subtypes contain different concentrations of CH_2OH as carbohydrates

Spectroscopic analysis of MV subtypes A_{230} for RNA showed the presence of carbohydrate (and –OH groups) associated with proteins (Fig 5.10A). Although RNA, carbohydrate and -OH could not be individually discriminated using this method, further investigation for CH_2OH using an adapted schiffs base test highlighted the significant presence of non-specific carbohydrate, although less than initially conjectured (Fig 5.10B). cMVs express ~17% more carbohydrate that sMVs when measured using schiffs reagent.

Although spectroscopic analysis A_{230} displayed a mixture of candidate molecules, it further highlights the significant differences between MV subtypes (Fig 5.10A). The carbohydrate expression was further qualified by a non-specific carbohydrate test, modified to measure total carbohydrate. Carbohydrate is often associated with protein and membrane receptors, however it is likely that the carbohydrate may also fulfil membrane marker roles such as HLA or MHC.

5.11 MV subtypes contain different concentrations of nucleic acids

DNA presence in MVs was first observed spectroscopically using NanoDrop A_{260}. This result shows significantly more nucleic acid in cMVs than is present in sMVs (Fig 5.11A and 5.14). This nucleic acid may be viral or mitochondrial in nature. Only sequencing of the DNA would reveal its origin and inferred function. However it is possible that the nucleic acids have a communicative function. This result was confirmed by gel electrophoresis of lysed cMVs (Fig 5.11B). FT-IR also showed the presence of fragmented nucleic acid in MV subtypes (Fig 5.14).

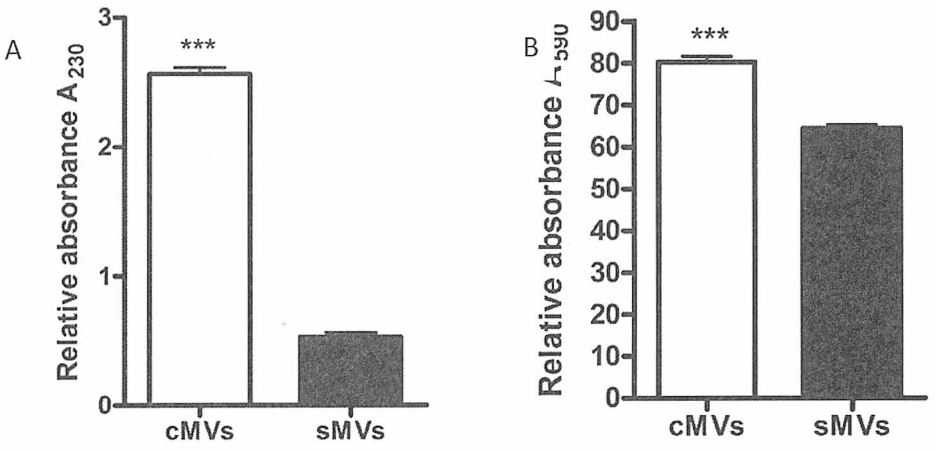

Fig 5.10 Investigation of MV subtype carbohydrate content. (**A**) A_{230} demonstrates x3 increase in absorbance for cMVs ~2.5 than sMVs ~0.5 due to the presence of RNA, carbohydrates, sugars and phenol groups, when 1 x 10^6 MVs/ml were measured with NanoDrop. (**B**) Schiffs base assay for nonspecific carbohydrates performed using FLUOstar Ω multiplate reader reveals differences between 1 x 10^6 /ml MV subtypes, cMVs expressing ~15% more carbohydrate than sMVs, confirming NanoDrop analysis.

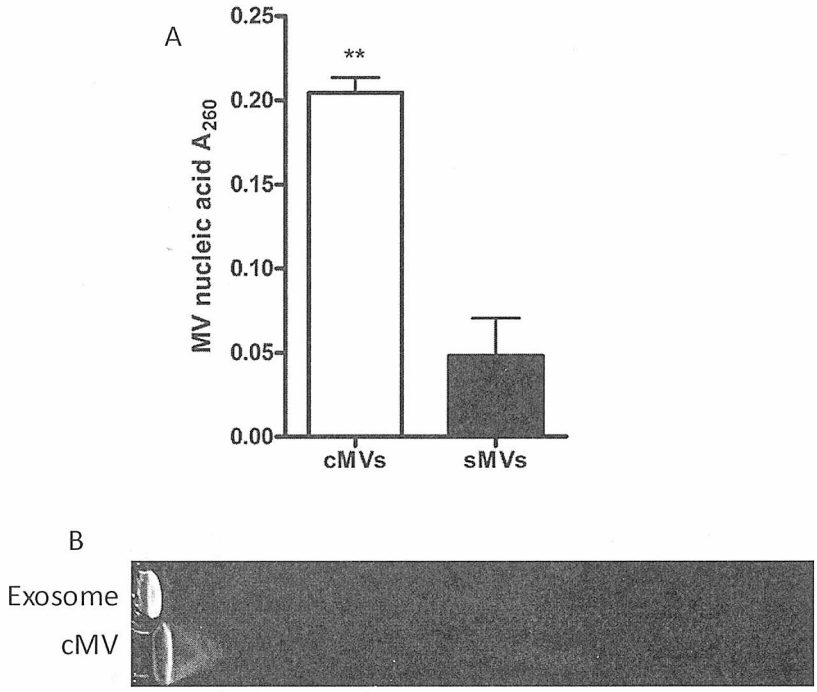

Fig 5.11 Measurements of nucleic acid, DNA A_{260} using NanoDrop. (**A**) NanoDrop analysis of 1 x 10^6 MVs subtypes/ml at A_{260} shows the presence of DNA, cMVs contain significantly more nucleic acid, ~4x more 0.21 ± 0.2 relative units than sMVs 0.045 ± 0.03 units. (**B**) Presumptive nucleic acid test using aragose gel electrophoresis, comparing exosomes to cMVs shows the presence of non descript nucleic acids, confirmed by FT-IR (Fig 5.13 and 5.14).

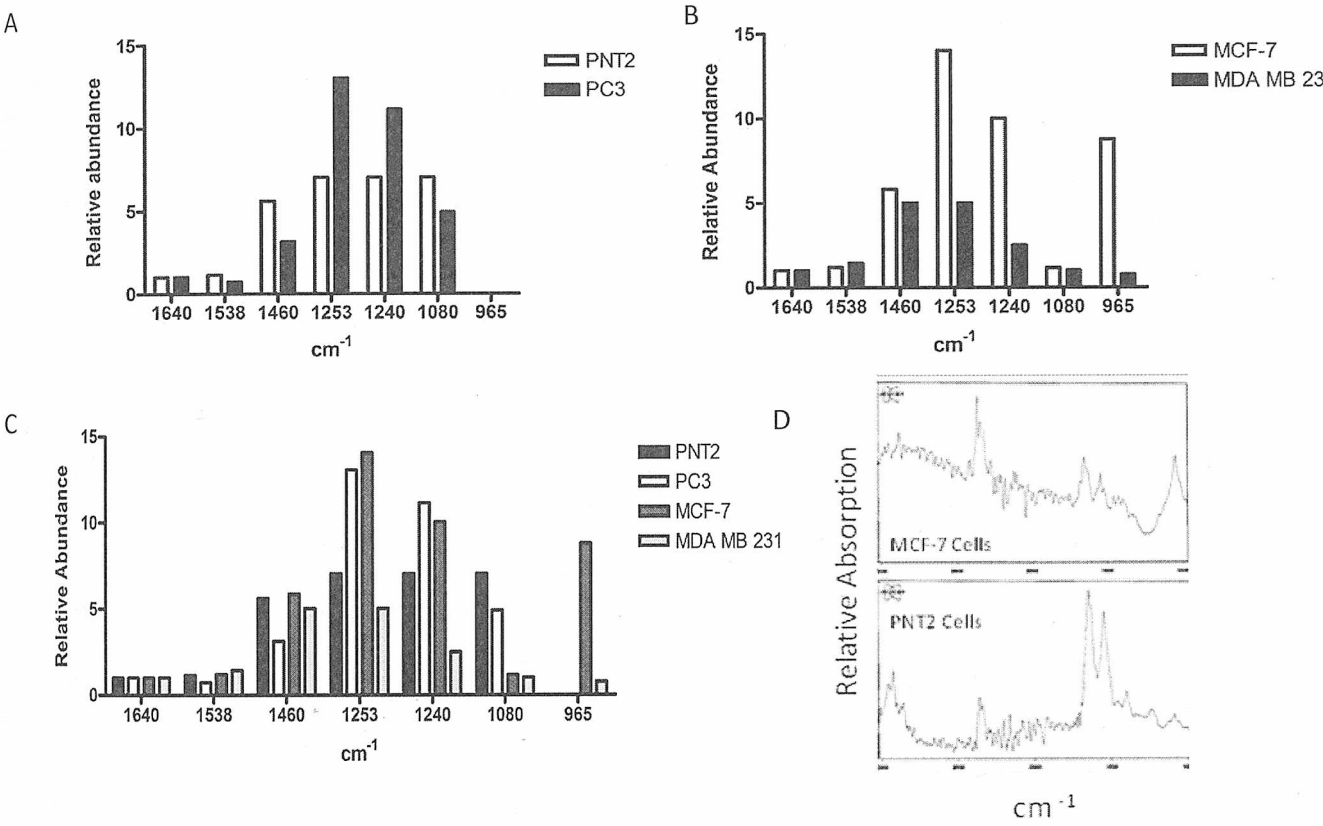

Fig 5.12 Graphical representation for FT-IR profiles of PNT2, PC3, MCF-7 and MDA MB 231 at all identification wavenumbers cm^{-1}. FT-IR analysis (absorption) using BRUKER revealed distinctive profiles of each cell type investigated. The results were obtained by normalising Amide I (1640 cm^{-1}) as an internal standard and comparing other wavenumbers cm^{-1} as a ratio. These results are based upon 5 x 10^5 cells/ml, grown to confluence on to sterile glass coverslips. (**A**) Prostate cell lines PNT2 and PC3 exhibit distinctly different FT-IR profiles, significantly Amide II (1538 cm^{-1}) and 1460 cm^{-1} in the protein region and at each of the DNA regions.(**B**) Breast cell lines MCF-7 and MDA MB 231 exhibit different FT-IR profiles, the results are significant at every wavenumber cm^{-1} except for Amide I (1640 cm^{-1}) and PO_2- bonds (1080 cm^{-1}). (**C**) Compares all cell types both highly metastatic and non metastatic. The FT-IR profiles for each cell type is unique, based upon 3x 10+ repeats for each cell type. (D) Representative FT-IR profile (3000 cm^{-1} to 1000 cm^{-1}) for MCF-7 and PNT2 cells.

5.12 FT-IR profiles generate unique cellular profiles

Cellular analysis by FT-IR shows that each cell type has unique profiles based upon the presence of various functional groups that are expressed on proteins, carbohydrates, DNA and lipids. The results presented are the average profile of 12 or more FT-IR absorption scans for a particular cell line (Fig 5.13 and 5.14).

The summarised key features of FT-IR data for the four cell types investigated (1640-965 cm^{-1}) shows that cell type has a highly reproducible, unique profile, demonstrated by the presence of functional groups associated with DNA, proteins, carbohydrates and lipids. Importantly the graphs show mathematically normalised data for the wave numbers analysed to allow qualitative analysis. Quantitative analysis was considered unnecessary as Amide I could be used as an internal standard, rather than stressing the cells using an external standard that would alter their typical FT-IR profiles. FT-IR protocol was standardised for use with all cell and MV types, the suspension media being PBS. PBS was assessed for the relevance of phosphate and other ions by producing a FT-IR profile. It was found the phosphate did not interfere with reading within the fingerprint region and therefore was a suitable suspension media for use with cells and MVs.

The data in Fig 5.12 clearly shows DNA at 965 cm^{-1}, 1080 cm^{-1}, 1240 cm^{-1} and 1253 cm^{-1}. This describes the DNA as double stranded, maybe even undergoing cell division as 1240 cm^{-1} shows asymmetric DNA. Proteins are present, importantly Amide I and Amide II.

The experimental concept was to examine both metastatic and non metastatic cancer cell lines; prostate (PC3 and PNT2) and breast (MCF-7 and MBA MB 231) cancers were chosen. They were cultured and analysed in optimal conditions. The results were highly reproducible.

PC3 is a highly metastatic and invasive prostate cancer cell line, PNT2 has low metastatic potential and grows slowly. MBA MB 231 has high metastatic and invasive potential (Mycielska *et al*, 2005; Wang et al, 2008), whilst MCF-7 has low metastatic potential (Levenson *et al*, 2005; Pang *et al*, 2009), but is able to grow rapidly.

5.13 FT-IR profiles of breast MV subtypes exhibit similarity to parent cell types

MV subtypes were compared to their parent cell types as well as one another to highlight similarities and differences. As expected MV subtypes expressed relatively high levels of proteins (1640 cm^{-1} amide I) compared to the parent cell type (Fig 5.13A and 5.13C).

The breast cancer cell lines each expressed a smaller but distinct peak at 1080, 1538 and 1460 cm^{-1}. MCF-7 MV subtypes had similar peaks although less magnitude (ratio to amide 1) at 1253 cm^{-1} (P=O) typical of lipid (Table 1.1) but also had a peak at 965 cm^{-1} (C-C) associated with DNA, that cells didn't express (Fig 5.13B). MBA MB 231, looking at MV subtypes, cMVs express significant peaks that sMVs do not express at 1240 and 1253 cm^{-1}.

5.14 FT-IR profiles of prostate MV subtypes exhibit similarity to parent cell types

The prostate cell lines had corresponding distinct peaks at 1640 cm^{-1} (amide I). However it was the PNT2 sMVs that showed the greatest similarity to parent cell across each wavenumber, reflecting a smaller, but typical biochemical profile, cMVs expressing smaller relative peaks than sMVs at every wavenumber.

PC3 cMVs had the greatest similarity to the parent cell types, at each wavenumber and expressed a larger peak at 965 cm^{-1} (C-C) typical of a complex structure such as DNA. sMVs expressed negligible peaks except 1640 cm^{-1}, indicating the presence of proteins in each MV subtype, but significant differences in their biochemical profile.

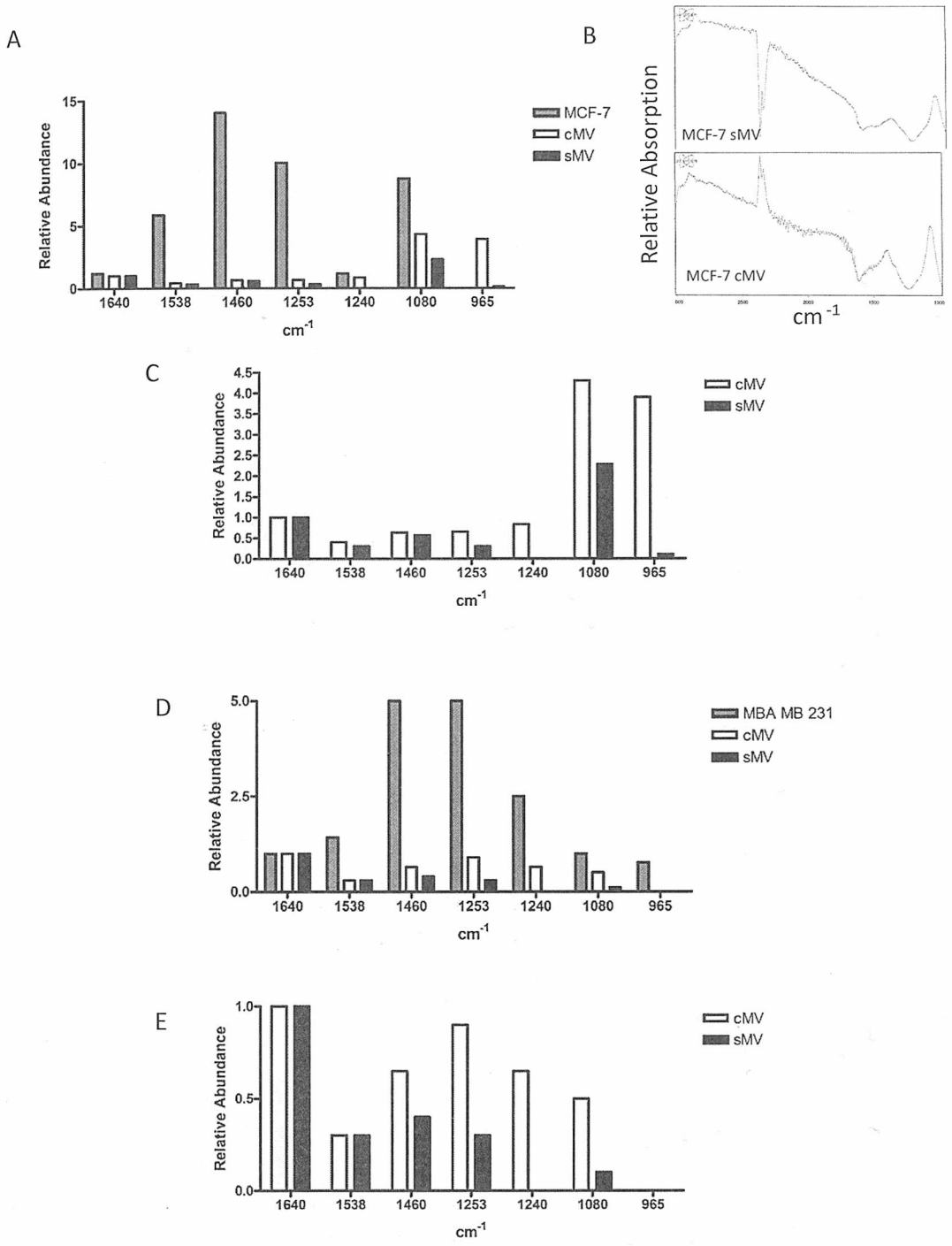

Fig 5.13 FT-IR analysis of MCF-7 and MDA MB 231 (breast) MV subtypes. (**A**) MCF-7 MV subtypes (1 x 10^6 /ml) resembled parent cell types at 1640, 1538, 1460 and 1253 cm^{-1}, there was some similarity at 1080 cm^{-1} but no similarities at 965 cm^{-1}. The parent cell type expressed significantly larger peaks at all wave numbers except 2350 cm^{-1}. (B) Representative FT-IR images taken from the Bruker software for PNT2 MV subtypes (**C**) cMVs had similar profile to sMVs at 1640 and higher at 1538 and 1080 cm^{-1}, but had higher peaks at all other wave numbers observed. The data was normalised using amide I (1640 cm^{-1}). (**D**) MDA MB 231 MV subtypes (1 x 10^6 /ml) MV subtypes resemble their parent cell type at 1640, 1538, 1460 and 1080 cm^{-1}, cMVs more closely resemble parent cells that sMVs. (**E**) cMVs have wavenumber peaks of greater magnitude than sMVs and cMVs have a greater array of peaks at 1253 and 1240 cm^{-1} that sMVs do not express.

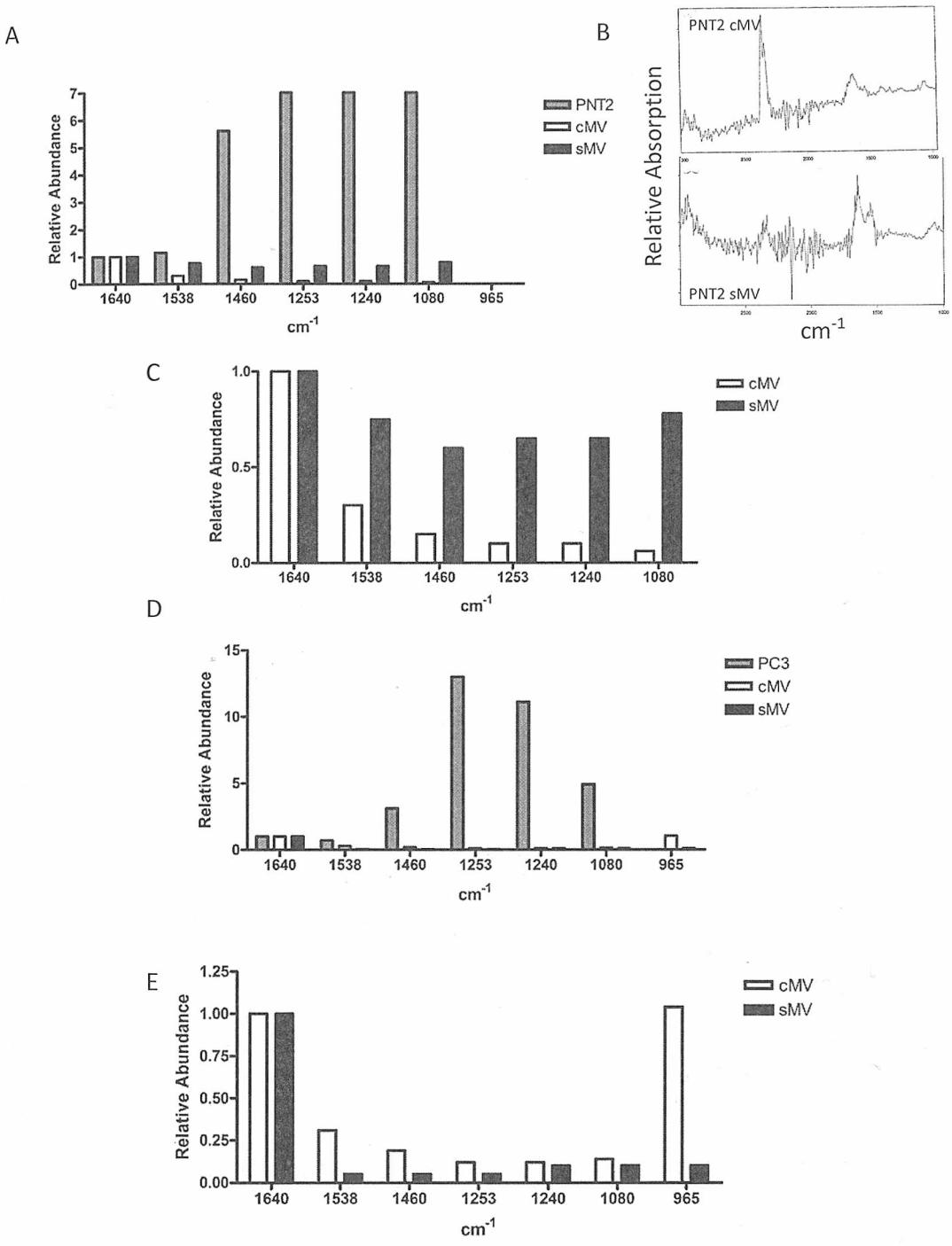

Fig 5.14 FT-IR analysis of PNT2 and PC3 (prostate) MV subtypes. (**A**) PNT2 MV subtypes (1 x 10^6 /ml) resembled the parent cell type only at 1640 cm^{-1}, sMVs expressed higher peaks at all wave numbers measured than cMVs. Parent cell types express significantly larger peaks at every wavenumber. (**B**) Representative FT-IR images taken from the Bruker software for PNT2 MV subtypes. (**C**) cMVs express smaller peaks than sMVs at every wave number except 1640 cm^{-1}. (**D**) PC3 MV subtypes (1 x 10^6 /ml) parent cell types have larger peaks than MV subtypes at every wave number except 1640 cm^{-1}. (**E**) cMVs have large peaks at every wavenumber analysed except 1640 cm^{-1}. In particular at 1538 1460 and 965 cm^{-1}.

5.15 FACs and oxygen electrode analysis of cMVs released from THP-1 cultured in α-tocopherol

THP-1 cultured in RPMI 1640 supplemented with 10% FBS, 1% penicillin and streptomycin and varying concentrations 0, 12 and 50 ng/L of α-tocopherol show 'typical' cMV morphology for 0 ng/L α-tocopherol, however with increasing (12 and 50 ng/L) α-tocopherol the cMV released are significantly smaller (Fig 5.15).

cMV derived from THP-1 cultured in elevated concentrations of α-tocopherol have significantly decreased natural GRN-HLog fluorescence. Indeed, 0 ng/L ~50% GRN-HLog, 12 ng/L ~20% GRN-HLog and 50 ng/L ~10% GRN-HLog. The natural decrease in GRN-HLog may be due to decreases in cellular lipofuscin levels. Lipofuscin is produced by the oxidation of saturated fats (Wassell and Boulton, 1997). Furthermore, MV subtypes collected form THP-1 cultured in α-tocopherol contain less oxygen free radicals that those cultured without α-tocopherol. It is reasonable to suppose that the MVs that have the lowest auto fluorescence are those with the least ROS, and that the auto-fluorescence is due to oxidised fats such as lipofuscin. This would also suggest that a primary function of cMVs are to export oxidised fats. Cancer cell types, such as those studied may also encourage cellular co-operation and spread virulence factors by increasing recipient cell cytoplasmic ROS (Komagoe *et al*, 2010).

5.16 THP-1 cultured in increasing concentrations of α-tocopherol for 24 h release successively smaller cMVs

FACs analysis revealed the increasing concentrations of α-tocopherol resulted in successively smaller cMV sizes (Fig 5.15 and 5.16A). Indeed, 0 ng/L lead to ~9 ± 1.25%

cMVs over 5 μm, 12 ng/L lead to significantly smaller cMVs ~4 ± 0.6% over 5 μm and 50 ng/L ~3 ± 0.1% over 5 μm (Fig 5.16A). α-tocopherol is a powerful anti oxidant, sequestering DNA damaging reactive oxygen species (ROS), likely generated by mitochondria or from vesicles containing peroxides (Donnelly *et al*, 1999).

THP-1 cultured (as before) in α-tocopherol significantly reduced the number of cMVs released over 24 h as concentration was increased from 0 – 12 ng/L and significantly fewer cMVs were released (from ~1 x 10^6 ± 0.15 /ml to 7 x 10^5 ± 1.75 /ml). However 50 ng/L α-tocopherol significantly increased cMVs released to ~9 x 10^5 ± 0.1 /ml, indicating a potential MV stimulatory role for excessive α-tocopherol concentration (Fig 5.16B).

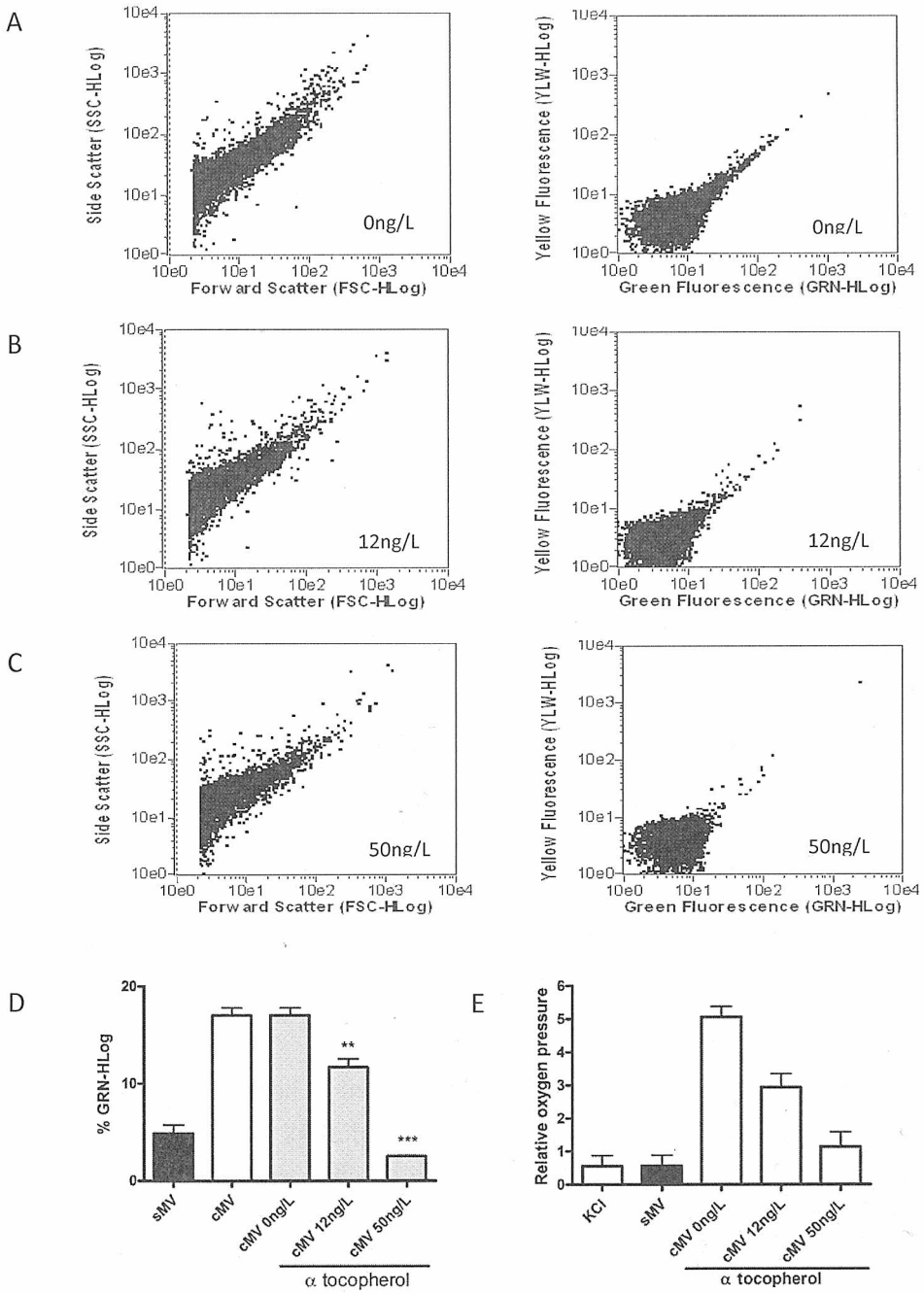

Fig 5.15 THP-1 cultured in complete growth media supplemented with increasing concentrations of α-tocopherol lead to changes in FACs morphology of released cMVs. (**A**) THP-1 in culture supplemented with 0 ng/L α-tocopherol show typical cMV morphology. (**B**) THP-1 in culture supplemented with 12 ng/L α-tocopherol release significantly smaller cMVs than in condition 'A'. (**C**) THP-1 in culture supplemented with 50 ng/L α-tocopherol release significantly smaller cMVs than in condition 'B'. (**D**) Increasing α-tocopherol concentration releases cMVs that express decreasing natural GRN-HLog fluorescence. 0 ng/L has a gated fluorescence ~17%; 12 ng/L ~11%; 50 ng/L ~2.5%. (**E**) The measurement of oxygen free radicals in MVs cultured in various concentrations of α-tocopherol show that as the cell culture concentration of α-tocopherol increased, the oxygen pressure decreased, from ~5.0 to ~1.0 relative units. sMVs had negligible oxygen pressure. Measured using an oxygen electrode.

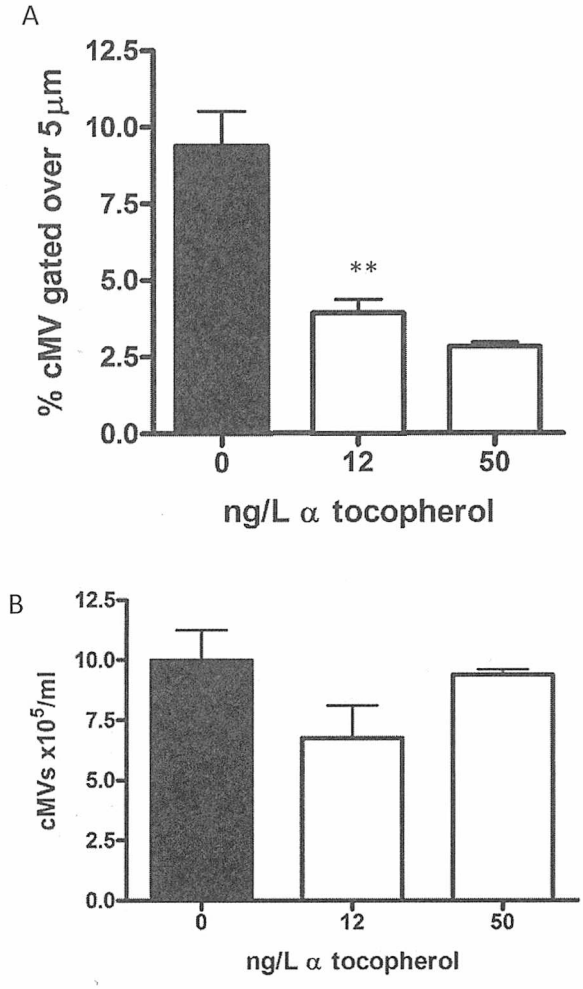

Fig 5.16 THP-1 cultured in increasing α-tocopherol concentration release smaller and fewer cMVs over 24 h. (**A**) As α-tocopherol dosage increases the relative sizes of the cMVs decreases. THP-1 cultured in 0 ng/L α-tocopherol release ~9 ± 1.5% cMVs over 5 µm, THP-1 cultured in 12 ng/L α-tocopherol release ~4 ± 0.5% cMVs over 5 µm and THP-1 cultured in 50 ng/L α-tocopherol release ~2.5% cMVs over 5 µm. (**B**) THP-1 cultured in 0 ng/L α-tocopherol release ~1 ± 1.5 x 10^6 /ml cMVs, when cultured in 12 ng/L they release significantly less ~6 ± 1.5 x10^5 /ml cMVs. However high dosage of α-tocopherol, 50 ng/L stimulated cMV release to increase to ~9.5 x 10^5/ml.

5.17 Discussion

MV subtypes differ significantly in their biochemistry and relative abundance of constituent molecules. Although cMVs are smaller and heavier (Fig 4.13, 4.14 and 4.20), they carry significantly more protein in the form of receptors, enzymes and structural proteins (Fig 5.4, 5.5 and 5.13), carbohydrate possibly associated with protein (Fig 5.10) and nucleic acid, possibly DNA, (Fig 5.11, 5.13B, 5.13D, 5.14B and 5.14D) than the larger, lighter sMV (Fig 4.13, 4.14 and 4.20). These biochemical differences are related to their functional roles (Fig 4.5B, 4.9A, 4.10, 5.1, 5.3, 5.13 and 5.16) and biogenesis (Fig 5.15). As consistently reported, sMVs are produced as a cellular response to stress agents, usurping apoptosis by exporting undesirable agents from the cell and maintaining calcium homeostasis (Fig 4.5A). sMVs are able to induce apoptosis in adjacent cells when stimulated for release using apoptotic causing agents by transmitting those agents to recipient cells (Jorfi *et al*, 2010) and sMVs express almost 5% more PS that cMVs (Fig 5.3A). When being produced, the cell has little time to release the sMV to circumvent apoptosis and repeated or constant insult will exhaust the cells ability to produce MVs (Fig 4.6) causing them to enter early/late apoptosis. Should the cell be critically wounded the sMV response will be insufficient to prevent apoptosis or necrosis.

Annexin V is expressed at different levels on MV subtypes, cMVs ~85% and sMVs ~90%, in part due to their different sizes, their surface areas expressing proportionate amounts of PS (Fig 5.9B). Their different modes of construction are probably more critical, as PS in sequestered to lipid rafts during early apoptosis (Ishii *et al*, 2005) as well as enrichment of various proteins and other lipids that give rise to their distinct physiological roles and may reflect potentially distinct MV subtype lipid profiles.

Indeed, annexin V expression and CD55 (both sequestered to lipid rafts) are more highly expressed on sMVs, or cellular expression was reduced by sMV release (Fig 5.6 and 5.9). sMVs will have an increased avidity for PS receptor than cMVs (Fig 5.3), and are more likely to encounter and be engulphed by macrophages (Antwi-Baffour *et al*, 2010). sMVs, therefore are more able to attract macrophages to the sight of cellular stress. The recruited macrophages are then able to ingest MVs, apoptotic cells and invading microorganisms.

Lipid rafts are enriched on MVs, however they are expressed significantly more on sMVs ~5.0% than cMVs ~3.0% (Fig 5.9A). This may reflect the difference in biogenesis or surface area of MV subtypes and account for differences of protein and lipid profiles in MV subtypes (Fig 5.5, 5.6, and 5.9). Lipid rafts carrying lipid and protein arrays may offer unique properties to recipient cells once transplanted.

As described above, CD55 (DAF) expression is reduced when cells are stimulated to release sMVs (Fig 5.6A and 5.6B). Indeed, sMVs express low levels of CD55, cMVs expressing ~10% CD55 more than sMVs (Fig 5.6B). H1R is carried by MV subtypes, sMVs expressing ~4.4% H1R and cMVs ~3.5% (Fig 5.7C). H1R is a transmembrane receptor anchored to the actin cytoskeleton, although actin (~42kDa) is not apparent on the protein gel for sMVs, cMVs have a protein band in this region (Fig 5.5).

Protein analysis of cMV and sMV lysates demonstrated that MV subtypes carry distinctive proteins and that cMVs reflect the protein profile of the parent cell more closely that sMVs. MV subtypes are enriched for a ~70 kDa protein (Fig 5.5) which may

correspond to HSP70 (Chaperon class protein) that translocates proteins derived from damaged organelles to lysosomes (Anand *et al*, 2010), HSP70 is often found associated with exosomes (Anand *et al*, 2010). However, sMVs appear to lack many of the proteins that are present in cMVs derived from the same parent cells or indeed the parent cells themselves (Fig 5.5). This affirms that MV subtypes biogenesis leads to distinctive protein profiles and to potentially MVs with different physiological roles.

In vitro, cells were stimulated using 5 – 10% NHS to produce sMVs, *in vivo* cells are bathed in NHS but would not produce MVs in response to this as they have complement protective features and would prevent binding of self antibody to self cells. MVs in plasma are produced as a result of regular cellular processes (communicative) or in response to some other stress (Fig 5.15) possibly ROS (Fig 5.15E). Furthermore the cells in the immune environment become tolerant to NHS. Cells grown in laboratory conditions are typically cultured in FBS and would not be able to fully tolerate NHS upon first exposure (Fig 4.1).

THP-1 cultured in increasing doses of α-tocopherol (vitamin E, an antioxidant) released smaller and less auto-fluorescent MVs (Fig 5.15 and Fig 5,16). It is reasonable to hypothesise that the green auto-fluorescence is due, at least in part to oxidised lipids such a lipofuscin. cMV ROS were shown to decrease as α-tocopherol concentration increased (Fig 5.15E), as expected. However this highlights that cMV release may be in response to increasing ROS concentration, or maybe that cancer cell types export ROS as a virulence agent to other cells. sMVs express negligible levels of ROS (measured using an oxygen electrode). THP-1 were shown to release more, significantly smaller

cMVs when cultured in 50 ng/L α-tocopherol, as the excess vitamin E stimulates the release of MVs via an undetermined mechanism (Fig 5.16B).

TEM of MV subtypes (Fig 4.13) visibly displays the larger sMVs are possibly composed of more water (possibly containing soluble ions and molecules) owing to their 'lack' of protein and carbohydrate contents, than cMVs, leading to an increased fragility when freezing (Fig 4.23). However, cMVs are composed of more protein (Fig 5.8) and they contain higher levels of nucleic acids and of bio-available calcium (Fig 4.5B and 5.1). Furthermore, cMVs are produced as a communicative vector. As demonstrated (Fig 4.9) they stimulate THP-1 to a different extent. However a unique cMV role has not been identified in this thesis, possibly as their effects may be subtle, or because any cell in culture will release cMVs and so cause confounding data; sMVs may contain a small population of cMVs (Fig 4.15).

FT-IR was used firstly to compare metastatic and non metastatic cancer types and to then analyse MV subtypes (Ami *et al*, 2012; Ojeda and Dittrich, 2012). No correlation was found between metastatic cell types or non-metastatic cell types, although similarities between cell types were observed. FT-IR analysis of parental cell types displayed a degree of correlation to their released MV subtypes, except for PNT2, where the cMVs expressed a clearer FT-IR profile than sMVs and exhibited a greater degree of similarity to parent cell types than sMVs (Fig 5.13A, 5.13C, 5.14A and 5.14C).

Although FT-IR is typically used to identify molecular groups, this study shows that this can be extended to the study of cell types (Ami *et al*, 2012). Within the fingerprint

region (1800 – 900 cm^{-1}), DNA, protein can be identified (Fig 5.12C) (Whelan et al, 2012). The profiles mathematically produced are unique for that cell type (Fig 5.12) (Ami *et al*, 2012), and FT-IR if properly developed may become a powerful, fast and cheap diagnostic tool that preserves the viability of the sample (Ami *et al*, 2012). However, FT-IR could not be used to identify individual molecules within a biological system *per se*, but rather identify the presence of features associated with types of molecule, i.e., phosphate back bone of DNA 1080 cm^{-1} (Fig 5.12)(Buttner *et al*, 2009; Du *et al*, 2009; Whelan et al, 2012). The research conducted for this thesis extended beyond the finger print region to encompass other molecules, increasing the resolving power of this technique. This study compared 4 cell lines and would need to be extensive and build a library of cell profiles. Scattering effects caused baseline distortions that were compensated for using OPUS software and multiple repeats of sample scans from 4000 – 950 cm-1 (Bassan *et al*, 2012).

Using FT-IR MV analysis as a diagnostic it would be very difficult to filter out interference from other MV cell types that would be present in a clinical sample. Indeed, all MV subtypes for all cell types analysed by FT-IR expressed a distinct peak at 1640 cm^{-1} (Amide 1) but did express weak but distinctive profiles (Fig 5.13 and 5.14).

CO_2 (2350 cm^{-1}) and H_2O (3000+ cm^{-1}) were observed in the profiles of the samples (Kargosha *et al*, 2001; Gousset *et al*, 2002). Future observations should consider real time atmospheric components rather than relying upon a 'blank' measurement taken before the samples were analysed. Indeed, CO_2 was expected and observed from bioactive cells. Future investigations could be performed using synchrotron infra-red

spectroscopy (Szeghalmi *et al*, 2007), to monitor real time CO_2 fluctuations that may affect the pH and therefore that behaviour of protein groups being analysed.

cMVs have been shown to carry a significant concentration of calcium (Fig 4.5B). Unlabelled cMVs were incubated with calcium green labelled THP-1 to assess the increase in calcium concentration upon binding of cMV to THP-1. The results show that cMVs deliver a significant concentration of calcium to THP-1 (Fig 5.1). Very small quantities of cMVs were used to simulate physiological conditions (1 cMV : 50 THP-1). sMVs also carry calcium, although in much lower concentrations than cMVs (Fig 4.5B). A larger quantity of sMVs was selected to observe any results. sMVs deliver approximately the same amount of calcium delivered to THP-1 (1x sMV : 1x THP-1). The implication of this result id that low concentrations of cMVs can deliver enough calcium to cells that may affect its metabolism. However sMVs would have to bind to cells in greater numbers (≥50 fold) to deliver the same concentration of calcium that cMVs deliver (Fig 5.1).

MVs transfer protein receptors between cell types, in particular, DAF^+ HeLa MVs will briefly transplant a working receptor onto DAF^- CHO-K1, enhancing its ability to evade complement mediated lysis (Fig 5.2). This type of 'novel' protein transfer has now been described for other receptors, such as Fas-R, CD81 and CCR5 (Inal *et al*, 2012), however, this thesis demonstrates cross species receptor transfer with associate beneficial results, leading to questions about host/parasite relationships.

MVs carry many receptors (Fig 10.7) and calcium originating from the parent cell. If x represents the total expression of a cellular feature, such as calcium or receptors, then x =100%, cell – MV ≤ x, transplanted MVs to recipient cell ≤ MV. This indicates that receptor transplantation is relatively inefficient, only transplanting ≥100% of MV receptors. Experimentally this figure is 5 - 10%.

MV subtypes both carry complement suppressing receptors as a part of their plasma membranes. When they were co-incubated in serial dilution with THP-1 and lytic concentrations of NHS and their avidity assessed (Fig 5.3). sMVs were found to offer a greater degree of protection to THP-1 from complement mediated lysis (Fig 5.3A) than cMVs that offered significantly less lysis protection at 64x THP-1: 1x cMV (Fig 5.3B). This result reflects the protection against lysis that MV subtypes offer to *Salmonella typhimurium* (Fig 4.10). This may be due to the size of cMVs and that they either do not carry as much C4b as sMVs or that their surface area is not large enough to incorporate as much MAC as sMVs.

MVs role in cellular communication includes transfer of proteins and receptors offering many potential undetermined benefits to the recipient cells. The research presented offers obvious benefits for exploitation by pathogens and protection from the host's innate immune responses, i.e., complement mediated lysis. Detailed proteomic studies would reveal striking differences in the array of proteins expressed and carried by MV subtypes across all cells investigated. The necessity of this type of study is growing as more functions are being attributed to MVs.

6. ULTRA LOW-FREQUENCY MAGNETIC FIELDS STIMULATE MICROVESICLE RELEASE AND AFFECT CELLULAR BEHAVIOUR.

6.0 Introduction

Low frequency electromagnetic fields are generated by most electronic devices in common use, but are specifically used in medical imaging. Epidemiological studies indicate possible links to cancer development (Lacy-Hulbert *et al*, 1998; Ansari and Hei, 2000; Dini *et al*, 2010; Repacholi, 2012) leading to concerns about their ever growing occurrence and a more general effect on human development, health and disease (WHO, 2007; Hung *et al*, 2010; Repacholi, 2012).

Although the Earth has a static variable ~15 - 50μT (microteslas) 0Hz magnetic field, it is alternating current (A/C) generated magnetic fields that are able to exert electromotive force (Pham *et al*, 2009), capable of interacting with polar molecules such as H_2O and more complex organic molecules such as lipid (Liburdy *et al*, 1986). A/C currents are used in almost all appliances and power lines that generate magnetic fields that extend into the microtesla range, capable of interacting with molecules (Liburdy *et al*, 1986; WHO, 2007; Repacholi, 2012).

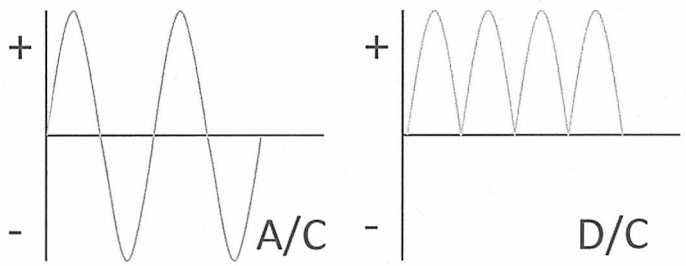

Fig 6.18 Alternating current (A/C) and direct current (D/C). A/C current are both positive and negative as a part of one complete oscillation, frequency (Hz) is the number of oscillations a wave has in one second (s). Amplitude (amp) is the size of the wave and voltage (v) is the potential difference across a circuit or electromotive force. An A/C current has a net neutral charge, D/C are only positive and therefore generate static magnetic fields.

Studies into the role of magnetic fields and cancer progression have given conflicting results (Nakahara *et al*, 2002; Nikolva *et al*, 2005; Hung *et al*, 2010) likely due to diverse tissue types responding differently to magnetic stimuli (Ventura *et al*, 2000; Dini *et al*, 2010). Studies on cell lines derived from different tissues and organisms show many positive or even, negligible effects (Lacy-Hulbert *et al*, 1998; Nikolva *et al*, 2005). Electromagnetic exposure of neuronal progenitor cells resulted in DNA damage and up-regulation of genes relating to apoptosis (Blank and Goodman, 2011; Seyyedi *et al*, 2010). These effects were transient and it is conjectured that cellular mechanisms compensate for these magnetic effects (Nikolova *et al*, 2005). For tumour development, a minimum of three mutations in the genome must occur (in most cases) (Lacy-Hubert *et al*, 1998). Although magnetic fields may contribute to tumour development (Simko and Mattsson, 2004), they may not necessarily be the only causative agent; however low frequency magnetic fields could contribute a mutagen or interfere with cellular signalling pathways (Lacy-Hubert et al, 1998; Simko and Mattsson, 2004; Hung *et al*, 2010).

Studies have shown the growth effects of magnetic fields on particular cell lines (Lacy-Hulbert *et al*, 1998; Ventura *et al*, 2000; Gartzek and Lange, 2002) Typically, *in vitro* magnetic studies demonstrate a proliferative stimulus to particular cell lines, initiating G_1 from cells in the G_0 phase (Lacy-Hulbert *et al*, 1998). Furthermore, Hung *et al*, 2010 demonstrated that low frequency magnetic fields caused *C. elegans* to develop and age more rapidly than the control group due to atypical gene transcription of *age-1, unc-3, lim-7 and chk-1* (human homologues). THP-1 promonocytic cells usually terminally differentiate within three days when cultured with PMA, however when stimulated with a 6mT magnetic field, THP-1 differentiation is halted (Dini *et al*, 2010). Low

frequency magnetic fields alter cell morphology via cytoskeletal interactions or remodelling (Dini *et al*, 2010; Hung *et al*, 2010). Furthermore, cells stimulated by low frequency magnetic fields up-regulate HSP70 (Dini *et al*, 2010). As chaperones assist in protein folding and protein repair (Lado *et al*, 2004), this suggests that structural protein stress due to low frequency magnetic fields causes the increased production of chaperone class proteins.

Calcium influx (in the range 50 – 300 nM) across plasma membrane in conjunction with magnetic fields is well documented (Glogauer et al 1995; Nakahara *et al*, 2002; Hung *et al*, 2010), the subsequent biological effects often being attributed to the excess calcium (Simko and Mattsson, 2004), in as much as calcium is vital for both cytoskeleton remodelling and apoptosis. How low frequency magnetic fields interact with calcium and transfer free energy is a matter for debate, with differing 'schools' of thought offering feasible theories (Gartzek and Lange, 2002). Indeed, this thesis proposes a simple model of diffusion down concentration gradients allowing enough free calcium to affect physiological responses (Simko and Mattsson, 2004). Other work proposes F-actin components of microfilaments to interact with magnetic fields, their polyelectrolyte properties allowing calcium ion conductance into the cytosol, analogous to a disjointed conductive cable (Gartzek and Lange, 2002).

The movement of Ca^{2+} along a concentration gradient down a magnetically induced 'conductive axis' leads to typical Calcium induced cellular responses. Once the induced Ca^{2+} conductance begins, the signal is amplified until V_{max} is achieved or the Magnetic field is removed (Gartzek and Lange, 2002). The F-actin affinity for cations causes a

barrier to anion entry. Furthermore, Ca^{2+} 'flow' and microvilli warping causes membrane stress and dissociation with cytoskeletal elements (Gartzek and Lange, 2002; Dini *et al*, 2010). Calcium also enters via stretch activated ion channels (Glogauer et al, 1995) during membrane deformation, leading to cytoskeletal remodelling (Dini *et al*, 2010; Hung *et al*, 2010), and magnetically induced calcium influx increases levels of apoptosis (Hung *et al*, 2010). No research so far has investigated the role of magnetically induced MVs as a response to increased intracellular calcium caused by ULMF stress.

The purpose of the research reported herein was to investigate the role of pulsed low-frequency magnetically-induced transient membrane pores play in microvesiculation (MV release), apoptosis as well as their effect on proliferation. This work went on to suggest that these membrane pores may be used therapeutically to increase the uptake of chemotherapeutic drugs in Ultra Low-frequency Magnetic Fields (ULMF) stimulated cells (0.3 μT 6V A/C 10Hz [ULMF]).

6.1 ULMFs initiate pseudoapoptosis by creating plasma membrane pores allowing membrane exclusion dyes to enter along a concentration gradient.

ULMFs (0.3 μT 6V A/C magnetic fields) disrupt the integrity of plasma membrane through transient interaction with polar groups associated with phospholipid species. Charged molecules then align with magnetic fields causing low lipid density regions and pores to allow the flow of extracellular molecules and ions into the cytoplasm along a concentration gradient (Fig 6.1A). Furthermore, the configuration of stretch activated ion channels may have been altered by magnetic forces allowing influx of ions such as Ca^{2+} this would in turn lead to the initiation of pseudoapoptosis, subsequent membrane damage allowing the uptake of membrane exclusion dyes (Fig 6.1A).

Once THP-1 were removed from the ULMF, molecular alignment of membrane phospholipids with magnetic fields rapidly dissipates and plasma membrane pores are immediately sealed (Fig 6.1B) as plasma membranes are constantly in motion, indicating that damage causing agents can only enter healthy cells (THP-1 were used as a model for normal cellular behaviour) when stimulated with ULMF. Damage accrued during ULMF stimulation lead to persisting decreased viability after ULMFs are removed. Dye uptake within ULMF ~6.3 ± 0.6% significantly more than when THP-1 cells were removed from the ULMF at 60 second intervals, ~2.0 ± 0.4% dye uptake compared to the control; viability of untreated THP-1 was 95%.

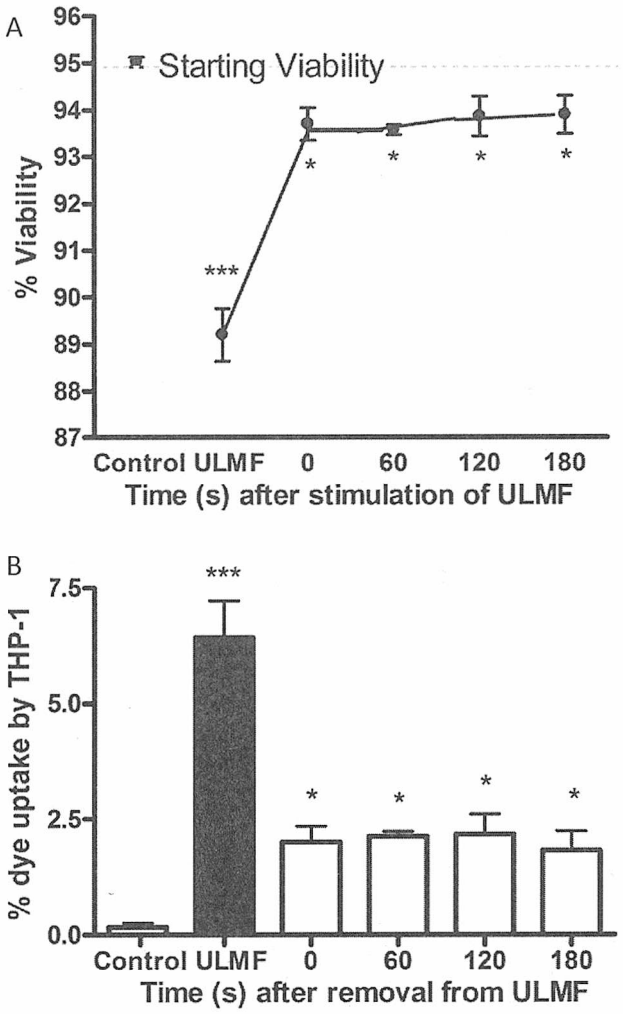

Fig 6.1 ULMFs cause membrane damage facilitating the influx of membrane exclusion dyes causing pseudoapoptosis for the duration of stimulation. THP-1 were stimulated with 0.3 μT 6V A/C ultra low frequency magnetic fields (ULMFs) for 30 min temporarily lowering the viability of the cells by forming transient membrane damage that allowed the passage of ViaCount, which contains a nuclear dye. (**A**) Once removed from the ULMFs, THP-1 were assessed for their viability (**A**) and (**B**) by adding nuclear dye containing ViaCount at 1 min intervals for 3 min to determine the level of membrane breaching. Transient membrane pores induced by ULMFs are unstable: once THP-1 were removed from the 30 min stimulation by ULMFs the membrane dye was unable to enter the cell. The results however demonstrate a consistent insignificant decrease in viability owing to ULMF damage, ≤1% for the duration of the experiment. Cells were assayed by flow cytometry.

6.2 Increasing ULMF density leads to decreased THP-1 viability

To ascertain the extent of ULMF density on membrane damage, four regimens of ULMF density were chosen: 0, 0.1, 0.3 and 0.6 μT 6V A/C 10Hz. It was found that with increasing magnetic field density there was a corresponding significant decrease in viability caused by ULMF induced membrane damage. (Fig 6.2A) High field densities beyond the optimal for membrane damage display negligible decreases in THP-1 viability over a 30 min duration (0.3 - 0.6 μT), possibly due to the small size of the cell in relation to the field density or that the increased field density may hinder the diffusion of ions across a rapidly remodelled membrane. Ion channels may also become increasingly distorted, eliminating a possible route of ion transport in denser magnetic fields.

Our earlier investigation into the nature of ULMF induced membrane damage showed that the 'pores' induced only existed within the field, and that once the cells were removed from the field that pores immediately closed (Fig 6.1B). Furthermore, membrane induced damage must allow the flow of ions and molecules into and out of the cytoplasm along a concentration gradient and we can speculate that ions and molecules included into the cytoplasm must be retained within the membrane once the ULMF is removed. However at 30 min incubation post stimulation with ULMFs there was a significant increase in viability of THP-1. This alludes to removal of damaging agents and restoration of homeostatic mechanisms via MV release (Fig 6.2B).

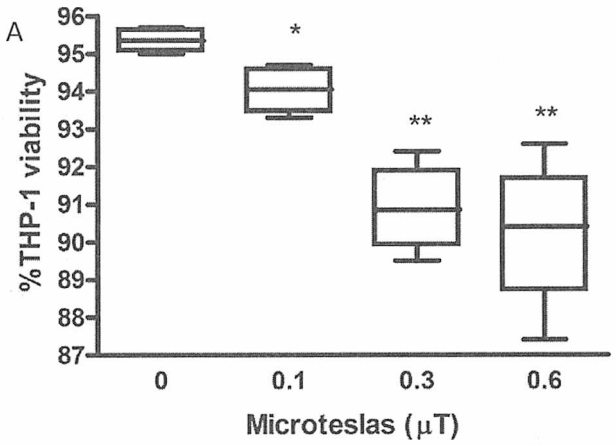

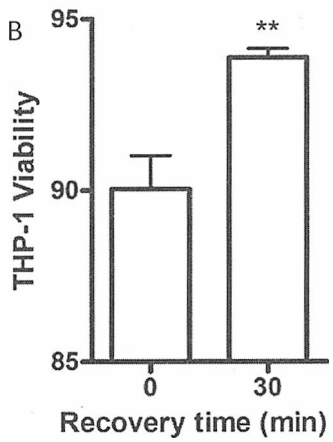

Fig 6.2 Increasing field density leads to an immediate transient decrease in viability. (**A**) 1 x 10^5 THP-1 /ml were subjected to three different ULMF density regimens, 0.1 ± 0.05 μT, 0.3 ± 0.5 μT and 0.6 ± 0.5 μT for 30 min. The THP-1 were immediately quantified for viability using ViaCount. Each regime caused a significant change in viability; 0.1 μT (low field density) showing the smallest drop in viability ≥ 1.5%, 0.3 μT field density ≥ 5% and 0.6 μT (high field density) ≥5.5%. (**B**) THP-1 were subjected to 0.6 μT ULMF strength for 30 min and their viability ascertained using ViaCount, either immediately afterwards (0 min) or after 30 min recovery period suspended in RPMI 1640 supplemented with 10% FBS and 1% penicillin and streptomycin. The THP-1 had shown a significant increase in viability as the ViaCount was exported.

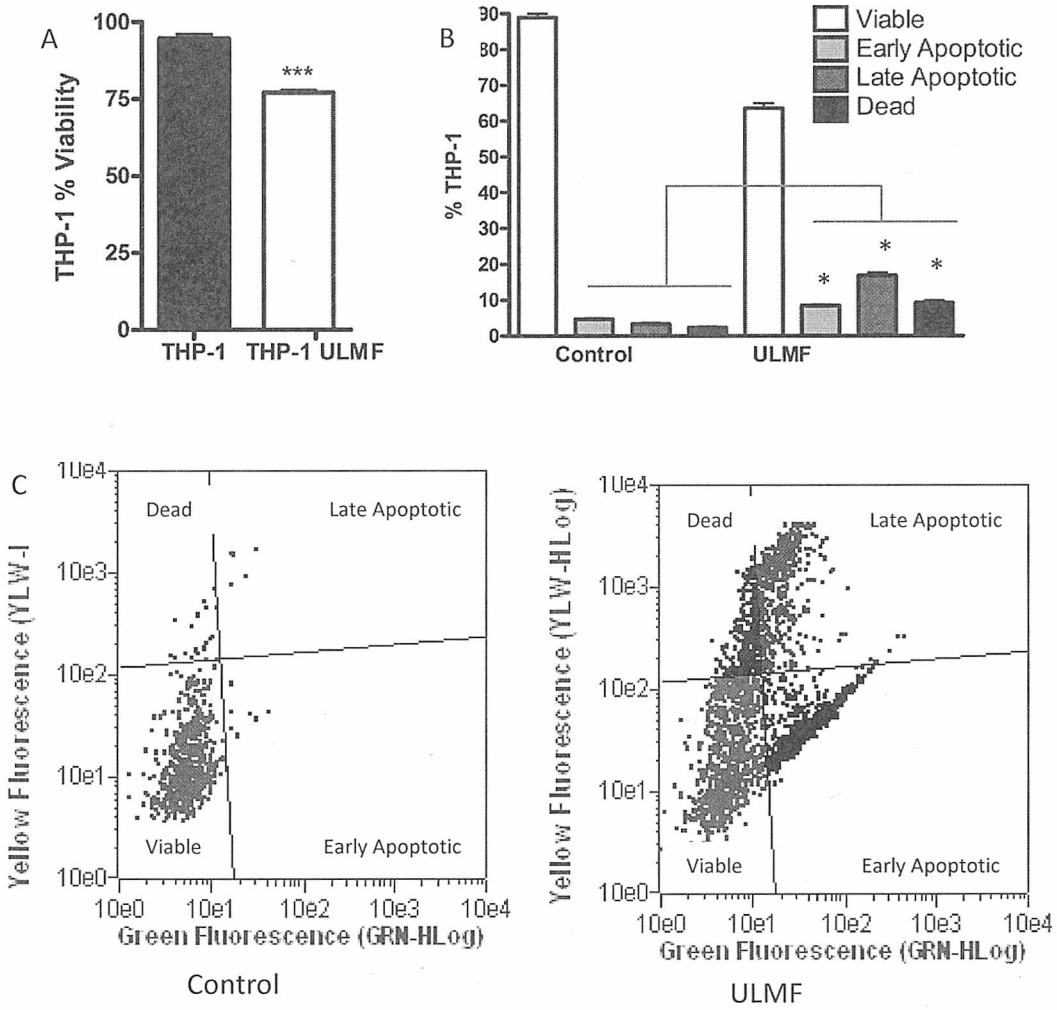

Fig 6.3 The prolonged effect of ULMF on THP-1. (**A**) 2 h 0.3 μT 6V A/C ULMF stimulation of THP-1 caused 18 ± 2% lower viability than un-stimulated control cells. (**B**) Nexin assay of THP-1 stimulated with 0.3 μT 6V A/C ULMF for 2 h. The ULMF exposed THP-1 population were significantly damaged ~18% THP-1 being characterised as late apoptotic. (**C**) FACs Nexin assay compares 95% viable THP-1 to 2 h 0.3 μT 6V A/C ULMF stimulated THP-1. The results demonstrate that ULMFs cause cellular damage through interaction with cellular mechanisms that are linked to pseudoapoptosis but also cause ionic imbalances by the induction of membrane pores, leading to cell death.

6.3 The effects of prolonged THP-1 exposure to ULMFs

The effects of ULMFs on sMV formation were assessed as an alternative method of stimulation without the use of biological or chemical activators. Prolonged (2 h) ULMF stimulation of THP-1 lead to a permanent 18 ± 2% decrease in total population viability (Fig 6.3A). Pseudoapoptotic events induced with ULMFs (Fig 6.3B) induce MV formation (Fig 6.4A) by allowing the Ca^{2+} to accumulate within the cytoplasm allowing MV formation (Fig 6.5A). ULMF stimulation beyond the normal MV release duration maintains an elevated $[Ca^{2+}]_i$ level causing the progression of irreversible apoptotic events (Fig 6.3).

Indeed, Nexin assay demonstrated that THP-1 were shunted to early (~10%) and late apoptosis (~18%) when stimulated with ULMFs. Furthermore, THP-1 express decreased PS expression by annexin V binding between 1 - 2 h ULMF stimulation, possibly due to PS export on sMVs. Flow cytometer Nexin assay confirmed the apoptotic stages (Fig 6.3B and 6.3C), highlighting the extent of the damage ULMFs caused to the cell populations. Incubation with ULMFs for 2 h lead to ~ 28% of cells to enter late apoptosis of die (Fig 6.3B and 6.3C). ULMF induced membrane pores promoted 7-AAD binding to dsDNA indicating that ULMFs cause membrane pores in nuclear membranes and possibly throughout the cell. This may cause mitochondria to leak cytochromes, forming the apoptosome and causing apoptosis.

6.4 ULMFs stimulate THP-1 to release MVs

0.3 μT 6V A/C ULMF causes a significant increase in MV release ~2.5x more than control cells rested in RPMI 1640 (Fig 6.4A and 6.4B). sMV release is possibly coupled

with pseudoapoptotic events (Fig 6.3B). The sMVs generated are identifiable by FACs analysis as 'typical' sMVs (Fig 6.4B) although they are produced in lower numbers than sMVs generated by other stimuli, such as 5%NHS (Fig 6.6A). ULMF stimulates sMVs express ~90% PS when quantified using annexin V (Fig 6.4B).

6.5 THP-1 loaded with calcium green-AM and stimulated with ULMFs demonstrate calcium influx.

It was found that sMV formation was indeed stimulated using ULMFs, producing x2.5 more vesicles than were constitutively released (Fig 6.4A). The effect of ULMFs on the integrity of sMV membrane was not assessed. As ULMFs induce the production of sMVs through membrane pores and are enriched by internalised PI therefore MV formation can be regarded as a similar process to MAC induced sMVs (Fig 6.8A).

As referred to earlier in the introduction, cMV release is in response to normal physiological processes of the cell and sMV release is due to cells having been subjected to various stresses to prevent the progression of pseudoapoptotic events to irreversible apoptosis. However, prolonged exposure to ULMFs ensures apoptosis by generating 'un-pluggable' or un-removable membrane pores, so much so that cells stimulated with ULMFs will initially produce sMVs but can progress to apoptosis. Subsequently fewer sMVs were produced by ULMFs than by other means, (e.g., 10% NHS) as the cells begin to die (Fig 6.3A).

Calcium enters cells stimulated with ULMF for 30 min, significantly increasing total cellular free calcium (Fig 6.5A). However, calcium influx occurs over 5 – 15 min and reaches significant levels at 30 min. The lag phase of calcium influx was between 0 – 5+ min (Fig 6.5B). This possibly occurs as cells are effective at calcium homeostasis and other mechanisms operate to hinder uncontrolled calcium influx. Cells are able to store 'free' calcium within the endoplasmic reticulum (ER), but stimulation with ULMFs cause trans-cellular plasma membrane poration and the cellular mechanisms to sequester calcium to the ER become less efficient as the ER is no longer capable of storing calcium, that enters the cytoplasm along a concentration gradient.

6.6 The consequence of calcium ion channels for calcium influx during ULMF stimulation

NHS (5 – 10%) caused sMV release ~5.2 x 10^6 /ml as previously described in this thesis. ULMFs generate a significant increase in sMV formation (Fig 6.4A). EGTA sequesters Ca^{2+} thus preventing it from entering the cell or initiating MV biogenesis, indicating that Ca^{2+} is essential of ULMF sMVs. However, ~5 x 10^5 sMVs are released in ULMFs, supporting the supposition that trans-cellular poration occurs and Ca^{2+} originating from sub-cellular organelles are capable of initiating sMV biogenesis (Fig 6.6).

Gadolinium Chloride ($GdCl_3$) is a non-specific calcium ion channel blocker, preventing the passage of Ca^{2+} by blocking the channel with atoms having approximately the same ionic radius as Ca^{2+}. sMVs are released as Ca^{2+} enters through membrane pores induced by ULMF and Ca^{2+} leaked from porated organelles. $GdCl_3$ stimulated more MVs that cells stimulated with ULMFs alone as $GdCl_3$ is highly toxic. Although $GdCl_3$ blocked stretch

activated calcium ion channels, when stimulated with ULMFs the free Gd^{3+} enters the cell via ULMF induced membrane pores and stimulated cytotoxic activity. In conjunction with ULMFs the viability of the cells decreased to ~1/5 the control cells and induced apoptosis and therefore elevated numbers of sMVs (Evens *et al*, 2005), data to support this hypothesis (Fig 10.11).

FACs analysis of sMVs released from cells cultured in RPMI 1640 supplemented with EGTA and those stimulated with ULMF display that ULMFs produce MVs that are larger and more uniformly distributed in size than ULMF un-stimulated cells. Also, cells whose stretch activated calcium ion channels were blocked with $GdCl_3$ and stimulated with ULMFs display larger, uniformly distributed sMVs with a more variable side scatter, than cells with $GdCl_3$ blocked stretch activated calcium ion channels that were un-stimulated with ULMFs (Fig 6.6).

ULMF stimulation of cells therefore create membrane pores and don't cause stretch ion channels to open *per se*, blocking the ion chnnels with $GdCl_3$ did not prevent sMV release, indicating that Ca^{2+} was influxing through membrane damage and not through ULMF interaction with the ion channels. Furthermore, EGTA chelating free calcium reduced sMV release but low levels of sMVs were released as ULMF generate membrane pores throughout the cells, causeing organelles to leak their free calcium, leading to MV release (Fig 6.6).

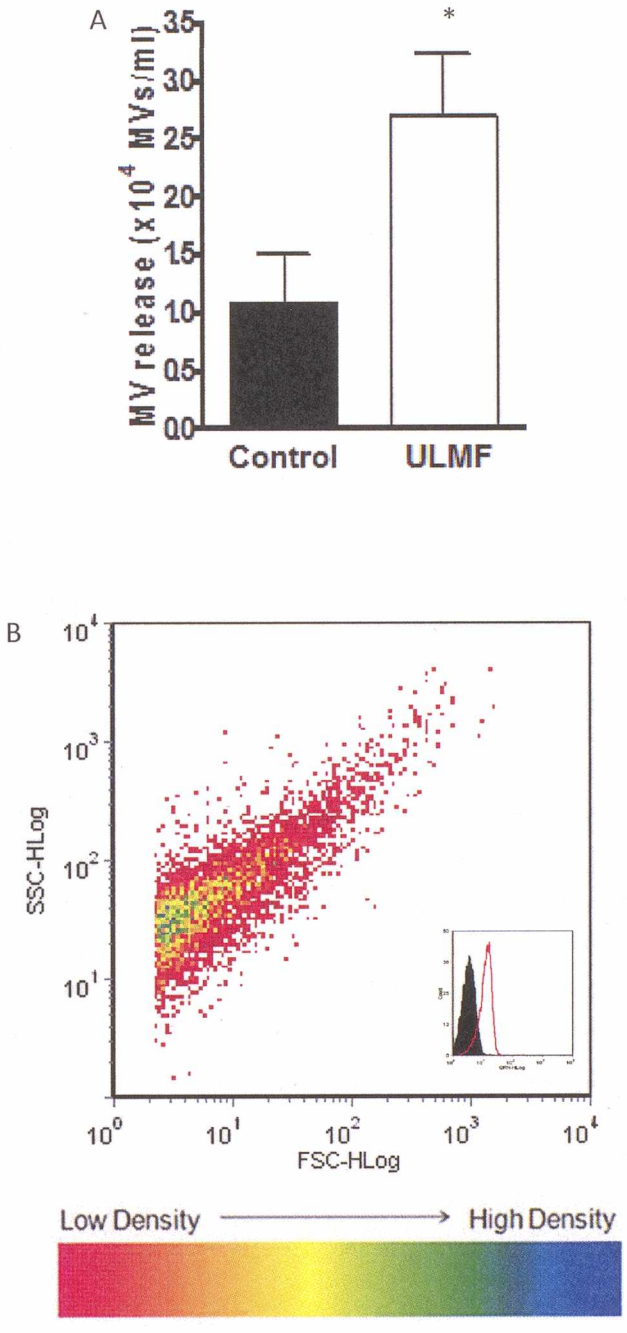

Fig 6.4 Quantification of ULMF stimulation of MVs. Cell-free culture supernatant was submitted for MV isolation and quantification by FACs analysis (Guava ExpressPlus). (**A**) There is a significant increase in MV release when cells are stimulated with 0.3 µT 6V A/C ULMFs for 1 h+. Although the MV levels released are lower than those obtained with other stimulating agents, ULMFs demonstrate that as cells enter 'early' apoptosis they release sMVs in an attempt to reduce cellular membrane damage inflicted by the magnetic field. (**B**) FACs morphology and the inset show's annexin V staining of PS ~90%, confirming MV release during ULMF stimulation.

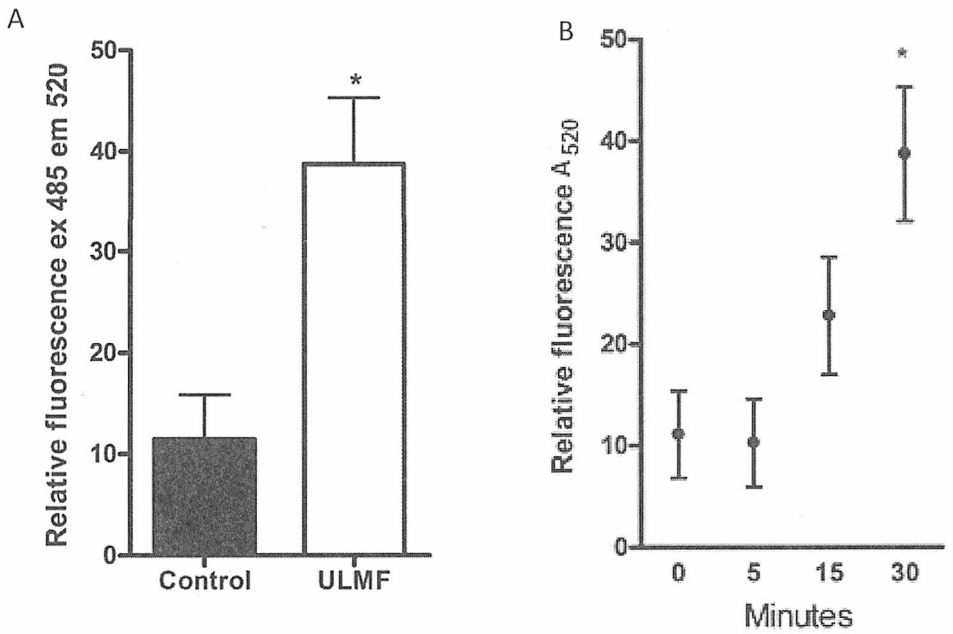

Fig 6.5 Relative fluorescence of THP-1 loaded with calcium green-AM dye. (**A**) THP-1 (5 x 10^5/ml) were loaded with calcium green and stimulated with 0.3 µT 6V A/C ULMF for 30 min. (**B**) The cells were quantified for cytoplasmic calcium levels using a FLUOstar Ω multiplate reader exciting A_{485} and recording A_{520} at set time points 0, 5, 15 and 30 min. Indeed after 30 min the cytoplasmic calcium levels had increased significantly (28 ± 5%). However, stimulation with ULMFs did not lead to an immediate calcium spike, rather a delayed significant increase between 5 - 15 min (11 ± 5%) leading to 28 ± 5% at 30 min.

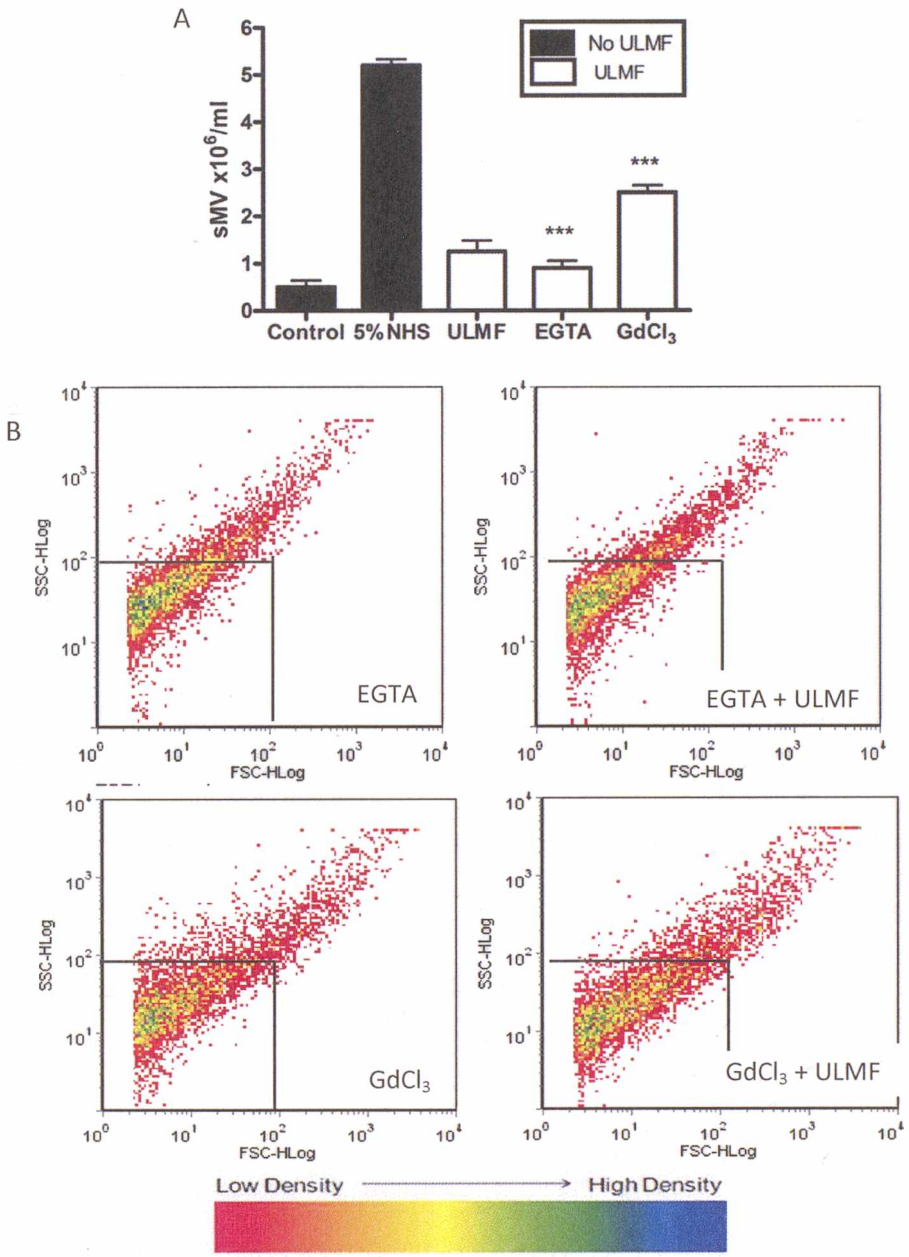

Fig 6.6 Assessment of the role calcium ion channels play in the calcium influx during ULMF stimulation. (**A**) sMVs were stimulated from THP-1 (5 x 10^5/ml) using 5% NHS and quantified (~5.2 x 10^6/ml). THP-1 were also cultured in EGTA or $GdCl_3$ to ascertain the role of external sources of calcium and calcium ion channels play in ULMF sMVs. Although EGTA significantly quenched external Ca^{2+} sources, sMVs were released (~8 x 10^5/ml) as calcium influx from ULMF membrane pores induced in cellular organelles was significant enough to cause damage. $GdCl_3$ blocked the calcium ion channels, however calcium entered the cell through ULMF induced membrane pores leading to sMV release (~2.25 x 10^6/ml). (**B**) FACs dot plots displaying differences in typical MV morphology when subjected to the stressing constraints supplemented with either EGTA or EGTA and ULMF, demonstrating that ULMF with EGTA lead to increased larger MVs. $GdCl_3$ or $GdCl_3$ and ULMFs, demonstrating that ULMFs in conjunction with $GdCl_3$ leads to a larger and more general distribution of MV sizes. The lines intersecting at FSC-HLog 10^2 and SSC-HLog 10^2 were chosen to highlight differences in MV sizes and surface topographical features.

6.7 ULMFs enhance THP-1 ability to produce sMVs when stimulated with NHS

THP-1 (1 x 10^6 /ml) release sMV with incubated with RPMI 1640 supplemented with 10% NHS and 2 mM Ca^{2+} as previously described generating ~5 x 10^5 MVs/ml, (Fig 6.7A). However, when THP-1 (1 x 10^6 /ml) were incubated with RPMI 1640 supplemented with 10% NHS and 2 mM Ca^{2+} and further stimulated with ULMF ~6 x 10^5 MVs/ml were released (Fig 6.7A). FACs ExpressPlus analysis confirmed that their morphology was similar to NHS stimulated THP-1 without ULMFs but they were generally more concentrated in the 0 – 0.3 μm size range.

6.8 ULMF formation of membrane pores allows the cytoplasmic inclusion of PI

THP-1 stimulated with ULMF generated membrane pores large enough to allow the influx of PI (RMM 668.3) along a concentration gradient that was retained within THP-1 cytoplasm once ULMF stimulation was removed, significantly increasing relative fluorescence ~18% A_{626} (Fig 6.8A) and when quantified by FACs ExpressPlus, PI inclusion had significantly increased ~22% (Fig 6.8B)

ULMFs cause the formation of membrane pores within sub-cellular organelles, including the nucleus allowing PI to bind to DNA (Fig 6.8C). This signifies that the double membrane bound nucleus is prone to ULMF induced damage, allowing the free passage of undesirable agents in to the nucleus to interact with DNA. It is conjectured that DNA damage could also result from interaction with ROS (resulting from ULMF damaged mitochondria by inducing membrane pores) or other genetically hostile agents, leading to apoptosis (Fig 6.3B) or promotion or suppression of desirable gene products via an undetermined mechanism.

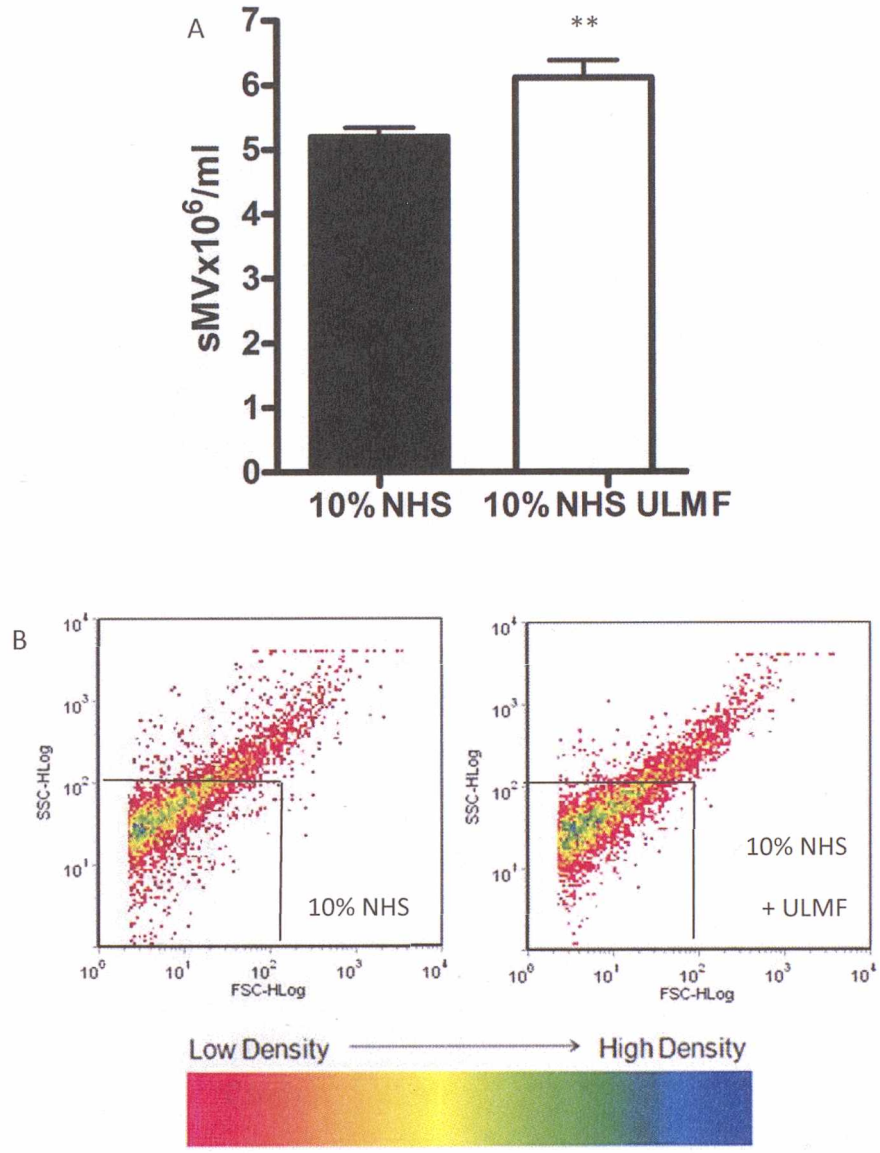

Fig 6.7 The increased effect of ULMF on sMV release in conjunction with 10% NHS. (**A**) THP-1 (1 x 10^6 /ml) were incubated with 10% NHS in RPMI 1640 supplemented with 2 mM $CaCl_2$ and stimulated using ULMF. 10% NHS stimulated ~5.2 x 10^6 /ml sMVs, however 10% NHS in conjunction with ULMFs stimulated significantly more ~6 x 10^6 /ml sMVs. (**B**) FACS ExpressPlus morphology of sMVs released from THP-1 stimulated with 10% NHS and 10% NHS in conjunction with ULMFs. There is a distinct difference in sMV population morphology. 10% NHS derived sMVs exhibit a more uniform size distribution than 10% NHS with ULMF, where there is an increase in population density for sMVs 0 - 3.0 μm.

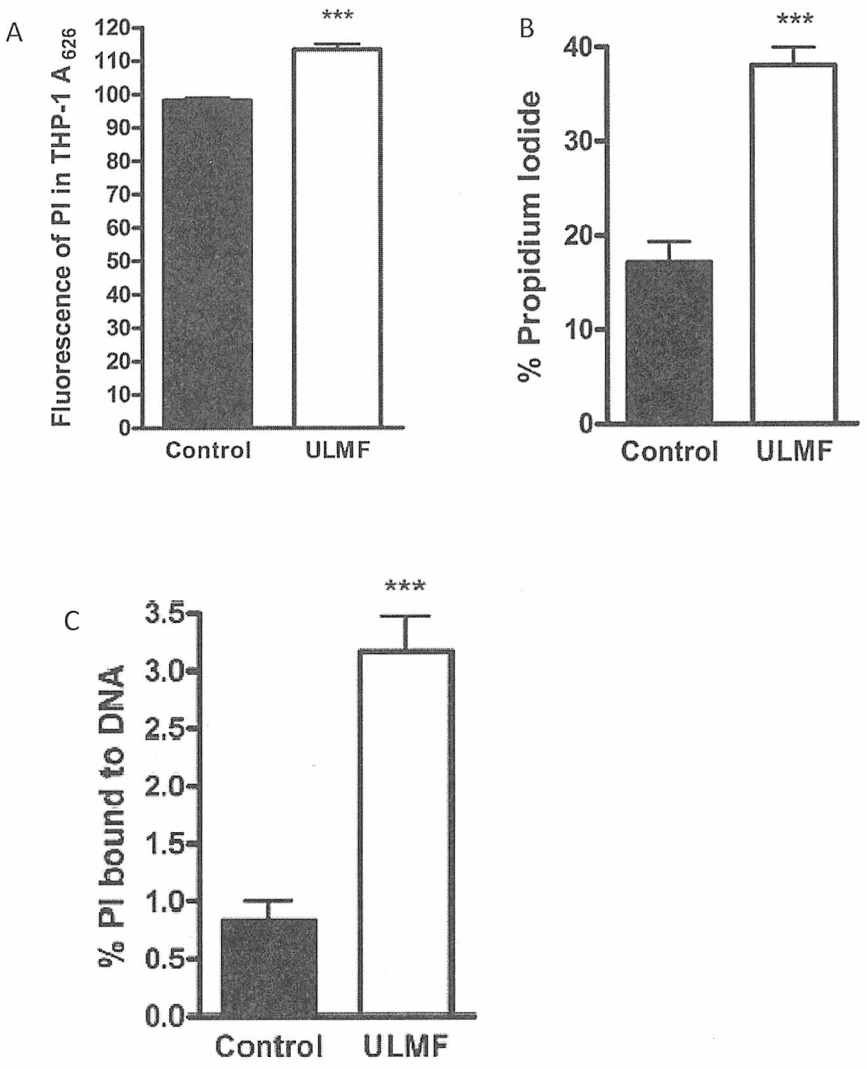

Fig 6.8 ULMF formation of membrane pores allows the cytoplasmic inclusion of PI. (**A**) The mechanism for cellular damage and subsequent sMV release was assessed using PI. If was found that cells stimulated with ULMFs had significantly more PI fluorescence at A_{626} than those cultured normally. The results were relative rather than absolute, but confirmed previous results. Furthermore, the likely method of PI entry was by ULMF induced, transient membrane pores. (**B**) Membrane PI levels were quantified using FACs Guava viacount analysis, but measuring % PI internalised by cells both stimulated or not by 30 min stimulation with ULMFs. The stimulated cells show 22 ± 2% more internalised PI than the control cells. (**C**) ULMFs cause nuclear membrane pores, PI passes through ULMF (30 min) induced pores throughout the entire membrane architecture of the cell; significantly, PI is bound to DNA by passing through pores formed in the nuclear membrane, 2.5% above the established base line. PI was quantified (**A**) using FLUOstar Ω multiplate reader (Thermo) (**B**) and (**C**) using flow cytometry.

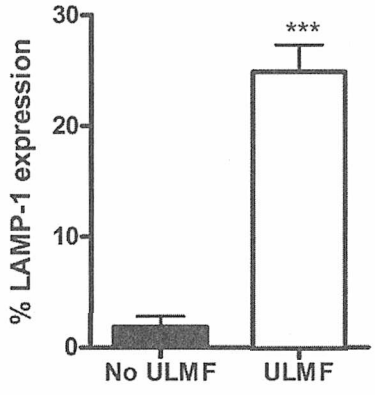

Fig 6.9 LAMP-1 expression in THP-1 stimulated with ULMF. THP-1 (5 x 10^5 /ml) were stimulated using 'standard' ULMF regime and assessed for cell surface membrane expression of LAMP-1 (CD 107a). THP-1 stimulated with ULMF for 30 min express significantly more Lamp-1; 23 ± 2% than un-stimulated THP-1. LAMP-1 was quantified using FLUOstar Ω multiplate reader, (Thermo).

6.9 Outer leaflet LAMP-1 expression increases during ULMF stimulation

Lamp-1 (lysosome associated membrane protein 1; CD107a) is highly expressed on the outer membrane of THP-1 stimulated with ULMFs, 23 ± 2% more than the control (Fig 6.9). ULMFs cause the formation of outer membrane pores by causing the polar groups on phospholipids to align with magnetic fields. The resultant pores allow the influx of ions down a concentration gradient, causing the cell to enter apoptosis. MVs are produced in response to membrane pores (Fig 6.4 and 6.5A). Increased cytosolic free Ca^{2+} leads to increased plasma membrane LAMP-1 by increasing the speed and frequency of lysosomal trafficking to the plasma membrane by Ca^{2+} sensitive secretory pathways (Thomas *et al*, 2009). Lysosomes are released to 'plug' the ULMF induced pore by fusing with the plasma membrane, preventing the loss of membrane selective permeability and maintaining the membranes ion gradients (Fig 6.9). (Thomas *et al*, 2009).

6.10 THP-1 loaded with PI using ULMFs display a decrease in PI after MV release

PI (5 mM) loaded into THP-1 using ULMF lead to a significant increase ~4.1% in internalised PI. The THP-1 loaded with PI using ULMFs were rested and then stimulated for sMV release, for 45 min at 37 °C in 5% CO_2 and then analysed for internalised PI. The THP-1 had negligible PI levels above the control (Fig 6.10). It can be surmised that PI was excreted as non cellular waste and exported via sMVs as with free Ca^{2+} to prevent pseudoapoptotic events (Fig 4.5).

6.11 Incubation of THP-1 with H_2O_2 decrease cell population viability, co-incubation with ULMFs significantly reduces THP-1 viability.

H_2O_2 (1 mM) incubated with THP-1 for 1 h at 37 ^oC in 5% CO_2 caused a significant loss of viability ~67.2 ± 5%. When THP-1 loaded with H_2O_2 for 1 h at 37 ^oC in 5% CO_2 were co-stimulated with ULMFs for 30 min, this caused a further significant loss of viability down to ~49.1 ± 3.6% (Fig 6.11). The decrease of THP-1 viability when stimulated with H_2O_2 is well documented, moving the cells into late apoptosis. Furthermore, Fig 6.2B suggests that THP-1 also enter early and late apoptosis with ULMF stimulation, indeed the ULMFs enhanced the effects of H_2O_2 nearly two fold. THP-1 were assayed using flow cytometry, ViaCount.

6.12 ULMFs stimulate increased proliferation of THP-1 and PC12

Cells stimulated with 0.3 μT 6V A/C ULMFs for 30 min and subsequently incubated in RPMI 1640 supplemented with 10% FBS and 1% penicillin and streptomycin proliferate significantly more than the control cells. Indeed, THP-1 that were stimulated with ULMFs and allowed to proliferate in culture for 24 h have a population ~11 ± 1% significantly larger than the un-stimulated control cells. Furthermore, PC12 that were stimulated with ULMFs and allowed 24 h to proliferate (as before) had a significantly larger population 15 ± 1% than the un-stimulated control PC12 (Fig 6.12).

The viability of both cell types remained high, with no significant difference, although THP-1 appears to have a post ULMF viability ~1% higher than the control, conversely PC12 have viabilities ~1 ± 1% lower than their control cells (Fig 6.12).

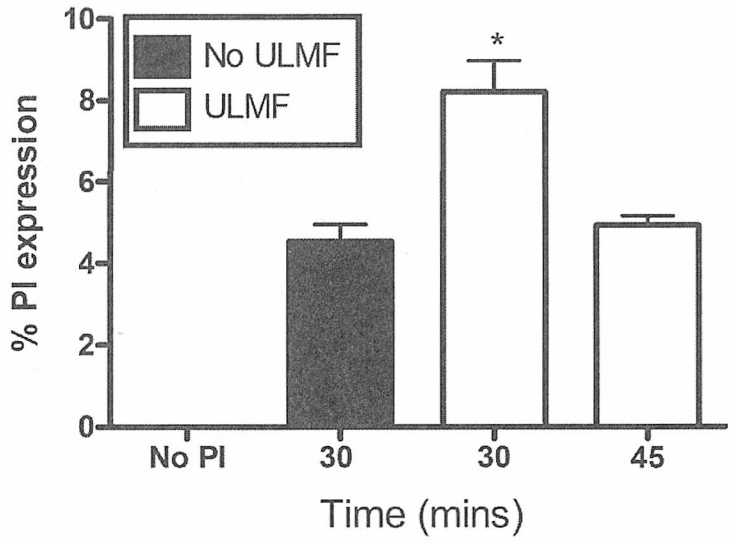

Fig 6.10 THP-1 stimulated with ULMF lead to PI influx along a concentration gradient. THP-1 were cultured with CGM supplemented with 5 mM PI and stimulated with ULMF for 30 min where upon the cells were assessed using FACs ExpressPlus for cytoplasmically included PI demonstrating a significant increase in PI inclusion ~4 ± 1% more than the no ULMF control. Cells stimulated with ULMFs allowing PI uptake were allowed to microvesiculate leading to a decline in cell included PI to 'normal' levels ~5%. PI was quantified using flow cytometry.

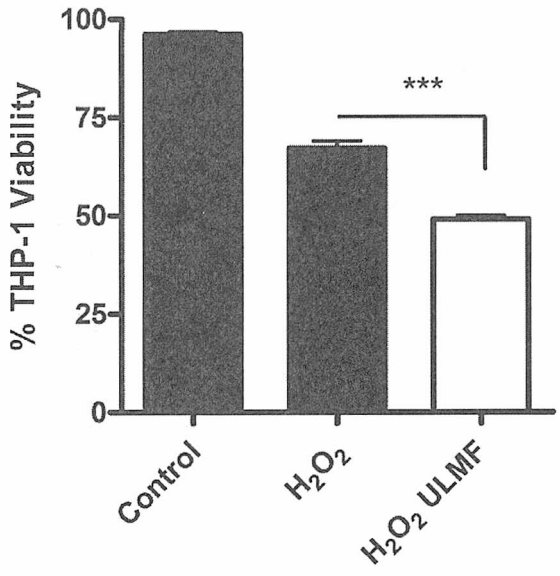

Fig 6.11 Incubation of THP-1 with H_2O_2 decreases viability and co-incubation with ULMFs significantly reduces THP-1 viability. THP-1 treated with 1 mM H_2O_2 reported ~67.2% viability and THP-1 treated with 1 mM H_2O_2 and 0.3 μT ULMF reported a significant decrease in viability ~49.1%. THP-1 were assayed using ViaCount and flow cytometry.

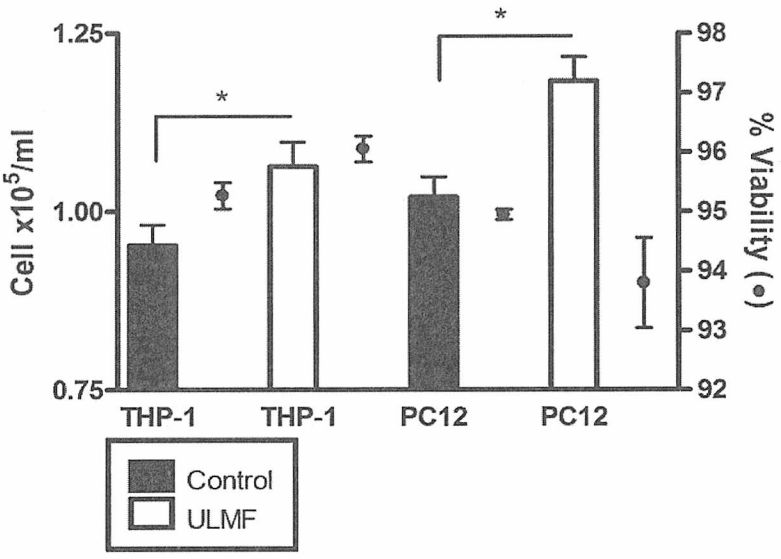

Fig 6.12 ULMFs stimulate increased proliferation of THP-1 and PC-12. THP-1 and PC-12 (1 x 10^5 /ml) were exposed to ULMFs for 30 min and cultured at 37°C 5% CO_2 for 24 h. Their viability and cell number was quantified using Guava Millipore Viacount analysis. THP-1 experienced both increased growth (~11% higher than the control) and viability (1% higher than the control). PC-12 showed an increase in cell number (~15% higher than the control) but a decrease in population viability (1.5 ± 1.0% lower than the control). Cells were assayed using ViaCount and flow cytometry.

6.13 Methotrexate (MTX) potency is enhanced by directed ULMFs

ULMFs enhance the potency of methotrexate when treating THP-1 (5 x 10^5 /ml). This significant finding was produced when administering methotrexate in conjunction with ULMFs within an acceptable time frame to prevent drug half life decay. The drug enters the cells through a magnetically induced membrane pore, down a concentration gradient. When the ULMF stimulus was removed, the drug was 'trapped' within the cytoplasm. This method allows a larger bio-available dose of methotrexate to enter the cell, so much so, that smaller therapeutic doses such as 1 μM can be administered while larger intracellular concentrations can be achieved. Indeed, THP-1 treated with 1 μM methotrexate, administered in conjunction with ULMFs lead to population ~4.0 x 10^5 /ml and viability ~51%, similar to those treated with 10 μM methotrexate and not stimulated with ULMFs (~4.25 x 10^5 /ml with ~53% viability). Furthermore, 10 μM of methotrexate loaded cells stimulated with ULMF lead to ~3.2 x 10^5 /ml THP-1 and ~49% viability (Fig 6.13A). Compared to the starting concentration of 1.9 x 10^6 cells/ml, the additional effect of ULMF over MTX alone increased the % decrease in cell concentration by ~75%.

The combined use of methotrexate and ULMFs yields similar results with PC12 as were observed using THP-1. The full data is provided in the appendix. Although the effects of methotrexate therapy in conjunction with ULMFs against PC12 were less dramatic than with THP-1, the effects were statistically significant. PC12 (5 x 10^5 /ml) treated with 1 μM methotrexate yielded a cell concentration of ~1 x 10^5 /ml and cell viability ~32%. However when treated with ULMF this was significantly reduced to ~7.8 x 10^4 /ml and 29% viable. Furthermore, 0.1 μM methotrexate and ULMF treated PC12 lead to ~5 x 10^4 /ml and ~29% viability (Fig 6.13B). There may be a balance between ULMF

generating membrane pores that sensitise cells to anti-cancer drugs or initiating sMV release (containing the drug) effectively desensitising the cells to anti-cancer drugs. PC12 is a model for brain cancer or an inaccessible solid mass tumour, indeed the PC12 were not differentiated in to neurones for this purpose.

6.14 Varying ULMF density leads to a plateau effect when stimulating membrane damage

THP-1 (1 x 10^5 /ml) were chosen for the field density study. THP-1 treated with methotrexate and 0.3 μT 6V A/C ULMFs lead to significant loss of viable cells (Fig 6.13A). It was shown earlier that THP-1 were significantly affected by varying ULMF density (Fig 6.2A) leading to a plateau of viability loss as field density increased. However, reproducing the experiment (as described in section 6.2) and supplementing the media with 10 μM methotrexate produced results with no significance at all field densities tested. Nevertheless THP-1 subjected to 0.3 μT 6V A/C ULMFs lead to ~1 x 10^4 /ml lower viable cells than the other densities tested (Fig 6.14A) and ~2% lower population viability (Fig 6.14B).

6.15 Comparison of the effects of etoposide, docetaxel and methotrexate with or without 0.3μT 6V A/C ULMF stimulation over 48 h

The use of therapeutic doses of etoposide, docetaxel and methotrexate on THP-1 lead to significant proliferation of THP-1 over 24 – 48 h (Fig 6.15). This is documented and apart of the drug's mode of action. THP-1 (5 x 10^5 /ml) were cultured in RPMI 1640 supplemented with 10% FBS and 1% penicillin and streptomycin for 48 h and quantified using ViaCount assay by flow cytometry. Furthermore THP-1 were cultured

with a variety of regimes of therapeutic doses of anti cancer drugs in conjunction with or without ULMFs. ULMFs had a stimulatory effect on THP-1 cultured with etoposide and docetaxel, significantly increasing their proliferation beyond that obtained with the drug alone (Fig 6.15). In the case of methotrexate the ULMFs significantly inhibited proliferation to ~30% that of the drug control.

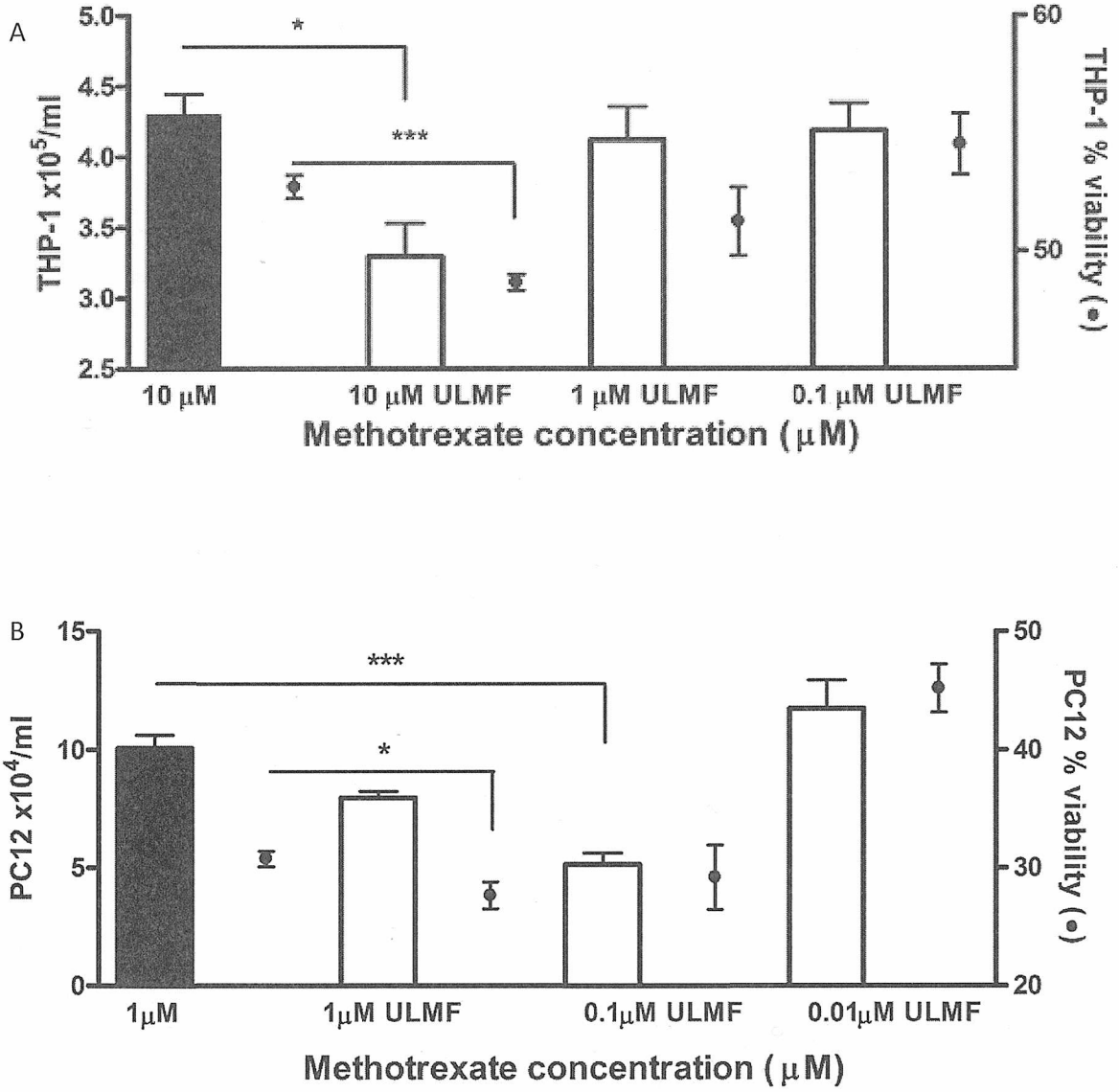

Fig 6.13 Methatrexate potency is enhanced by directed ULMFs. (**A**) Therapeutic doses of methatrexate were used to treat THP-1 in conjunction with 0.3 μT 6V A/C ULMFs, control not shown viability 97.1% and cell count ~1.9 x 10^6 /ml. (**B**) Therapeutic doses of methatrexate were used to treat PC-12 *in vitro*, assessing both cell number and population viability. When used in conjunction with 0.3 μT 6V A/C ULMFs, the potency of methatrexate is significantly enhanced, so much so that 1/10^{th} dosage with ULMFs produced lower, but approximating that of the control regimen (no ULMF, 10 μM) and 10 μM with ULMF produces significant effects both lowering viability and cell number. Furthermore 1/100 dose with ULMF produces acceptable chemotherapeutic effects. Cells were assayed using ViaCount and flow cytometry.

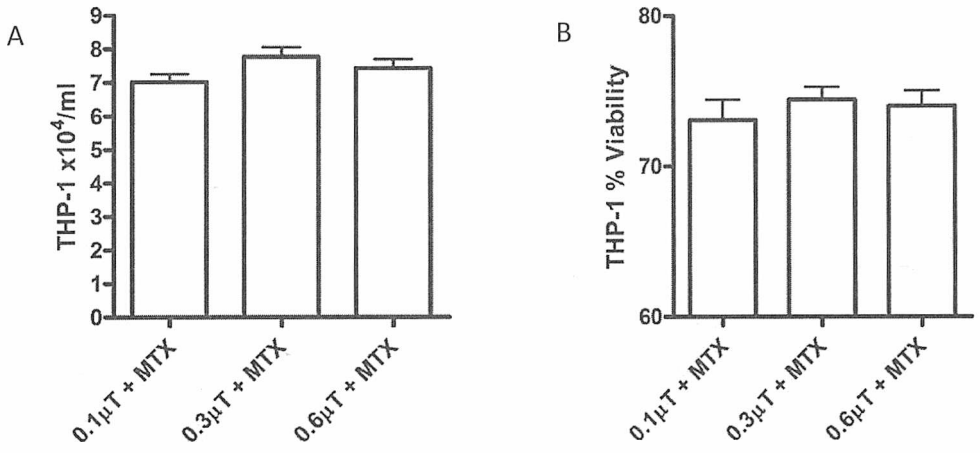

Fig 6.14 Varying the ULMF density leads to a plateau effect during treatment with methotrexate (MTX) and co-stimulating plasma membrane damage. THP-1 (1 x 10^5 /ml) were exposed to ULMFs with 3 magnetic field densities. (**A**) ~1 x 10^5 THP-1 /ml were cultured with 10 μM MTX and 0.1, 0.3 and 0.6 μT 6V A/C ULMF for 30 min and allowed to proliferate for 24 h. Insignificant differences in THP-1 population numbers were found, although the lowest field density is the most effective ~7 x 10^4 /ml when compared to THP-1 stimulated with an increased density (8 x 10^4 /ml). (**B**) The THP-1 viabilities also show no significant difference, although the low field density with 10 μM MTX has a 2% lower viability than the higher field density populations. THP-1 were assayed by flow cytometry using ViaCount assay.

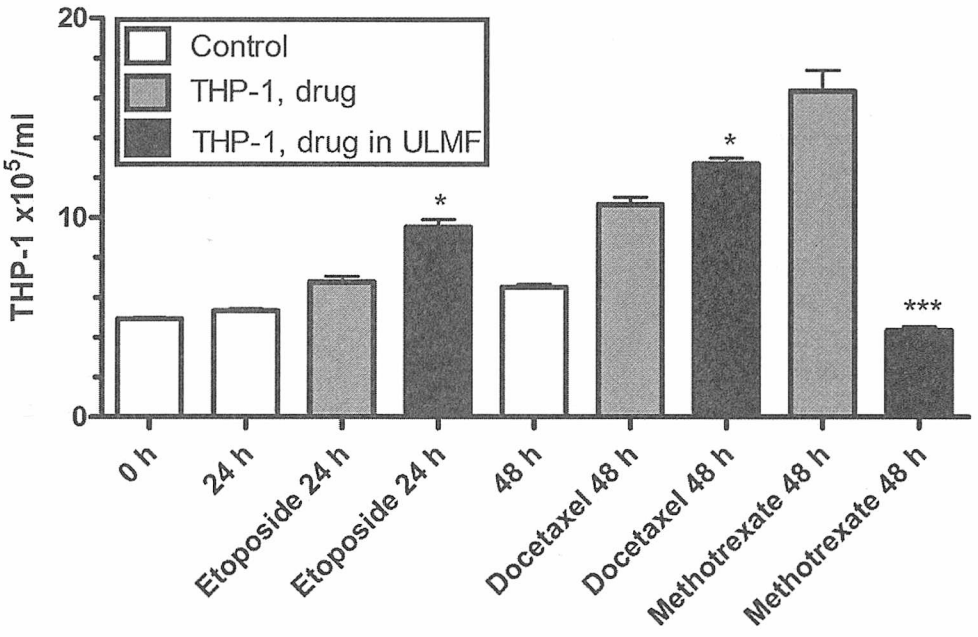

Fig 6.15 Summary of the effects on THP-1 promonocytes of various chemotherapeutic drugs both with and without ULMFs used against THP-1. The control shows the standard growth for THP-1 in culture (CGM) over 48 h. quantified at 24 h time intervals. The use of the chemotherapeutic drugs show an enhanced growth for all drugs tested, significantly higher than the control. The proliferation was significantly exaggerated by using ULMF in the case of etoposide (~30% proliferation) and docetaxel (~18% proliferation) above that of THP-1 treated with the drug. However methatrexate therapy used with ULMF shows a significant decrease in THP-1 cell numbers at 48 h to ~30% that of the methotrexate treated cells without ULMF. Cell populations were assayed using ViaCount and flow cytometry.

6.16 HeLa scratch injury treated with ULMFs

To see if ULMF had any effect on cell migration, HeLa were grown to confluence (~1.1 x 10^5 /ml) in sterile 12 well plates in RPMI supplemented with 10% FBS and 1% penicillin and streptomycin. HeLa were inflicted with a 1500 μm scratch along the equator of the confluent culture and immediately washed with RPMI and suspended in RPMI supplemented with 10% FBS and 1% penicillin and streptomycin. The control cells were incubated for 48 h at 37 °C in 5% CO_2 and the scratch measured at 24 h intervals. HeLa (non control) were stimulated with 0.3 μT 6V A/C ULMFs for 30 min at 37 °C and 5% CO_2 and then removed from the ULMF and incubated at 37 °C and 5% CO_2 for 48 h, the scratch measured at 24 h intervals.

Control HeLa scratch injury shows that cell migration and proliferation into the scratch is significant by 24 h and by 48 h the scratch has significantly shrunk, no longer being apparent. However, HeLa treated with 0.3 μT 6V A/C ULMFs show little migration at 24 h and by 48 h and although the scratch has shrunken, the edge of the scratch is still visible and 'clean' (Fig 6.16) The measurements for the scratch were made along its entire length at multiple points.

6.17 Migration and proliferation of HeLa are significantly affected by ULMFs

The migration of cells into a wound is essential for healing. HeLa migration into the wound site was measured at 24 h intervals for 48 h. Surprisingly, control HeLa migrated into the wound and over 48 h the scratch healed ~68% (480 μm scratch), however 0.3 μT 6V A/C ULMF treated HeLa had migrated less over 48 h and the scratch healed ~56% (650 μm scratch) (Fig 6.17A). Indeed, the ULMF stimulated HeLa

proliferation levels were ~10.1% more than non ULMF stimulated HeLa over 48 h, maintaining a high viability ~97% (Fig 6.17B) as seen with THP-1 and PC12 (Fig 6.12). Furthermore, ULMFs stimulate HeLa (1 x 10^5 /ml) to release significantly more MVs (~2x) than un-stimulated cells (Fig 6.17C).

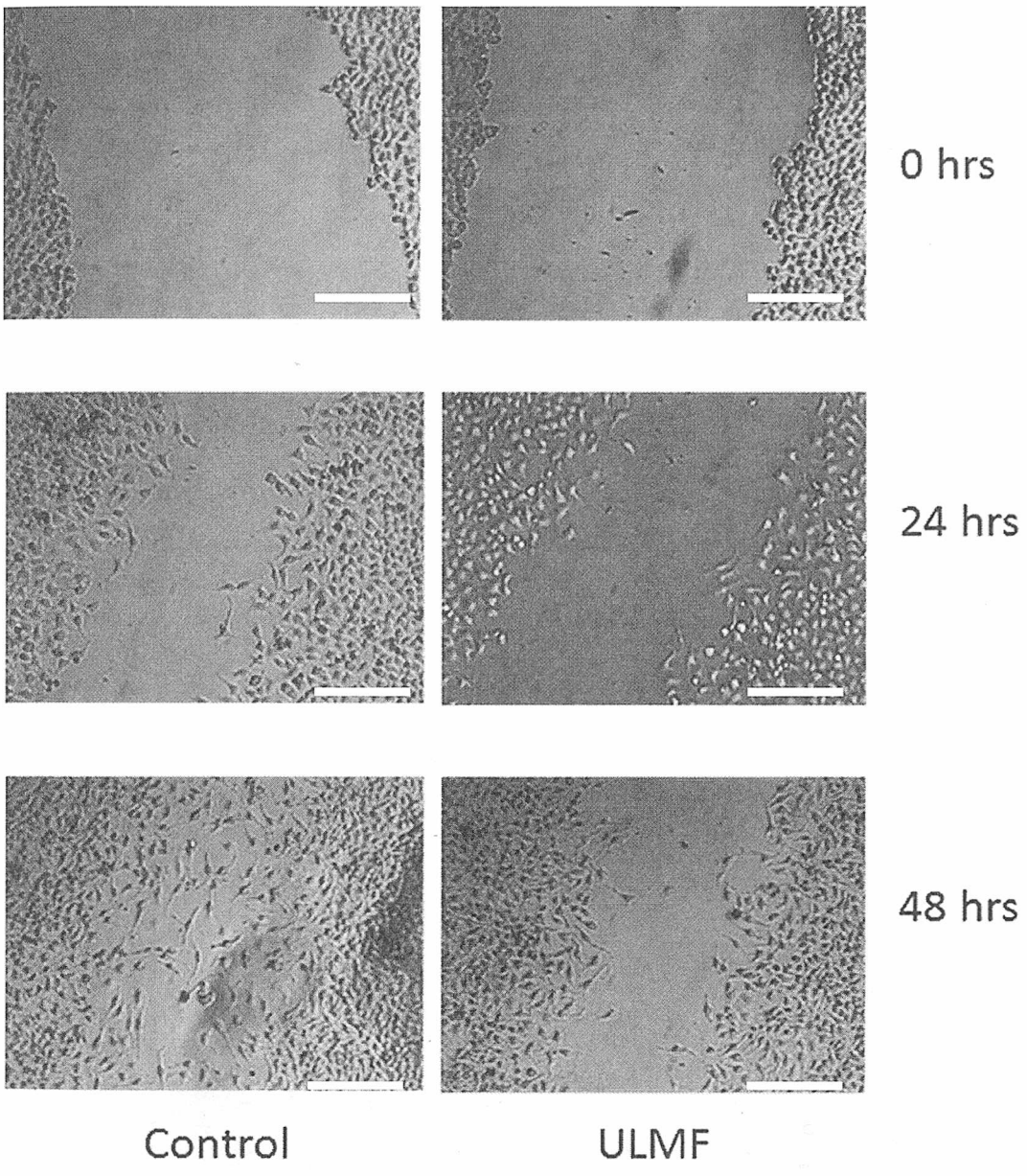

Fig 6.16 HeLa scratch injury treated with ULMFs. A 1.5 ± 0.05 mm scratch injury was inflicted on confluent HeLa before being subjected to 0.3 μT 6V A/C ULMF for 30 min. The HeLa were cultured for 48 h and the injury measured randomly at 15 sites, 90^{o} angle to the scratch per repeat (inset scale bar is 400 μm). Control HeLa migrated into the injury site significantly faster than ULMF treated HeLa. At 48 h the Control HeLa had significantly populated the scratch. Although the ULMF treated HeLa had migrated but the scratch was still apparent. The scratch was measured using 1X81 motorised inverted fluorescence microscope, Olympus Corporation.

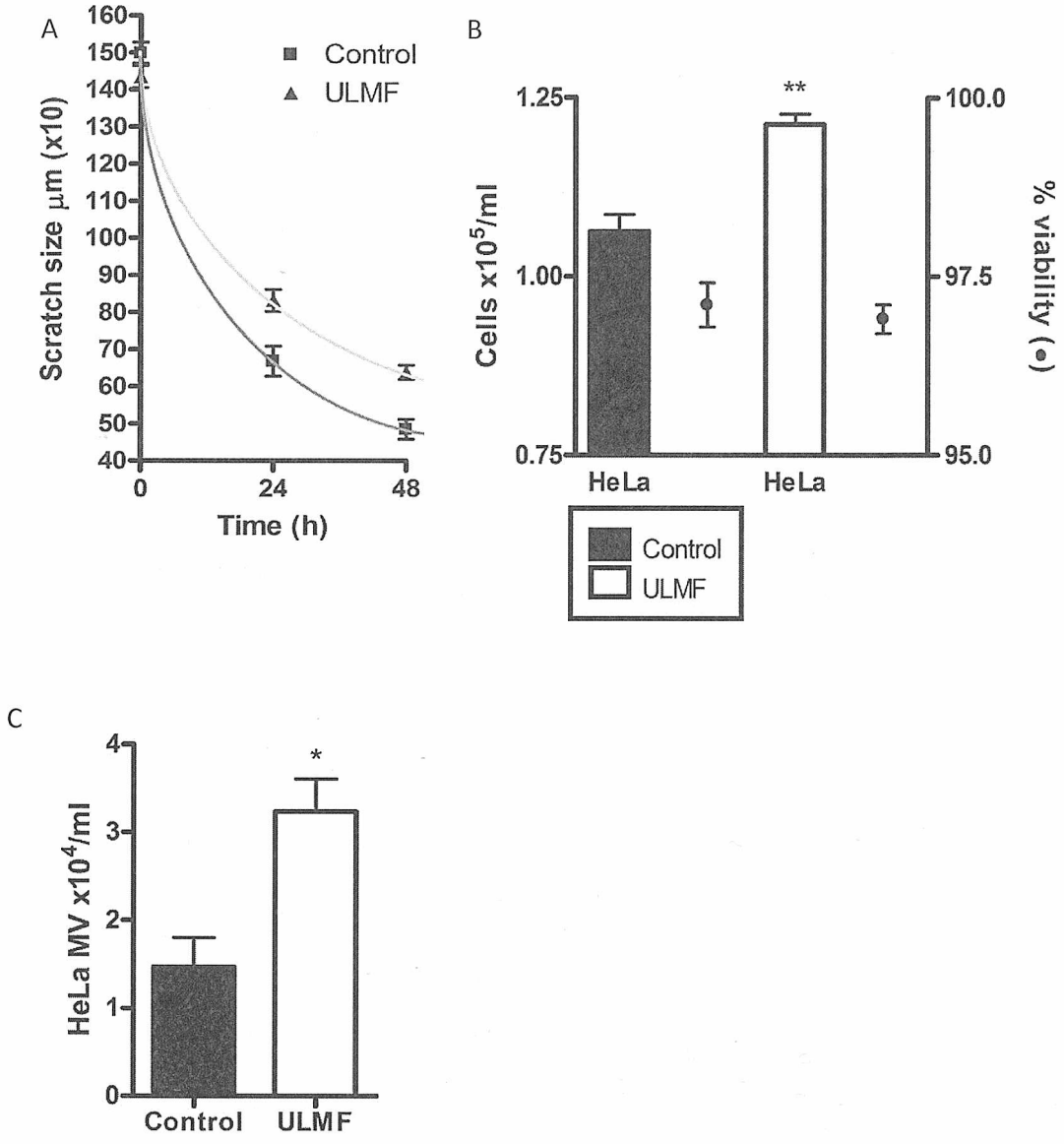

Fig 6.17 Migration and HeLa number are significantly affected by ULMFs. (**A**) The initial scratch injury was 1.5 ± 0.05 mm, control HeLa at 24 h was 0.7 ± 0.1 mm compared to 0.3 µT 6V A/C ULMF treated HeLa (0.85 ± 0.05 mm) and at 48 h the control HeLa were 0.48 ± 0.05 mm whereas the ULMF treated HeLa were 0.65 ± 0.05 mm. (**B**) At 48 h control HeLa were quantified at ~1.05 ± 0.2 x 10^5 /ml, 0.3 µT 6V A/C ULMF treated HeLa were significantly more (~1.22 ± 0.05 x10^5 /ml). Both control (black filled) and ULMF HeLa (white filled) maintained ≥96% viability. Cells were quantified using flow cytometry and ViaCount assay. (**C**) HeLa stimulated with ULMFs released (~1.5 x 10^4 /ml) significantly more MVs than un-stimulated HeLa (~3 x 10^4 /ml). The supernatant was collected directly after ULMF stimulation for 30 min.

6.18 Discussion

Ultra Low-frequency Magnetic Fields 0.3 μT 6V A/C 10 Hz (ULMFs) have an immediate effect on cells (Pillar, 2012), causing a recoverable, significant decrease in viability or related cellular responses for the duration of the magnetic stimuli (Fig 6.1) (Seyyedi *et al*, 2010). However prolonged stimulation leads to more dramatic decreases in irreversible viability (Fig 6.3) (Seyyedi *et al*, 2010). The viability was assessed by using a membrane impermeable dye (ViaCount and PI) that typically enters the cytoplasm via membrane pores, this being an accepted model for assessing cell viability. ULMFs cause the formation of membrane pores allowing the transit of ViaCount, PI, calcium (Simko and Mattsson, 2004) and chemotherapeutic drugs (Fig 6.1, 6.5A, 6.8, 6.11 and 6.13). Although ULMFs cause stretch activated calcium ion channels to open (Cho *et al*, 1999), allowing calcium influx, when the stretch activated calcium ion channels were blocked with $GdCl_3$ (Cho *et al*, 1999) calcium influx occurred through ULMF stimulated membrane pores (Fig 6.1 and 6.6) that had non-uniform size and symmetry (Liburdy *et al*, 1986; Deng *et al*, 2005) through ULMF/lipid interactions (Liburdy *et al*, 1986).

Extracellular calcium influx was the main cause for sMV release within ULMFs, releasing excess and cellular stores of Ca^{2+} (Deng *et al*, 2005), although calcium stored within organelles also contributed to total free cytoplasmic calcium (Jai *et al*, 2011; McKeown *et al*, 2012). When extracellular calcium was quenched with EDTA, sMVs were released at a significantly lower levels but higher than would have been expected through cMV release (Fig 6.6). Although sub-cellular organelle pores were stimulated with ULMF (Lui *et al*, 2012), in particular the mitochondria (Tenorio *et al*, 2012), releasing calcium, they may release other toxic substances such as peroxide, ROS (Simko and Mattsson, 2004), Cyt 450 and so on (Parihar *et al*, 2012) leading to changes

in cell viability. sMVs would export these toxins to prevent subsequent apoptosis (Jorfi *et al*, 2010), prolonged ULMF treatment would ensure their continued supply to the cytoplasm, well beyond the cell's ability to produce and release sMVs leading to irreversible apoptosis (Liu *et al*, 2012). Ca^{2+} influx acts as a second messenger stimulating many potential cellular responses (Pilla *et al*, 2011) before Ca^{2+} can be exported (as ULMF prevents effective organelle sequestering). Furthermore, organelles may lose their ultrastructure and function (Tenorio *et al*, 2012).

ULMF induced membrane pores were plugged rapidly (100 ms) by lysosomes expressing LAMP-1 upon fusion with plasma membrane (Fig 6.9) in response to membrane damage and localised increases in cytoplasmic Ca^{2+} concentration (Bergsbaken *et al*, 2011; Han *et al*, 2012). However, over a 30 min duration the cells exhaust their supply of lysosomes and membrane pores remain for longer allowing the increased influx of dyes and calcium down a concentration gradient (Fig 6.5), that when removed from the ULMF are retained within the membrane (Fig 6.8B). The increased calcium, trapped within the membrane once ULMF stimuli was removed causing the release of sMVs through the usual pathways (Fig 6.4 and 6.6).

Although all of the chemotherapeutic drugs studied are membrane permeable (Leonce and Cudennec, 1990), it was surmised that induction of membrane pores could lead to increased potential for lethal dose of the drug by uptake through ULMF membrane pores (Fig 6,13) using H_2O_2 as a model (Fig 6.11), as the plasma membrane offered some impedance to membrane permeable drugs (Leonce and Cudennec, 1990). Indeed the data for ULMF stimulated cells loaded with chemotherapeutic drugs was surprising.

Docetaxel and etoposide lead to exaggerated proliferation (Fig 10.10), however methotrexate lead to significant cell death, so much so that $1/10^{th}$ therapeutic dose lead to similar results as the non ULMF cells (Fig 6.13). ULMFs stimulate sMV release by causing plasma membrane pores in cell populations, thereby allowing Ca^{2+} influx, and so initiating MV biogenesis. EGTA chelation of Ca^{2+} lead to reduced MV release. However, as ULMFs stimulate pores throughout the cells organelles (Fig 6.3B and 6.8C) free calcium is able to leak into the cytoplasm so stimulating sMV biogenesis (Fig 6.6A) and un-quantified stimulatory roles (Pilla *et al*, 2011).

$GdCl_3$ was used to examine the role of stretch activated Ca^{2+} channels during ULMF stimulation of sMV release. Its cytotoxicity (Fig 10.11) increased eMV (extracellular microvesicle) release (Fig 6.6A) but not necessarily sMV release (Fig 6.6B). However, it may be that $GdCl_3$ more readily induced apoptosis (Fig 10.11) and in conjunction with Ca^{2+} influx this may contribute to sMV biogenesis.

THP-1 and PC12 were used as models for non-adherent and solid mass cancers respectively. H_2O_2 caused significant decrease in cell viability and was enhanced when used in conjunction with ULMF (Fig 6.11). It was hypothesised that anti-cancer drugs' apoptotic potential would be enhanced when used in conjunction with ULMFs (Liburdy *et al*, 1986; Pillar, 2012), and this was indeed found to be the case (Fig 6.13). Using the same concentration of methotrexate but stimulating with ULMFs there was a ~25% decrease in viability of THP-1 promonocytes (Acute monocytic leukaemia) and ~18% decrease in the viability of PC12. However the dose of methotrexate was reduced 90% (1μM) when stimulated with ULMF and yielded statistically similar results to un-

stimulated cells given 10 μM of the drug. Furthermore, PC12 showed an increased sensitivity to methotrexate at lower doses (0.1 μM) when used in conjunction with ULMF. This may be due to the release of higher doses of methotrexate in sMVs, as the cell circumvents apoptosis (Fig 6.13B).

The exciting potential for this therapy is obvious, namely ULMFs can potentially be targeted to a cell cluster or tissue in conjunction with significantly smaller doses of methotrexate drug, therefore minimising the drugs side effects while its delivery into cancer cells is enhanced. A repeated regime of methotrexate treatment in conjunction with directional ULMFs could result in a greater degree of targeted cell death and a better prognosis for the patient.

ULMFs significantly enhance the proliferative potential of the cell lines studied (Fig 6.12 and 6.17B) (Simko and Mattsson, 2004; Liu *et al*, 2012; Zhang *et al*, 2012b). As was earlier shown in this chapter that ULMF creates pores in the cell's membranes, including the plasma membrane. The increased proliferation is interesting in view of a similar observation due to another surface pore, this time due to sublytic complement deposition (Ansa-Addo *et al*, 2010). Indeed, low frequency pulsed magnetic fields caused permanent change in body tissues for prolonged exposure (Li *et al*, 2012). HeLa were selected for scratch injury studies for their relative ease of culturing and relative speed of cell division. Surprisingly scratches stimulated with ULMFs for 30 min did not 'heal' as quickly as the un-stimulated HeLa (Fig 6.16 and 6.17A). Analysis confirmed that the ULMF stimulated cells ~15% larger population but the cells had not migrated into the scratch, but rather grew much more densely, where as un-stimulated cells

migrated relatively quickly but didn't proliferate to such an extent (Fig 6.17). The mechanism for migration retardation was not eluded, however A/C ULMFs have been reported to change cell migration velocity (Aly *et al*, 2008) by damage of cell polarisation (Deng *et al*, 2005). It can be speculated that the process of sMV release causes increased cellular proliferation, however for cells to migrate as they move by pseudopodia (Brahmbhatt and Klemke, 2003; Avraamides *et al*, 2007) extending from the anterior of the cell and they vesiculate (internally or externally) from the posterior of the polar cell (Shen *et al*, 2011). ULMFs cause indiscriminate membrane pores from which sMV biogenesis (incorporating lipid rafts [Fig 5.9A]) occurs and possibly temporarily hinder the cells ability to migrate by disruption of their lipid rafts (Gomez-Moulton *et al*, 2001; Gomez-Moulton *et al*, 2004; Kindzelskii *et al*, 2004) or by exporting the lipid rafts on sMVs (Fig 5.9A and 6.17C). Furthermore, sMVs generated by ULMFs may export receptors necessary for the cells to identify missing or damaged neighbours (Kindzelskii *et al*, 2004; Shen *et al*, 2011) and the transient increase in intracellular calcium may lead to un-observed cellular responses (Pilla *et al*, 2011). The significantly reduced migration would indicate a ULMF induced biochemical constraint and may be an important tool for disrupting metastatic cancer *in vivo*.

Other groups have however published conflicting results, that magnetic therapy can increase wound healing through migration as well as proliferation using 1GHz ULMFs on fibroblasts (Sunkari *et al*, 2011). Higher levels of ULMFs slow proliferation but increased differentiation of osteoblasts (Zhou *et al*, 2011). DNA damage was not assessed although nuclear pore formation was observed by PI binding to DNA (Fig 6.8) (Blank and Goodman, 2011). DNA analysis could have been performed by PCR.

It is reasonable to assume that studies into the effects of ultra low frequency magnetic fields report conflicting results as the potential biological effects will vary between cell types and the strength, density, amplitude and duration of the treatment (Patruno *et al*, 2011). However, the use of electromotive weak oscillating fields generated transient membrane pores allowing uncontrolled calcium influx that lead to sMV release and possibly other calcium mediated cellular responses. The membrane pores allowed the increased influx of anticancer drugs, leading to smaller doses of drug causing a similar effect to a therapeutic dose. Finally, ULMFs cause increased cellular proliferation but slowed migration of cells into a wound, possibly by disruption of lipid rafts or another undetermined mechanism.

7. Discussion

Extracellular microvesicles (eMVs) of all types have been implicated with many physiological conditions ranging from cellular communication (Biancone *et al*, 2012), viral (Gan and Gould, 2011; Inal *et al*, 2012; Wurdinger *et al*, 2012) and parasite protection (Cestari *et al*, 2012), stress responses (Jorfi *et al*, 2010; Lo Cicero *et al*, 2011), tissue remodelling (Biancone *et al*, 2012) and tumour protection (Baj-Krzyworzeka *et al*, 2010). eMV research is mainly dominated by exosome studies, although there is a growing interest within the scientific community towards MV research to fully explain confounding data and unexplained microvesicle mediated responses. Characterisation of MVs was crucial in order to understand their biogenesis and their roles within an organism.

The importance of contrasting eMV types underpins this research and this thesis employed Guava Millipore flow cytometry capable of identifying vesicles as small as 0.7 μm, NanoSight particle tracking, qNano, Dynamic light scattering and Transmission electron microscopy to confirm and consolidate MV subtype characterisation.

As with many labs, MVs were initially treated as a single population and it was assumed that stimulating MV release would allow large numbers of them to be collected rapidly and be identical to constitutively released MVs, however FACs plots and annexin V labelling distinguished two distinct MV populations across all cell types studies depending upon their biogenesis. Indeed, cMVs and sMVs have been studied in detail and exhibit markedly different physical and biochemical properties.

Initially microvesicles were isolated using a standard protocol (Antwi-Baffour *et al*, 2010) that was adapted to allow the purest population of microvesicles to be collected and eliminate exosomes as a contaminating vesicle (Grant et al, 2011). The addition of a sonicating step was to break up exosome clumps that approximated the mass of MVs and could be pelleted with them during centrifugation. The sonicating step resulted in dramatically purer MV isolates (Fig 4.11).

Isolation of eMVs from differing media produces three distinct eMV subtypes, exosomes, constitutively released MVs (cMVs) and stimulated MVs (sMVs) (Muller, 2012). Exosomes are small vesicles whose detectible range ~0.4 – 1 μm (Fig 4.12, 4.14 and 4.19) and highly express CD63 but lowly express PS and they have distinctive physical morphology (Fig 4.14) (Gan and Gould, 2011). cMVs are small extracellular vesicles ~1.0 – 3 μm (Fig 4.14, 4.15) that accumulate in culture medium at a steady rate as a result of normal cellular functioning (Fig 4.5) and express ~85% PS (Fig 5.5B). cMVs are distinct from exosomes (Muralidharan-Chari *et al*, 2010; Muller, 2012) (Fig 5.5B) expressing a variety of different biomarkers such as PS (Angelot *et al*, 2009; Kushlich *et al*, 2010; Muller, 2012) (Fig 5.5, 5.6 and 5.9). sMVs are stimulated to be released, they accumulate rapidly and at high quantities in culture media over 30 min (Fig 4.5, 4.7 and 4.11A), they are larger than cMVs and exosomes, ~1.0 to 10+ μm and express ~90% PS (Fig 5.5B). sMVs, cMVs and exosomes have characteristically different sizes with distinct physical morphologies (Fig 4.12 and 4.14), biochemistries (Heijnen *et al*, 1999; Akoi *et al*, 2007) and pathways for cellular release (Muralidharan-Chari *et al*, 2010; Iglesias *et al*, 2012).

To ensure MV population purity differential centrifugation was used to remove cells, then debris and then sonicated the media to disaggregate exosomes before ultracentrifugation to pellet MVs. Concern over shearing forces within the media during ultracentrifugation lead to investigation of different centrifugation times to quantify the amount and quality of pelleted MVs. The final protocol produced high purity MVs with little observable population depletion (Grant *et al*, 2011).

MV isolation techniques were assessed for their effectiveness; a range of centrifugation speeds were selected and MVs stimulated from THP-1 and isolated identically until the final centrifugation step (Fig 4.17 and 4.18). MVs were isolated at different published (Heijnen *et al*, 1999; Akoi *et al*, 2007; Grant *et al*, 2011; Iglesias *et al*, 2012) centrifugation speeds however the quantities increased significantly at 25,000 *g* for 90 min (Fig 4.18), furthermore as the centrifugation speed were increased, the more smaller sized MVs were isolated (Fig 4.17) (Grant *et al*, 2011), eliminating shearing forces at a possible MV degrading step.

Analysis of eMVs constitutively released over 24 h reveals that both exosomes and cMVs accumulate in the culture medium (Muller, 2012), however significantly more cMVs are present then exosomes. Published data suggests differently, although this thesis shows a distinct co-population of MVs and a discrete exosome population (Fig 4.11C and 4.19A) it is likely that the exosomes are absorbed by the cells rapidly and cMVs take longer to interact with the cells.

The technique employed in this thesis varies to some extent to published data, where some groups isolate MVs antibody affinity to remove MVs from media (Chen *et al*, 2010), some use filtration techniques through porous nitrocellulose membranes ~0.1 - 0.22 μm (Gan and Gould, 2011) and some used differential ultracentrifugation (Chung *et al*, 2007; Grant *et al*, 2011; Iglesias *et al*, 2012) or combinations of these techniques (Gyorgy *et al*, 2011). Although there is no current consensus on isolation techniques (Chen *et al*, 2010), this thesis used a modified ultracentrifugation technique due to financial constraints, furthermore the filtration techniques investigated tended to produce submicron particles of nitrocellulose when freeing MVs attached to the membrane. However great attention was paid to detail and a detailed characterisation of MVs ensured purity of the samples collected (Fig 4.11, 4.12, 4.13, 4.14 and 4.18).

Cells cultured in different media release different types of eMVs, exhibiting distinctive FACs morphologies (Fig 4.11), physical morphology (Fig 4.14) and are released in different numbers (Fig 4.11, 4.12 and 4.19). The TEM of sMVs (a) reveal them to be larger, approximately 600+ nm, less dense vesicles than (b) cMVs, that are smaller, sizes approximately 200 nm and electron dense. (c) exosomes have a biconcave morphology with sizes up to 100 nm (Koga *et al*, 2005; Akoi *et al*, 2007). The MV subtypes were released in different quantities, cMVs accumulated in media 24 h old number 1.5×10^4 /ml however sMVs number 2.5×10^6 /ml (Fig 4.11).

Depending upon their origin, MV subtypes exhibit distinctly different FACs morphologies, FSC-HLog and SSC-HLog (Fig 4.11) cMVs appear smaller and more granular with approximately 80% of the population ranging from 0.1 - 0.3 μM (Fig 4.11,

4.15 and 4.20) measured using dynamic light scattering and using FACs megamix beads (Fig 4.15, 4.16 and 4.17) however sMVs display a larger, more dispersed population size (Fig 4.13 and 4.15) with approximately 60% ranging from 0.3 - 0.5 μM (Fig 4.15 and 4.20) when measured as before.

Typical MV subtypes were weighed using NanoDrop microbalance 2 x 10^3 MVs were weighed, the highly consistent results demonstrate that cMVs, although much smaller, weigh (10 ng/μl for 2 x 10^3 cMVs) significantly more than sMVs (3.8 ng/μl for 2 x 10^3 sMVs). When MV subtype density was measured by quartz crystal microbalance, it was found the cMVs have a higher density than sMVs (Fig 4.21).

sMVs are released from the cell surface responding to stressing agents as a mechanism to circumvent apoptosis. Typically, most mammalian cells exist in a state of pseudoapoptosis as their environments, although well maintained are fragile and micro environments constrain cells, such as local changes in osmolarity or ion concentration and so forth (Mackenzie *et al*, 2005; Bevilacqua *et al*, 2010). Furthermore, cells are also subject to a host of potential stress triggers including pathogen related stresses (Brereton and Blander, 2011; Delabranche *et al*, 2012). These stresses, if left to accrue will ultimately result in apoptosis or in extreme cases necrosis (Janssen *et al*, 2009; Bevilacqua *et al*, 2010). Membrane pores, such as MACs, typically cause an uncontrolled rise in intracellular calcium that could lead to many types of metabolic damage. Calcium drives many biochemical reactions and instigate or act as second messengers for many intracellular signalling pathways (Rizzuto and Pozzan, 2006). However this calcium influx may be localised to a micro-environment adjacent to the membrane breach

rather than completely cytosolic and therefore recoverable (Rizzuto and Pozzan, 2006). Homeostatic mechanisms cause the formation of a membrane bleb containing damaged cell components, the excess intracellular calcium (Gutwein *et al*, 2005; Mackenzie *et al*, 2005; Delabranche *et al*, 2012) (Fig 4.5) and the MAC that will 'pinch off' to form sMVs (Moskovich and Fishelson, 2007), expelling the breach that would allow continuing damage (Moskovich and Fishelson, 2007). Indeed optimal media calcium concentrations for sMV production are 1 – 2 mM (Fig 4.4) in conjunction with membrane breaches, 4+ mM causes significant irreversible cell damage that leads to apoptosis (Vindis *et al*, 2005). The degree of plasma membrane damage directly influences the number of sMVs released, Fig 4.3 shows that increasing THP-1 cell number in an absolute volume of RPMI supplemented with 10% NHS and 2 mM $CaCl_2$ decreases the sMV number. If one MAC caused the formation of one sMV, changing the cell number would not affect the number of sMV released, thus demonstrating that multiple MACs and therefore more than one membrane breach is required. The Q-sense QCM measures a significant change in cellular mass at 27 min typical of sMV release (Fig 4.7), measured at 2 sub-harmonics (shown). Not shown, the quartz crystal microbalance detected a decrease in media fluidity, attributed to increases of membrane blebbing on THP-1 (Mackenzie *et al*, 2005) and at 27 min MV release.

Once released, sMVs export significant amounts of calcium, so that immediate re-stimulation is not possible and a 30 min refractory begins (Fig 4.5, 4.6 and 4.7), whereby the cell recovers sufficient intracellular calcium concentration to enable subsequent microvesiculation (Fig 4.5 and 4.6). Calcium induced refractory periods are a typical feature of many cellular vesicle pathways (Rizzuto and Pozzan, 2006). The sMVs contain low levels of calcium (Fig 4.5), that is deliverable to cells thus temporarily

increasing intracellular calcium of the recipient cell (Fig 5.1), whose typical resting Ca^{2+} potential is ~100 nM (Rizzuto and Pozzan, 2006). Although sMVs have low calcium levels ~20% that of cMVs, they are released in large numbers, all capable of delivering a small calcium cargo (Muralidharan-Chari *et al*, 2010).

cMVs are released as communicative vectors and are produced in a different manner to sMVs. They are not produced as a response to observable or immediate stress agents and do not respond to extracellular calcium concentration per-se (Fig 4.6). cMVs are released at a low constant rate (Fig 4.6) accumulating in the culture media. No significant differences in numbers released were observed over the course of these experiments. cMVs contain significantly more calcium than sMVs (Fig 4.5), It was found that calcium was deliverable to recipient cells. Indeed, MV subtypes deliver different amounts of free calcium derived from the parent cells. cMVs (2×10^3 /ml) were delivered to THP-1 (1×10^5 /ml) significantly increasing intercellular calcium, however 5x sMVs were delivered (1×10^4 /ml) to THP-1 to achieve a significant level of calcium (approximately equal to cMVs). This suggests that the smaller cMV carries 5x the free calcium that sMVs carry, however sMVs are released in significantly larger amounts. Furthermore, sMVs are produced in response to free calcium influx causing intercellular damage, and are crucial for calcium homeostasis.

The initial observable role of MV subtypes is the removal or export of stress agents, receptors and cellular components (Fig 4.5, 4.8, 5.3, 5.5, 5.6, 5.7, 5.9 and 6.10) (Chen *et al*, 2010; Iglesias *et al*, 2012). The nature and relative amounts of this export and

relative amounts is due to MV subtype differences in biogenesis (Fig 4.11) (Delabranche *et al*, 2012; Muller, 2012).

Receptor transfer between cell types allows the transient expression of a transplanted protein/receptor to a recipient cell via MVs expressing the receptor derived from a parent cell (Fig 5.9) (Inal *et al*, 2012; Muller, 2012). Although the exact nature of this interaction was not elucidated (Gan and Gould, 2011), it is likely that MVs fuse with the membrane of the recipient cell, allowing protein and lipid mixing that is expressible on the outer leaflet (Cestari et al, 2012) although this was not observed the presence of a working DAF receptor between HeLa (DAF^+) and CHO-K1 (DAF^-), offering CHO-K1 protection against complement mediated lysis, increasing cell population survival ~5% confirms membrane fusion and lipid/receptor mixing.

sMVs also transmit apoptotic signals between cells (Jorfi *et al*, 2010; Lo Cicero *et al*, 2011) or other protein/lipid/carbohydrate agents (Chen *et al*, 2010; Batista *et al*, 2011; Iglesias *et al*, 2012). miRNA derived from cells undergoing stress is also deliverable to cells (Camussi et al, 2011), MV subtypes express significantly different levels of nucleic acids (Fig 5.11 and 5.14) although the exact nature and sequence of the nucleic acids remain undertermined it is certain that they exert a desirable effect on the recipient cell (Chen *et al*, 2010; Camussi *et al* 2011; Iglesias *et al*, 2012). Though it is also likely that parasites such as virus use microvesicles and exosomes to envelope themselves (even non-enveloped virus) and may also be able to infect different cell types (Gan and Gould, 2011).

cMV biogenesis contain miRNA, high calcium and so forth, and released as a communicative vector, although they contain high ROS, this may be as the cell lines studies are cancer and this may be a method of transmitting pathenogenicity (Delabranche *et al*, 2012) (Fig 5.15).

Observable change is more relevant in biological terms for the releasing cells (Fig 4.5, 4.6, 5.2, 5.5, 5.6, 5.7, 5.9 and 5.10) as there are significant changes in receptor, calcium, proteins, carbohydrates and so forth (Batista *et al*, 2011; Iglesias *et al*, 2012). However, recipient cells respond to MVs in a dose dependent manor (Lo Cicero *et al*, 2011; Iglesias *et al*, 2012) (Fig 4.9, 4.10 and 5.4).

sMVs produced using MACs release the stress agent (MAC) on the MVs (Fig 4.11 and 4.13), they are released in larger numbers that MVs produced by other stressing agents such as ULMFs and fMLP. It is possible to conjecture that the nature and severity of the stress agent varies the significance of the sMV release.

FT-IR was used to differentiate broad differences in cancer cell types (Lee-Montiel *et al*, 2011), in particular, metastatic and non metastatic Breast (MCF-7 and MBA MB 231) and prostate (PC3 and PNT2) to identify primarily whether differences in cell profile generates unique wave forms (Argov *et al*, 2002) (Fig 5.13)The fingerprint region (Nara *et al*, 2006; Buttner et al, 2009; Ceylan *et al*, 2012) was used to identify the presence of DNA, protein and lipid (Fig 5.13 and 5.14) (Buttner *et al*, 2009). Unfortunately there was not observable commonality with metastatic and non

metastatic cell types of different types, however, there were similarities between cells of the same type but different metastatic potentials.

Further work revealed distinguishable similarities of MV subtypes to their cell of origin (Batista *et al*, 2011; Muller, 2012). This work initially offered an exciting avenue for diagnostics, however this particular technique was effective at identifying cells and MVs of the same type, when mixed the profile generated would be additive or mixed and without reference to the original types in the mix, no identification can be achieved.

THP-1 incubated with α-tocopherol (12+ ng/L) produced cMVs that were significantly smaller and less auto-fluorescent that the control (Fig 5.15 and 5.16). Free reactive oxygen species (ROS) were cleaned up by an excess of α-tocopherol leading to less protein-protein cross linking (de Oliveira *et al*, 2012; Klychnikova *et al*, 2012; Salinthone *et al*, 2012) and oxidisation of fats that would cause the formation of the auto-fluorescent lipofuscin (Yang and Honaramooz, 2012). Indeed, the larger cMVs may exhibit properties closely resembling apoptotic bodies, containing ROS. The formation of increased MV release ~50 ng/L α-tocopherol may be due to a stressing effect that excess α-tocopherol has on cells.

ULMFs stimulate sMV release, although significantly fewer than other stimulating agents (Fig 6.4). ULMFs generate the formation of transcellular membrane pores allowing free $Ca^{2+}{}_i$ to leak from organelles, such as the rough endoplasmic reticulum, contributing to pseudoapoptotic events and increasing the likelihood of sMV formation, even in the absence of extracellular Ca^{2+} (Nakamichi *et al*, 2009) (Fig 6.6). Prolonged

cellular exposure to ULMFs lead to cells entering late apoptosis (Narita *et al*, 1997) (Fig 6.3) as they are unable to constantly release sMVs (sMV release requires a 30 min refractory period [Fig 4.5, 4.6 and 4.7]) and cytotoxic agents accrue in the cell (Rajendra *et al*, 2004), unsanctioned nuclear membrane pores appear (Fig 6.8) and mitochondria leak apoptosome forming agents (Liu *et al*, 2012).

A 30 min stimulation of the cell lines studied with ULMFs cause proliferation (Iwasaka *et al*, 2004; Nakamichi *et al*, 2009). The proliferation of cells may be due to the release of MVs from a cell and therefore the removal of an inhibitory protein rather than the stimulatory event. Indeed, sublytic levels of MAC cause sMV release and cellular proliferation (Fig 6.12, 6.17B and 6.17C).

Stimulated membrane pores allow the unimpeded influx of anti-cancer drugs (and other cytotoxic agents) along a concentration gradient that accrues a lethal dose within the cell at ~1/10 the 'therapeutic' level (Fig 6.13). The implications of this type of therapy is immediately obvious, however *in vivo* trials are required. This effect was observed with methotrexate, however docetaxel was also a promising candidate (Fig 10.10).

Scratch injury's stimulated with ULMFs lead to an increase in HeLa proliferation (as previously described) but significantly less migration into the scratch than the control (Fig 6.16 and 6.17A) It is likely that the release of sMVs and ULMFs affect the distribution and disrupt the formation of lipid rafts that lead to the development of

uropods, or an unobserved biochemical side effect that lead to the inhibition of the cells ability to migrate.

8. Conclusion

The work presented in this thesis supports the hypothesis of the existence of two distinct MV subtypes offering unique properties depending upon their biogenesis. Furthermore, these subtypes resemble their parent cells and can confer parental cell properties, albeit transiently, to recipient cells. However, it can be supposed that MVs have a greater biological significance to the cells releasing the MVs than the recipient cells that may need more than one MV to fuse in order to achieve a desired response.

ULMFs cause increases in cellular proliferation and sMV release by calcium induction and cause irreversible damage when exposed for extended durations. ULMFs also inhibit a polar cells ability to migrate through some undetermined mechanism, it may be speculated that disruption of lipid rafts may prevent uropod formation and subsequently prevent the cells moving.

ULMFs generate membrane pores transiently for the duration of the cells exposure, once removed the cells seal their membrane breaches. During ULMF pore generation anti cancer drugs enter the cells to a greater extent and is trapped for longer once removed from the field, leading to a reduction of the therapeutic dose to ~1/10, however, further research is recommended.

9. Bibliography

Agouni, A., Mostefai, H. A., Porro, C., Carusio, N., Favre, J., Richard, V., Henrion, D. and Martinez, M. C., (2007) Sonic hedgehog carried by microparticles corrects endothelial injury through nitric oxide release, FASEB, Vol. **21**, pp 2735-2741

Alder, E. M. (2010) Sending a Package Through the Blood, Science, Vol. 3, pp ec220

Aleo, E., Henderson, C. J., Fontanini, A., Solazzo, B. and Brancolini, C., (2006) Identification of New Compounds That Trigger Apoptosome-Independent Caspase Activation and Apoptosis, Cancer Res, Vol. **66**, pp 9235-9244

Aliotta, J. M., Pereria, M., Amaral, A., Dooner, M., Goldberg, L. and Quesenberry, P. J., (2011) Microvesicle-mediated transfer of genetic phenotype from lung to marrow cells, Tumor Biology, Vol. **29**, e21092

Aly, A. A., Cheema, M. I., Tambawala, M., Laterza, R., Zhou, E., Rathnabharathi, K. and Barnes, F. S., (2008) Effects of 900-MHz radio frequencies on the chemotaxis of human neutrophils in vitro, IEEE Trans Biomed Eng., Vol. **55**, pp 795-797

Ami, D., Natalello, A. and Doglia, S. M., (2012) Fourier transform infrared microspectroscopy of complex biological systems: from intact cells to whole organisms, Methods Mol Biol., Vol. **895**, pp 85-100

Anand, P. K., Anand, E., Bleck, C. K. E., Anes, E and Griffiths, G., (2010) Exosomal Hsp70 induces a Pro-Inflammatory Response to Foreigh Particle Including Mycobacteria, PLoS ONE, Vol. **5**, e10136

Andreola, G., Rivoltini, L., Castelli, C., Huber, V., Perego, P., Deho, P., Squarcina, P., Accornero, P., Molinari, A., Arancia, G., Gentile, M., Parmiani, G. and Fais, S. (2002) Induction of Lymphocyte Apoptosis by Tumor Cell Secretion of FasL-bearing Microvesicles, J, Exp. Med., Vol. **195**, pp1303-1316

Angelot, F., Seilles, E., Biichle, S., Berda, Y., Gaugler, B., Plumas, J., Chaperot, L., Dignat-George, F., Tiberghien, P., Saas, P and Garnache-Ottou, G. (2009) 'Endothelial cell-derived microparticles induce plasmacytoid dendritic cell maturation: potential implications in inflammatory diseases', Haematologica, Vol. **94**, pp 1502-1512.

Ansa-Addo, E. A., dos Santos Cestari, I., Pathak, P., Ramirez, M. I. and Inal, J. M., (2009) Monocytic THP-1 cells stimulated by normal human serum (NHS) release cytokine-bearing plasma membrane-derived vesicles (PMVs), and can be inhibited by methyl-beta-cyclodextrin, alcpeptin and Pho-kinase inhibitor, Y-27632, J. Immunol. Vol. **182**, 98.27

Ansa-Addo, E., Lange, S., Stratton, D., Antwi-Baffour, S., Cestari, I., Ramirez, M. I., McCrossan, M. and Inal, J., (2010) Human Plasma Membrane-Derived Vesicles Halt Proliferation and Induce Differentiation of THP-1 Acute Monocytic Leukemia Cells, J. Immunol. Vol. **185**, pp 5236-5246

Antwi-Baffour, S., Kholia, S., Aryee, Y. K. D., Ansa-Addo, E. A., Stratton, D., Lange, S and Inal, J. M., (2010) Human plasma membrane-derived vesicles inhibit the phagocytosis of apoptotic cells – Possible role in SLE, BBRC, Vol. **396**, pp 278-283

Aoki, N., Jin-no, S., Nakagawa, Y., Asai, N., Arakawa, E., Tamura, N., Tamura, T. And Matsuda, T. (2007) Identification and Characterization of Microvesicles Secreted by 3T3-L1 Adipocytes: Redox- and Hormone- Dependent Induction of Milk Fat Globule-Epidermal Growth Factor 8- Associated Microvesicles, Endocrinology, Vol. **184**, No. 8, pp 3850-3862

Argov, S., Ramesh, J., Salman, A., Sinelnikov, I., Goldstein, J., Guterman, H. and Mordechai, S., (2002) Diagnostic potential of Fourier-transform infrared microspectroscopy and advanced computational methods in colon cancer patients, Journal of Biomedical Optics, Vol. **7**, pp 248-254

Avraamides, C., Bromberg, M. E., Gaughan, J. P., Thomas, S. M., Tsygenkov, A. Y. and Panetti, T. S., (2007) Hic-5 promotes endothelial cell migration to lysophosphatic acid, Am J Physiol Heart Circ Physiol, Vol. **293**, pp 193-203

Baj-Krzyworzeka, M., Baran, J., Weglarczyk, K., Szatanek, R., Szaflarska, A., Siedlar, M. and Zembala, M., (2010) Tumour-Derived Microvesicles (TMV) Mimic the Effect of Tumour Cells on Monocyte Subpopulations, Anticancer Res., Vol. **30**, pp 3515-3519

Bassan, P., Sachdeva, A., Kohler, A., Hughes, C., Henderson, A., Boyle, J., Shanks, J. H., Brown, M., Clarke, N. W. and Gardner, P., (2012) FTIR microscopy of biological cells and tissue: data analysis using resonant Mie scattering (RMieS) EMSC algorithm, Analyst, Vol. **137**, pp 1370-1377

Bastos-Amador, P., Perez-Cabezas, B., Inzquierdo-Useros, N., Puertas, M. C., Martinez-Picado, J., Pujol-Borrell, R., Naranjo-Gomez, M. and Borras, F. E., (2012) Capture of cell-derived microvesicles (exosomes and apoptotic bodies) by plasmacytoid dendritic cells, Journal of Leukocyte Biology, Vol. **91**, pp 751-758

Batista, B. S., Eng, W. S., Pilobello, K. T., Hendricks-Munoz, K. D. and Mahal, L. K., (2011) Identification of a conserved glycan signature for microvesicles, J Proteome Res., Vol. **10**, pp 4624-4633

Bauman, S. J. And Kuehn, M. J. (2006), 'Purification of outer membrane vesicles from *Pseudomonas aeruginosa* and their activation of an IL-8 response', Microbes and Infection, Vol. **8**, pp 2400-2408

Benes, E., (1984) Improved quartz crystal microbalance technique, J. Appl. Phys, Vol. **56**, pp 608-626

Benjaminin, E., Coico, R. and Sunshine, G., (2000) 'Cytokines', *Immunology: A short course* 4th edition, Wiley-Liss, Chichester, pp 229-252

Bergsbaken, T., Fink, S. L., den Hartigh, A. B., Loomis, W. P. and Cookson, B. T., (2011) Coordinated Host Responses during Pyroptosis: Inflammatory Cytokine Maturation, J. Immunol., Vol. **187**, pp 2748-2754

Bevilacqua, E., Wang, X., Majumber, M., Gaccioli, F., Yuan, C. L., Wang, C., Zhu, X., Jordan, L. E., Scheuner, D., Kaufman, R. J., Koromilas, A. E., Snider, M. D., Holcik, M and Hatzoglou, M., (2010) eIF2α Phosphorylation Tips tha Balance to Apoptosis during Osmotic Stress, Journal of Biological Chemistry, Vol. **285**, pp 17098-17111

Bianco, F., Pravettoni, E., Colombo, A., Schenk, U., Moller, T., Matteoli, M. and Verderio, C., (2005) Astrocyte-Derived ATP Induces Vesicle Shedding and IL-1{beta} Release from Microglia, Journal of Immunology, Vol. **174**, pp 7268-7277

Biancone, L., Bruno, S., Deregibus, M.C., Tetta, C. and Camussi, G., (2012) Therapeutic potential of mesenchymal stem cell-derived microvesicles, Nephrol. Dial. Transplant., Vol. **27**, pp 3037-3042

Biasi, F., Tessitore, L., Zanetti, D., Cutrin, J. C., Zingaro, B., Chiarpotto, E., Zarkovic, N., Serviddio, G. and Poli, G., (2002) Associated changes of lipid peroxidation and transforming growth factor β1 levels in human colon cancer during tumour progression, Cancer, Vol. **50**, pp 361-367

Bishop, A. L., Schild, S., Patimalla, B., Klein, B. and Camilli, A., (2010) Mucosal Immunization with Vibrio cholera Outer Membrane Vesicles Provides Maternal Protection Mediated by Antilipopolysaccharide Andibodues That Inhibit Bacterial Motility, Infect. Immun., Vol. **78**, pp 4402-4420

Blank, M. and Goodman, R., (2011) DNA is a fractal antenna in electromagnetic fields, Int J Radiat Biol., Vol. **87**, pp 409-415

Bomberger, J. M., MacEachran, D. P., Coutermarsh, B. A., Ye, S., O'Toole, G. A. and Stanton, B. A., (2009) Long-Distant Delivery of Bacterial Virulence Factors by Pseudomonas aeruginosa Outer Membrane Vesicles, PLoS Pathogens, Vol. **5**, No. 4, pp 1-13

Boulanger, C. M., Amabile, N., Guerin, A. P., Pannier, B., Leroyer, A. S., Mallat, Z., Nguyen, C., Tedgui, A and London, G. M., (2007), 'In Vivo Shear Stress Determines Circulating Levels of Endothelial Microparticles in End-Stage Renal Disease', Hypertension, Vol. **49**, pp 902-908

Brahmbhatt, A. A. and Klemke, R. L., (2003) ERK and PhoA Differentially Regulate Pseudopodia Growth and Retraction during Chemotaxis, JBC, Vol **278**, pp 13016-12025

Bratton, D, L., Fadok, V. A., Richter, D.A., Kailey, J. M., Guthrie, L. A and Henson, P. M., (1997) 'Appearance of Phosphotidylserine on Apoptotic Cells Requires Calcium-mediated Nonspecific Flip-Flop and Is Enhanced by Loss of the Aminophospholipid Translocase', Journal of Biological Chemistry, Vol. 272, No **42**, pp 26159-26165

Brereton, C. F and Blander, J. M., (2011) The unexpected link between infection-induced apoptosis and a TH12 immune response, JLB, Vol. **89**, pp 565-576

Brodsky, S. V., Malinowski, K., Golightly, M., Jesty, J and Goligorsky, M. S., (2002) 'Plasminogen Activator Inhibitor-1 Promotes Formation of Endothelial Microparticles With Procoagulant Potential', Circulation, Vol. **106**, pp 2372-2378.

Brooks, M. B., Catalfamo, J. L., Brown, H. A., Ivanova, P. And Lovaglio, J., (2002) Ahereditary bleeding disorder of dogs caused by a lack of platelet procoagulant activity, Blood, Vol. **99**, pp 2432-2441

Broom, R. J., Tang, P. A., Simmons, C., Bordeleau, Mulligan, A. M., O'Malley, F. P., Miller, N., Andrulis, I. L., Brenner, D. M. and Clemons, M. J., (2009) Changes in Estrogen Receptor, Progesterone Receptor and Her-2/neu Status with Time: Discordance Rates Betweem Primary and Metastatic Breast Cancer, Anticancer Research, Vol. **29**, pp 1557-1562

Brown, D. R. and Price, L. D., (2007) Characterization of *Salmonella* enteric serovar Typhimurium DT104 invasion in an epithelial cell line (IPEC J2) from porcine small intestine, Vet Microbiology, Vol. **120**, pp 328-333

Buttner, L., Guidolin, M., Murakami, L. S., Nomizo, A. and Bachmann, L., (2009) Fourier Transform Spectroscopy of Skin Cancer Cells and Tissues, Applied Spectroscopy Reviews, Vol. **44**, pp 438-455

Cain, R. J., Hayward, R. D. and Koronakis, V., (2004) Deciphering Interplay between Solmonella Invasion Effectors, PLoS Pathogens, Vol. **4**, pp 1-16

Cestari, I., Ansa-Addo, E., Deolindo, P., Inal, J. M. and Ramirez, M., (2012) *Trypanosoma cruzi* Immune Evasion Mediated by Host Cell-Derived Microvesicles, J. Immunol., Vol. **188**, pp 1942-1952

Ceylan, C., Severcan, F., Ozkul, A., Severcan, M., Bozoglu, F. and Taheri, N., (2012) Biophysical and microbiological study of high hydrostatic pressure inactivation of Bovine Viral Diarrheavirus type 1 on serum, Vet Microbiol., Vol. **154**, pp 266-271

Chang, J., Wasser, J. S., Cornelussen, R. N. M. and Knowlton, A. A., (2001) Activation of Heat-Shock Factor by Stretch- Activated Channels in Rat Hearts, Circulation, Vol. **104**, pp 209-214

Chaput, N., Flament, C., Viaud, S., Taieb, J., Roux, S., Spatz, A., Andre, F., LePecq, J., Boussac, M., Garin, J., Amigorena, S., Thery, C. and Zitvogel, L., (2006) Dendritic cell derived-exosomes: biology and clinical implementations, Journal of Leukocyte Biology, Vol. **80**, pp471-479

Chattopadhyay, P. K., Lai, J. and Wu, H. C., (1979) Incorporation of Phosphatidylglycerol into Murein Lipoprotein in Intact Cells of *Salmonella typhimurium* by Phospholipid Vesicle Fusion, Journal of Bacteriology, Vol. **137**, pp 309-312

Chen, C., Skog, J., Hsu, C., Lessard, R. T., Balaj, L., Wurdinger, T., Carter, B. S., Breakefield, X. O., Toner, M. and Irimia, D., (2010) Microfluidic isolation and transcriptome analysis of serum microvesicles, Lab Chip, Vol. **4**, pp 505-511

Chen, X., Xiong, W., Chen, X., Lu, C., Liu, F., Huang, S. and Li, H., (2011) Analysis of Microparticle Microrna Expression Profiles and Their Functional Roles in ALL Subtypes, Blood, Vol. **118**, Abstract 1488

Cheviet, S., Bezzi, P., Ivarsson, R., Renstrom, E., Vierti, D., Kasas, S., Catsicas, S. and Regazzi, R., (2006) Tomosyn-1 is involved in a post-docking even required from pancreatic β-cell exocytosis, Journal of Cell Science, Vol. **119**, pp 2921-2920

Chitcholtan, K., Hampton, M. B. and Keenan, J. I., (2008) Outer membrane vesicles enhance the carcinogenic potential of Helicobacter pylori, Carcinogenesis, Vol. **29**, No. 12, pp 2400-2405

Cho, M. R., Thatte, H. S., Silvia, M. T and Golan, D. E., (1999) Transmembrane calcium influx by ac electric fields, FASEB, Vol. **13**, pp 677-683

Chou, S., Hsu, W., Hwang, J. and Chen, C., (2002) Determination of α-Fetoprotein in Human Seru, by a Quartz Crystal Microbalance-based Immunosensor, Clinical Chemistry, Vol. **48**, pp 913-918

Chung, S., Bae, O., Lim, K., Noh, L., Jung, Y. and Chung, J., (2007) Lysophosphatidic Acid Induces Thrombogenic Activity Through Phosphatidylserine Exposure and Procoagulant Microvesicle Generation in Human Erythrocytes, Arteriosclerosis, Thrombosis and Vascular Biology, Vol. **27**, pp 414-412

D'Souza-Schorley, C. and Clancy, J. W., (2012) Tumor-derived microvesicles: shedding light on novel microenvironment modulators and prospective biomarkers, Genes and Development, Vol. **26**, pp 1287-1299

Dagneaux, C., Gousset, H., Shchyolkina, A. K., Ouali, M., Letellier, R., Liquier, J., Florentiev, V. L. and Taillandier, E., (1996) Parallel and antiparallel A*A-T intramolecular triple helices, Nucleic Acids Research, Vol. **24**, pp 4506-4512

de Gassart, A., Geminard, C., Fevier, B., Raposo, G. and Vidal, M., (2003) Lipid raft-associated protein sorting in exosomes, Blood, Vol. **102**, pp 4336-4344

de Oliveira, B. F., Veloso, C. A., Nogueira-Machado, J. A. and Martins Chavesm M., (2012) High Doses of In vitro Beta-carotene, Alpha-Tocopherol and Ascorbic Acid Induce Oxidative Stress and Secretion of IL-6 in Peripheral Blood Mononuclear Cells from Healthy Donors, Curr Aging Sci., Vol. **5**, pp 148-156

del Conde, I., Shrimpton, C. N., Thiagarajan, P. and Lo'pez, J. A., (2005) Tissue-factor-bearing microvesicles arise from lipid rafts and fuse with activated platelets to initiate coagulation, Blood, Vol. **106**, pp 1604-1611

Delabranche, X., Berger, A., Boisrame-Helms, J. and Meziani, F., (2012) Micropatricles and infectious disease, Med Mal Infect., Vol. 8, pp 335-343

Dell'Angelica, E. C., Mullins, C., Caplan, S. and Bonifacino, J. S., (2000) Lysosome-related organelles, FASEB, Vol. **14**, No. 10, pp 1265-1278

Deng, H., Wang, D., Peng, R., Wang, S., Chen, J., Zhang, S., Dong, B. and Wang, X., (2005) The electroporation effects of high power pulse microwave and electromagnetic pulse irradiation on the membranes of cardiomyocyte cells and the mechanism therein involved, Sheng Wu Yi Xue Gong Cheng Xue Za Zhi, Vol. **22**, pp 672-676

Deregibus, M. C., Cantaluppi, V., Calogero, R., Lo Iacono, M., Tetta, C., Biancone, L., Bruno, S., Bussolati, B. and Camussi, G., (2007) Endothelial progenitor cell-derived microvesicles activate an angiogenic program in endothelial cells by a horizontal transfer of mRNA, Blood, Vol. **110**, pp 2440-2448

Donnelly, E. T., McClure, N. and Lewis, S. E., (1999) The effect of ascorbate and alpha-tocopherol supplementation in vitro on DNA integrity and hydrogen peroxide-induced DNA damage in human spermatozoa, *Mutagenesis,* Vol. 14, pp 505-512

Dourdin, N., Bhatt, A. K., Dutt, P., Greer, P. A., Arthur, J. S. C., Elce, J. S. and Huttenlocher, A., (2001) 'Reduced Cell Migration and Disruption of the Actin Cytoskeleton in Calpain-deficient Embryonic Fibroblasts', The Journal of Biological Chemistry, Vol. **276**, No. 51, pp 48382-48388

Du, J., Shi, J., Sun, X., Wang, J., Zu, Y., Wu, J., Zhang, Y. and Weng, S., (2009) Fourier transform infrared spectroscopy of gallbladder carcinoma cell line, Hepatobiliary Pancreat Dis Int, Vol. 8, pp 75-78

DuBmann, H., Rehm, M., Kogel, D. and Prehn, J. H. M., (2003) Outer mitochondrial membrane permeabilization during apoptosis triggers caspase-independent mitochondrial and caspase-dependent plasma membrane potential depolarization: a single-cell analysis, Journal of Cell Science, Vol. **116**, pp 525-536

Duclos, S., Corsini, R. and Desjardins, M., (2003) Remodeling of endosomes during lysosomes biogenesis involves 'kiss and run' fusion events regulated by rab5, Journal of Cell Science, Vol. **116**, No. 5, pp 907-918

Emori, Y. and Saigo, K., (1994), 'Calpain Localization Changes in Coordination with Actin-related Cytoskeletal Changes during Early Embryonic Development of *DrosophiZu*', The Journal of Biological Chemistry, Vol. 269, No. 40, pp 25137-25142

Evens, A. M., Lecane, P., Magda, D., Prachand, S., Singhal, E., Nelson, J., Miller, R. A., Gartenhaus, R. B. and Gordon, L. I., (2005) Motexafin gadolinium generates reactive oxygen species and induces apoptosis in sensitive and highly resistant multiple myeloma cells, Vol. 23, pp 1265-1273

Fox, J. E. B, Austin, C. D., Boyles, J. K. and Steffen, P. K., (1990) Role of the Membrane Skeleton in Preventing the Shedding of Procoagulant-rich Microvesicles from the Platelet Plasma Membrane, Journal of Cell Biology, Vol. **111**, pp 483-493

Gan, X. and Gould, S. J., (2011) Identification of an inhibitory budding signal that blocks the release of HIV particles and exosome/microvesicle proteins, Mol. Biol. Cell., Vol. **22**, pp 817-830

Garver, W. S., Jelinek, D., Meaney, F. J., Flynn, J., Pettit, K. M., Shepherd, G., Heidenreich, R. A., Walsh Vockley, C. M., Castro, G. and Francis, G. A., (2010) The National Niemann-Pick Type C1 Disease Database: correlation of lipid profiles, mutations, and biochemical phenotypes, J. Lipid Res, Vol. **51**, pp 406-415

Gasser, O. and Schifferli, J. A., (2004) Activated polymorphonuclear neutrophils disseminate anti-inflammatory microparticles by ectocytosis, Blood, Vol. **104**, pp 2543-2548

Gazi, E., Gardner, P., Lockyer, N. P., Hart, C. A., Brown. M. D. and Clarke, N. W., (2007) Direct evidence of lipid translocation between adipocytes and prostate cancer cells with imaging FTIR microspectroscopy, Journal of lipid research, Vol. **48**, pp 1846-1856

Ghosal, R., Lewis, K. E., Kloer, P., Bayliss, S., Mur, L. and Lewis, P. D., (2010) S38 Fourier transform infra-red (FTIR) spectroscopy on sputum from lung cancer patients, healthy controls and a high-risk cohort, Thorax, Vol. **65**, A19-A20

Ghosh, T. K., Bian, J. and Gill, D. L., (1994) Sphingosine 1-Phosphate Generated in the Endoplasmic Reticulum Membrane Activates Release of Stored Calcium, The Journal of Biological Chemistry, Vol. **269**, No. 36, pp 22628-22635

Giannella, R. A., Washington, O., Gemski, P. and Formal, S. B., (1973) Invasion of HeLa cells by *Salmonella typhimurium*: A model for the study of invasiveness of Salmonella, The Journal of Infectious Diseases, Vol. **128**, No. 1, pp 69-75

Gigli, I., Fujita, T. and Nussenzweig, V., (1979) Modulation of the classical pathway C3 convertase by plasma proteins C4 binding protein and C3b inactivator, Proc. Natl. Acad. Sci. USA, Vol. **76**, pp 6596-6600

Giorgi, C., Baldassari, F., Bononi, A., Bonora, M., De Marchi, E., Missiroli, S., Patergnani, S., Rimessi, A., Suski, J. M., Wieckowski, M. R. and Pinton, P., (2012) Mitochondrial Ca(2+) and apoptosis, Cell Calcium, Vol. **52**, pp 36-43

Gitz, E., Koekman, C. A., van den Heuvel, D., Deckmyn, H., Akkerman, J. W., Gerritsen, H. C. and Urbanus, R. T., (2012) Improved platelet survival after cold storage by prevention of Glycoprotein Ibα clustering in lipid rafts, Haematol., Vol. **10**, pp 1-8

Gomez-Moulton, C., Abad, J. L., Mira, E., Lacalle, R. A., Gallardo, E., Jimenez-Baranda, S., Illa, I., Bernad, A., Manes, S. and Martinez-A, C., (2001) Segregation of leading-edge and uropod components into specific lipid rafts during T cell polarization, PNAS, Vol. **98**, pp 9642-9647

Gomez-Moulton, C., Lacanelle, R. A., Mira, E., Jimenez-Baranda, S., Barber, D. F., Carrera, A. C., Martinez-A, C. and Manes, S., (2004) Dynamic redistribution of raft domains as an organizing platform for signalling during cell chemotaxis, JCB, Vol. **164** , pp 759-768

Gonzalez, L. J., Gibbons, E., Bailey, R. W., Fairbourn, J., Nguyen, T., Smith, S. K., Best, K. B., Nelson, J., Judd, A. M. and Bell, J. D., (2009) The influence of membrane physical properties on microvesicle release in human erythrocytes, Biophysics, Vol. **2**, pp 1-14

Gould, S. J., Booth, A. M. and Hildreth, J. E. K., (2003) The Trojan exosome hypothesis, PNAS, Vol. **100**, No. 19, pp 10592-10597

Gousset, K., Wolkers, W. F., Tsvetkova, N. M., Oliver, A. E., Field, C. L., Walker, N. J., Crowe, J. H. and Tablin, F., (2002) Evidence for a physiological role of membrane rafts in human platelets, Journal of Cellular Physiology, Vol. **190**, pp 117-128

Grant, R., Stratton, D., Ansa-Addo, E., Antwi-Baffour, S., Jorfi, S., Kholia, S., Krige, L., Lange, S. and Inal. J., (2011) A filtration-based protocol to isolate human Plasma Membrane-derived Vesicles and exosomes from blood plasma, Journal of Immunological Methods, Vol. **371**, pp 143-151

Gross, T. and Blasius, B., (2008) Adaptive coevolutionary networks: a review, Interface, Vol. **5**, pp 259-271

Gurr, M. I., Harwood, J. L. and Frayn, K. N., (2002) ' Lipids in cellular structures', *Lipid Biochemistry* 5th edition, Blackwell Science, Oxford, pp 215-263

Gutwein, P., Stoeck, A., Riedle, S., Gast, D., Runz, S., Condon, T. P., Marme, A., Phong, M., Linderkamp, O., Skorokhod, A. and Altevogt, P., (2005) Cleavage of L1 in Exosomes and Apoptotic Membrane Vesicles Released from Ovarian Carcinoma Cells, Clinicak Cancer Research, Vol. **11**, pp 2492-2501

Gyorgy, B., Modos, K., Pallinger, E., Paloczi, K., Pasztoi, M., Misjak, P., Deli, M. A., Sipos, A., Szalai, A., Voszka, I., Polgar, A., Toth, K., Csete, M., Nagy, G., Gay, S., Falus, A., Kittel, A. and Buzas, E. I., (2011) Detection and isolation of cell-derived microparticles are compromised by protein complexes resulting from shared biophysical parameters, Blood, Vol. **117**, pp 39-48

Halperin, J. A., Taratuska, A., Rynkiewicz, M. and Nicholson-Weller, A., (1993) Transient Changes in Erythrocyte Membrane Permeability Are Induced by Sublytic Amounts of the Complement Membrane Attack Complex (C5b-9), Blood, Vol. **81**, No. 1, pp 200-205

Han, W., Xia, M., Xu, M., Boini, K. M., Ritter, J. K., Li, N. and Li, P., (2012) Lysosome fusion to the cell membrane is mediated by dysferlin C2A domain in coronary arterial endothelial cells, J Cell Sci, Vol. **125**, pp 1225-1234

Hansen, T. V. O., Simonsen, M. K., Nielsen, F. C. and Hundrup, Y. A., (2007) Collection of Blood, Saliva, and Buccal Cell Samples in a Pilot Study on the Danish Nurse Cohort: Comparison of the Response Rate and Quality of Genomic DNA, Cancer Epidemiol Biomarkers, Vol. **16**, pp 2072-2076

Hardin, C. D., Raeymaekers, L. and Paul, R. J., (1992) Comparison of Endogenous and Exogenous Sources of ATP in Fuelling Ca 2+ Uptake in Smooth Muscle Plasma Membrane Vesicles, Journal of General Physiology, Vol. **99**, pp 21-40

Harriman, G. R., Podack, E. R., Braude, A. I., Corbeil, L. C., Esser, A. F. and Curd, J. G., (1982) Activation of Complement by Serum-resistant *Neisseria Gonorrhoeae* Assembly of the Membrane Attack Complex without Subsequent Cell Death*, J. Exp. Med., Vol. **156**, pp 1235-1249

Harry, S., Stratton, D. and Heugh, S., (2012) Gadolinium chloride blocks calcium ion channel activity leading to down regulation of erythrocyte microvesicle activity, JBC, abstract.

Heijnen, H. F. G., Schiel, A., Fujnheer, R., Geuze, H. J. and Sixma, J. J., (1999) Activated Platelets Release Two Types of Membrane Vesicles: Microvesicles by Surface Shedding and Exosome Derived From Exocytosis of Multivesicular Bodies and ?-Granules, Blood, Vol. **94**, pp 3791-3799

Henderson, B. R., Pfister, G., Boeck, G., Kind, M. and Wick, G., (2003) Expression levels of heat shock protein 60 in human endothelial cells in vitro are unaffected by exposure to 50 Hz magnetic fields, Cell Stress Chaperones, Vol. **8**, pp 172-182

Hindmarsh, E. J. and Marks, R. M., (1998) Decay-accelerating factor is a component of subendothelial extracellular matrix *in vitro*, and is augmented by activation of endothelial protein kinase C, Eur. J. Immunol, Vol. **28**, pp 1052-1062

Hogan, M. C., Manganelli, L., Woollard, J. R., Masyuk, A. I., Masyuk, T. V., Tammachote, R., Huang, B. Q., Leontovich, A. A., Beito, T. G., Madden, B. J., Charlesworth, M. C., Torres, V. E., LaRusso, N. F., Harris, P. C. and Ward, C. J., (2009) Characterization of PKD Protein-Positive Exosome-Like Vesicles, J Am Soc Nephrol, Vol. **20**, pp 278-288

Hristov, M., Eri, W., Linder, S. and Weber, P. C., (2004) Apoptotic bodies from endothelial cells enhance the number and initiate the differentiation of human endothelial progenitor cells in vitro, Blood, Vol. **104**, No. 9, pp 2761-2766

Hugel, B., Carmen Martinez, M., Kunzelmann, C. and Freyssinet, J., (2004), 'Membrane Microparticles: Two Sides of the Coin', Physiology, Vol. **20**, pp 22-27

Humphreys, D., Hume, P. J. and Koronakis, V., (2009) The *Salmonella* Effector SptP Dephosphorylates Host AAA+ ATPase VCP to Promote Development of its Intracellular Replicative Niche, Cell Host Microbe, Vol. **5**, pp 225-233

Iglesias, D. M., El-Kares, R., Taranta, A., Bellomo, F., Emma, F., Besouw, M., Levtchenko, E., Toelen, J., van den Heuvel, L., Chu, L., Young, Y. K., Eliopoulos, N. and Goodyer, P., (2012) Stem Cell Microvesicles Transfer Cystinosin to Human Cytinotic Cells and Reduce Cystine Accumulation In Vitro, PLoS ONE, Vol. **7**, e42840

Inal, J. M., Ansa-Addo, E. A., Stratton, D., Kholia, S., Antwi-Baffour, S. S., Jorfi, S. and Lange, S., (2012) Microvesicles in health and disease, Archivum Immunologiae Therapiae et Experimentalis, Vol. **60**, pp 107-121

Ioria, F., Bosotti, R., Scacheri, E., Belcastro, V., Mithbaokar, P., Ferriero, R., Murino, L., Tagliaferri, R., Brunetti-Pierri, N., Isacchi, A. and di Bernardo, D., (2010) Discovery of drug mode of action and srug repositioning from transcriptional responses, PNAS, Vol. **107**, pp 14621-14626

ISEV 1st Annual Meeting Goteborg, (2012)

Ishii, H., mori, T., Shiratsuchi, A., Nakai, Y., Shimada, Y., Ohno-Iwashits, Y. and Nakanishi, Y., (2005) Distinct localization of lipid rafts and externalized phosphatidylserine at the surface of apoptotic cells, BBRC, Vol. **327**, pp 94-99

Iwasaka, M., Ikehata, M., Miyakoshi, J. and Ueno, S., (2004) Strong static magnetic field effects on yeast proliferation and distribution, Bioelectrochemistry, Vol. **65**, pp 59-68

Izquierdo-Useros, N., Naranjo-Gomez, Archer, J., Hatch, S. C., Erkizia, I., Blanco, J., Borras, F. E., Puertas, M. C., Connor, J. H., Fernandez-Figueras, M. T., Moore, L., Clotet, B., Gummuluru, S. and Martinez-Picado, J., (2009) Capture and transfer of HIV-1 particles by mature dendritic cells converges with the exosomes-dissemination pathway, Blood, Vol. **5**, pp 2732-2741

Jai, W., Pua, H. H., Li, Q. and He, Y., (2011) Autophagy Regulates Endoplasmic Reticulum Homeostasis and Calcium Mobilization in T Lymphocytes, J. Immunol., Vol. **186**, pp 1564-1574

Janssen, K., Horn, S., Niemann, M. T., Daniel, P. T., Schulze-Osthoff, K. and Fischer, U., (2009) Inhibition of the ER Ca^{2+} pump forces multidrug-resistant cells deficient in Bak and Bax into necrosis, Journal of Cell Science, Vol. **122**, pp 4481-4491

Jayachandran, M., Miller, V. M., Heit, J. A. and Owen, W. G., (2012) Methodology for isolation, identification and characterization of microvesicles in peripheral blood, J Immunol Methods., Vol. **375**, pp 207-214

Jones, G. W. and Richardson, L. A., (1981) The attachment to, and invasion of HeLa cells by *Salmonella typhimurium*: The contribution of Mannose-sensitive and Mannose-resistant Haemagglutination activities, Journal of General Microbiology, Vol. **127**, pp 361-370

Jorfi, S. and Inal, J. M., (2012) Coxackie virus entry and spread in HeLa cells is aided by microvesicle release, JBC, Abstract

Jorfi, S., Ansa-Addo, E., El dine, S. and Inal, J., (2010) Plasma membrane-derived vesicles (PMVs) released from apoptotic Jurkat cells express unregulated surface Fas and induce apoptosis in recipient viable cells, J. Immunol., Vol. **184**, 89.45

Kargosha, K., Khanmohammadi, M. and Ghadiri, M., (2001) Vapour phase Fourier transform infrared spectrometric determination of thiourea, Analyst, Vol. **126**, pp 1432-1435

Kawakubo, T., Naruse, K., Matsubara, T., Hotta, N. and Sokabe, M., (1999) Characterization of newly found stretch-activated $K_{Ca,ATP}$ channel in cultured chick ventricular myocytes, Am J Physiol Heart Circ Physiol, Vol. **276**, pp 1827-1838

Kern, S. E. and Shibata, D., (2007) The Fuzzy Math of Solid Tumor Stem Cells: A Perspective, Cancer Res, Vol. **67**, pp 8985-8988

Kesimer, M., Scull, M., Brighton, B., DeMaria, G., Burns, K., O'Neal, W., Pickles, R. J. and Sheehan, J. K., (2009) Characterization of exosome-like vesicles released from human tracheobronchial ciliated epithelium: a possible role in innate defense, The FASEB Journal, Vol. **23**, No 6, pp 1858-1868

Kim, J. W., Wieckowski, E., Taylor, D. D., Reichert, T. E., Watkins, S. and Whiteside, T. L., (2005) Fas Ligand-Positive Membranous Vesicles Isolated form Sera of Patients with Oral Cancer Induce Apoptosis of Activated T Lymphocytes, Clinical Cancer Research, Vol. **11**, pp 1010-1020

Kindzelskii, A. L., Sitrin, R. G. and Petty, H. R., (2004) Cutting Edge: optical Microspectrophotometry Supports the Existence of Gel Phase Lipid Rafts at the Lamellipodium of Neutrophils: Apparent Role in Calcium Signaling, J. Immunol., Vol **172**, pp 4681-4685

Klychnikova, E. V., Matveev, S. B., Riabinin, V. A., Godkov, M. A., Golikov, A. P., Akhmetov, V. V. and Milkhailov, I. P., (2012) The oxidation stress, lipid metabolism and their relationship in patients with severe course of hypertension disease in aggregate with carotid stenosis, Klin Lab Diagn., Vol **5**, pp 20-22

Koga, K., Matsumoto, K., Akiyoshi, T., Kubo, M., Yamanaka, N., Tasaki, A., Nakashima, H., Nakamura, M., Kuroki, S., Tanaka, M. and Katano, M., (2005) Purification, Characterization and Biological Significance of Tumor-derived Exosomes, Anticancer Research, Vol. **25**, pp 3703-3708

Komagoe, K., Takeuchi, H., Inoue, T. and Katsu, T., (2010) Application of an oxygen electrode to evaluate superoxide anion-scavenging ability, Anal Sci., Vol. **26**, pp 903-906

Kouokam, J. C., Wai, S. N., Fallman, M., Dobrindt, U., Hacker, J. and Uhlin, B. E., (2006) Active Cytotoxic Necrotizing Factor 1 Associated with Outer Membrane Vesicles from Uropathogenic *Escherichia coli*, Infection and Immunity, Vol. **74**, No. 4, pp 2011-2030

Kushlich, C., Pawlowski, T. L., Deng, T., Tinder, T., Kim, J., Kimbrough, J. and Spetzler, D., (2010) A sensitive exosomes-based biosignature for the diagnosis of prostate cancer, Journal of Clinical Oncology, Vol. **28**, pp 4636

Laytin, V., Allen, D. J., Mutlu, A., Gyulkhandanyan, A. V., Mykhaylov, S. and Freedman, J., (2009) Mitochondrial control of platelet apoptosis: effect of cyclosporin A, an inhibitor of the mitochondrial permeability transition pore, Laboratory Investigation, Vol. **89**, pp 374-384

Lederman, L. M., (1982) A report on high-energy physics*, PNAS, Vol. **79**, pp 7963-7969

Lee, S. R., Kim, S. H., Jeong, K. J., Kim, K. S., Kim, Y. H., Kim, S J., Kim, E., Kim. J. W. and Chang, K. T., (2009) Multi-Immunogenic Outer Membrane Vesicles Derived from a MsbBDeficient Salmonella enteric Serovar Typhimurium Mutant, Journal of Microbiology and Biotechnology, Vol. **19**, pp 1271-1279

Lee-Montiel, F. T., Reynolds, K. A. and Riley, M. R., (2011) Detection and quantification of poliovirus infection using FTIR spectroscopy and cell culture, J Biol Eng., Vol. **5**, pp 1-12

Legate, K. R., Wickstrom, S. A. and Fassler, R., (2009) Genetic and cell biological analysis of integrin outside-in signalling, Genes & Development, Vol. **23**, pp 397-418

Leonce, S. and Cudennec, C. A., (1990) Modification of membrane permeability measured by Texas-Red during cell cycle progression and differentiation, Anticancer Res, Vol. **10**, pp 369-374

Leroyer, A. S., Ebrahimian, T. G., Cochain, C., Recalde, A., Blanc-Brude, O., Mees, B., Vilar, J., Tedgui, A., Levy, B. I., Chimini, G., Boulanger, C. M. and Silvestre, J., (2009) Microparticles From Ischemic Muscle Promotes Postnatal Vasculogenisis, Circulation, Vol. **119**, pp 2807-2817

Leroyer, A. S., Isobe, H., Leseche, G., Castier, Y., Wassef, M., Mallat, Z., Binder, B. R., Tedgui, A. and Boulanger, C. M., (2007), 'Cellular Origins and Thrombogenic Activity of Microparticles Isolated From Human Atherosclerotic Plaques', Atherosclerosis, Vol. **49**, pp 772-779

Levenson, A. S., Thurn, K. E., Simons, L. A., Velicesas, D., Jarrett, J., Osipo, C., Jordan, V. C., Volpert, O. V., Satcher Jr, R. L. and Gartenhaus, R. B., (2005) MCT-1 Oncogebe Contributes to Increased *In vivo* Inhibition of Apoptosis, Cancer Res., Vol. **65**, pp 10651-10656

Levitan, I., Fang, Y., Rosenhouse-Dantsker, A. and Romanenko, V., (2010) Cholesterol and Ion Channels, Subcell Biochem, Vol. **51**, pp 509-549

Li, C., Yu, S., Nakamura, F., Penrikainen, O. T., Singh, N., Yin, S., Xin, W. and Sy, M., (2010) Pro-prion binds filamin A facilitating its interaction with integrin β and contributes to melanomagenesis, JBC, Vol. **10**, pp 1-25

Li, G, Yan, Y. J., Huang, Y., Zhou, Y. and Pang, X. F., (2012) FTIR spectra investigation of rat sensitive tissues explore exposure to ELF-EMF, Guang Pu Yu Guang Pu Fen Xi , Vol. **32**, pp 1194-1197

Liburdy, R. P., Tenforde, T. S. and Margin, R. L., (1986) Magnetic field-induced drug permeability in liposome vesicles, Radiat Res., Vol. **108**, pp 102-111

Liu, S. Y., Chen, C. L., Yang, T. T., Huang, W. C., Hsieh, C. Y., Shen, W. T., Tsai, T. T., Shieh, C. C. and Lin, C. F., (2012) Albumin prevents reactive oxygen species-induced mitochondrial damage, autophagy, and apoptosis during serum starvation, Apoptosis, Epub ahead of print

Liu, Y. X., Tai, J. L., Li, G. Q., Zhang, Z. W., Xue, J. H., Liu, H. S., Zhu, H., Cheng, J.D., Liu, Y. L., Li, A. M. and Zhang, Y., (2012) Exposure to 1950-MHz TD-SCDMA Electromagnetic Fields Affects the Apoptosis of Astrocytes via Caspase-3-Dependent Pathway, PLoS One, Vol. **7**, e42332

Lo Cicero, A., Schinera, G., Proia, P., Saladino, P., Savettieri, G., Di Liegro, C. M. and Di Liegro, I., (2011) Oligodendroglioma cells shed microvesicles which contain TRAIL as well as molecular chaperones and induce cell death in astrocytes, Int J Oncol., Vol. **39**, pp 1353-1357

Lourido, S., Shuman, J., Zhang, Chao, Shokat, K. M., Hui, R. and Sibley, L. D., (2010) Calcium-dependent protein kinase 1 is an essential regulator of exocytosis in *Toxoplasma*, Nature, Vol. **465**, pp 359-362

Luo, Y., Chen, M., Wen, Q., Zhao, M., Zhang, B., Li, X., Wang, F., Huang, Q., Yao, C., Jiang, T., Cai, G. and Fu, W., (2006) Rapid and Simultaneous Quantification of 4 Urinary Proteins by Piezoelectric Quartz Crystal Microbalance Immunosensor Array, Clinical Chemistry, Vol. **52**, pp 2273-2280

Mack, M., Klienschmidt, A., Bruhl, H., Klier, C., Nelson, P. J., Cihak, J., Plachy, J., Stangassinger, M., Erfle, V. and Schlondorff, D., (2000), 'Transfer of the chemokine receptor CCR5 between cells by membrane-derived microparticles: A mechanism for cellular human immunodeficiency virus 1 infection', Nature America, Vol. **6**, No. 7, pp 769-775

Mackenzie, A. B., Young, M. T., Adinolfi, E. and Surprenant, A., (2005) Pseudoapoptosis Induced by Brief Activation of ATP-gated $P2X_7$ Receptors, The Journal of Biological Chemistry, Vol. **280**, No. 40, pp 33968-33976

Mandal, D., Mazumder, A., Das, P., Kundu, M. and Basu, J., (2005) Fas-, Caspase 8-, and Caspase 3-dependent Signaling Regulates the Activity of the Aminophospholipid Translocase and Phosphatidylserine Externalization in Human Erythrocytes, The Journal of Biological Chemistry, Vol. **280**, No. 47, pp 39460-39467

Manno, S., Takakuwa, Y. and Mohandas, N., (2001) Identification of a functional role for lipid asymmetry in biological membranes: Phosphatidylserine-skeletal protein interactions modulate membrane stability, Biophysics, Vol. **99**, No. 4, pp 1943-1948

Martin, F. L., (2011) Shining a new light into molecular workings, Nature Methods, Vol. **8**, No. 5, pp 385-387

Martinez-Seara, H., Rog, T., Karttunen, M., Vattulainen, I. and Reigada, R., (2010) Cholesterol Induces Specific Spatial and Orientational Order in Cholesterol/Phospholipid Membranes, PLoS ONE, Vol. **5**, pp 1-11

McBroom, A. J., Johnson, A. P., Vemulapalli, S. and Kuehn, M. J., (2006) Outer Membrane Vesicles Production by *Escherichia* coli Is Independent of Membrane Instability, Journal of Bacteriology, Vol. **188**, No. 15, pp 5385-5392

McKeown, L., Moss, N. K., Turner, P., Li, J., Heath, N., Burke, D., O'Regan, D., Gilthorpe, M.S., Porter, K. E. and Beech, D. J., (2012) Platelet-Derived Growth Factor Maintains Stored Calcium Through a Nonclustering Orai1 Mechanism But Evokes Clustering If the Endoplasmic Reticulum Is Stressed by Store Depetion, Cellular Biology, Vol. **111**, pp 66-76

Meckes Jr, D. G. and Raab-Traub, N., (2011) Microvesicles and Viral Infection, J. Virol, Vol. **85**, pp 12844-12854

Merk, M., Baugh, J., Zierow, S., Leng, L., Pal, U., Lee, S. J., Ebert, A. D., Mizue, Y., Trent, J. O., Mitchell, R., Nickel, W., Kavathas, P. B., Bernhagen, J. and Bucala, R., (2009) The Golgi-Associated Protein p115 Mediates the secretion of Macrophage Migration Inhibitiry Factor, Journal of Immunology, Vol. **182**, pp 6896-6906

Molecular Probes., (2003) Vybrant® Lipid Raft Labeling Kits, pp 1-3

Morel, O., Jesel, L., Freyssinet, J. and Toti, F., (2011) Cellular Mechanisms Underlying the Formation of Circulating Microvesicles, Arteriosclerosis, Thrombosis and Vascular Biology, Vol. **31**, pp 15-26

Moskovich, O. and Fishelson, Z., (2007) Live Cell Imaging of Outward and Inward Vesiculation Induced by the Complement C5b-9 Complex, The Journal of Biological Chemistry, Vol. **282**, pp 29977-29986

Muller, G., (2012) Microvesicle/exosome as potential novel biomarkers of metabolic disease, Diabetes, Metabolic Syndrome and Obesity: Targets and Therapy, Vol. **5**, pp 247-282

Muralidharan-Chari, V., Clancy, J. W., Sedgwick, A. and D'Souza-Schorey, C., (2010) Microvesicles: Mediators of extracellular communication during cancer progression, Journal of Cell Science, Vol. **123**, pp 1603-1611

Muralinath, M., Kuehn, M. J., Roland, K. L. and Curtiss, R., (2011) Immunization with *Salmonella enterica* Serocar Typhimurium-derived Outer Membrane Vesicles delivering the pneumococcal protein PspA confers protection against challenge with *Streptococcus pneumonia*, Vol. **79**, No. 2, pp 887-894

Mycielska, M. E., Palmer, C. P., Brackenbury, W. J. and Djamgoz, M. B. A., (2005) Expression of Na^+-dependant citrate transport in a strongly metastatic human prostate cancer PC-3M cell line: regulation by voltage-gated Na^+ channel activity, Cell Physiology, Vol. **563**, pp 393-408

Nakamichi, N., Ishioka, Y., Hirai, T., Ozawa, S., Tachibana, M., Nakamura, N., Takarada, T. and Yoneda, Y., (2009) Possible promotion of neuronal differentiation in fetal rat brain neural progenitor cells after sustained exposure to static magnetism, J Neurosci Res., Vol. **87**, pp 2406-2417

NanoDrop., (2008) 'Nucleic acids', NanoDrop 1000 Spectrophotometer V3.7 User's Manual, Thermo Scientific, pp 27-30

Nara, M., Yonezawa, N., Shimada, T., Takahashi, K., Tanokura, M., Yumoto, F., Nakagawa, H., Ohashi, K., Hamano, S. and Nakano, M., (2006) Fourier Transform Infrared Spectroscopic Analysis of the Intact Zona Pellucida of the Mammalian Egg: Changes in the Secondary Structure of Bovine Zona Pellucida Proteins During Fertilization, Experimental Biology and Medicine, Vol. **231**, pp 166-171

Narita, K., Hanakawa, K., Kasahara, T., Hisamitsu, T. and Asano, K., (1997) Induction of apoptotic cell death in human leukemic cell line HL-60, by extremely low frequency electric magnetic fields: analysis of the possible mechanisms in vitro, In Vivo, Vol. **11**, pp 329-335

Narula, J. and Strauss, W., (2003) P.S. *I Love You: Implications of Phosphatidyl Serine (PS) Reversal in Acute Ischemic Syndromes, Journal of Nuclear Medicine, Vol. **44**, pp 397-399

Nasse, M. J., Walsh, M. J., Mattson, E. C., Reininger, R., Kajdacsy-Balla, A., Macias, V., Bhargava, R. and Hirschmugl, C. J., (2011) High-resolution Fourier-transform infrared chemical imaging with multiple synchrotron beams, Nature Methods, Vol. **8**, No. 5, pp 413-416

Nolan, S., Dixon, R., Norman, K., Hellewell, P., and Ridger, V., (2008) Nitric Oxide Regulates Neutrophil Migration through Microparticle Formation, The American Journal of Pathology, Vol. **172**, No. 1, pp 265-273

Ohata, H., Tanaka, K., Maeyama, N., Yamamoto, M. and Momose, K., (2001) Visualization of elementary mechanosensitive Ca^{2+} influx events, Ca^{2+} spots, in bovine lens epithelial cells, Journal of Physiology, Vol. **532**, pp 31-42

Oheim, M., Kirchhoff, F. and Stuhmer, W., (2006) Calcium microdomains in regulated exocytosis, Cell Calcium, Vol. **40**, pp 423-439

Ojeda, J. J. and Dittrich, M., (2012) Fourier transform infrared spectroscopy for molecular analysis of microbial cells, Methods Mol Biol., Vol. **811**, pp 187-211

Palmisano, G., Jensen, S. S., Le Bihan, M. C., Laine, J., McGuire, J. N., Pociot, F. and Larsen, M. R., (2012) Characterization of Membrane-shed Microvesicles from Cytokine-stimulated β-Cells Using Proteomics Strategies, Mol Cell Proteomics, Vol. **11**, pp 230-243

Pang, H., Flinn, R., Patsialou, A., Wyckoff, J., Roussos, E. T., Wu, H., Pozzuto, M., Goswami, S., Condeelis, J. S., Bresnick, A. R., Segall, J. E. and Backer, J., (2009) Differential Enhancement of Breast Cancer Motility and Metastasis by Helical and Kinase Domain Mutations of Class IA Phosphositide 2-Kinase, Cancer Res., Vol. **69**, pp 8868-8876

Parihar, A., Parihar, M. S., Zenebe, W. J. and Ghafourifar, P., (2012) Statins lower calcium-induced oxidative stress in isolated mitochondria, Toxicol., Vol. **31**, pp 355-363

Parolini, I., Federici, C., Raggi, C., Lugini, L., Palleschi, S., De Milito, A., Coscia, C., Iessi, E., Logozzi, M., Molinari, A., Colone, M., Tatti, M., Sargiacomo, M. and Fais, S., (2009) Microenvironmental pH Is a Key Factir for Exosome Traffic in Tumor Cells, Journal of Biological Chemistry, Vol. **284**, pp 34211-34222

Pasciak, M., Holst, O., Lindner, B., Mordarska, H. and Gamian, A., (2003) Novel Bacterial Polar Lipids Containing Ether-linked Alkyl Chains, the Structures and Biological Properties of the Four Major Glycolipids from *Propionibacterium propioicum* PCM 2431 (ATCC 14157^T)*, JBC, Vol. **278**, pp 3948-3956

Patel, J. C. and Galan, J. E., (2008) Investigating the Function of Rho Family GTPases during Salmonella/Host Cell Interactions, Methods Enzymol., Vol.**439**, pp 145-158

Patruno, A., Tabrez, S., Amerio, P., Pesce, M., Vianale, G., Franceschelli, S., Grilli, A., Karmal, M. A. and Reale, M., (2011) Kinetic study on the effects of extremely low frequency electromagnetic field on catalase, cytochrome P450 and inducible nitric oxide synthase in human HaCaT and THP-1 cell lines, CNS Neurol Disord Drug Targets, Vol. **10**, pp 936-944

Pereira, C. S., de Regt, A. K., Brito, P. H., Miller, S. T. and Xavier, K. B., (2009) Identification of Functional LsrB-Like Autoinducer-2 Receptors, Journal if Bacteriology, Vol. **191**, pp 6975-6987

Petrache, H. I., Tristram-Nagle, S., Harries, D., Kucerka, N., Nagle, J. F. and Parsegian, V. A., (2006) Swelling of phospholipids by monovalent salt, J. Lipid Res., Vol. **47**, pp 302-309

Pham, N. H., Ohya, S., Tanaka, M., Barnes, S. E. and Maekawa, S., (2009) Electromotive force and huge magnetoresistance in magnetic tunnel junctions, Nature, Vol. **458**, pp 489-492

Pilla, A. A., (2012) Electromagnetic fields instantaneously modulate nitric oxide signalling in challenged biological systems, BBRC, Epub ahead of print

Pilla, A., Fitzsimmons, R., Muehsam, D., Wu, J., Rohde, C. and Casper, D., (2011) Electromagnetic fields as first messenger in biological signalling: Application to calmodulin-dependent signalling in tissue repair, Biochim Biophys Acta, Vol. **12**, pp 1236-1245

Pizzirani, C., Ferrari, D., Chiozzi, P., Adinolfi, E., Sandona, D., Savaglio, E. and Di Virgilio, F., (2007) Stimulation of P2 receptors causes release of IL-1β-loaded microvesicles from human dendritic cells, Blood, Vol. **109**, No. 9, pp 3856-3864

Popova, A. V. and Hincha, D. K., (2005) Effects of the sugar headgroup of a glycoglycerolipid on the phase behaviour of phospholipid model membranes in the dry state, Glycobiology, Vol. **15**, No.11, pp 1150-1155

Potter, D. A., Tirnauer, J. S., Jassen, R., Croall, D. E., Hughes, C. N., Fiacco, K. A., Mier, J. W., Maki, M. and Herman, I. M., (1998) 'Calpain Regulates Actin Remodeling during cell spreaing', The Journal of Cell Biology, Vol. **141**, No. 3, pp 647-662

Pryor, P. R., Mullock, B. M., Bright, N. A., Gray, S. R. and Luzio, J. P., (2000) The role of Intraorganellar Ca^{2+} in late Endosome-Lysosome Hetertypic Fusion and in the Reformation of Lysosomes from Hybrid Organelles, The Journal of Chemical Biology, Vol. **149**, pp 1053-1062

Putz, U., Howitt, J., Lackovic, J., Foot, N., Kumar, S., Silke, J. and Tan, S., (2008) Nedd4 Family-interacting Protein 1 (Ndfip1) Is Required for the Exosomal Secretion of Nedd4 Family Proteins, Journal of Biological Chemistry, Vol. **283**, pp 32621-32627

Qu, Y., Franchi, L., Nunez, G. and Dubyak, G. R., (2007) Nonclassical IL-1β Secretion Stimulated by P2X7 Receptors is Dependent in Inflammasome Activation and Correlated with Exosome Release in Murine Macrophages, The Journal of Immunology, Vol. **179**, pp 1913-1925

Quesenberry, P. J. and Aliotta, J. M., (2010a) Cellular phenotype switching and microvesicles, Advanced Drug Delivery Reviews, Vol. **10**, pp 1016-1024

Quesenberry, P. J., Dooner, M. S. and Aliotta, J. M., (2010b) Stem cell plasticity revisited: The continuum marrow model and phenotypic changes mediated by microvesicle, Experimental Hematology, Vol. **38**, pp 581-592

Rajendra, P., Sujatha, H. N., Devendranath, D., Gunasekaran, B., Sashidhar, R. B., Subramanyam, C. and Channakeshava., (2004) Biological effects of power frequency magnetic fields: Neurochemical and toxicological changes in developing chick embryos, Biomagnetic Research and Technology, Vol. **2**, pp 1-9

Repacholi, M., (2012) Concern that "EMF" magnetic fields from power lines cause cancer, Science of the total Environment, Vol. **426**, pp 454-458

Rizzuto, R. and Pozzan, T., (2006) Microdomains of Intracellular Ca^{2+}: Molecular Determinants and Functional Consequences, Physiol Rev, Vol. **86**, pp 369-408

Robertson, C., Booth, S. A., Beniac, D. R., Coulthart, M. B., Booth, T. F. and NcNicol, A., (2006) Cellular prion protein is released on exosomes from activated platelets, Blood, Vol. **107**, pp 3907-3911

Rodriguez-Escudero, I., Rotger, R., Cid, V. J. and Molina, M., (2006) Inhibition of Cdc42-dependent signalling in *Saccharomyces* cerevistae by phosphatise-dead SigD/SopB from *Salmonella typhimurium*, Microbiology, Vol. **152**, pp 3437-3452

Roos, D., Seeger, R., Puntel, R. and Vargas Barbosa, N., (2012) Role of Calcium and Mitochondria in MeHg-Mediated Cytotoxicity, J Biomed Biotechnol., pp 1-15

Rosenfeld, J. L., Moore, R. H., Zimmer, K. P., Foster, E. A., Dia, W., Zarka, M. N. and Knoll, B. J., (2001) Lysosome proteins are redistributed during expression of a GTP-hydroylsis-defective reb5a, Journal of Cell Science, Vol. 114, No. 24, pp 4499-4508

Salinthone, S., Kerns, A. R., Tsang, V. and Carr, D. W., (2012) α-Tocopherol (vitamin E) stimulates cyclic AMP production in human peripheral mononuclear cells and alters immune function, Mol Immunol., Vol. **53**, pp 173-178

Sarkar, A., Mitra, S., Mehta, S., Raices, R. and Wewers, M. D., (2009) Monocyte Derived Microvesicles Deliver a Cell Death Message via Encapsulated Caspase-1, PLoS ONE, Vol. **4**, pp 1-9

Sato, T., Machida, T., Takahashi, S., Iyama, S., Sato, Y., Kuribayashi, K., Takada, K., Oku, T., Kawano, Y., Okamoto, T., Takimoto, R., Matsunaga, T., Takayama, T., Takahashi, M., Kato, J. and Niitus, Y., (2004) Fas-Mediated Apoptosome Formation Is Dependent on Reactive Oxygen Species Derived from Mitochondrial Permeability Transition in Jurkat Cells, The Journal of Immunology, Vol. **173**, pp 285-296

Scanu, A., Molnarfi, N., Brandt, K. J., Grauz, L., Dayer, J. and Burger, D., (2008) Stimulated T cells generate microparticles, which mimic cellular contact activation of human monocytes: differential regulation of pro- and anti-inflammatory cytokine production by high-density lipoproteins, Journal of Leukocyte Biology, Vol. **83**, pp 921-927

Schlumberger, M. C., Muller, A. J., Ehrbar, K., Winnen, B., Duss, I., Stecher, B. and Hardt, W., (2005) Real-time inaging of type III secretion: *Salmonella* SipA injection into host cells, PNAS, Vol. **102**, No. 35, pp 12548-12553

Schuck, S. and Simons, K., (2004) Polarized sorting in epithelial cells: raft clustering and the biogenesis of the apical membrane, J. Cell Sci., Vol. **117**, pp 5955-5964

Schutz, E., Urnovitz, H. B., Iakoubov, L., Schulz-Schaeffer, W., Wemheurer, W. and Brenig, B., (2005) Bov-tA Short Interspersed Nucleotide Element Sequences in Circulating Nucleic Acids from Sera of Cattle with Bovine Spongiform Encephalopathy (BSE) and Sera of Cattle Exposed to BSE, Immunology, Vol. **12**, No. 7, pp 814-820

Setty, B. N. Y., Kulkarni, S., Rao, A. K. and Stuart, M. J., (2000) Fetal haemoglobin in sickle cell disease: relationship to erythrocyte phosphatidylserine exposure and coagulation activation, Blood, Vol. **96**, pp 1119-1124

Seyyedi, S. S., Mozdarani, H., Tavirani, M. R., Heydari, S., (2010) Induction of chromosomal aberrations in human primary fibroblasts and immortalized cancer cells exposed to extremely-low-frequency electromagnetic fields, Iran. J. Radiat. Res., Vol. **8**, pp 25-29

Shah, F. D., Shukla, S. N., Shah, P. M., Patel, H. R. H. and Patel, P. S., (2008) Significance if Alterations in Plasma Lipid Profile Levels in Breast Cancer, Integr Cancer Ther, Vol. **7**, pp 31-41

Shen, B., Fang, Y., Wu, N. and Gould, S. J., (2011) Biogenesis of the Posterior Pole Is Mediated by the Exosome/Microvesicle Protein-sorting Pathway, JBC, Vol. **286**, pp 44162-44176

Shi, B., Farboud, B., Nuccitelli, R. and Isseroff, R. R., (2003) Power-line frequency electromagnetic fields do not induce changes in phosphorylation, localisation, or expression of the 27-kilodalton heat shock protein in human keratinocytes, Environ Health Perspect, Vol. **111**, pp 281-288

Silverman, J. M., Clos, J, de'Olivera, C. C., Shirvani, O., Fang, Y., Wang, C., Foster, L. J. and Reiner, N., (2010) An exosomes-based secretion pathway is responsible for protein export from *Leishmania* and communication with macrophages, Journal of Cell Science, Vol. **123**, pp 842-852

Simko, M. and Mattsson, M., (2004) Extremely Low Fequency Electromagnetic Fields as Effectors of Cellular Responses In Vitro: Possible Immune Cell Activation, Journal of Cellular Biochemistry, Vol. **93**, pp 83-92

Smith, J. D., Waelde, C., Horwitz, A. and Zheng, P., (2002) Evaluation of the Role of Phosphatidylserine Translocase Activity in ABCA1-mediated Lipid Efflux, Journal of Biological Chemistry, Vol. **277**, No. 20, pp 17797-17803

Solun, N. O., (1999) Procoagulant Expression in Platelets and Defects Leading to Clinical Disorders, Arterioscler Thromb Vasc Biol, Vol. **99**, pp 2841-2846

Stowell, S. R., Karmakar, S., Arthur, C. M., Ju, T., Rodrigues, L. C., Riul, T. B., Dias-Baruffi, M., Miner, J., McEver, R. P. and Cummings, R. D., (2009) Galectin-1 Induced Reversible Phosphatidylserine Exposure at the Plasma Membane, Molecular Biology of the Cell, Vol. **20**, pp 1408-1418

Stratton, D., Antwi-Baffour, S., Williams, G., Grant, R., Lange, S. and Inal, J., (2012) Characterisation of microvesicles released from cells constitutively and upon stimulation, ISEV, Vol. **1**

Subra, C., Grand, D., Laulagnier, K., Stella, A., Lambeau, G., Paillasse, M., De Medina, P., Monsarrat, B., Perret, B., Silvente-Poirot, S., Poirot, M. and Record, M., (2010) Exosomes account for vesicle-mediated transcellular transport of activatable phospholipases and prostaglandins, J. Lipid Res., Vol. **51**, pp 2105-2120

Sun, H., Lin, K. and Yin, H. L., (1997) Gelsolin Modulates Phospholipase C Activity In Vivo through Phospholipid Binding, JBC, Vol. **138**, pp 811-820

Sunkari, V. G., Aranovitch, B., Portwood, N. and Nikoshkov, A., (2011) Effects of a low-intensity electromagnetic field on fibroblast migration and proliferation, Electromagn Biol Med., Vol. **30**, pp 80-85

Szajnik, M., Czystowska, M., Szczepanski, M. J., Mandapathil, M. and Whiteside, T. L., (2010) Tumor-Derived Microvesicles Induce, Expand and Up-Regulate Biological Activities of Human Regulatory T Cells, PLoS ONE, Vol. **5**, e11469

Szeghalmi, A., Kaminskyj. S. and gough, K. M., (2007) A synchrotron FTIR microscopy investigation of fungal hypae growth under optimal and stressed conditions, Anal Bioanal Chem., Vol. **387**, pp 1779-1789

Temme, S., Eis-Hubinger, A. M., McLellan, A. D. and Koch, N., (2010) The Herpes Simples Virus-1 Encoded Glycoprotein B Diverts HLA-DR into the Exosome Pathway, The Journal of Immunology, Vol. **184**, pp 236-243

Tenorio, B. M., Jimenez, G. C., de Morais, R. N., Peixoto, C. A., de Albuguergue Nogueira, R. and de Silve, V. A. Jr., (2012) Evaluation of testicular degeneration induced by low-frequency electromagnetic fields, J Appl Toxicol., Vol. **32**, pp 210-218

Terstrappen, L. W. M. M., Nguyen, M., Lazarus, H. M. and Medof, E., (1992) Expression of DAF (CD55) and CD59 antigens during normal hematopoietic cell differentiation, Journal of Leukocyte Biology, Vol. **56**, No. 6, pp 652-660

Thomas, D. D. H., Martin, C. L., Weng, N., Byrne, J. A. and Groblewski, G. E., (2009) Tumor protein D52 expression and Ca^{2+} -dependent phosphorylation modulates lysosomal membrane protein trafficking to the plasma membrane, Am J Physiol Cell Physiol, Vol. **298**, pp 725-739

Thomas, L. M. and Salter, R. D., (2010) Activation of Macrophages by $P2X_7$-Induced Microvesicles from Myeloid Cells Is Mediated by Phospholipids and Is Partially Dependent on TLR4, The Journal of Immunology, Vol. **185**, pp 3740-3749

Tomas, A., Yermen, B., Min, L., Pessin, J. E. and Halban, P. A., (2006) Regulation of pancreatic β-cell insulin secretion by actin cytoskeleton remodelling: role of Gelsolin and cooperation with the MAPK signalling pathway, Journal of Cell Science, Vol. **119**, No, 10, pp 2156-2167

Torrado, L. C., Temmerman, K., Muller, H, Mayer, M. P., Seelenmeyer, C., Backhaus, R. and Nickel, W., (2009) An intrinsic quality-control mechanism ensures unconventional secretion of fibroblast growth factor 2 in a folded conformation, Journal of Cell Science, Vol. **122**, No. 18, pp 3322-3329

Vallhov, H., Gutzeit, C., Johansson, S. M., Nagy, N., Paul, M., Li, Q., Friend, S., George, T. C., Kleim, E., Scheynius, A. and Gabrielsson, S., (2011) Exosomes Containing Glycoprotein 350 Released by EBV-Transformed B Cells Selectively Target B Cells through CD21 and Block EBV Infection In Vitro, The Journal of Immunology, Vol. **186**, pp 73-82

Viaud, S., Thery, C., Ploix, S., Tursz, T., Lapierre, V., Lantz, O., Zitvogel, L. and Chaput, N., (2010) Dendritic Cell-Derived Exosomes for Cancer Immunotherapy: What's Next?, Cancer Res, Vol. **70**, pp 1281-1285

Vidakovics, M. L., Jendholm, J., Morghelin, M., Mansson, A., Larsson, C., Cardell, L. O. and Riesbeck, K., (2010) B cell activation by outer membrane vesicles—a novel virulence mechanism, PLoS Pathogens, Vol. **15**, pp 1-19

Vindis, C., Elbaz, M., Escargueil-Blanc, I., Auge, N., Heniquez, A., Thiers, J., Negre-Salvayre, A. and Salvayre, R., (2005) Two Distinct Calcium-Dependent Mitochondrial Pathways are Involved in Oxidized LDL-Induced Apoptosis, Journal of the American Heart Association, Vol. **24**, pp 639-645

Vineis, P., (2008) Methodological insight: fuzzy sets in medicine, J Epidemiol Community Health, Vol. **62**, pp 273-278

Walsh, G., (2002) 'Interferons, interleukins and additional regulatory factors', Proteins Biochemistry and Biotechnology, Wiley, Chichester, pp 317-345

Wang, C., Yoo, Y., Fan, H., Kin, E., Guan, K. and Guan, J., (2010) Regulation of integrin β1 recycling to lipid rafts by RAB1A to promote cell migration, JBC, Vol. **10**, pp 1-13

Wang, Y., Makker, P. and Raz, A., (2008) Down-regulation of galectin-3 inhibits cell growth and metastasis in human prostate cancer PC3 cells, Growth Control, Gene Regulation: Abstract 104

Wassell, J. and Boulton, M., (1997) A role for vitamin A in the formation of ocular lipofuscin, British Journal of Ophthalmology, Vol. **81**, pp 911-918

Whelan, D. R., Bamberry, K. R., Pulskar, L., McNaughton, D. and Wood, B. R., (2012) Quantification of DNA in simple eukaryotic cells using Fourier transform infrared spectroscopy, J. Biophotonics, Epub ahead of print

Winder, L., Lefley, M. and Smith, B., (1997) A key for freshwater invertibrates using fuzzy logic, Comput Appl Biosci, Vol. 13, pp 169-174

Winnen, B., Schlumberger, M. C., Sturm, A., Schupbach, K., Siebenmenn, S., Jenny, P. and Hardt, W., (2008) Hierarchial Effector Protein Transport by the Salmonella Typhimurium SPI-1 Type III Secretion System, PLoS ONE, Vol. **3**, No. 5, pp 1-8

Woolf, P. J. and Wang, Y., (2000) A fuzzy logic approach to analysing gene expression data, Physiol. Genomics, Vol. **3**, pp 9-15

World Health Organisation (WHO)., (2007) Electromagnetic fields and public health: Exposure to extremely low frequency fields, www.who.int/mediacentre/factsheets/fs322/en/index.html (Accessed on 20th September 2012)

Wright, M., (2012) Nanoparticle tracking analysis for the multiparameter characterization and counting of particle suspensions, Methods Mol Biol., Vol. **906**, pp 511-524

Wurdinger, T., Gatson, N, N., Balaj, L., Kaur, B., Breakefield, X. O. and Pegtel, D. M., (2012) Extracellular Vesicles and Their Convergence with Viral Pathways, Advances in Virology, Vol. **10**, pp 1-12

Xie, Y., Bai, O., Yuan, J., Chibbar, R., Slattery, K., Wei, Y., Deng, Y. and Xiang, J., (2009) Tumor Apoptotic Bodies Inhibit, CTL Responses and Antitumor Immunity via Membrane-Bound Transforming Growth Factor-β1 Inducing CD8+ T-Cell Anergy and CD4+ Tr1 Cell Responses, Cancer Research, Vol. **69**, pp 7756-7766

Yang, Y. and Honaramooz, A., (2012) Characterization and quenching of autofluorescence in piglet testis tissue and cells, Anat Res Int., 820120

Yao, K., Paliyath, G. and Thomson, J. E., (1993) Localization of Peroxidized Lipids in Non-Sedimentable Microvesicles of Senescing Bean Cotyledons, Journal of Experimental Botany, Vol. **44**, pp 1267-1274

Yao, K., Paliyath, G., Humphrey, R. W., Hallett, F. R. and Thompson, J. E., (1991) Identification and characterization of nonsedimentable lipid-protein microvesicles, PNAS, Vol. **88**, pp 2269-2273

Yen, J., Liu, X. and Teh, S. H., (1994) A Fuzzy Logic-based Methodology for the Acquisition and Analysis of Imprecise Requirements, Concurrent Engineering, Vol. **2**, pp 265-277

Yermen, B., Tomas, A. and Halban, P. A., (2007) Pro-Survival Role of Gelsolin in Mouse β-Cells, Diabetes, Vol. **56**, No. 1, pp 80-87

Zeelenberg, I. S., Ostrowiski, M., Krumeich, S., Bobrie, A., Jancic, C., Boissonnas, A., Delcayre, A., Le Pecq, J., Combadiere, B., Amigorena, S. and Thery, C., (2008) Targeting Tumor Antigens to Secreted Membrane Vesicles *In vivo* Induces Efficient Antitumor Immune Responses, Cancer Res, Vol. **86**, pp 1228-1235

Zhang, H. C., Liu, X. B., Huang, S., Bi, X. Y., Wang, H. X., Xie, L. X., Wang, Y. Q., Cao, X. F., Lv, J., Xiao, F. J., Yang, Y. and Guo, Z. K., (2012a) Microvesicles derived from human umbilical cord mesenchymal stem cells stimulated by hypoxia promote angiogenesis both in vitro and in vivo, Stem Cells, Epub ahead of print

Zhang, M., Li, X., Bai, L., Uchida, K., Bai, W., Wu, B., Xu, B., Xu, W., Zhu, H. and Huang, H., (2012b) Effects of low frequency electromagnetic field on proliferation of human epidermal stem cells: An in vitro study, Bioelectromagnets, Epub ahead of print

Zhang, X., Meng, L., He, B., Chen, J., Liu, P., Zhao, J., Zhang, Y., Li, Ming, L. and An. D., (2009) The role of P2X7 receptor in ATP-mediated human leukemia cell death: calcium influx-independent, Acta Biochim Biophys Sin, Vol. **41**, pp 362-369

Zhou, J., Ming, L. G., Ge, B. F., Wang, J. Q., Zhu, R. Q., Wei, Z., Ma, H. P., Xian, C. J. and Chen, K. M., (2011) Effects of 50 Hz sinusoidal electromagnetic fields of different intensities on proliferation, differentiation and mineralization potentials of rat osreoblasts, Bone, Vol. **49**, pp 7530761

Zielstorff, R. D., (1998) Online Practise Guidelines: Issues, Obstacles, and Future Prospects, Journal of the American Medical Informatics Association, Vol. **5**, pp 227-236

10. Appendix

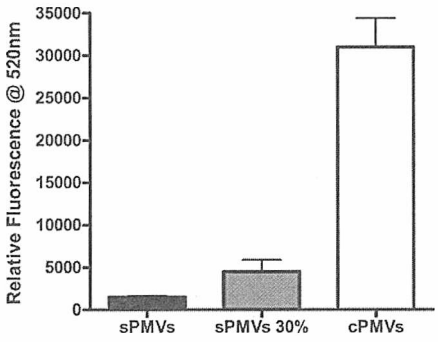

Fig 10.1 MV subtypes contain significantly different concentrations of free calcium. sMVs were released in ~11 fold greater amount that cMVs, however cMVs contain a relatively higher level of free calcium, 1x sMV ~1500 RFU:1x cMV ~35000 RFU. 3X sMVS have increased free calcium ~5000 RFU.

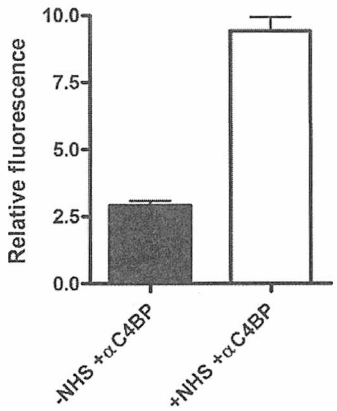

Fig 10.2 NHS derived C4 binding protein binds to MVs. The significant increase in αC4 binding protein (αC4BP) on MVs indicates a possible mechanism for the survival of THP-1 and Salmonella incubated at lytic levels of MAC, as the MVs would sequester C4 and therefore limit ativation of the complement pathways.

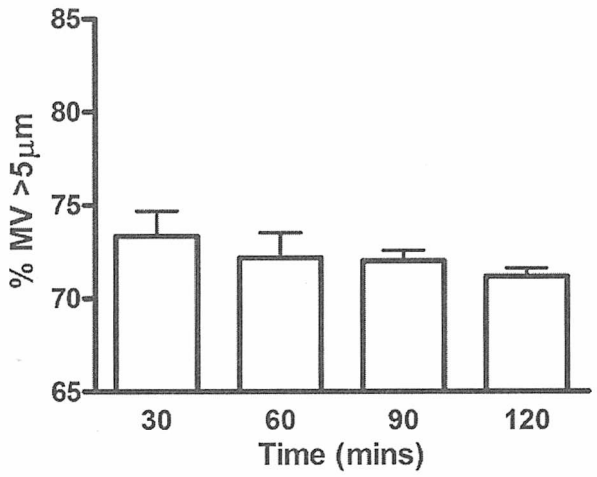

Fig 10.4 Restimulation of MVs leads to generally smaller sized sMVs. After an initial stimulatory event, THP-1 were rested in RPMI 1640 at 37°C in 5% CO_2 for ascending time points before being restimulated for MV release. Once incubated with 10% NHS and 2mM Ca^{2+} the MVs were isolated and quantified for their size. It was found the the sMVs released were significantly smaller after 120 min resting.

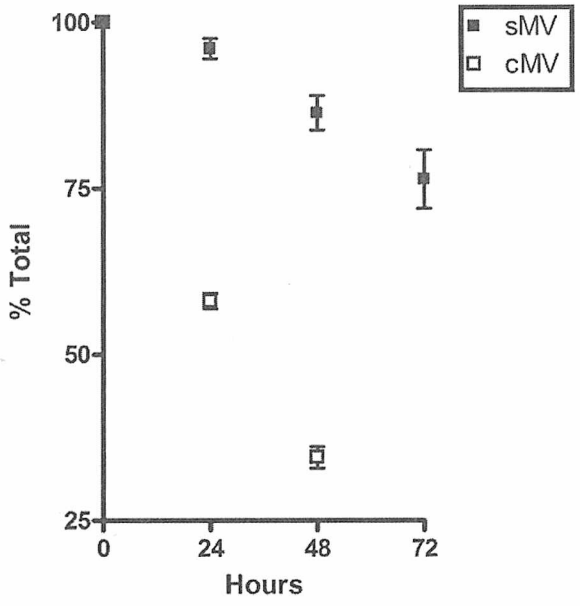

Fig 10.4 MV subtype half life. sMVs (2.5 x 10^6/ml) and cMVs (2.5 x 10^6/ml) were incubated at 4^{0}C for 60 h. At 24 h time points the MV subtypes were assessed for changes in population numbers. From 0 h to 48 h, there was a significant decline in sMV numbers that continued to 60 h. cMVs numbers decrease highly significantly, from 0 to 24 h there was ~ 50% decline, 24 to 48 h there was a further significant decline ~ 40% decline, however at 72 h the MVs were obscured by MV derived debris and no result was obtainable. The MV subtype numbers were quantified by FACs ExpressPlus programme.

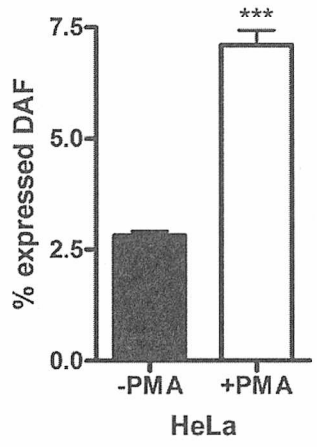

Fig 10.5 HeLa DAF expression was significantly enhanced by 50μM incubation with PMA for 72 h. HeLa DAF was significantly enhanced from ~2.75% to 7.0±0.5% by 72 h incubation with PMA. DAF expression was ascertained using flow cytometry.

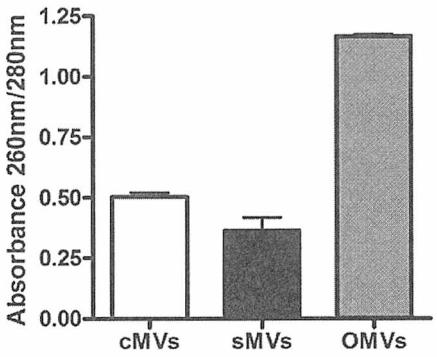

Fig 10.6 DNA and protein content of MV subtypes and Outer Membrane Vesicles (OMVs) derived from *Salmonella typhimurium*. OMVs express much more protein that MV subtypes, possibly as *salmonella* expresses a higher amount of protein on their plasma membrane.

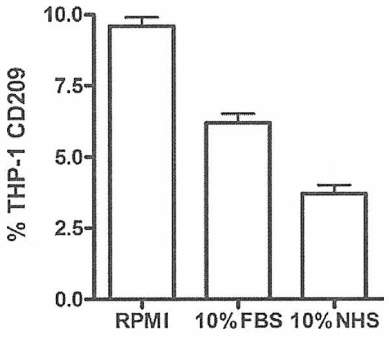

Fig 10.7 CD209 expression decreases after MV subtype release. CD209 in a pathogen receptor present on immature dendritic cells (THP-1) and is important for adhesion and antigen recognition. THP-1 express depressed levels after microvesiculation events. The control was gated against an unlabelled blank expressed ~9% CD209. THP-1 stimulated to release sMVs express ~ 4% and cMVs ~6%.

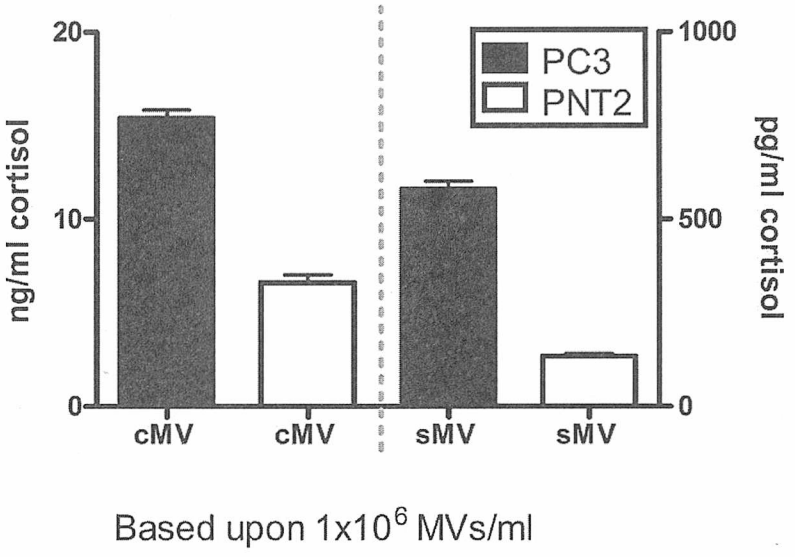

Fig 10.8 PC3 and PNT2 MV subtypes carry different concentrations of cortisol. PC3 and PNT2 were cultured in RPMI 1640 supplemented with 10% FBS and 1% penicillin and streptomycin. Although neither of these cells can synthesize cortisol, it was conjectured that they absorb the cortisol from the FBS. Cortisol was exported during microvesiculation, $1x10^6$MV subtypes/ml were assayed. Highly metastatic PC3 released ~15ng/ml in cMVs and ~550pg/ml in sMVs, lowly metastatic PNT2 released ~7ng/ml in cMVs and ~150pg/ml in sMVs. The cortisol ELISA from AB CAM (108665). Optical density was determined by FLUOstar Ω multiplate reader as per manufacturers' instructions.

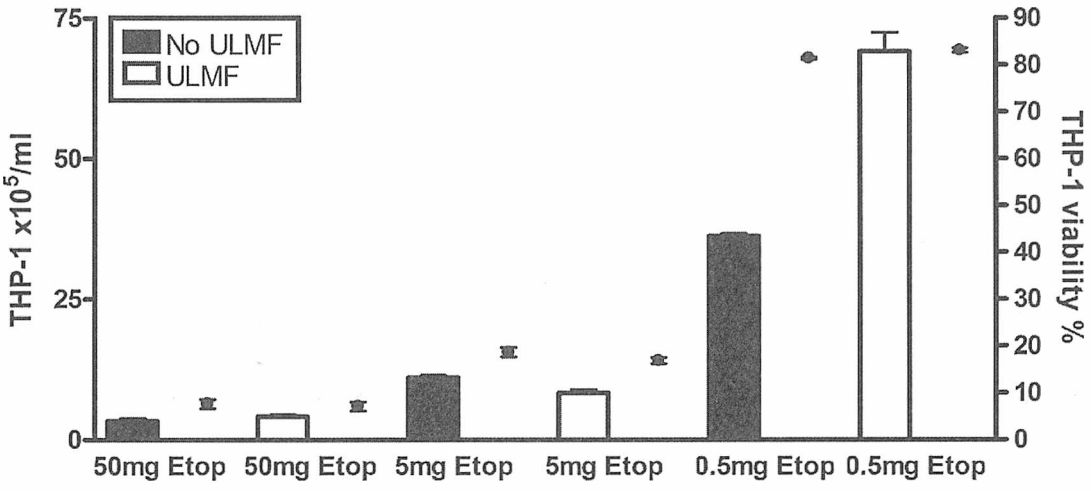

Fig 10.9 THP-1 incubated with ULMFs and reducing concentration of etoposide. THP-1 were incubated with 10x reducing concentrations of etoposide and ULMFs demonstrated small but significant cell death and significantly lower viability than cells treated with etoposide but no ULMFs. 0.5mg/ml etoposide treated with ULMF underwent either MV export of the cytotoxic drug compared to the control or significant levels of proliferation due to MV release.

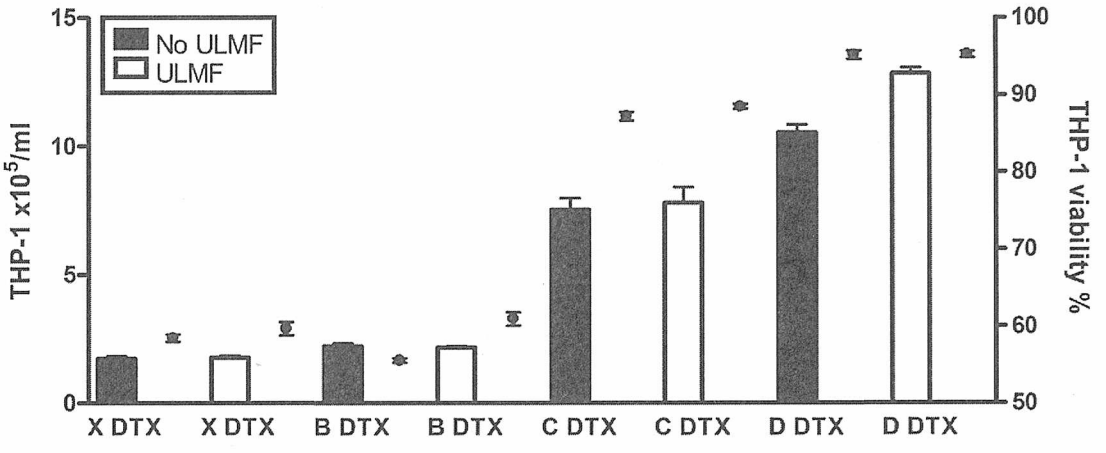

Fig 10.10 THP-1 treated with docetaxel and ULMF show no difference to the control. THP-1 were treated with 10x reducing concentrations of docetaxel (X was the therapeutic dose 50μM, B was 5μM, C was 0.5μM and D was 0.05μM). D ULMF treated THP-1 demonstrated typical proliferation of cells stimulated with ULMF (as before)

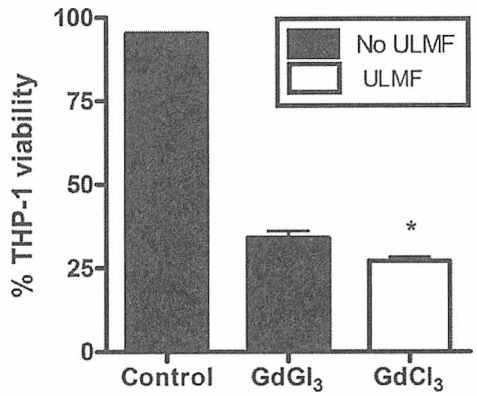

Fig 10.11 $GdCl_3$ causes THP-1 apoptosis. $GdCl_3$ incubated with THP-1 causes apoptosis due to its highly toxic nature, furthermore ULMFs cause a significant decrease in $GdCl_3$ treated THP-1 viability. Viability assayed using flow cytometry, ViaCount.

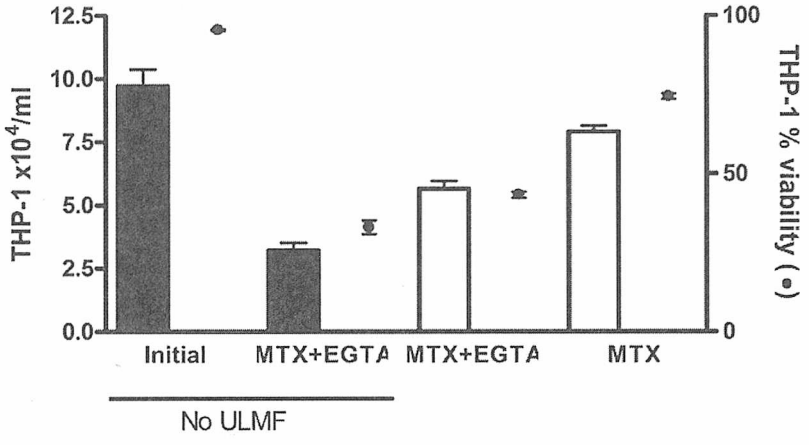

Fig 10.12 MV release lessens the therapeutic effects of methotrexate and 0.3μT 6V A/C ULMF. EGTA chelates extracellular Ca^{2+}, stimulation of THP-1 with ULMFs cause transcellular pores. Internal organelles leak Ca^{2+} into the cytoplasm leading to MV release.

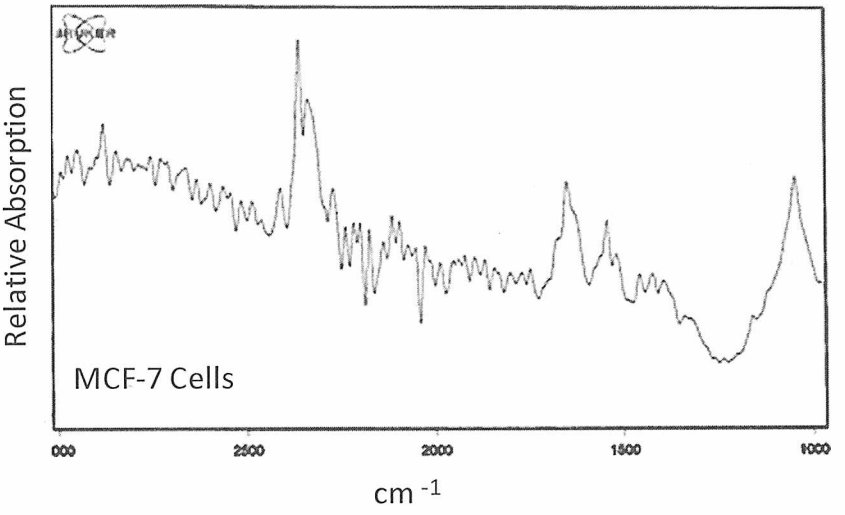

Fig 10.13 Typical FT-IR absorption profile for MCF-7. The profile generater from FT-IR spectroscopy (Bruker) was a composite of 12+ individual profiles, each generated from 100 scans from 4000cm-1 to 950cm-1. Although only the fingerprint region was of interest, all wave numbers were collected to compare unique cell profiles without assuming differences outside of the fingerprint region.

Analysis of calcium homeostasis has revealed that MVs contain high calcium levels, that are deliverable to cells via MVs as cargo. Furthermore, the MV subtypes express different arrays of deliverable proteins and receptors that were transiently expressible upon the recipient cell.

Novel research into the role of ultra low-frequency magnetic fields (ULMFs) on cellular viability was explored. Results suggested that 0.3μT 6V A/C 10Hz ULMF exposure to cells increased intracellular Ca^{2+} levels via transiently induced plasma membrane pores. Furthermore, ULMFs stimulated MV release from cells and negated apoptosis by export of pro-apoptotic agents, increasing the health of the cells. ULMFs can be used to significantly enhance the uptake promoting cellular sensitivity to anti-cancer drugs, such that 10% of the therapeutic dose used with ULMFs was able to achieve current levels of therapeutic response. ULMFs significantly reduce HeLa migration during wound healing although they increased cell proliferation, possibly by releasing MVs.

The exciting potential of this research may lead to new possibilities in cancer therapy. Using ULMFs in conjunction with chemotherapy may increase the success rates of existing therapies and reduce unwanted side effects. The data presented in this thesis will allow researchers to better understand subtle differences in MV biogenesis, how this reflects in their composition and morphology. It is the hoped that this research will lead to more laboratories engaging MV research using the techniques pioneered in this thesis to engage within many new areas of biology and biochemistry. This work offers a significant contribution to the field of MV research, but represents the tip of the iceberg.